PREDICTION OF MOTION AND WAVE LOAD OF MONO AND TWIN HULL SHIPS IN WAVES

by

Xing Zheng, B.Sc.

A Thesis Submitted for the Degree of

Doctor of Philosophy

in the Faculty of Engineering of University of Glasgow

ProQuest LLC.
789 East Eisenhower Parkway
P.O. Box 1346
Ann Arbor, MI 48106 – 1346

DEDICATION

TO THE MEMORY OF MY FATHER

SUMMARY

The main aim of this thesis is to improve the computational efficiency of three dimensional method and to investigate its applications to prediction of motion responses and wave loads for mono and twin hull vessels with emphasis on twin hull SWATH ships and crane vessels during heavy lifting operation . The result is to provide a more advanced tool for practical ship designers to use at the primary design stage.

In order to improve the computational efficiency of the three dimensional theory, the existing three dimensional panel method is modified in two different manners, firstly by making use of the properties of Green's function and then by introducing the higher order panel methods. It has been found that the first approach is simple and can save considerable computation time, while the improvement by the second approach is not significant at present but it has potential for future developments.

A mono hull Series 60 and a small waterplane area twin hull (SWATH) model are calculated by the modified three dimensional method (from the first approach). The emphasize is drawn on the SWATH model which is traditionally treated by the two dimensional strip theory. The viscous effect on the motion of SWATH is taken into account by a semi-empirical method . The comparison with two dimensional prediction and experimental results has been made. In addition, the standing wave phenomenon in the vicinity of twin hull ships and its effect on hydrodynamic coefficients and wave loads are extensively discussed.

The ordinary motion equation is modified to predict the motion responses of crane vessels during heavy lifting operation. The coupling effect between the motion of the vessel and the load being lifted and the viscous effect are considered in the prediction. The results are compared with the available experiments to validate the prediction method.

A general three dimensional method for predicting wave loads on cross deck structures of twin hull ships has been introduced. The predictions are fully three dimensional, so this method has ability to predict the wave loads and the wave load distributions at arbitrary wave heading . The predictions have been compared with experimental data.

In order to evaluate the seakeeping quality of a ship design in certain ocean environment, a seakeeping quality evaluation method has been presented. This method is based on the irregular wave results which can be deriv ed from regular wave results and the observed ocean environmental data in certain area and season. In addition, some design criteria for SWATH ships have been discussed and an example has been given for evaluation of the seakeeping quality for a SWATH design.

Finally, the overall conclusions regarding the above investigations are drawn, and some possible proposals for future development based on the present study are suggested.

ACKNOWLEDGEMENT

The author wishes to record his thanks to Professor D. Faulkner, Head of the Department of Naval Architecture and Ocean Engineering, University of Glasgow, and to his supervisor, Dr. R.C. McGregor, for their help and encouragement.

Thanks are also due to Dr. A. Incecik and Dr. M. Atlar for their very helpful discussions and moral support during his research at University of Glasgow. To Mr. E. Djatmiko for supplying some experimental results and tracing some of drawings.

The author would also like to express his heartfelt gratitude to his mother for her continuous encouragement and to his wife Jiang Hong who has supported and encouraged him throughout the research.

Finally, the author is grateful to the Chinese Government and the British Council for their financial support and to the Committee of Vice-Chancellors and Principals of the Universities of the United Kingdom for the O.R.S. Scholarship.

DECLARATION

Except where reference is made to the work of others

This thesis is believed to be original.

NOMENCLATURE

A_{ij}	added masses or inertia
A^0_{ij}	added masses or inertias at zero speed
$A_{ij}(x)$	added masses or inertias per unit ship length at position x along hull

$$A_{ij}' = \begin{cases} A_{ij} / \rho \Delta & \text{non-dimensional added mass (i,j = 1, 2, 3)} \\ A_{ij} / \rho \Delta L^2 & \text{non-dimensional added inertia (i,j = 4, 5, 6)} \\ A_{ij} / \rho \Delta L & \text{non-dimensional coupling added inertia } \begin{cases} i = 1,2,3;\ j = 4,5,6 \\ i = 4,5,6;\ j = 1,2,3 \end{cases} \end{cases}$$

A_W	water plane area
a	wave amplitude
a_0	viscous lift coefficient
B	beam
B_0	maximum beam for twin hull ships
B_{ij}	damping coefficient
B^0_{ij}	damping coefficient at zero speed
$B_{ij}(x)$	damping coefficient per unit ship length at position x along hull

$$B_{ij}' = \begin{cases} B_{ij}/\rho \Delta \sqrt{(g/L)} & \text{non-dimensional damping (i,j = 1, 2, 3)} \\ B_{ij}/\rho \Delta L^2 \sqrt{(g/L)} & \text{non-dimensional damping (i,j = 4, 5, 6)} \\ B_{ij}/\rho \Delta L \sqrt{(g/L)} & \text{non-dimensional damping } \begin{cases} i = 1,2,3;\ j = 4,5,6 \\ i = 4,5,6;\ j = 1,2,3 \end{cases} \end{cases}$$

B_{vij}	viscous damping coefficient
b	aspect ratio of panel element
b(x)	one half distance between centrelines of each hull
b_0	breadth of strut at waterline
b_z	breadth of strut at vertical position z
C_b	block coefficient
C_D	crossflow drag coefficient
C_o	contour around intersection of body surface and free surface

C_{ij}	hydrostatic restoring coefficient
$\overline{C}ij$	hydrostatic restoring coefficient of a crane vessel with the load at the jib extreme
F_n (= U/√(Lg))	Froude number
F_i	wave exciting force or moment due to wave
F_{vi}	viscous wave exciting force or moment
f_i	component of the tension force on the sling cable in ith direction
f_d (= f-mg)	dynamic sling tension of the cable
G	G (ξ, ζ, η; x, y, z) Green's function
G_i	Green's function associated with the position (x_i, y_i, z_i) in fluid
GM_T	transverse metacentric height
GM_L	longitudinal metacentric height
g	gravitational acceleration
$H_{1/3}$	significant wave height
h_0	height of cross deck above the free surface for twin hull ships
I_W	inertia of waterplane area
I_{ii}	moment of inertia in ith mode
I_{ij}	product of inertia
k	wave number
L	ship length
l	length of lifting cable
M	mass of body
Mb	bending moment
M_T	torsional moment
M_W	moment of waterplane area
M_{ij}	general mass matrix for ship
$\overline{M}_{ij}$	general mass matrix for crane vessel with the load at jib extreme
m	mass of the load being lifted
m_d	mass per unit area of cross deck
m_s	mass per unit ship length per unit height along strut

N	number of panels
$\mathbf{n}$ (n_1, n_2, n_3)	outward unit normal
p	pressure
$\mathbf{q}$	matrix of source densities
q_i	source density on ith panel
R	$\sqrt{(r^2 + (z - \eta)^2)}$
R'	$\sqrt{(r^2 + (z + \eta)^2)}$
r	$\sqrt{((x - \xi)^2 + (y - \zeta)^2)}$
S	mean wetted surface area
S_t	instantaneous wetted surface area
S_0	surface in waterplane
S_f	free surface outside waterplane
T	ship draught
T_{ij}	hydrodynamic action on ith panel per unit oscillatory displacement in jth mode
T_0	modal wave period
T_1	average wave period
t	time
U	forward speed
V	fluid volume
V_2	horizontal side force
V_3	vertical shear
$\mathbf{v}$	fluid velocity vector
$\mathbf{v_n}$	velocity in direction normal to the body surface
$\mathbf{W}$	steady state velocity vector
x, y, z	axis system defined as Fig. 2.1
x_0, y_0, z_0	axis system fixed in the space
x', y', z'	axis system fixed in body
$\bar{x}, \bar{y}, \bar{z}$	local element axis system
z_C	vertical co-ordinate of centre of gravity
β	heading angle of incident wave with respect to x-axis

ΔC_i	waterline length of ith element adjacent to free surface
ΔS_i	area of ith panel
∇	displacement of ship
λ	wave length
ε	small quantity
ξ_i	displacement in ith mode of motion
ξ_{io}	complex amplitude of ξ_i
ζ	free surface elevation
$\overline{\zeta}$	steady state free surface elevation
λ	wave length
$\overline{\xi}, \overline{\eta}$	local element system
ρ	density of fluid
σ	source strength
ψ	doublet strength
Φ	total velocity potential
$\overline{\phi}$	steady velocity potential
ϕ	unsteady velocity potential
ϕ_0	incident wave potential
ϕ_i	velocity potential associated with ith mode of motion (i = 1,2,...6)
ϕ_i^0	forward speed independent part of ϕ_i
ϕ_D	diffraction potential
φ_1, φ_2	swing angles of the lifting cable with respect to x, y axes respectively
χ_1, χ_2, χ_3	co-ordinates of the jib extreme in x, y, z, direction respectively
ω	wave frequency
ω_e	encounter wave frequency

CONTENTS

CHAPTER ONE

INTRODUCTION

1.1 General Consideration

A ship or marine vehicle operating in ocean environments, which are uncomfortable and often hostile, must fulfill its function namely transportation or exploration with safety, prudence operation of the ship, and with effectiveness of the ship's crew and its equipment. In extreme conditions, it must withstand waves which cause it to bend and twist without structural failure and seas which might overturn it without capsizing. It should also retain its manoeuvrability and reduce deck wetness, slamming and speed reduction in waves.

To design such a vessel, naval architects face a formidable task and must rely to a large extent on the methods which can predict the way a ship behaves in a seaway. Since Euler[1] and Bernoulli[2] published the earliest work on the ship motion problem in the middle of 18th century, naval architects have expended considerable efforts in deriving such a prediction method for use in ship design. Unfortunately, this was something of a 'black art' over a long period primarily because of the absence of any technique that could describe the complex nature of the problem involving free surface waves which behave in a random way. For this reason, naval architects were forced to rely heavily on empirical or semi-empirical rules based on past experience. The result is that designs changed only slowly from one vessel to another. Seldom is a radical departure made in the hull form of a ship. The improvement of the seakeeping quality of a ship design is a rather difficult and time consuming task.

The well known paper of St. Denis and Pierson[3] in 1953 on the application of the principle of superposition to the ship motion problem started a new era in this field by hypothesizing that the responses of a ship to irregular wave can be considered as the

summation of the responses to regular waves of all frequencies. Today, the validity of the application of superposition to the ship motion and wave load problem is generally accepted. In termsof the principle of superposition, the complex problem of predicting ship motions and wave loads in a seaway can be replaced by two problems,

1, the prediction of the motions and wave loads in regular sinusoidal waves and,

2, the prediction of statistical responses in irregular waves by using the regular wave results.

This first problem can be solved directly by measurements using model tests or indirectly by a hydrodynamic theory to predict the ship responses in regular waves. Since the St. Denis and Pierson's paper, there have been spectacular developments in both experimental and theoretical methods for predicting ship responses in regular waves. Large experimental facilities for testing models in oblique waves were built in many places around the world. Furthermore, most of the tanks originally designed for resistance and propulsion test have been equip ed with wavemakers, so that they can be used for head and following wave experiments. Numerous ship motion and wave loads test have been conducted in those facilities. Perhaps the most significant and comprehensive tests are the systematic experiments carried out at NSMB in Wageningen on sixteen different Series 60 hull forms in 1960's. The motions, power increases and wave loads were measured for each hull in head, following and oblique waves. Unfortunately, even this kind of data has been invaluable in the study of the hull form effect on seakeeping characteristics. However, for non-Series 60 hull forms there exists no similar systematic experimental data.

While experimental study is always desirable, it can be very expensive and time consuming and so it is not usually feasible to perform these experiments for each individual ship design option. On the other hand, the experiments are difficult to give insight into why a ship behaves in a particular way. Therefore, the paper of St. Denis and Pierson has further emphasized the importance of the development of theoretical and numerical methods for predicting the ship responses in regular waves.

The main purpose of this thesis is to investigate the hydrodynamic theories which

can predict the motion responses and wave loads of mono and twin hull ships in regular and irregular waves. In particular, the predictions for Small Waterplane Area Twin Hull (SWATH) ship and crane vessels during heavy lifting operations will be given emphasis. Before the investigation is described, a literature review on the seakeeping theories will be presented.

1.2 Literature Review

The study of seakeeping problem has been continued over a long period, but it is only recently that much progress has been made in solving the total problem. However, there are today a variety of different theoretical formulations based on a range of assumptions in both two and three dimensional cases which are valid in particular circumstances. Before going on to discuss the efficiencies and deficiencies of different theories and set up the main aims of this thesis, a brief review of the development of seakeeping theory is necessary.

1.2.1 The development of strip theory

Among many theoretical methods, the two dimensional strip theory has been recognized as 'the most practical tool' for prediction of motions and wave loads of a ship so far. The strip theory was first applied by Korvin-Kroukovsky and Jacobs[4] in 1957 to the prediction of heaving and pitching motion of a ship in regular head waves. This was the first motion theory suitable for numerical computations, which had adequate accuracy for engineering applications. This theory was then extended by Jacobs[5] to include the wave vertical shear forces and bending moments in regular head waves. Their approach has made use of the characteristic shape of a ship which has a length many times its beam and draught, so the ship can be divided into a number of transverse strips in the longitudinal direction of the hull. Then, the wave excitations and hydrodynamic forces on each strip can be evaluated separately. The interaction between one strip and another is ignored. It is, therefore, termed 'strip theory'.

The theory of Korvin-Kroukovsky and Jacobs has since modified and extended. Gerritsma and Beukelman[6] employed the multipole expansion technique to calculate the

added mass and damping coefficients of each strip. Smith[7] showed their approach predicted the head sea motions for a destroyer hull form which agree quite well with experiments. Ursell[8] found analytical solutions to the hydrodynamic forces of an infinitely long half immersed cylinder oscillating on the free surface in both heave and pitch modes. He employed the multipole expansion technique which has been discussed in detail by Thorne[9]. By applying a transformation to the results of Ursell's circular cylinder it is possible to calculate the added mass and damping for a unit length of ship shaped section. The multipole technique was also used by Porter[10] and Tasai[11].

The use of close-fit methods pioneered by Frank[12] was another significant improvement in the development of strip theory. In Frank's approach a number of segments with unknown sources are distributed on the section to calculate the added mass and damping coefficients. Smith and Salvesen[13] have demonstrated that the head sea motions can be predicted quite accurately even for a high speed hull with large bulbous bow when such close-fit method is applied. They also attempted to extend the original head sea strip theory to the case of oblique seas, but the theories are not that accurate since the diffraction effect on the exciting forces was not treated properly.

It is worth to note that the original strip theory of Korvin-Kroukovsky and Jacobs was based on a relative motion concept which was not derived in a rational mathematical manner but rather by use of physical intuition, and so this concept was considered suspect. It was found that some terms must be missing from the formula since the forward speed terms in the coefficients of the motion equations do not satisfy the symmetry relationship proved by Timman and Newman[14]. Timman and Newman gave rigorous analyses of the hydrodynamic coupling for a symmetric point-ended ship. They revealed that the forward speed dependent terms in hydrodynamic coefficients have the following relationship, (for five degrees of freedom)

A,	heave induced pitch moment	=	- pitch induced heave force
	sway induced yaw moment	=	- yaw induced sway force
	Yaw induced roll moment	=	- roll induced yaw moment
B,	Sway induced roll moment	=	- roll induced sway force

This is so called Timman-Newman relationship in the case of five degree freedom. For above reason , the work on strip theory was consequently concentrated on providing a rigorous derivation of the theory using the more rational approach.

It should be mentioned that the most general derivation of strip theory was made by Ogilvie and Tuck[15] to produce they called rational strip theory. They formulated the full three dimensional boundary value problem and used the high frequency slender body assumption with a systematic perturbation expansion to make consistent simplifications throughout the analyses. Their formulae satisfy the Timman-Newman relationship (A), but is only valid for the vertical modes of motion in head seas. There are some integral terms in their theory which have not yet been evaluated, thus their theory is difficult to use.

Strip theory formulations which have been derived less rigorously, but still give good results are those due to Salvesen, Ogilvie and Tuck[16] and Vugts[17]. They agree with Ogilvie and Tuck's results at zero speed, but include forward speed terms which Ogilvie and Tuck described as higher order terms. Their theories satisfy the Timman-Newman relationship (A) and (B) and also can be applied to the oblique waves. The correlation study made by Kim, Chou and Tien[18] shows that the predictions from this theory agree well with experiments, except when the ship oscillates at low encounter frequencies or moves with high speed. These limitations are consequences of the basic assumptions of the strip theory.

On the other hand, Newman[19] pointed out that in strip theory it was difficult to calculate the wave exciting forces and moments due to the diffraction directly in some cases. Troesch[20] has obtained solution in oblique waves, but in head seas Newman[19] has found the solution singular. Consequently, the Haskind[21] relationship is usually employed in strip theory to calculate the diffraction forces in terms of the radiation potential. The original formulae of the Haskind relationship is based on a three dimensional potential problem, but when used with strip theory the resultant form of the wave excitation acting on the ends of the ship is not strictly valid since three dimensional influences may be important in these regions. Newman has shown that for high frequencies of oscillation this

discrepancy does not cause significant differences on a slender ship since the wave propagates almost entirely in the broadside direction as explained by Ogilvie[22]. However, Faltinsen[23] found serious differences occurring at $\lambda/L=0.45$, and Maruo[24] found that strip theory fails to predict accurately the distribution of wave exciting forces and moments on a ship in head seas. In particular, good agreement between measurements and calculations for force distribution at bow was achieved, but the prediction of the pressure decay along the hull was poor. This resulted in considerable error between measurement and predictions on the sections over the after body. These findings were confirmed by Ursell[25] and Moeyes[26].

Another important improvement on the strip theory was made by Kim[27,28], Lee, Jones and Curphey[29]. They modified Salvesen, Tuck and Faltinsen's theory which is original for mono hulls to twin hull ships by taking the hydrodynamic interaction between the twin hulls in transverse direction into account. Later Lee and Curphey[30] applied this method to predict the motion response of SWATH ships in oblique waves with forward speed. They also modified this approach to predict the dynamic wave loads on the cross-deck structure of SWATH. In their approach the ship is approximated by uniform twin cylinders for wave loads calculation, so it is only valid in case of pure beam seas. They also compared the predictions with measurements and found generally good agreement, except for those in following waves when the encounter frequencies were very low. The pitch moment in head and following seas predicted by this approach was not good enough as found by Fein and Lamb[31]. The unified slender body theory of Newman[32] has been applied to SWATH by Hong[33] in order to improve the prediction especially for following seas. But in the limited comparisons that have been made with strip theory and experiments in head and following seas, it was found that the computed motion were not significantly improved by the application of the slender body theory.

1.2.2 Limitations of strip theories and the need for three dimensional theories

As reviewed foregoing the strip theories have been significantly improved both on the rigours of the theory and the accuracy of its prediction since it was first introduced by

Korvin-Kroukovsky and Jacobs thirty years ago. However, all the strip theories have deficiencies in one way or another. Takagi[34] suggested that a major failing of such approach was their inability to treat adequately three dimensional effects. From engineering application point of view, there are some key points on the limitation of strip theories and the need of three dimensional theories which can be identified as follows.

The strip theories can be applied to the most of mono hulls which usually have large length to beam ratios. Particularly, the prediction of motion responses of mono hull by strip theories agree well with the experimental results in head, beam and oblique waves as long as the forward speed is not very high and the oscillation frequency is not very low. The wave load predictions from bow to midship section are reasonable, but the values on the sections over the after body may cause considerable error. Therefore, the strip theories could provide a very useful practical tool for motion and wave load prediction of mono hulls before three dimensional theories become acceptable for engineering applications.

Unlike mono hulls, the twin hull or multi hull vessels, such as SWATH or semi-submersible, generally have long slender hulls but fairly large beams. The application of strip theory to such vessels still needs justification, as argued by Eatock Taylor and Hung[35]. The correlation study between experiments and theoretical predictions have shown that the motion responses predicted by strip theory are good in head and beam waves, but in oblique waves Djatmiko[36] showed the predictions from strip theory were poor for a tandem strut SWATH. This may be caused by the unfair treatment of hydrodynamic interaction between the twin hulls by strip theories which only take these interaction in transverse direction into account.

At early stage of SWATH research, the researchers were primarily concerned on the most serious motion conditions which were the pitch responses in head or following seas and the roll responses in beam seas. The strip theories were, therefore, quite acceptable. Nowadays, the designer are also interested in evaluating the seakeeping quality of SWATH in certain ocean environments[37]. In the latter case, the predictions of the motion response in any wave heading are equally important from the point of view of evaluating

seakeeping quality[37,38]. Therefore, the accuracy of predictions from strip theory still need further justification.

Wu[39], Eatock Taylor and Hung[35] indicated that for certain combinations of wave frequencies and the inner distances between the twin hulls the standing waves may occur. Those standing waves are caused by the hydrodynamic interaction either in transverse direction[39] or in longitudinal direction[35]. The computational results in this thesis show that both cases of standing waves may occur. The longitudinal standing waves are very important. The longitudinal standing waves with the lowest frequency may cause the maximum side loads and bending moment on cross deck structure of twin hull ships. As discussed by Eatock Taylor, the longitudinal standing waves are induced by three dimensional hydrodynamic effect. To investigate such effect the three dimensional theories are, therefore, necessary.

The wave loads, i.e. side forces and bending moments, on cross deck structure in pure beam seas were seen to be the worst wave loading conditions. The recent research[40] has found that the seas approaching from just forward or aft of beam give biased load distributions which may cause the maximum local stress on the cross deck structure. Since the present strip theories for predicting wave loads on super structure of twin hull ships are only valid in pure beam seas, they are unable to predict such load distributions along the hull. To overcome this problem the three dimensional theory must be applied.

On the other hand, the advanced structural analyses for SWATH or other twin hull ships are mainly based on three dimensional methods. If the strip theory is used for hydrodynamic load calculation, a rough approximation of load distribution along the hull must be employed. The three dimensional theory has ability to calculate the wave load distribution directly and so can provide more accurate wave load input for the structural analyses not only for beam sea case but also for any wave heading.

Owing to the slender body assumption, the strip theory is unable to treat a ship which is not slender. This is a limitation for vessels such as semi-submersible crane vessels which usually have columns with the similar size in diameter to the beam of each demihull

and the hull separation. To predict the motions and wave loads of such a vessel the three dimensional effect must be taken into account.

The major advantage of strip theories is that it is computationally less expensive than three dimensional theories. This is why strip theories are recognized as a very practical tool to predict the ship motion and wave load problem in the past decades when computations for three dimensional body in free surface were impractical if not impossible. Computer technology has drastically improved during the past decades. Not only has the memory space been expanded, but the speed of computation has increased and the relative cost has been reduced drastically. With further improvements of the computer technology, the advantage of strip theory will become less and less significant. The technology for calculating three dimensional ship motion and wave loads have been under development for a number of years, while general application of these techniques were restricted by the limitation of computers and the cost. The majority of the previous work was, therefore, concentrated on the development of the theories based on monohulls or stationary structures. Before going to set up the main aims of thesis and to investigate the application of three dimensional theories to engineering problem especially for twin hull ships, it is necessary to briefly review the existing three dimensional theories.

1.2.3 Existing three dimensional theories

The pioneer work on three dimensional method was made by Hess and Smith[41] for the problem of nonlifting potential flow about arbitrary three dimensional bodies in an infinite fluid. In their approach, a number of panels with simple fundamental sources which do not satisfy the free surface boundary conditions are used to approximate the body surface. This approach is, therefore, termed 'panel method'. Hess and Smith's method is unable to treat the free surface wave problem. However, this original panel method provides the basis for the further development of three dimensional theories.

In the early seventies the advent of the offshore oil boom brought the need to analyse structures which were large in all dimensions and for which strip theories were invalid. Consequently, three dimensional theories which coped with the free surface wave

problem were developed. Garrison[42,43], Faltinsen and Michelsen[44], Hogben and Standing[45] introduced the free surface Green's function which satisfied the linear free surface boundary condition at zero forward speed, i.e. pulsating sources, to the original panel method instead of fundamental sources. The result was that their panel methods had the ability to treat the free surface wave problem. The comparisons with experiments shown the prediction by their method are generally good for large number of offshore structures under stationary conditions.

In a different manner, Bai and Yeung[46] introduced another way to deal with the free surface wave problem. They modified the original panel method of Hess and Smith by distributing source panels on not only body surface but free surface, sea bed and a vertical control surface at infinity and choosing the source strength on each panel to satisfy body surface kinetic boundary conditions, linear free surface, sea bed and radiation conditions. Their approach only uses fundamental sources which has much simpler form than pulsating source , but the method is computational less efficient than Garrison's approach for the problems with an infinite extent of free surface[47]. However this approach does have its advantages, e.g. it can be used to treat the problem where the sea bed is not flat or the fluid domain is restricted such as the sloshing in oil tanks.

Besides the above two approaches, there are many other three dimensional theories. Zienkiewicz et al[48] applied the finite element method which has scored spectacular successes in structural mechanics to fluid mechanics with free surface effect. Eatock Taylor and Zietsman[49] introduced a hybrid method which used the finite element method in the inner region close to body surface and the panel method in the outer region. All the different three dimensional theories have their own efficiencies and deficiencies which depend on the problem to be solved.

All the 3D theories mentioned so far only deal with bodies without forward speed and are mainly applied to the stationary offshore structures. The work by Chang[50] applied the three dimensional theory to the ship motion problem with the forward speed effect. She introduced translating and pulsating sources which satisfied the speed dependent free

surface conditions to the ordinary panel method to take the forward speed effect into account. The results by this approach agree well with experiments with or without forward speed. Unfortunately, this approach is computationally very expensive because the double integral in the formulations of translating and pulsating source is very time consuming for numerical evaluation.

In order to reduce the computational effort for forward speed problem, Inglis[51] developed so called simplified three dimensional theory. He employed a similar approach as the strip theory of Salvesen, Tuck and Faltinsen to simplify the forward speed dependent terms on the free surface conditions under the assumptions of the oscillation frequency is high and the forward speed is low. In his approach the pulsating source is used instead of translating and pulsating source, so it is computationally much cheaper than Chang's approach. Inglis has also investigated the full three dimensional theory which is similar as Chang's approach and compared it with simplified three dimensional theory and experimental results. The comparisons confirm that the simplified three dimensional theory can give very reasonable predictions as long as its assumptions are valid. This approach is now recognized as one of the most practical three dimensional tool for ship motion and wave load problem and has been used by various of investigators, such as Chen, Torng and Shin[52], Wu and Price[53].

From the review of the previous work published in this field, some conclusions can be drawn as follows:

1, the motion and wave load problems of twin hull vessels, especially for SWATH, have been mainly treated by strip theories in the past but there are still some practically important problems which are difficult to solve due to the three dimensional effects,

2, the three dimension methods are still computationally time consuming, and

3, the majority of three dimensional work was concentrated on mono hulls or stationary offshore structures and its application to some special twin hull vessels, such as SWATH and crane vessels during heavy lifting operation that are primarily concerned in this thesis, are still lack of justification.

These form the main aim of this thesis.

1.3 Main Aim of this Thesis

The main aim of this thesis is to improve the computational efficiency of three dimensional method and to investigate its applications to prediction of motion responses and wave loads for mono and twin hull vessels with emphasis on twin hull SWATH ships and semi-submersible crane vessels during heavy lifting operation . The result is to provide a more advanced tool for practical ship designers to use at the primary design stage. The particular attention has been devoted to certain aspects as follows.

1, The existing three dimensional panel method has been modified to improve its computational efficiency which is the major restriction on the application of three dimensional theory to practical uses. Two approaches have been investigated in this thesis, firstly by making use of properties of Green's function which is presented in Chapter 3 and then by introducing higher order panel methods which is given in Appendix A.

2, The modified three dimensional method (by the first approach) was used to predict the hydrodynamic coefficients, wave excitations and motion responses of mono hull Series 60 model and compared the present predictions with other theoretical and experimental results to validate the modification. This is described in the Chapter 4.

3, The three dimensional theory has been employed to predict the hydrodynamic coefficients, wave excitations and motion responses of SWATH for different wave headings and forward speeds. The correlation study has been made with the strip theory predictions and experiments. Attention is paid to the discussion about the improvements of three dimensional predictions over the traditional strip theory approach. The presentation is

made in Chapter 4.

4, Unlike monohulls, the viscous effect on the motion responses of SWATH and semisubmersibles is significant specially near the motion resonant frequencies. In order to predict those motion responses correctly the semi-empirical cross flow approach which was originally used with strip theories has been introduced to the three dimensional panel method to estimate the viscous effect. An iterative method is employed in the solution of motion equations. Comparison has been made with measurements. This is also in Chapter 4.

5, The standing wave phenomenon in the vicinity of twin hull ships has been discussed in detail. The three dimensional hydrodynamic effect on the standing waves and its effect on the wave loads on the structures of twin hull ships has been given particular attention. Those discussions are presented in both Chapter 4 and 6.

6, The ordinary motion prediction methods have been modified to predict the motion responses of the crane vessels during heavy lifting operations. The motion coupling effect between the vessel and the load being lifted and the viscous effect on the motion of the vessel has been considered in the prediction. The two examples, for a mono hull and a semisubmersible crane vessels, are given. Some comparison with experimental data have been made as well. The details can be found in Chapter 5.

7, A general three dimensional method for predicting wave loads on cross deck structures of twin hull ships has been introduced. The predictions are fully three dimensional, so this method has ability to predict the wave loads and the wave load distributions for arbitrary wave headings. In addition, some special features of three dimensional predictions such as

a, its ability to predict the biased load distribution in just forward or aft beam seas which may give rise to maximum local stress on the structure.

b, to predict the maximum torsional moment on cross deck structure which usually occurs at quartering seas and

c, to produce more accurate wave distribution input for structural analyses

have also been discussed. Some of the results have been compared with the experiments to validate the three dimensional predictions. This is presented in Chapter 6.

8, Finally, the traditional wave spectral methods were employed to predict the statistic responses of the motion responses and wave loads of a ship in irregular waves by using its regular results. These statistical results can be used to evaluate the significant values of motion response and wave loads in given ocean conditions. In order to evaluate the seakeeping quality of a ship design in certain ocean environment,a seakeeping quality evaluation method has been presented. This method is based on the irregular wave results for a given design and the observed ocean environmental data for certain area and season . Furthermore, some design criteria for SWATH ships have been discussed and an example has been given for evaluation of the seakeeping quality for a SWATH design. Those are given in Chapter 7.

In the final chapter the conclusions of present study have been drawn and the proposals for the future development based on the present work have been suggested as well.

CHAPTER TWO

THREE DIMENSIONAL POTENTIAL THEORY

This chapter summarises the method based on 3D diffraction theory for predicting motion and wave load of a 3D arbitrary body in regular waves with and without forward speed. The analysis is primarily based on irrotational (inviscid), incompressible potential flow theory. The viscous effect will be discussed in Chapter 4 and the random sea procedure will be discussed in Chapter 7.

The general definition of the hydrodynamic problem is firstly outlined. This is followed by the analysis of the different methods for solving the boundary value problem to get a suitable method for the present study. Finally a detailed discussion on the singularity distribution method is given.

2.1 Formulation of the Problem

2.1.1 Definition of the problem

The hydrodynamic theory which deals with the problem of a 3D arbitrary body moving at a constant speed in regular sinusoidal waves is developed based on the assumption that the fluid surrounding the body is inviscid, irrotational, homogeneous and incompressible. Therefore, a velocity potential must exist satisfying Laplace's equation and the respective boundary conditions. When linearization is considered permissible the harmonic motion of the body becomes primarily important. In that case only the boundary conditions for velocity potential remain. Summarizing, the velocity potential must satisfy the following requirements:

1- Laplace's equation,

2- the linearized free surface condition,

3- the radiation condition,

4- sea bed condition, and

5- body surface kinematic condition.

The underlying assumptions are:

1- the fluid is inviscid, incompressible and irrotational,

2- the surface tension may be neglected,

3- the free surface domain is infinitely large,

4- the seabed is flat or infinitely deep, and

5- the incident wave and resulting motion responses is sufficiently small in amplitude.

By means of the velocity potential the fluid velocity vector **v** can be represented as

$$\mathbf{v} = \nabla\Phi \tag{2.1}$$

with

$$\Phi = \Phi(\mathbf{x}, t) \tag{2.2}$$

where Φ is velocity potential satisfying the conditions mentioned above, **x**, t are respectively the position vector and time. The pressure p is determined by Bernoullis equation

$$p = -\rho\left(\Phi_t + \frac{1}{2}\,\mathbf{v}\cdot\mathbf{v} + p_0\right) \tag{2.3}$$

in which ρ is the fluid density, g is the gravitation acceleration and p_0 is the atmospheric pressure which is assumed constant. In equation (2.3) and hereafter when the independent variables, x, y, z, t appear as subscripts, partial differentiation is indicated, i.e. $\phi_t = \partial\Phi/\partial t$, etc.

1.1.2 Co-ordinate systems

In dealing with the 3D ship motion problem defined above, it will be convenient to consider three co-ordinate systems, one of these is the $o\text{-}x_0y_0z_0$ co-ordinate system fixed in space in such a way that the $o\text{-}x_0y_0$ plane coincides with undisturbed free surface and $o\text{-}z_0$ is directed vertically upward, $o\text{-}y_0$ is chosen to make the system right handed. The other o-xyz is taken to be fixed in the ship, and in such a way that the origin, o, is at the point of intersection of the calm water surface, the longitudinal plane of symmetry and the vertical

plane passing through the centre of gravity of the ship, the o-xy plane coincides with the undisturbed water surface when the ship is at rest, the o-xz plane coincides with the longitudinal plane of symmetry of the ship. o-x towards the bow and o-y to the port side. If the ship is moving in such a way that one may define average position around which the axes o-xyz fluctuate, this can be denoted by the co-ordinate system o'-x'y'z' (see Fig.2.1) The aim of the ship motion theory is to find the mutual relationship of these sets of co-ordinate systems.

2.1.3 Decomposition of the velocity potential

A total potential $\Phi(x,y,z,t)$ exists which can be expressed in following form

$$\Phi\ (x,y,z,t) = U\left[\ \bar{\phi}\ (x,y,z,) - x\ \right] + \phi\ (x,y,z,t) \qquad (2.4)$$

where U is the forward speed of the body, $U\left[\ \bar{\phi}\ (x,y,z) - x\right]$ is the time independent potential due to the steady forward motion of the floating body travelling in calm water with speed U and $\phi\ (x,y,z,t)$ is the unsteady time dependent potential due to the body motion in waves.

Since the incident wave and the resulting responses have been assumed sufficiently small in amplitude, the unsteady motion problem can be assumed to be a linear superposition of the following boundary value problems as suggested by Haskind[1]:

1- the incident wave encountered by the body will be diffracted from it assuming the body is rigidly held in its fixed position. This is called the 'Diffraction Problem'.

2- as soon as the incident waves are diffracted due to the presence of the body, it is assumed that the motion can be represented by the oscillation of this body in initial calm water with the same frequency as it encountered in the wave. The six degrees of rigid body motions can be further decomposed linearly. This is known as 'Radiation Problem'.

The total unsteady potential for a sinusoidal wave excitation with encounter frequency, ω_e, can thus be expressed as

$$\phi(x,y,z,t) = \left[\phi_0(x,y,z) + \phi_D(x,y,z) + \sum_{i=1}^{6} \xi_i \phi_i \right] e^{-i\omega_e t} \qquad (2.5)$$

where $\phi_0(x,y,z)$ is the incident wave potential representing the incident waves, $\phi_D(x,y,z)$ is the diffraction potential representing the disturbance of the incident waves diffracted from the body, $\phi_i(x,y,z)$, i=1,2,...6, are the radiation potentials due to oscillations of the body in calm water with unit amplitude in each of six degrees of freedom, i=1,2,...6 represent surge, sway, heave, roll, pitch and yaw respectively and ξi, i=1,2,...6 are the appropriate amplitudes of the oscillation.

The incident wave potential is of the form

$$\phi_0 = -\frac{iga}{\omega} e^{kz} e^{i(kx\cos\beta + ky\sin\beta)} \qquad (2.6)$$

and the encounter frequency, ω_e, in Eqn.(2.5) is represented by

$$\omega_e = |\omega - Uk\cos\beta| \qquad (2.7)$$

where ω is wave frequency, a is the wave amplitude, k is the incident wave number, $k=\omega^2/g$, and β is an arbitary heading angle (180^0 for head sea).

2.1.4 Boundary conditions

The nature of the boundary value problem under the foreging assumptions described in section 2.1.1 imposes the following conditions which should be satisfied in fluid domain, on the free surface, the immersed surface of the body, a suitable closure at infinity and sea bed.

1, Laplace equation

$$\nabla^2\phi = 0 \qquad \text{in fluid domain} \qquad (2.9)$$

2, Linear free surface condition

$$U^2 \frac{\partial}{\partial x^2} \bar{\phi} + g \frac{\partial}{\partial z} \bar{\phi} = 0 \qquad \text{on } z=0 \qquad (2.10)$$

$$(i\omega_e + U\frac{\partial}{\partial x})^2 \phi + g \frac{\partial}{\partial z} \phi = 0 \qquad \text{on } z=0 \qquad (2.11)$$

for the zero forward speed

$$- \omega^2 \phi + g \frac{\partial}{\partial z} \phi = 0 \qquad \text{on } z=0 \qquad (2.12)$$

3, Body boundary condition[2]

$$\frac{\partial}{\partial n} (\bar{\phi} - x) = 0 \qquad \text{on S} \qquad (2.13)$$

$$\frac{\partial}{\partial n} (\phi_0 + \phi_D) = 0 \qquad \text{on S} \qquad (2.14)$$

$$\frac{\partial}{\partial n} \phi_i = -i\omega_e n_i + U m_i \qquad \text{on S} \qquad (2.15)$$

where

$(n_1, n_2, n_3) = \mathbf{n}$

$(n_4, n_5, n_6) = \mathbf{r} \times \mathbf{n}$

with **n** the outward unit normal vector and **r** the position vector with respect to the origin of reference frame

$(m_1, m_2, m_3) = - (\mathbf{n} \cdot \nabla) \nabla(\bar{\phi} - x)$

$(m_4, m_5, m_6) = - (\mathbf{n} \cdot \nabla) [\mathbf{r} \times \nabla(\bar{\phi} - x)]$.

Salvesen, Tuck and Faltinsen[2] showed that the cross products of the steady perturbation potential $\bar{\phi}$ and the unsteady potential ϕ are of higher order and $\bar{\phi}$ may be neglected in the computation of m_i in above equation, this leads to

$$m_i = 0 \qquad i=1,2,3,4$$

$$m_5 = n_3, \quad m_6 = - n_2 \qquad (2.16)$$

4, Sea bed condition

For finite depth

$$\frac{\partial}{\partial z}\phi = 0 \qquad \text{for } z=-d \qquad (2.17)$$

and the infinite depth

$$\frac{\partial}{\partial z}\phi = 0 \qquad \text{for } z \to -\infty \qquad (2.18)$$

where d is the depth of water.

5, Radiation condition at infinity

A radiation condition, which states that wave energy flux is directed away from the body at infinity, must be satisfied. This restriction imposes a uniqueness for the solution of the boundary problem, which would not otherwise be presented. The radiation condition takes various mathematical forms depending on the nature of the velocity potential. The detailed discussions are given by John[3], Newman[4], and Wehausen and Laitone[5].

2.1.5 Evaluation of the hydrodynamic forces

If the velocity potential ϕ is known, the pressure on the body surface can be obtained by applying the Eqn.(2.4) to the Bernoullis' equation, Eqn.(2.3), i.e.

$$p = -\rho \left[\left| -i\omega_e \phi + U\nabla(\bar{\phi} - x)\nabla\phi \right| e^{-i\omega_e t} + \frac{1}{2}\left(\nabla\phi e^{-i\omega_e t}\right)^2 + \frac{1}{2}U^2 \left|\nabla(\bar{\phi} - x)\right|^2 + \rho g z \right] \qquad (2.19)$$

in which the last two terms on the right hand side are time independent, the first of them is associated with wave making resistance and the lift, the second is the hydrostatic buoyancy force contribution. The other terms in Eqn.(2.19) are time dependent due to the factor $e^{-i\omega_e t}$ and give rise to unsteady forces.

The linearized hydrodynamic pressure is obtained by disregarding higher order terms in ϕ as well as terms involving cross products of $\bar{\phi}$ and ϕ from the time dependent terms in Eqn.(2.19), as follows

$$p = -\rho \left(-i\omega_e - U \frac{\partial}{\partial x} \right) \phi \, e^{-i\omega_e t} \quad . \tag{2.20}$$

Since the oscillation displacement is assumed small, the total oscillation force and moment on the body can be obtained by integrating the pressure(2.20) (ignoring the time factor $e^{-i\omega_e t}$) over the mean wetted body surface instead of the instaneous wetted surface, thus

$$\begin{aligned} H_i &= - \iint_S p n_i \, ds \\ &= - \rho \iint_S n_i \left(i\omega_e + U \frac{\partial}{\partial x} \right) \phi \, ds \end{aligned} \quad . \tag{2.21}$$

By substituting Eqn.(2.5) to Eqn.(2.21), the total force, H_i, can be divided into the wave exciting force, F_i, and the motion induced forces, E_i, i.e.

$$H_i = F_i + E_i \tag{2.22}$$

and the wave exciting force can be further divided into the incident wave part, F_i^O, and the diffraction part, F_i^D, so that

$$F_i = F_i^I + F_i^D = - \iint_S n_i \left(i\omega_e + U \frac{\partial}{\partial x} \right) (\phi_0 + \phi_D) \, ds \tag{2.23}$$

with

$$F_i^I = - \iint_S n_i \left(i\omega_e + U \frac{\partial}{\partial x} \right) \phi_0 \, ds \tag{2.24}$$

and

$$F_i^D = - \iint_S n_i \left(i\omega_e + U \frac{\partial}{\partial x} \right) \phi_D \, ds \quad . \tag{2.25}$$

The motion induced force is

$$E_i = - \iint_S n_i \left(i\omega_e + U \frac{\partial}{\partial x} \right) \sum_{j=1}^{6} \xi_j \phi_j \, ds \quad . \tag{2.26}$$

Since the derivative in Eqn.(2.26) is not easy to deal with, the following form which is

derived from the Stokes' theorem has been suggested by Salvesen[2].

$$\iint_S n_i \, U\frac{\partial}{\partial x}\phi \, ds = U \iint_S m_i \, \phi \, ds - U \int_{C_0} n_i \, \phi \, dl \qquad (2.27)$$

where ϕ is any differentiable scalar function, C_0 is the intersection of the body surface and the free surface.

In accordance with classical linear gravity wave theory, the potential for the incident wave, Eqn (2.6), is introduced in the expression for the incident wave part of exciting force Eqn.(2.24) and gives

$$F_i^0 = -\rho \, i \iint_S n_i \, (\omega_e + Uk\cos\beta) \, \phi_0 \, ds \qquad (2.28)$$

and Eqn.(2.7) reduces this to

$$F_i^0 = -\rho \, i \, \omega \iint_S n_i \, \phi_0 \, ds. \qquad (2.29)$$

This is well known Froude-Krylov force which is independent of the forward speed.

By applying the Stokes' theorem, Eqn.(2.27), to Eqn.(2.25), the diffraction part of the wave exciting force can be expressed as

$$F_i^D = -\rho \iint_S (i \omega_e n_i + U m_i) \, \phi_D \, ds - \rho U \int_{C_0} n_i \, \phi_D \, ds. \qquad (2.30)$$

The motion induced forces on moments, Eqn.(2.26) can be rewritten as

$$\begin{aligned} E_i &= -\rho \iint_S (i \omega_e n_i + U m_i) \sum_{j=1}^{6} \xi_j \, \phi_j \, ds + U \int_{C_0} n_i \sum_{j=1}^{6} \xi_j \, \phi_j \, dl \\ &= \sum_{j=1}^{6} T_{ij} \, \xi_j \qquad \text{for } i=1,2,\ldots 6 \end{aligned} \qquad (2.31)$$

where

$$\begin{aligned} T_{ij} &= -\rho \iint_S (i \omega_e n_i + U m_i) \, \phi_j \, ds + U\rho \iint_S n_i \, \phi_j \, ds \\ &= -\omega_e^2 A_{ij} - i \omega_e B_{ij} \end{aligned} \qquad (2.31)$$

The terms A_{ij} and B_{ij} are added mass and damping coefficients respectively. The subscript ij denotes jth mode of motion induced ith mode of added mass and damping coefficient. Furthermore, A_{ij} and B_{ij} can be expressed as the following form by extending Eqn.(2.32).

$$A_{ij} = -\frac{\rho}{\omega} \mathrm{Im}\left[\iint_S n_i \phi_j \, ds \right] + \frac{\rho U}{\omega^2} \mathrm{Re}\left[\iint_S m_i \phi_j \, ds \right] - \frac{\rho U}{\omega^2} \mathrm{Re}\left[\int_{C_0} n_i \phi_j \, dl \right]$$

$$B_{ij} = \rho \, \mathrm{Re}\left[\iint_S n_i \phi_j \, ds \right] + \frac{\rho U}{\omega} \mathrm{Im}\left[\iint_S m_i \phi_j \, ds \right] - \frac{\rho U}{\omega} \mathrm{Im}\left[\int_{C_0} n_i \phi_j \, dl \right] \tag{2.33}$$

2.1.6 Haskind relationship

In terms of Eqn.(2.29)-(2.30), the wave exciting forces can be obtained by direct integral of incident and diffraction wave potential over the mean wetted body surface. This is the so called direct integration method. There is an indirect way to do it by using 'Haskind relationship'.

For any two functions ϕ_A and ϕ_B satisfying the same Laplace equations, the free surface condition, the radiation condition and the sea bed condition, from Green's second identity

$$\iiint_V \left(\phi_A \nabla^2 \phi_B - \phi_B \nabla^2 \phi_A \right) dv = \iint_{SF} \left(\phi_A \frac{\partial \phi_B}{\partial n} - \phi_B \frac{\partial \phi_A}{\partial n} \right) ds \tag{2.34}$$

it can be found that

$$\iint_{SF} \phi_A \frac{\partial \phi_B}{\partial n} \, ds = \iint_{SF} \phi_B \frac{\partial \phi_A}{\partial n} \, ds \tag{2.35}$$

This is the so called 'Haskind relationship'. Since this relationship is also valid for the two dimensional case, it can be applied to both the surface integral and the line integral in Eqn.(2.23), so that the wave exciting force can be written by means of the boundary

condition (2.15) as following

$$F_i = -\rho \iint_S \frac{\partial \phi_i}{\partial n} (\phi_0 + \phi_D) \, ds = -\rho \iint_S (\frac{\partial \phi_i}{\partial n} \phi_0 - \frac{\partial \phi_0}{\partial n} \phi_i) \, ds. \qquad (2.36)$$

Here the boundary condition, $\partial\phi_i/\partial n = -\partial\phi_D/\partial n$, Eqn.(2.14) has been used.

The use of 'Haskind relationship' enable to the total wave exciting forces or moments acting on a ship to be determined from the velocity potential associated with the forced oscillation of the ship in calm water without recourse to the diffraction problem. However, the results obtained by the two approaches are completely equivalent.

2.1.7 Evaluation of motion

Under the assumptions that the responses are linear and harmonic, the six linear coupled differential equations of motion can be written in following form

$$\sum_{j=1}^{6} \left[-\omega_e^2 (M_{ij} + A_{ij}) - i\omega_e B_{ij} + C_{ij} \right] \xi_i = F_i \quad \text{for } i=1,2,...6. \qquad (2.37)$$

where M_{ij} is the generalized mass matrix for the ship, A_{ij}, B_{ij}, and C_{ij} are added mass, damping and restoring force matrices respectively, ξ_i is complex amplitude of the responses motion in each of six degrees of freedom, and F_i is the complex amplitude of wave exciting force.

If it is assumed that the ship has lateral symmetry and the centre of gravity is located at $(0,0,z_c)$, then the generalized mass matrix has the form of

$$[M_{ij}] = \begin{bmatrix} M & 0 & 0 & 0 & Mz_c & 0 \\ 0 & M & 0 & -Mz_c & 0 & 0 \\ 0 & 0 & M & 0 & 0 & 0 \\ 0 & -Mz_c & 0 & I_{44} & 0 & -I_{46} \\ Mz_c & 0 & 0 & 0 & I_{55} & 0 \\ 0 & 0 & 0 & -I_{64} & 0 & I_{66} \end{bmatrix}, \qquad (2.38)$$

where M is the mass of the ship, I_{ii} is the moment of inertia in ith mode and I_{ij} are the products of inertia. The inertia terms are with respect to co-ordinate system shown in Fig.2.1. The only product of inertia which appears is I_{46}, the roll-yaw product, which vanishes if the ship has fore-aft symmetry The other nondiagonal elements all vanish if the origin of the co-ordinate system coincides with the centre of gravity of the ship. However, it is frequently more convenient to take the origin in the water plane, in which case, z_c is not equal to zero.

For ship with lateral symmetry it also follows that the added mass and damping matrices are

$$[A_{ij}] = \begin{bmatrix} A_{11} & 0 & A_{13} & 0 & A_{15} & 0 \\ 0 & A_{22} & 0 & A_{24} & 0 & A_{26} \\ A_{31} & 0 & A_{33} & 0 & A_{35} & 0 \\ 0 & A_{42} & 0 & A_{44} & 0 & A_{46} \\ A_{51} & 0 & A_{53} & 0 & A_{55} & 0 \\ 0 & A_{62} & 0 & A_{64} & 0 & A_{66} \end{bmatrix} \qquad (2.39)$$

and

$$[B_{ij}] = \begin{bmatrix} B_{11} & 0 & B_{13} & 0 & B_{15} & 0 \\ 0 & B_{22} & 0 & B_{24} & 0 & B_{26} \\ B_{31} & 0 & B_{33} & 0 & B_{35} & 0 \\ 0 & B_{42} & 0 & B_{44} & 0 & B_{46} \\ B_{51} & 0 & B_{53} & 0 & B_{55} & 0 \\ 0 & B_{62} & 0 & B_{64} & 0 & B_{66} \end{bmatrix} . \qquad (2.40)$$

Furthermore, for a ship in the free surface the linear hydrostatic restoring coefficient matrix is

$$[C_{ij}] = \rho g \begin{bmatrix} 0 & 0 & 0 & 0 & 0 & 0 \\ 0 & 0 & 0 & 0 & 0 & 0 \\ 0 & 0 & A_w & 0 & -M_w & 0 \\ 0 & 0 & 0 & \nabla GM_T & 0 & 0 \\ 0 & 0 & -M_w & 0 & \nabla GM_L & 0 \\ 0 & 0 & 0 & 0 & 0 & 0 \end{bmatrix} \quad (2.41)$$

where A_W is the waterplane area, M_W is the moment of waterplane, ∇ is the displacement of ship, GM_T is the transverse metacentric height and GM_L is the longitudinal metacentric height.

If all those matrices are substituted in equation (2.37), it is seen that for ship with lateral symmetry, the six coupled equations of motion reduce to two sets of coupled equations: a set of three coupled equations for surge, heave and pitch and another set of three coupled equations for sway, roll and yaw. Thus, for a ship with lateral symmetry, surge, heave and pitch are not coupled with sway, roll and yaw.

With the present method, the added mass, damping and wave exciting force terms are yielded from the 3D diffraction theory. From a knowledge of these hydrodynamic coefficients, the equations of motion (2.37) can be solved for ship responses ξ_i (i=1,2,...6).

The motion equations described above only contain the potential terms and viscous effect is not included in the prediction of motion. In some cases, such as the roll responses of mono hull ships, and the heave and pitch motions of SWATH ships or semisubmersibles, the viscous effect is significant. In fact, the viscous forces are nonlinear and not readily amenable to computation, even in relatively simple configuration. Consequently, it has been found to be necessary to introduce equivalent, i.e.

$$\sum_{j=1}^{6} [- \omega_e^2 (M_{ij} + A_{ij}) - i\omega_e (B_{ij} + B_{vij}) + C_{ij}] \xi_j = F_i + F_{vi} \qquad i=1,2,...6 \tag{2.42}$$

where B_{vij} is an equivalent linear damping matrix and F_{vi} is viscous wave exciting forces. Both of them can be determined by empirical or semi-empirical method, which will be discussed in Chapter 4.

2.2 The Solution of the Boundary Value Problem and the Singularity Distribution Method

There are many techniques which may be considered for obtaining the solution of the boundary value problem formulated in previous sections for arbitrary 3D bodies. Quite comprehensive reviews in this field have been made by Shen[6], Mei[7] and Yeung[8]. In order to choose a suitable method for the present problem, it is necessary to have a brief view of several major techniques and their advantages and disadvantages.

One widely used method is finite element technique which has successfully used in structural analysis for many years, but only recently is introduced into hydrodynamic field. The finite element method is based on the variational principle. In order to solve the boundary value problem and determine the velocity potential, the whole fluid domain is described by a number of finite elements and the velocity potential within each element may be approximated by a set of polynomial trial functions which are ultimately chosen to satisfy the required boundary conditions. As reviewed by Yeung[8], this technique can be satisfactorily used to solve the problem where the fluid domain is restricted, for example, in canals, harbours, even for the interior flow problem like oil sloshing in the tank which is in a seaway. But it is faced with the difficulty of imposing an effective open boundary problem because of large number of elements required. There are some variations on this method to overcome this problem. The hybrid method described by Bai and Yeung[9] combines finite element idealization close to the body with an analytic solution away from the body where the boundaries are simple. The infinite element method of Bettess[10] divides the fluid domain into two parts, the finite elements are used in the inner region which is close to the

body and the infinite element in the outer region. The idea of the both methods is to reduce the number of elements required for the open boundary problem.

Alternatively, the boundary integral or singularity distribution method is another in which to make use of Green's identity to reduce the 3D potential flow problem to a 2D boundary surface problem. It generally involves distributing singularities (sources, dipoles or source-dipoles) over the body surface and using Green's theorem to obtain an integral equation for the strength of these surface singularities to satisfy the body boundary condition. The velocity potential associated with the singularity satisfies all the boundary conditions except the one on the body surface which is used to determine the strength of the singularities. Integral equations for the velocity potential can generally be derived from Green's identity in order to satisfy the body surface condition. So this approach needs to solve a Fredholm integral equation with a complicated kernel function. In order to avoid this problem a small departure from tradition was made by Yeung[9] which utilizes only the fundamental source function (1/R in 3D case). However, since the fundamental source function does not satisfy any of the required boundary conditions the sources must be distributed over the fluid boundaries,the strengths are chosen to meet these boundary conditions. Like the finite element method. this approach is particularly useful for the problems where the fluid domain is restricted or seabed is not flat. But for the problem with open water, this method not efficient.

In the current study, ships on the surface of infinite fluid is of primary interest, so the singularity distribution method in its basic form will be used.

There are at least three different way to formulate the Fredholm integral equations in the singularity distribution method:

1. source and dipole distribution by the second kind of integral equation,
2. source distribution by the second kind of integral equation, and
3. dipole distribution by the first kind of integral equation.

For the convenience of discussion, the three different distribution methods will

firstly be formulated for each case at zero forward speed, then they will be modified to take into account of forward speed.

2.2.1 Source-dipole distribution method

Apply Green's second identity to the exterior flow

$$\iint_{SF} [\, \phi(Q) \frac{\partial G(P,Q)}{\partial n_Q} - \frac{\partial \phi}{\partial n_Q} G(P,Q) \,] \, ds(Q)$$
$$= \iiint_{V} [\, \phi(Q) \nabla_Q^2 G(P,Q) - G(P,Q) \nabla_Q^2 \phi \,] \, dv \qquad (2.43)$$

where Green's function, G (P,Q), represents the potential at field point P(x,y,z) due to a source of strength 4π at point Q (ξ,η,ζ)

$$G(x,y,z;\xi,\eta,\zeta) = 1/R + G^*(x,y,z:\xi,\eta,\zeta) \qquad (2.44)$$

where

$$\nabla^2 G^*(x,y,z;\xi,\eta,\zeta) = 0 \qquad \text{in V}$$
$$R^2 = (x-\xi)^2 + (y-\eta)^2 + (z-\zeta)^2,$$

SF represents all the boundary surface, that is, body surface, surface at infinity, bottom surface and control surface around point P, V is the volume surrounded by SF, as shown in Fig.2.2. ϕ is the unknown velocity potential which also satisfies the Laplace equation $\nabla^2\phi = 0$, in volume V, but it should be noted that G is not a harmonic function at point $Q(\xi,\eta,\zeta)$, so

$$\nabla^2 G = \nabla^2 \left(\frac{1}{R}\right) = \lim_{\varepsilon \to \infty} \left(\frac{-2\varepsilon}{R(R+\varepsilon)^3}\right) = \begin{cases} 0 & R \neq 0 \\ \infty & R = 0 \end{cases} \qquad (2.45)$$

If a small sphere isolating the singularity for the case of P in V or a small hemisphere for the case of P on SF is used then G is harmonic outside this isolated region and the volume integral of $\phi\nabla^2 G$ gives, in limit as the radius of the sphere, r, approaches zero,

$$\iiint_V \phi \nabla^2 G \, dv = \lim_{\varepsilon \to 0} \phi(P) \int_0^{r_0} \left[\frac{-2\varepsilon}{R(R+\varepsilon)^3} 4\pi R^2 \right] dr$$

$$= \begin{cases} -4\pi \phi(P) & \text{for P in} \\ -2\pi \phi(P) & \text{for P on S} \\ 0 & \text{for P outside VUS} \end{cases} \qquad (2.46)$$

Substituting Eqn.(2.46) into Eqn.(2.44), the principle value integral yields the basic integral equation of the method

$$\iint_{SF} \left[\phi(Q) \frac{\partial G(P,Q)}{\partial n_Q} - \frac{\partial \phi}{\partial n_Q} G(P,Q) \right] ds(Q) = \begin{cases} -4\pi \phi(P) & \text{for p outside } SUS_0 \\ -2\pi \phi(P) & \text{for p on S} \\ 0 & \text{for p inside } SUS_0 \end{cases} \qquad (2.47)$$

for the case of the body floating on the free surface without forward speed, the surface integrals over free surface, the surface at infinity and bottom do not give any contribution. G and ϕ satisfy the same boundary condition on those surfaces, so putting those conditions into Eqn.(2.47), it can be found the integral terms cancel each other on those surfaces and the Eqn.(2.47) reduces to

$$\iint_{S} \left[\phi(Q) \frac{\partial G(P,Q)}{\partial n_Q} - \frac{\partial \phi}{\partial n_Q} G(P,Q) \right] ds(Q) = \begin{cases} -4\pi \phi(P) & \text{for P outside } SUS_0 \\ -2\pi \phi(P) & \text{for P on S} \\ 0 & \text{for P inside } SUS_0 \end{cases} \qquad (2.48)$$

where S_0 is the waterplane area of the floating body or zero for submerged body.

Let P on the body surface S and make use of body boundary condition, Eqn(2.14) and (2.15), the equation can be rewritten as

$$2\pi \phi(P) + \iint_S \phi(Q) \frac{\partial G(P,Q)}{\partial n_Q} ds(Q)$$

$$= \iint_S v_n(Q) \, G(P,Q) \, ds(Q) \qquad (2.49)$$

where v_n is the normal component of the velocity on the body surface and equal to $-i\omega_e n_i$ for i=1,2,...6 at zero forward speed or $-\partial\phi_0/\partial n$ for diffraction potential.

This is so called source-dipole distribution of second kind of integral equation.

It should be noted that the Eqn.(2.49) is only valid for a body without forward speed otherwise the integral over the free surface would not vanish.

This method has been discussed from a strict mathematical point of view by John[3] and is called Green's integral equation method (Mei[7]) or direct boundary integral equation method (Zienkiewicz et al [11]).

2.2.2 Source distribution method

In the Eqn.(2.48) the potential ϕ is only dealt with outside the volume V' which is enclosed by the body surface S and the waterplane area S_0. It is termed exterior problem and ϕ outside V' is of physically interest. For the convenience of the solution, a complementary interior problem can also be formulated similarly. Let $\phi'(P)$ be a solution of 3D Laplace equation for P' inside V' which is an artificial potential without any physical meaning. If ϕ' satisfies the free surface condition, a similar expression is obtained from Green's identity by keeping the same sign of **n**.

$$\iint_S [\, (\phi'(Q) \frac{\partial G(P',Q)}{\partial n_Q} - \frac{\partial \phi'}{\partial n_Q} G(P',Q) \,] \, ds(Q) = 0 \qquad \text{for P' outside } SUS_0 . \tag{2.50}$$

Subtracting Eqn.(2.50) from Eqn.(2.48) gives

$$\iint_S \left[[\, \phi(Q) - \phi'(Q) \,] \frac{\partial G(P,Q)}{\partial n} - G [\, \frac{\partial \phi}{\partial n} - \frac{\partial \phi'}{\partial n} \,] \right] ds(Q) = -4\pi \phi(P) \qquad \text{for P outside } SUS_0 . \tag{2.51}$$

If the definitions are made for

$$\psi = \phi - \phi' \tag{2.52}$$

$$\sigma = \frac{\partial \phi}{\partial n} - \frac{\partial \phi'}{\partial n} , \tag{2.53}$$

where ψ is termed the dipole strength and σ is termed the source strength. The velocity potential in Eqn.(2.51) is represented by source and dipole distribution over the body surface, but it involves the interior potential terms. This kind of integral equation is therefore not used as commonly as Eqn.(2.49) which is simpler and moves straight forward. The use of the artificial; interior potential is only for convenience of the solution by other kind of singularity distributions.

Furthermore, if the specification

$$\psi = \phi(Q) - \phi'(Q) = 0 \qquad \text{for Q on S} \qquad (2.54)$$

is made, then the potential can be represented by the source distribution with the density $\sigma(Q)$ on the surface S.

$$\iint_S \sigma(Q)\, G(P,Q)\, ds(Q) = 4\pi\, \phi\,(P) \qquad \text{for P outside SUS}_0 \qquad (2.55)$$

The unknown source density σ can be found by imposing the body boundary condition, Eqn.(2.14) and (2.15), and it gives

$$\frac{1}{2}\sigma(P) + \frac{1}{4\pi}\iint_S \sigma(Q)\frac{\partial G(P,Q)}{\partial n}\, ds(Q) = v_n \qquad \text{for P on S.} \qquad (2.56)$$

The first term of Eqn.(2.56) represents the contribution of local source strength to the normal velocity since $\partial G/\partial n$ becomes singular as P approaches to Q. This is the two dimensional Fredholm integral equation of second kind which can be solved by various methods.

This distribution is related to that of the mixed distribution, Eqn.(2.49), by a similarity transformation. It is the version used in most studies, such as Frank[12], Garrison and Rao[13], Faltinsen and Michelsen[14], Inglis and Price[15].

2.2.3 Dipole distribution method

If the specification is made in another way, i.e.

$$\sigma = \frac{\partial\phi(Q)}{\partial n} - \frac{\partial\phi'(Q)}{\partial n} = 0 \qquad \text{Q on SUS}_0 \qquad (2.57)$$

then the potential in Eqn.(2.51) is represented only by dipole distribution with the density ψ on the body surface S_0.

$$\iint_S \psi(Q) \frac{\partial G(P,Q)}{\partial n_Q} ds(Q) = -4\pi \phi(P) \quad \text{for P outside } SUS_0. \tag{2.58}$$

For the case $\phi_n = \phi'_n = n_3$, $\phi'(P) = Uz$, and so on for the case of other rigid body motions. Eatock Taylor has found ϕ' for the rectangular box. For an arbitrary ϕn this procedure breaks down since ϕ' is unknown, but from Eqn.(2.58), one can get

$$\iint_S \psi(P) \frac{\partial^2 G(P,Q)}{\partial n_P \partial n_Q} ds(Q) = -4\pi \frac{\partial \phi(P)}{\partial n_P} \quad P \text{ on } S. \tag{2.59}$$

This is a Fredholm equation of the first kind. Once ψ is found, ϕ follows from Eqn.(2.58) by quadrature. This method has been applied by Pien[16] and Chang and Pien[17] to submerged bodies. Compared with second kind of Fredholm equation (2.48) and (2.56), the first kind of Fredholm equation(2.59) is much less amenable to iterative solution, because its dominant is off the diagonal. Yeung[8] pointed out that for the cases that for which Eqn.(2.58) can be used, the dipole distribution method can be 50% more efficient than the other two distributions because it only needs the evaluation of $\partial G/\partial n$, not both G and $\partial G/\partial n$. If Eqn.(2.59) is used for the case of arbitrary ϕ_n, it results in second derivatives of Green's function, which compounds the already difficult task of evaluating a highly oscillatory Green's function.

2.2.4 Influence of forward speed

The fundamental integral equations of singularity distribution methods in previous Sections were derived for a body without forward speed. The zero speed free surface boundary condition, Eqn.(2.12), was used to simplify the integrals over the free surface. When a body moving forward in the free surface, the velocity potential must satisfy the free surface condition which is speed dependent, Eqn.(2.11). The basic equation of the method must therefore be modified to account for the influence of forward speed. Brard[18] has given a result, equivalent to Eqn.(2.49), for a body moving with forward speed in the free surface, i.e.

$$\iint_S \left(\psi \frac{\partial G}{\partial n} - G\sigma \right) ds - \frac{U^2}{g} \int_{C_0} \left(\psi \frac{\partial G}{\partial x} - G \frac{\partial \psi}{\partial x} \right) dy$$

$$= -4\pi \phi (P) \qquad \text{for P outside } SUS_0, \tag{2.60}$$

where ψ and σ are the strength of dipole and source respectively as defined by Eqn.(2.52) and (2.53), and contour C_0 is the intersection of the body surface and mean calm water surface.

Brard treated the term $\partial\psi/\partial x$ by letting a point on the contour C_0 with $\mathbf{t}$ to be a unit vector tangential to C_0 in the positive direction and $\tau = \mathbf{t} \times \mathbf{n}$, τ is tangential to the body surface S and normal to contour C_0. $\alpha_t = \cos(t,x)$, $\alpha_\tau = \cos(\tau,x)$ and $\alpha_n = \cos(n,x)$, so

$$\frac{\partial \psi}{\partial x} = \frac{\partial \psi}{\partial t} \alpha_t + \frac{\partial \psi}{\partial \tau} \alpha_\tau - \frac{\partial \psi}{\partial n} \alpha_n \,. \tag{2.61}$$

Noting $\alpha_n = n_1$, the Eqn.(2.60) becomes

$$\iint_S \left(\psi \frac{\partial G}{\partial n} - \sigma G \right) ds - \frac{U^2}{g} \int_{C_0} \left(\psi \frac{\partial G}{\partial x} - G t_x \frac{\partial \psi}{\partial t} - G \tau_x \frac{\partial \psi}{\partial \tau} + G n_x \sigma \right) dy$$

$$= -4\pi \phi(P) \qquad \text{for P outside } SUS_0 \,. \tag{2.62}$$

Here the potential is in general form and represented by source and dipole distribution. Eqn.(2.62) is the extension of Eqn.(2.49). If ψ or σ are set to be zero as in the zero speed case, Eqn.(2.62) reduces to source or dipole distribution.

In the usual approach, the solution is found to ship motion problem using only sources in order to have same kind of distribution both in the surface integral and line integral, i.e. by letting $\psi = 0$ on S, Eqn.(2.62) reduces to

$$\iint_S \sigma (Q)\, G (P,Q)\, ds + \frac{U^2}{g} \int_{C_0} \sigma (Q)\, G (P,Q)\, n_1\, dy = -4\pi \phi (P). \tag{2.63}$$

This kind of source distribution method with forward speed effect has been

examined by Chang[19], Inglis and Price[15]. Taking the normal directional derivative of ϕ in Eqn.(2.63) on the body surface S and applying the boundary condition, Eqn.(2.15), yields the following integral equation for σ.

$$-\frac{1}{2}\sigma(Q)+\frac{1}{4\pi}\left[\iint_S \sigma(Q)\frac{\partial G(P,Q)}{\partial n}ds(Q)+\frac{U^2}{g}\int_{C_0}\sigma(Q)\frac{\partial G(P,Q)}{\partial n}n_1 dy\right] = v_n \tag{2.64}$$

The first term of Eqn.(2.64) represents the contribution of local source density to the local normal velocity since $\partial G/\partial n$ becomes singular as P approaches Q.

The dipole distribution could used instead of, or as well as, a source distribution. However, if a source distribution is used the contribution from line integral is much smaller than if a dipole distribution were used, i.e. letting $\sigma=0$ in Eqn.(2.62). In view of the simplification that will be needed to evaluate the line integral, the source distribution method may be more accurate.

In deriving Eqn.(2.62) and (2.63), it has been assumed that a linear body surface boundary condition is valid. This assumption is suspect for a bluff body moving in free surface and so the method can no longer be applied to arbitrary bodies with forward speed. The body must be thin or flat for the method to give accurate results.

2.3 Irregular Frequency

2.3.1 Occurrence of irregular frequency

The integral equation methods by source, dipole or source-dipole distributions are all plagued by the presence of irregular frequencies when the body is surface piercing. This was first pointed out by John[3] in the context of source distribution method. John showed that the integral equation by source, Eqn.(2.56) can be approximated by a set of the simultaneous linear algebraic equations which can be solved by matrix inversion. However, the integral equation fails to produce solutions at certain frequencies associated with the resonance of interior flow. At these frequencies, called irregular frequencies or

eigenfrequencies, the determinant of the kernel matrix becomes singular. In practice, however, the matrix is never completely singular due to rounding errors in the numerical procedure and the solution is ill conditioned.

John pointed out that the irregular frequencies are the solutions of interior eigenvalue problem defined by the set of equations for source distribution at zero forward speed.

$$\begin{cases} \nabla^2 \phi' = 0 & \text{in } V' \\ -\omega^2 \phi' + g \dfrac{\partial \phi'}{\partial z} = 0 & \text{on } S_0 \\ \phi' = 0 & \text{on } S \end{cases} \qquad (2.65)$$

where the interior velocity potential ϕ' defined in the region V' inside the body with a surface S and waterplane S_0. as shown in Fig.2.2.

The solution of such equations, however, is only available for some simple geometries, such as boxes, circular or triangular cylinders. The solution for a box was given by Eatock Taylor[20] as follows

$$\phi' = \sin\left[p\pi \left(\frac{x}{L} - \frac{1}{2} \right) \right] \sin\left[m\pi \left(\frac{y}{B} - \frac{1}{2} \right) \right] \sin\left[\gamma (z + T) \right]$$

for $-L/2 \le x \le L/2$, $-B/2 \le y \le B/2$ and $-T \le z \le 0$, where L, B, T are length, beam, and draught of the box respectively.

The irregular frequencies occur at

$$\omega_{pm} = \left[g \gamma \coth \gamma T \right]^{\frac{1}{2}} \qquad (2.66)$$

with

$$\gamma = \left[\left(\frac{p\pi}{L} \right)^2 + \left(\frac{m\pi}{B} \right)^2 \right]^{\frac{1}{2}} \qquad p, m = 1,2,\ldots .$$

For an arbitrary 3D body, there are no exact solution available, but a semi-empirical formula given by Wu and Price[21] may be used to predict irregular frequencies. This

formula make use of equivalent box approximation for the prediction.

$$\omega_{pm} = \left[g\,\gamma \coth \gamma T_e \right]^{\frac{1}{2}} \tag{2.67}$$

with

$$\gamma = \left[\left(\frac{p\pi}{L_e}\right)^2 + \left(\frac{m\pi}{B_e}\right)^2 \right]^{\frac{1}{2}} \qquad p,\ m = 1,2,...,$$

where

$$L_e = \beta_1 (\beta_0)^{\alpha_1} L, \quad B_e = \beta_2 (\beta_0)^{\alpha_2} B, \quad T_e = \frac{V}{L_e B_e}$$

are equivalent length, beam and draught of the body respectively with

$$\alpha_1 = \frac{L^2}{L^2 + B^2}, \qquad \alpha_2 = \frac{B^2}{L^2 + B^2}$$

$$\beta_0 = (C_W)^{C_0}, \quad \beta_1 = (C_C)^{C_1}, \quad \beta_2 = (C_m)^{C_2},$$

where V is the displacement, $C_W = A_W/LB$, $C_m = A_m/BT$ and $C_c = A_c/LT$ are waterplane, midsection and central longitudinal section coefficients with A_W, A_m and A_c the relevant plane area. The correction coefficients are expressed as

$$C_0 = \frac{2}{3}, \quad C_1 = \left[1 + 6\left|\frac{L-B}{L+B}\right| \ln(p) \right] / 8, \quad C_2 = \left[1 + 6\left|\frac{L-B}{L+B}\right| \ln(m) \right] / 8.$$

In their limiting case, the Eqn.(2.67) reduces to the Eqn.(2.66) for the solutions of a box, otherwise it approximates solutions.

It can be considered that the integral equation by source-dipole distribution, Eqn.(2.49) derived directly from Green's identity is more general in the sense of that no assumption about the interior flow has been made. However, Mei[7] and Shin[22] have proven that this alternative form of integral equation also has the same difficulty at those irregular frequencies of the interior Dirichlet problem. Both source, Eqn(2.56), and source-dipole, Eqn.(2.49), distributions have the same irregular frequencies since the kernel of one integral equation is transferable from the other. Furthermore, a subtle distinction

between the two integral equations is that the inhomogeneous term of the source-dipole distribution equation is orthogonal to the interior eigensolution at these frequencies, whereas that of the source distribution equation is generally not. Delves and Walsh[23] have shown that the source-dipole distribution method actually has a solution, though not unique, whereas source distribution method has none. Neither situation is entirely desirable.

For the dipole distribution method, the reason for the irregular frequencies is the same as the source method, but the irregular frequencies in the dipole distribution don't generally coincide with those of the source distribution as discussed by Chertock[24].

2.3.2 Avoiding of irregular frequency

Several ways devoted to prevent the occurrence of irregular frequencies can be found from the literature by Ursell[25][26], Faltinsen[27], Ohmatsu[28], Soding[29], Soding and Lee[30], Ogilvie and Shin[31], Mei[7], and Sclavounos and Lee[32]. The Sclavounos and Lee method is suitable for 3D ship motion problem with zero speed and appears to give reasonable good results. Their theory originally comes from the method of Burton and Miller[33] in an acoustic problem. It depends on the fact that irregular frequencies for the second kind integral equation by source-dipole distribution do not coincide with those of the first kind one by dipole distribution. Actually their formulation is a linear combination of those two distributions, but it involves the second order derivative of Green's function.

In the results presented in the thesis, no attempt has been made to avoid irregular frequencies since for ship shaped bodies they are often a high frequency phenomenon, the most of interesting frequency range is under the first irregular frequency. Even when the irregular frequency occurs, its influence only appears within a very narrow bandwidth at each irregular frequency. It is easy for them to be distinguished and removed. If however the method is extended to calculate the hydrodynamic properties associated with flexible bodies in which the higher frequency range is needed then some avoidance procedure would be necessary.

2.4 Use of source distribution method

To decide which method will be used in the present study, the comparison among the methods discussed above will be concluded first.

1, The source and source-dipole distribution methods involves the same amount of computational effort (G and $\partial G/\partial n$), since ϕ, being proportional to the pressure, is the desired quantity. Actually, the source-dipole distribution method has a slight advantage over the source one because it can solve for ϕ directly. The dipole distribution method may be more efficient (only $\partial G/\partial n$ needed) than the other two if ϕ' is known, but for arbitrary ϕ' it needs the second derivatives of Green's function which may eliminate its advantage.

2, Both the source and source-dipole distribution methods give the Fredholm integral equation of second kind which is diagonally dominant in the matrix equation and much more amenable to iterative solutions than the dipole one with the Fredholm integral equation of the first kind, which is dominant off the diagonal of the matrix equation.

3, All three distributions are subject to irregular frequencies.

4, For the non-zero speed case, the source distribution has the same form of distribution in the surface and contour integral, so it is simpler and more straightforward than the other two.

Considering the above distribution methods, the source distribution method is the one which has more advantages at present especially for the forward speed case and also considerable numerical experience has been accumulated in the past. Therefore, it is used in the present study.

The other two distributions may have their advantages in other cases. As mentioned earlier, the dipole distribution with first kind of integral equation may be more efficient than the other two if ϕ' can be found. The linear combination of the second kind of integral equation from the source-dipole distribution with the first kind of integral equation from the dipole

distribution can eliminate the irregular frequencies. But these are not part of this study.

2.5 Solution by Source Distribution Method

2.5.1 Green's functions

The Green's function,or source potential, is fundamental to the singularity methods. A collection of appropriate formula for this function can be found in the well known paper by Wehausen and Laitone[5] in various cases involving a ideal fluid, a linearized free surface, and a fluid domain which is otherwise unbounded except by a fixed horizontal bottom at a finite depth beneath the free surface. If attention is restricted to the conventional point source beneath a free surface, a summary can be made in various time dependence including:

1, oscillatory motion,

2, steady translation,

3, combined oscillatory motion with steady translation, and

4, transient motion with source strength described by a step or delta function.

Each of them has four different conditions, that is, two and three dimensions, finite and infinite depth. From this list alone there are 16 cases.

Nor will the list above satisfy every need. For example, in numerical techniques where the free surface Green's function is employed on a matching boundary, maximum efficiency is achieved by choosing a special Green's function which satisfies an appropriate boundary condition on that boundary. In the present study, the problem of a body moving in regular waves, the interesting cases are 1 and 2. Table 2.1 gives the general formula of Green's functions for 3D. Actually, in the limiting case (3) reduces to case (1) by the forward speed approaching zero and case (2) approaches (1) if the oscillating frequency approaches to zero. On the other hand, if the oscillating frequency in case (1) approaches zero or infinity it gives the two different Green's functions for rigid wall free surface condition which are shown in Table 2.1 as well. The point source in case (1) is called a pulsating source and in case (3) is called a translating and pulsating source.

Table 2.1 Green's Functions

Name	Free Surface Condition	Sea Bed Condition	Function
Tanslating and Pulsating Source	$(i\omega_e + U\frac{\partial}{\partial x})^2\phi + g\frac{\partial}{\partial z}\phi = 0$	Infinite Depth $\frac{\partial}{\partial z}\phi = 0$ on $z = -\infty$	$G = \frac{1}{R} + \frac{1}{R'} + \frac{2g}{\pi}\int_0^{\gamma} d\theta \int_0^{\infty} dm\, F(\theta, m) + \frac{2g}{\pi}\int_{\gamma}^{\frac{\pi}{2}} d\theta \int_{L_2} dm\, F(\theta, m) + \int_{\frac{\pi}{2}}^{\pi} d\theta \int_{L_1} dm\, F(\theta, m)$ where $\tau = \omega U/g < 0.25 \quad \gamma = 0$; $\tau \geq 0.25 \quad \gamma = \cos^{-1}[1/(4\tau)]$ $F(\theta, m) = \frac{m \exp\left[m[z + \zeta - i(x - \xi)\cos\theta]\right]\cos\left[m(y - \eta)\sin\theta\right]}{gm - (\omega_e - mU\cos\theta)}$
Pulsating Source	$-\omega_e^2\phi + g\frac{\partial\phi}{\partial z} = 0$	Infinite Depth $\frac{\partial}{\partial z}\phi = 0$ on $z = -\infty$	$G = \frac{1}{R} + \frac{1}{R'} + 2k\int_0^{\infty} d\upsilon \frac{e^{\upsilon Y}}{\upsilon - 1} J_0(\upsilon X) + i\,2k\, e^{k(z+\zeta)} J_0(X)$ Where $X = k\left[(x - \xi)^2 + (y - \eta)^2\right]^{\frac{1}{2}}$ $Y = k(z - \zeta)$
Pulsating Source	$-\omega_e^2\phi + g\frac{\partial\phi}{\partial z} = 0$	Finite Depth $\frac{\partial}{\partial z}\phi = 0$ on $z = -d$	$G = \frac{1}{R} + \frac{1}{R'} + 2\int_0^{\infty} \frac{(\upsilon + k)e^{-\upsilon d}\cosh\upsilon(\zeta + d)\cosh\upsilon(z + d)J_0(\upsilon r)\,d\upsilon}{\upsilon\sinh\upsilon d - k\cosh\upsilon d} + i\frac{2\pi(\mu^2 - k^2)\cosh\mu(\zeta + d)\cosh\mu(z + d)}{\mu^2 d - k^2 d + k} J_0(\mu r)$ where $\mu\tanh(\mu d) = k$ $r = \left[(x - \xi)^2 + (y - \eta)^2\right]^{\frac{1}{2}}$
Rigid Wall Free Surface	$\frac{\partial\phi}{\partial z} = 0$ i.e. $\omega_e = 0$	Infinite Depth	$G = \frac{1}{R} + \frac{1}{R'}$
Rigid Wall Free Surface	$\phi = 0$ i.e. $\omega_e = \infty$	Infinite Depth	$G = \frac{1}{R} - \frac{1}{R'}$

2.5.2 Solution by translating and pulsating source

When the body is moving in regular waves, the source potential should satisfy the speed dependent free surface condition, Eqn.(2.11), which can be rewritten as

$$U^2 \frac{\partial^2 \phi}{\partial x^2} + 2\, i\, \omega_e \frac{\partial \phi}{\partial x} - \omega_e^2\, \phi + g \frac{\partial \phi}{\partial z} = 0 . \qquad (2.68)$$

Such a source potential is obtained by a translating and pulsating source which includes the combined effects from oscillatory motion and steady translation. Its form is listed in Table 2.1. By means of the translating and pulsating source and the body boundary condition Eqn.(2.13)-(2.15), the source distribution integral equation (2.64) can be solved directly for the velocity potential ϕ. Consequently, all other results, such as forces and motion responses of the ship, can be obtained.

This approach has been used by Chang[19], Inglis and Price[15]. Good agreement with experimental results has been achieved, but a translating and pulsating source requires a considerable amount of computational effort, which restricts its use, since the efficient way to evaluate its Green's function involves a double integral has faced a difficult task. There are several ways to evaluate such a double integral. Inglis[34] divided the integral into two parts with respect to $\tau>0.25$ or $\tau\leq 0.25$. For the case of $\tau<0.25$, the integral can be reduced to the single integral, but when $\tau\geq 0.25$, the double integral is still necessary. Unfortunally, the case of $\tau\geq 0.25$ is of practical interest. Guevel and Bougis[35], Wu and Eatock Taylor[36] introduced two alternative forms of this Green's function which only contain a single integral involving an exponential function. Their approaches have a better numerical performance than the form given by Inglis and Price, but is still very expensive since the complex exponential function must be evaluated by a series expansion or an asymptotic expansion at every step of the numerical integral. In order to reduce the computing cost, an alternative method was suggested by Salvesen, Tuck and Faltinsen, refered to as the simplified approach by a pulsating source.

2.5.3 Solution by pulsating source

To simplify the problem and use the pulsating source, some assumptions must be made: - that the ship hull is thin or flat, that the forward speed is low and the oscillatory frequency is high, thus the boundary conditions of the problem become

$$\frac{\partial}{\partial n}\phi_i = -i\omega_e n_i + Um_i \qquad \text{on S} \qquad (2.69)$$

with

$$m_i = 0 \qquad i=1,2,3,4$$

$$m_5 = n_3, \quad m_6 = -n_2$$

and

$$\frac{\partial}{\partial n}(\phi_0 + \phi_D) = 0 \qquad \text{on S.} \qquad (2.70)$$

The forward speed free surface condition Eqn.(2.68) reduces to

$$-\omega_e^2 \phi + g\frac{\partial \phi}{\partial z} = 0 \qquad \text{on z=0} \qquad (2.71)$$

This is equivalent to the zero speed free surface boundary condition Eqn.(2.12) with the wave frequency ω replaced by encounter frequency ω_e , so the pulsating source is valid.

Under the above assumptions, It has been suggested that the contour integral can be neglected since its effect is small. The only speed dependent boundary condition is now Eqn.(2.69). Substituting Eqn.(2.69) into integral equation (2.64), Salvesen et al.[2] showed that the speed dependent velocity potential can be expressed in terms of the correspondent zero speed velocity potential. Thus

$$\phi_i = \phi_i^0 \qquad i = 1,2,3,4$$

$$\begin{Bmatrix} \phi_5 \\ \phi_6 \end{Bmatrix} = \begin{Bmatrix} \phi_5^0 \\ \phi_6^0 \end{Bmatrix} \pm \frac{U}{i\omega_e}\begin{Bmatrix} \phi_3^0 \\ \phi_2^0 \end{Bmatrix}, \qquad (2.72)$$

where ϕ_i^0, i=1,2,...6, denotes the correspondent zero speed velocity potential. Introducing Eqn.(2.72) to Eqn(2.33) gives the speed dependent added mass and damping coefficients expressed in terms of the correspondent zero speed coefficients. These formula are listed in Table 2.2.

In present study the pulsating source is used. Although the translating and pulsating

Table 2.2 Speed Dependent Hydrodynamic Coefficients

$A_{11} = A_{11}^0$ $\quad B_{11} = B_{11}^0$

$A_{33} = A_{33}^0$ $\quad B_{33} = B_{33}^0$

$A_{55} = A_{55}^0 + \frac{U^2}{\omega_e^2} A_{33}^0$ $\quad B_{55} = B_{55}^0 + \frac{U^2}{\omega_e^2} B_{33}^0$

$A_{15} = A_{15}^0 - \frac{U}{\omega_e^2} B_{13}^0$ $\quad B_{15} = B_{15}^0 + U A_{13}^0$

$A_{51} = A_{51}^0 + \frac{U}{\omega_e^2} A_{13}^0$ $\quad B_{51} = B_{51}^0 - U A_{13}^0$

$A_{13} = A_{13}^0$ $\quad B_{13} = B_{13}^0$

$A_{13} = A_{13}^0$ $\quad B_{13} = B_{13}^0$

$A_{53} = A_{53}^0 + \frac{U}{\omega_e^2} B_{33}^0$ $\quad B_{53} = B_{53}^0 - U A_{33}^0$

$A_{35} = A_{35}^0 \quad \frac{U}{\omega_e^2} B_{13}^0$ $\quad B_{35} = B_{35}^0 + U A_{33}^0$

$A_{22} = A_{22}^0$ $\quad B_{22} = B_{22}^0$

$A_{44} = A_{44}^0$ $\quad B_{44} = B_{44}^0$

$A_{66} = A_{66}^0 + \frac{U^2}{\omega_e^2} A_{22}^0$ $\quad B_{66} = B_{66}^0 + \frac{U^2}{\omega_e^2} B_{22}^0$

$A_{24} = A_{24}^0$ $\quad B_{24} = B_{24}^0$

$A_{24} = A_{24}^0$ $\quad B_{24} = B_{24}^0$

$A_{26} = A_{26}^0 + \frac{U}{\omega_e^2} B_{22}^0$ $\quad B_{26} = B_{26}^0 - U A_{22}^0$

$A_{62} = A_{62}^0 - \frac{U}{\omega_e^2} B_{22}^0$ $\quad B_{62} = B_{62}^0 + U A_{22}^0$

$A_{46} = A_{46}^0 + \frac{U}{\omega_e^2} B_{24}^0$ $\quad B_{46} = B_{46}^0 - U A_{24}^0$

$A_{64} = A_{64}^0 - \frac{U}{\omega_e^2} B_{24}^0$ $\quad B_{64} = B_{64}^0 + U A_{24}^0$

source gives a better description of the problem, it required a considerable amount of computational effort (an order higher than the pulsating source) which restricts its use. With the computer facility in the University when the program was developed, i.e. ICL 2988, the translating and pulsating source was impossible to use because of the huge CPU time required for this method. The pulsating source is computationally much cheaper. A considerable amount of successful numerical solutions has been achieved by previous investigators and reasonable agreement they achieved with experimental results was encouraging. Finally, the greater part of the program based on the pulsating source method is compatible with the translating and pulsating source method. As long as the translating and pulsating source can be evaluated efficiently or a new more powerful computer becomes available, replacing the pulsating source with a translating and pulsating source would upgrade the program immediately. For this reason, the contour integral in Eqn.(2.64) is kept in the program, although its effect is small with the pulsating source method, since it may not be negligible when the translating and pulsating source is used.

CHAPTER THREE

NUMERICAL PROCEDURE

As described in Chapter 2, several singularity distribution methods have been studied and some of them have been developed into powerful tools for engineering applications in predicting motion responses and wave loads for ships or offshore structures in seaway. Until recently, the 2D strip theory is still the most universally used technique in practical applications. The restriction on the use of 3D theory is the large computing time and memory space required for it. Improving the numerical efficiency of 3D theory is important for practical purposes. In this chapter, a modified numerical procedure is introduced based on the traditional procedure employed by most previous authors, such as Garrison and Michelsen[1], Shin[2] and Inglis[3] etc. The modified procedure makes use of the symmetric property of Green's function and its derivatives. The comparison with the traditional numerical procedure has been made. The results show that considerable computing time saving can be achieved.

3.1 Approximation by Matrix Equations

In order to be able to implement the source distribution method described in Chapter 2, it is necessary to adopt a technique pioneered by Hess and Smith[4]. The body surface is replaced by large number of small panels, so the method is also called 'panel method', of area ΔS_i (i=1,2,...N), where N is the number of the panels. The continuous formulation of the solution indicates that Eqn.(2.63) and (2.64) are to be satisfied at all points(P) on the immersed surface S, but in order to obtain a discretized numerical solution it is necessary to relax this requirement and apply the condition at only N control points. The location of these control point may, in principle, be chosen arbitrarily, but for convenience the N points at the panel centroids are used. Thus, in the discretization process Eqn.(2.64) is replaced by the N equations

$$-\frac{1}{2}\sigma_i + \frac{1}{4\pi}\left[\iint_S \sigma(Q)\frac{\partial G(P,Q)}{\partial n}\,ds(Q) + \frac{U^2}{g}\int_{C_0} \sigma(Q)\frac{\partial G(P,Q)}{\partial n}\,n_1\,dy \right]$$

$$= v_{ni} \qquad (3.1)$$

Furthermore, the surface integral in Eqn.(3.1) may be written as the sum of the integral over the N panels of area ΔS_i, and as an approximation, the source strength function $\sigma(Q)$ may be taken as constant over each panel,so that Eqn.(3.1) becomes

$$\sum_{j=1}^{N} q_j \iint_{\Delta S_j} \frac{\partial G_j}{\partial n}\,ds + \frac{U^2}{g}\sum_{j=1}^{M} q_j \int_{\Delta C_j} \left(\frac{\partial G_j}{\partial n}\,n_1\right) dy \qquad (3.2)$$

$$= v_{ni} \qquad \text{for } i = 1,2,...N$$

where

$$q_j = \frac{1}{4\pi}\sigma(x_j, y_j, z_j) \qquad \text{for } j = 1,2,...N$$

is the source density on the jth panel to be determined,which has its centroid at (x_j, y_j, z_j) and v_{ni} is the component of the body velocity normal to the body surface at (x_i, y_i, z_i). When i=j, the first term of Eqn.(3.2) becomes singular and gives the contribution of $(1/2)\sigma_i$ which is the first term of Eqn.(3.1). Here the panels numbered 1 to M are distributed along the mean waterline and the jth panel on the waterline has a horizontal length of ΔC_j along its upper side which coincides with the mean waterline. The term $(\partial G_j/\partial n)n_1$ should be integrated along the intersection ΔC_j, but for simplicity, this integration can be achieved by evaluating $(\partial G_j/\partial n)n_1$ at the centroid of the jth panel and multiplying by the y component, δ_j, of ΔC_j passing through the centroid. Thus, Eqn.(3.2) becomes

$$\sum_{j=1}^{M} q_j \left(I_{ij} + \frac{U^2}{g} J_{ij} \right) + \sum_{j=M+1}^{N} q_j I_{ij} = v_{ni} \quad \text{for } i = 1,2,...N. \qquad (3.3)$$

Here the 'complex influence coefficients I_{ij} and J_{ij} are defined as

$$I_{ij} = \iint_{\Delta S_j} \frac{\partial}{\partial n} G(x_i, y_i, z_i; \xi_j, \eta_j, \zeta_j)\, ds$$

$$J_{ij} = n_{1j}\, \delta_j \frac{\partial}{\partial n} G(x_i, y_i, z_i; \xi_j, \eta_j, \zeta_j)\, ds \qquad (3.4)$$

and (n_{1j}, n_{2j}, n_{3j}) are direction cosine of the unit normal vector **n** on jth panel about x, y, and z axes respectively.

The Eqn.(3.3) represents a set of N simultaneous equations for N unknown source densities q_i (i=1,2,...N) and may be expressed in the matrix form

$$\mathbf{axq} = \mathbf{v}_n, \qquad (3.5)$$

where **a** is a N x N matrix of influence coefficients, **q** and $\mathbf{v}_n$ are column matrices of order N. The element of matrix **a** is

$$a_{ij} = I_{ij} + \frac{U^2}{g} J_{ij} \qquad \text{for } j = 1,2,...M$$

$$a_{ij} = I_{ij} \qquad \text{for } j = M+1,...N \qquad (3.6)$$

The Eqn.(3.5) can be solved for **q** by using any standard matrix inversion or iterative techniques. The Crout's factorisation method[5] (iterative method) was found to be convenient and is available as a NAG routine[6]. In order to make the solution more efficient for present use, a small modification has been made in the use of the NAG routine.

Having found the unknown source density, the potential at any point in the fluid (x_i, y_i, z_i), not necessary on the body surface, can be found by discretized form of Eqn.(2.63)

$$\phi(x_i, y_i, z_i) = \sum_{j=1}^{N} q_j \iint_{\Delta S_j} G_j\, ds + \frac{U^2}{g} \sum_{j=1}^{M} q_j \int_{\Delta C_j} (n_1 G_j)\, dy$$

$$i = 1,2,...N \qquad (3.7)$$

or

$$\phi_i = \sum_{j=1}^{M} q_j \left(I'_{ij} + \frac{U^2}{g} J'_{ij} \right) + \frac{U^2}{g} \sum_{j=M+1}^{N} q_j I'_{ij}$$

$$1 = 1,2,...N \qquad (3.8)$$

with

$$I'_{ij} = \iint_{\Delta S_j} G(x_i, y_i, z_i; \xi_j, \eta_j, \zeta_j)\, ds$$

$$J'_{ij} = n_{1j}\, \delta_j\, G(x_i, y_i, z_i; \xi_j, \eta_j, \zeta_j) \,. \qquad (3.9)$$

The above equation can be expressed in matrix form as

$$\phi = \mathbf{b} \cdot \mathbf{q} \,, \qquad (3.10)$$

where **b** is also N x N matrix, ϕ is column of order N representing N unknown potentials on N panels. The element of matrix **b** is

$$b_{ij} = \left(I'_{ij} + \frac{U^2}{g} J'_{ij} \right) \qquad \text{for } j = 1,2,...M$$

$$b_{ij} = I'_{ij} \qquad \text{for } j = M+1,...N \qquad (3.11)$$

3.2 Integration over one panel

Once the body surface has been approximated by a number of panels on which the source strength is constant, it is necessary to integrate the Green's function and its derivatives over each panel in order to evaluate the Eqn.(3.3) and (3.7). For the convenience of the discussion, the Green's function is written in the form of Eqn.(2.44) as

$$G(x, y, z; \xi, \eta, \zeta) = \frac{1}{R} + G^*(x, y, z; \xi, \eta, \zeta) \,. \qquad (3.12)$$

The first term here and its derivatives are not gradually varying when the field point (x_i, y_i, z_i) is near the panel over which the integration is to be carried out and are in fact, singular as $R \to 0$, i.e. when (x_i, y_i, z_i) is inside the panel. On the other hand, the second term and its derivatives are regular throughout the field domain except the case that $R \to 0$ at free

surface. In practice, this case can be avoided. So the first term is termed 'singular part' and the second term is termed 'regular part'. Because of the different nature of the two parts of the Green's function, their integral sill be treated in different ways and discussed as follows.

3.2.1 Integration for the singular part of Green's function over a panel

3.2.1.1 Integration of contribution due to (1/R)

Due to the singular nature of the source, 1/R, the integration of it over each panel must be carried out properly when the field point (x_i,y_i,z_i) is near the panel. For the integral

$$\iint_{\Delta S} \frac{1}{R}\, ds,$$

there are two numerical procedures given by Faltinsen and Michelsen[1]. Hogben and Standing[7] have been used by many previous investigators which are briefly reviewed here.

Following a procedure similar to Hess and Smith[4] for the velocity components, Faltinsen and Michelsen integrated above integral by means of local co-ordinates $\bar{x}$, $\bar{y}$, $\bar{z}$, and $\bar{\xi}$, $\bar{\eta}$,where the $\bar{x}$, $\bar{\xi}$ and $\bar{y}$, $\bar{\eta}$ axes lie in the plane of the panel as indicated in Fig.3.1. They gave the results of the integral as

$$\iint_{\Delta S} \frac{1}{R}\, ds = -\sum_{i=1}^{4} \int_{\bar{\xi}_i}^{\bar{\xi}_{i+1}} \ln \left[\bar{y} - \bar{\eta}_{1,i+1} + \left|(\bar{y} - \bar{\eta}_{i,i+1})^2 + (\bar{x} - \bar{\xi})^2\right|^{\frac{1}{2}} \right] d\bar{\xi} \qquad (3.13)$$

where

$$\bar{\eta}_{1,\,i+1} = \bar{\eta}_i + \frac{\bar{\eta}_{i+1} - \bar{\eta}_i}{\bar{\xi}_{i+1} - \bar{\xi}_i} (\bar{\xi} - \bar{\xi}_i)$$

$$\bar{\eta}_5 = \bar{\eta}_1, \qquad \bar{\xi}_5 = \bar{\xi}_1 .$$

This integral may be directly evaluated through numerical integral in most cases. However,

the integrand of Eqn.(3.13) is singular when $\bar{z}=0$, $\bar{\xi}=\bar{x}$, $\bar{y}-\bar{\eta}_{i,i+1}<0$. In this case, the integration may be replaced by

$$\int_{\bar{\xi}_i}^{\bar{\xi}_{i+1}} \ln\left[(\bar{x}-\bar{\xi})^2+\bar{z}^2\right] d\bar{\xi} - \int_{\bar{\xi}_i}^{\bar{\xi}_{i+1}} \ln\left[-(\bar{y}-\bar{\eta}_{i,i+1}) + \left[(\bar{y}-\bar{\eta}_{i,i+1})^2+(\bar{x}-\bar{\xi})^2+\bar{z}^2\right]^{\frac{1}{2}}\right] d\bar{\xi}. \tag{3.14}$$

The first integral in this expression can be integrated analytically and the second term can be integrated numerically since it contains no singularities.

Hogben and Standing treated the integration in the different way. They used the approximation of a point source, i.e.

$$\iint_{\Delta S} \frac{1}{R}\, ds = \frac{1}{R}\Delta S, \tag{3.15}$$

to evaluate the integration except the case where the field point (x_i,y_i,z_i) lies at the panel, i.e. i=j in Eqn.(3.8). It has been shown that if the field point (x_i, y_i, z_i) is right at the centroid of the quadrilateral panel, i.e. R=0, the integration becomes

$$\iint_{\Delta S} \frac{1}{R}\, ds = 2\gamma\sqrt{\pi\,\Delta S} \tag{3.16}$$

with

$$\gamma = \frac{1}{\sqrt{\pi\, b}}\left[\ln\left(b+\sqrt{1+b^2}\right) + b\ln\left(\frac{1+\sqrt{1+b^2}}{b}\right)\right],$$

where b is the aspect ratio of the quadrilateral panel.

Generally, the method of Faltinsen and Michelsen gives better approximation but needs more computing time and storage space. Both approaches have been tried in this study. From the results in Fig.3.3 it can be seen that the method of Hogben and Standing gives adequate results for the panels which are almost square, this is the case in the study of the

offshore structures which usually are well rounded or rectangular bodies. However, when analyzing bodies with a thin structure, such as the struts of SWATH ships or even the skeg area of the conventional ships, Faltinsen and Michelsen's method is preferable. This is because the sides of the bodies may be close together and a point source approximation leads to serious error. The procedure adopted in this study is to use different formula for the different cases and the strategy is described as follows:

1, when $R \leq R_c$, the exact formulation, Eqn.(3.13), is adopted, where R_c is criterion distance,

2, when $R > R_c$, the point source approximation,Eqn.(3.15),

3, when $R = 0$, The Eqn.(3.16) is used, and

4, $R_c = 3\sqrt{(\Delta S)}$.

The setting of the R_c can be justified by the results in Fig.3.2.

3.2.1.2 Integration of contribution due to $\frac{\partial}{\partial n}(\frac{1}{R})$

The integration of the contribution due to $\frac{\partial}{\partial n}(\frac{1}{R})$ can be written as

$$\iint_{\Delta S} \frac{\partial}{\partial n}\left(\frac{1}{R}\right) ds = \iint_{\Delta S} \left(n_1\frac{\partial}{\partial x} + n_2\frac{\partial}{\partial y} + n_3\frac{\partial}{\partial z} \right)\left(\frac{1}{R}\right) ds \qquad (3.17)$$

where

$$\iint_{\Delta S} \frac{\partial}{\partial x}\left(\frac{1}{R}\right) ds = \iint_{\Delta S} -\frac{(x_i - \xi)}{R^3} ds$$

$$\iint_{\Delta S} \frac{\partial}{\partial y}\left(\frac{1}{R}\right) ds = \iint_{\Delta S} -\frac{(y_i - \eta)}{R^3} ds$$

$$\iint_{\Delta S} \frac{\partial}{\partial z}\left(\frac{1}{R}\right) ds = \iint_{\Delta S} -\frac{(z_i - \zeta)}{R^3} ds$$

Table 3.1 Integration for the Derivatives of Singular Part of Green's Function over a Quadrilateral Panel

Exact Integral Formulae

$$\iint_{\Delta S} \frac{\partial}{\partial \bar{x}}\left(\frac{1}{R}\right) d\bar{\xi}\, d\bar{\eta} = \frac{\bar{\eta}_2 - \bar{\eta}_1}{d_{12}} \ln \frac{r_1 + r_2 - d_{12}}{r_1 + r_2 + d_{12}} + \frac{\bar{\eta}_3 - \bar{\eta}_2}{d_{23}} \ln \frac{r_2 + r_3 - d_{23}}{r_2 + r_3 + d_{23}}$$
$$+ \frac{\bar{\eta}_4 - \bar{\eta}_3}{d_{34}} \ln \frac{r_3 + r_4 - d_{34}}{r_3 + r_4 + d_{34}} + \frac{\bar{\eta}_1 - \bar{\eta}_4}{d_{41}} \ln \frac{r_4 + r_1 - d_{41}}{r_4 + r_1 + d_{41}}$$

$$\iint_{\Delta S} \frac{\partial}{\partial \bar{y}}\left(\frac{1}{R}\right) d\bar{\xi}\, d\bar{\eta} = \frac{\bar{\xi}_2 - \bar{\xi}_1}{d_{12}} \ln \frac{r_1 + r_2 + d_{12}}{r_1 + r_2 - d_{12}} + \frac{\bar{\xi}_3 - \bar{\xi}_2}{d_{23}} \ln \frac{r_2 + r_3 + d_{23}}{r_2 + r_3 - d_{23}}$$
$$+ \frac{\bar{\xi}_4 - \bar{\xi}_3}{d_{34}} \ln \frac{r_3 + r_4 + d_{34}}{r_3 + r_4 - d_{34}} + \frac{\bar{\xi}_1 - \bar{\xi}_4}{d_{41}} \ln \frac{r_4 + r_1 + d_{41}}{r_4 + r_1 - d_{41}}$$

$$\iint_{\Delta S} \frac{\partial}{\partial \bar{z}}\left(\frac{1}{R}\right) d\bar{\xi}\, d\bar{\eta} = \tan^{-1} \frac{m_{12} e_1 - h_1}{\bar{z}\, r_1} - \tan^{-1} \frac{m_{12} e_2 - h_2}{\bar{z}\, r_2} + \tan^{-1} \frac{m_{23} e_2 - h_2}{\bar{z}\, r_2} - \tan^{-1} \frac{m_{23} e_3 - h_3}{\bar{z}\, r_3}$$

$$+ \tan^{-1} \frac{m_{34} e_3 - h_3}{\bar{z}\, r_3} - \tan^{-1} \frac{m_{34} e_4 - h_4}{\bar{z}\, r_4} + \tan^{-1} \frac{m_{41} e_2 - h_4}{\bar{z}\, r_4} - \tan^{-1} \frac{m_{41} e_1 - h_1}{\bar{z}\, r_1}$$

where $d_{12}^2 = (\bar{\xi}_2 - \bar{\xi}_1)^2 + (\bar{\eta}_2 - \bar{\eta}_1)^2$ $\quad d_{23}^2 = (\bar{\xi}_3 - \bar{\xi}_2)^2 + (\bar{\eta}_3 - \bar{\eta}_2)^2$

$d_{34}^2 = (\bar{\xi}_4 - \bar{\xi}_3)^2 + (\bar{\eta}_4 - \bar{\eta}_3)^2$ $\quad d_{41}^2 = (\bar{\xi}_1 - \bar{\xi}_4)^2 + (\bar{\eta}_1 - \bar{\eta}_4)^2$

$m_{12} = \dfrac{\bar{\eta}_2 - \bar{\eta}_1}{\bar{\xi}_2 - \bar{\xi}_1}$, $\quad m_{23} = \dfrac{\bar{\eta}_3 - \bar{\eta}_2}{\bar{\xi}_3 - \bar{\xi}_2}$, $\quad m_{34} = \dfrac{\bar{\eta}_4 - \bar{\eta}_3}{\bar{\xi}_4 - \bar{\xi}_3}$, $\quad m_{41} = \dfrac{\bar{\eta}_1 - \bar{\eta}_4}{\bar{\xi}_1 - \bar{\xi}_4}$

$r_k^2 = (\bar{x} - \bar{\xi}_k)^2 + (\bar{y} - \bar{\eta}_k)^2 + \bar{z}^2$ $\qquad k = 1, 2, 3, 4$

$e_k = \bar{z}^2 + (\bar{x} - \bar{\xi}_k)^2$ $\qquad h_k = (\bar{y} - \bar{\eta}_k)(\bar{x} - \bar{\xi}_k)$

Point Source Approximation Formulae

$$\iint_{\Delta S} \frac{\partial}{\partial x}\left(\frac{1}{R}\right) ds = \frac{-(x - \xi)}{\left[(x - \xi)^2 + (y - \eta)^2 + (z - \zeta)^2\right]^{\frac{3}{2}}}$$

$$\iint_{\Delta S} \frac{\partial}{\partial y}\left(\frac{1}{R}\right) ds = \frac{-(y - \eta)}{\left[(x - \xi)^2 + (y - \eta)^2 + (z - \zeta)^2\right]^{\frac{3}{2}}}$$

$$\iint_{\Delta S} \frac{\partial}{\partial z}\left(\frac{1}{R}\right) ds = \frac{-(z - \zeta)}{\left[(x - \xi)^2 + (y - \eta)^2 + (z - \zeta)^2\right]^{\frac{3}{2}}}$$

Note: $\bar{x}, \bar{y}, \bar{z}$ are field points in local co-ordinate system

$\bar{\xi}_i, \bar{\eta}_i$, $i = 1,2,3,4$ are co-ordinates of the four corners of a quadrilateral in local co-ordinate system (see Fig. 3.1)

The exact formula of this integral is well known and derived by Hess and Smith[4] in terms of local co-ordinate system. Therefore it is not discussed here. The final formula are given in Table 3.1. The strategy of the integration is the same as that for (1/R) integral and also has several different ways to treat it for different cases, i.e.

1, when $R \leq R_c$, the exact formulae in Table 3.1 are used,

2, when $R > R_c$, the point source approximation formula in Table 3.1 is used, i.e.

$$\iint_{\Delta S} \frac{\partial}{\partial n}\left(\frac{1}{R}\right) ds = -\frac{1}{R^3}\left[n_1(x - \xi) + n_2(y - \eta) + n_3(z - \zeta) \right] \Delta S \qquad (3.18)$$

3, when $R = 0$

$$\iint_{\Delta S} \frac{\partial}{\partial n}\left(\frac{1}{R}\right) ds = -2\pi \qquad (3.19)$$

4, again $R_c = 3\sqrt{(\Delta S)}$

It should be noted that in the case of R=0, the integration of normal derivative has been shown to be independent of panel shape by Hogben and Standing[7].

3.2.1.3 Contour integrations of contributions due to $\left(\frac{1}{R}\right)$ and $\frac{\partial}{\partial n}\left(\frac{1}{R}\right)$

The line integration in Eqn.(3.3) and (3.8) are evaluated by Eqn.(3.4) and (3.9) in terms of point source approximation, that is

$$\int_{\Delta C_j} n_1 \left[\frac{1}{R(x_i, y_i, z_i; \xi_j, \eta_j, \zeta_j)} \right] dy = n_{1j}\, \delta_j \left[\frac{1}{R(x_i, y_i, z_i; \xi_j, \eta_j, \zeta_j)} \right] \qquad (3.20)$$

and

$$\int_{\Delta C_j} n_1 \frac{\partial}{\partial n}(R)\, dy = n_{1j}\, \delta_j \left[-\frac{1}{R^3}\left[n_1(x_i - \xi_j) + n_2(y_i - \eta_j) + n_3(z_i - \zeta_j) \right] \right] \qquad (3.21)$$

Both $(\frac{1}{R})$ and $\frac{\partial}{\partial n}(\frac{1}{R})$ are evaluated at the centroid of the panel using the source approximation formula. The above equations becomes singular at $x_i=\xi$, $y_i=\eta$, and $z_i=\zeta$, that is, when the field point at the centroid of the source panel. In this case, the results of Hogben and Standing can be used, i.e.

$$\int_{\Delta C_j} n_1 (\frac{1}{R})\, dy = n_{1j}\, \delta_j (2\gamma \sqrt{\frac{\pi}{\Delta S_j}}) \quad \text{for } i = j, \tag{3.22}$$

where

$$\gamma = \frac{1}{\sqrt{\pi\, b}} \left[\ln (b + \sqrt{1 + b^2}) + b \ln (\frac{1 + \sqrt{1+ b^2}}{b}) \right]$$

and

$$\int_{\Delta C_j} n_1 \frac{\partial}{\partial n} (\frac{1}{R})\, dy = n_{1j}\, \delta_j \left[\frac{2\pi}{\Delta S_j} \right] \qquad \text{for } i = j \tag{3.23}$$

3.2 Integration for the regular part of the Green's function

Owing to its complex form, the regular part of Green's function and its derivatives, $G^*(x_i, y_i, z_i; \xi_j, \eta_j, \zeta_j,)$ and $\partial G^*/\partial n$, cannot be integrated exactly over a panel like the singular part. However, the nature of the regular part of Green's function is not like the singular part either. It and its derivatives are regular throughout the fluid domain except the case that the field point (x, y, z) coincides with a source point (ξ, η, ζ) at free surface. G^* oscillates approximately with wave length λ. In practice, λ is at least of the same order as the length of the body hull for the frequency range of the present problem, so G^* and $\partial G^*/\partial n$ vary slowly over S and therefore, are nearly constant over ΔS. Thus, a valid and convenient approximation to the integrations of the regular part is to evaluate the integrand at the centroid of the panels and simply multiplied by ΔS as the point source approximation. The only difficulty comes from the contour integrations in Eqn.(3.3) and (3.7), where the G^* and $\partial G^*/\partial n$ may become singular. If the panels are arranged in the way described foregoing, that is the panels near the free surface have horizontal supersides

which coincide the mean free surface and making use of the contour integration approximation Eqn.(3.4) and (3.9), which has been used in the contour integration for singular part, the singularity difficulty can be simply avoided. Because of the good behaviour and slow varying nature of the regular part of the Green's function, the present calculations and many other papers have been shown the good approximation by this approach. The outline for the integration of the regular part can be drawn as follows:

1, surface integral

$$\iint_{\Delta S_j} G^*(x_i, y_i, z_i; \xi_j, \eta_j, \zeta_j)\, ds = G^*(x_i, y_i, z_i; \xi_j, \eta_j, \zeta_j)\, \Delta S \tag{2.24}$$

$$\iint_{\Delta S_j} \frac{\partial}{\partial n} G^*(x_i, y_i, z_i; \xi_j, \eta_j, \zeta_j)\, ds = \left[n_{1j} \frac{\partial}{\partial x} G^*(x_i, y_i, z_i; \xi_j, \eta_j, \zeta_j) + n_{2j} \frac{\partial}{\partial y} G^* + n_{3j} \frac{\partial}{\partial z} G^* \right] \tag{3.25}$$

2, contour integral

$$\int_{\Delta C_j} G^*(x_i, y_i, z_i; \xi_j, \eta_j, \zeta_j)\, n_1\, dy = n_{1j}\, \delta_j\, G^*(x_i, y_i, z_i; \xi_j, \eta_j, \zeta_j) \tag{3.26}$$

$$\int_{\Delta C_j} \frac{\partial}{\partial n} G^*(x_i, y_i, z_i; \xi_j, \eta_j, \zeta_j)\, n_1\, dy = n_{1j}\, \delta_j \left[n_1 \frac{\partial}{\partial x} G^*(x_i, y_i, z_i; \xi_j, \eta_j, \zeta_j) + n_2 \frac{\partial}{\partial y} G^* + n_3 \frac{\partial}{\partial z} G^* \right] \tag{3.27}$$

where (x_i, y_i, z_i) is field point and (ξ_j, η_j, ζ_j) is the centroid of jth panel.

3.3 Numerical Integration of Green's Function

The numerical solution of the present problem involves firstly the determination of the source density distribution function **q** in Eqn.(3.5). Once **q** is known, the problem is considered ' solved'. The ϕ and its derivatives at any point in the fluid region may be determined through the integration indicated in Eqn.(3.10) and ϕ leads to the pressure on

the body surface S.

The evaluation of the matrices **a** and **b** in Eqn.(3.5) and (3.10) represent the most important part of the numerical procedure since most of the CPU time is consumed in this process. An efficient way to evaluate the Green's function and its derivatives is the key to reduce the computing time and also to make the 3D theory of more practical value. Green's function has been studied extensively during the 1940's and 1950's, notably by Kochin[8], Havelock[9], Haskind[10] and Thorne[11]. These studies were reviewed in Wehausen and Laitone[12] where several alternative integrals were listed. A convergent expansion of Green's function involving spherical harmonics is given in Ursell[13]. The advent of fast computers, opening up the feasibility of numerical calculations for 3D flow, has caused a search of the expressions for the Green's function suited for efficient numerical evaluation which is the main interest of this section The modified form of the Haskind[10] expression for Green's function is given and used in Kim[14]. This modified Haskind expression was also used by Yeung[15] and rederived by Hearn[16] and Newman[17]. Recently, an integral presentation for the Green's function in terms of the exponential integral was obtained independently and in different ways by Guevel and Daubisse[18], Martine[19] and Noblesse[20]. Martine also gives asymptotic expansions of the Green's function. The study by Noblesse contains asymptotic expressions and convergent ascending series. The numerical evaluation of the Green's function was reviewed in Noblesse[20] and Newman[21]. recently with regard to the efficiency of different methods for various cases. The most efficient way to evaluate Green's function is to combine several suitable expressions in a program subroutine for different wave number space.

The present study is based on two different expressions of the Green's function. In the 3D case, the analogue of the Green's function for a pulsating source is

$$G = \frac{1}{R} + \frac{1}{R'} + 2k\, F(X, Y) + i\, 2\pi k\, e^{-Y} J_0(X) \qquad (3.28)$$

where

$$X = k\left[(x-\xi)^2 + (y-\eta)^2 \right]^{\frac{1}{2}}$$

$$Y = k(z+\zeta)$$

$$R = \left[(x-\xi)^2 + (y-\eta)^2 + (z-\zeta)^2 \right]^{\frac{1}{2}}$$

$$R' = \left[(x-\xi)^2 + (y-\eta)^2 + (z+\zeta)^2 \right]^{\frac{1}{2}}$$

and

$$F(X, Y) = \int_0^{\infty} d\upsilon \; (\upsilon - 1)^{-1} e^{\upsilon Y} J_0(\upsilon X). \qquad (3.28)$$

Here J_0 and J_1 are Bessel function of first kind of zero order and first order. The singular part and image part of Eqn.(3.27) and their derivatives can be evaluated in straight forward way since Jo and J_1 can be efficiently calculated by series expansion[22]. Therefore, the essential task for evaluating the Green's function is to evaluate the F(X, Y) for all possible values of two arguments throughout the quadrant where $X \geq 0$ and $Y \leq 0$.

In the case of $X \geq -Y$, the Bessel function J_0 in Eqn.(3.28) oscillates many times before the exponential term decays significantly and consequently numerical computation becomes inefficient. To overcome this situation, Eqn.(3.28) can be transformed to a finite form (due to Haskind) which gives the form

$$F(X, Y) = \left(\frac{\pi}{2}\right)\left[\bar{E}_0(X) - Y_0(X) \right] e^{Y} - \int_0^{-Y} e^{t+Y} (t^2 + X^2)^{-\frac{1}{2}} dt. \qquad (3.30)$$

The derivatives of F(X, Y) can be shown to be

$$\frac{\partial F}{\partial x} = \frac{\partial F}{\partial X}\frac{\partial X}{\partial x} = \frac{k(x-\xi)}{r}\frac{\partial F}{\partial X}$$

$$\frac{\partial F}{\partial y} = \frac{\partial F}{\partial X}\frac{\partial X}{\partial y} = \frac{k\,(y - \eta)}{r}\frac{\partial F}{\partial X}$$

$$\frac{\partial F}{\partial z} = \frac{\partial F}{\partial X}\frac{\partial X}{\partial z} = \frac{k\,(z - \zeta)}{r}\frac{\partial F}{\partial X}$$

where

$$r = \left[\, (x - \xi)^2 + (y - \eta)^2 \,\right]^{\frac{1}{2}}$$

$$\frac{\partial F}{\partial X} = \left(\frac{\pi}{2}\right)\left[\, \bar{E}_1(X) - Y_1(X) \,\right] e^{Y} - X \int_0^{-Y} e^{t+Y}(t^2 + X^2)^{-\frac{3}{2}}\, dt \,. \qquad (3.31)$$

Here E_0 and E_1 are Weber functions defined in Abramowitz and Stegun[22]. Y_0 and Y_1 are Bessel functions of the second kind of zero order and first order respectively.

The above formula can be easily evaluated by Simpson's first rule, clearly in the case of X=0, these formula break down and also for small X the Eqn.(3.30) is inefficient. Therefore, Monacella's[23] approach can be introduced for the case of X<-Y, that is

$$\text{P.V.} \int_0^{\infty} \frac{f(\upsilon)}{\upsilon - k}\, d\upsilon = \int_0^{2k} \frac{f(\upsilon) - f(k)}{\upsilon - k}\, d\upsilon + f(\upsilon)\ \text{P.V.} \int_0^{2k} \frac{d\upsilon}{\upsilon - k} + \int_{2k}^{\infty} \frac{f(\upsilon)}{\upsilon - k}\, d\upsilon \qquad (3.32)$$

since $\text{P.V.} \int_0^{2k} \frac{dk}{\upsilon - k} = 0$, the Eqn.(3.32) reduces to

$$\text{P.V.} \int_0^{\infty} \frac{f(\upsilon)}{\upsilon - k}\, d\upsilon = \int_0^{2k} \frac{f(\upsilon) - f(k)}{\upsilon - k}\, d\upsilon + \int_{2k}^{\infty} \frac{f(\upsilon)}{\upsilon - k}\, d\upsilon \qquad (3.33)$$

Applying Eqn.(3.33) to Eqn.(3.28) gives

$$F(X, Y) = \int_0^{2k} \frac{f(\upsilon) - f(k)}{\upsilon - k} d\upsilon + \int_{2k}^{\infty} \frac{f(\upsilon)}{\upsilon - k} d\upsilon \qquad (3.34)$$

where

$$f(\upsilon) = e^{\upsilon Y} J_0(\upsilon X)$$

$$f(k) = e^{kY} J_0(kX)$$

and the derivative is

$$\frac{\partial F}{\partial X} = \int_0^{2k} \frac{f'(\upsilon) - f'(k)}{\upsilon - k} d\upsilon - \int_{2k}^{\infty} \frac{f'(\upsilon)}{\upsilon - k} d\upsilon \qquad (3.35)$$

where

$$f'(\upsilon) = - \upsilon e^{\upsilon Y} J_1(\upsilon X)$$

$$f'(k) = - k e^{kY} J_1(kX).$$

Introducing (3.34) and (3.35) into Eqn.(3.30) gives the derivatives of F(X, Y).

The Eqn.(3.34) and (3.35) can be evaluated by a normal quadrature method. To do this more efficiently, Simpson's second rule is used for the first integral with the number of ordinates m used to attain the required accuracy, generated as m=6n+4 for n+1,2,.... This automatically avoids the calculation at υ=k. For the second integral, Simposon's first rule is used.

3.4 Use of Symmetry of Body Geometry

Most of the bodies in naval architecture and ocean engineering problem have at least one vertical plane of symmetry and this property can be used to save both computing time and the computer storage space. If the body has port-starboard symmetry, the co-ordinate system 0-xyz will be set in the way described in section 2.1.2 with the body symmetry plane coinciding with o-xz plane.

As mentioned earlier, in implementing the source distribution method most of the computing time is spent in calculating the influence of one source panel on another. If the total number of the panels of the body is N, the matrix **a** in Eqn.(3.5) and **b** in Eqn.(3.10) indicates the N x N operations. Taking advantage of the body symmetry, a considerable computing time can be saved. The scheme for use of this computing time is illustrated in following example.

For the sake of convenience, take the total panel number N=4, and the panel indices 1 and 2 be on one side, the indices 3 and 4 be on the opposite symmetric side, as shown in Fig.3.2, the Eqn.(3.5) becomes

$$\begin{bmatrix} a_{11} & a_{12} & a_{13} & a_{14} \\ a_{21} & a_{22} & a_{23} & a_{24} \\ a_{31} & a_{32} & a_{33} & a_{34} \\ a_{41} & a_{42} & a_{43} & a_{44} \end{bmatrix} \begin{bmatrix} q_1 \\ q_2 \\ q_3 \\ q_4 \end{bmatrix} = \begin{bmatrix} v_{n1} \\ v_{n2} \\ v_{n3} \\ v_{n4} \end{bmatrix}. \tag{3.36}$$

After partitioning, Eqn.(3.36) can be written as

$$\begin{bmatrix} \mathbf{a}_{11} & \mathbf{a}_{12} \\ \mathbf{a}_{21} & \mathbf{a}_{22} \end{bmatrix} \begin{bmatrix} \mathbf{q}_1 \\ \mathbf{q}_2 \end{bmatrix} = \begin{bmatrix} \mathbf{v}_{n1} \\ \mathbf{v}_{n2} \end{bmatrix} \tag{3.37}$$

where

$$\mathbf{a}_{11} = \begin{bmatrix} a_{11} & a_{12} \\ a_{21} & a_{22} \end{bmatrix}; \qquad \mathbf{a}_{12} = \begin{bmatrix} a_{13} & a_{14} \\ a_{23} & a_{24} \end{bmatrix}; \quad \text{etc.} \tag{3.38}$$

$$\mathbf{q}_1 = \begin{bmatrix} q_1 \\ q_2 \end{bmatrix}, \qquad \mathbf{q}_2 = \begin{bmatrix} q_3 \\ q_4 \end{bmatrix}, \qquad \mathbf{v}_{n1} = \begin{bmatrix} v_{n1} \\ v_{n2} \end{bmatrix}, \qquad \mathbf{v}_{n2} = \begin{bmatrix} v_{n3} \\ v_{n4} \end{bmatrix};$$

Due to the symmetry of the body, it can be shown that

$$\mathbf{a}_{11} = \mathbf{a}_{22}, \qquad \mathbf{a}_{12} = \mathbf{a}_{21}. \tag{3.39}$$

Furthermore, if the boundary values are also symmetric with respect to the 0-xz plane, i.e.

$\mathbf{v}_{n1}=\mathbf{v}_{n2}$, then it can be shown that $\mathbf{q}_1=\mathbf{q}_2$. Similarly, if the boundary values are asymmetric with respect to 0-xz plane, i.e. $\mathbf{v}_{n1}=-\mathbf{v}_{n2}$, then $\mathbf{q}_1=-\mathbf{q}_2$.

In Eqn.(3.31), the boundary values n_i are symmetric when i=1,3,5, i.e. for surge, heave and pitch modes, and are asymmetric when i=2,4,6, i.e. sway, roll and yaw modes. Summarizing, the Eqn.(3.37) can be rewritten in two special cases as follows:

1, for surge, heave and pitch modes

$$\mathbf{v}_{n1} = \mathbf{v}_{n2} \qquad \text{then} \qquad \mathbf{q}_1 = \mathbf{q}_2$$

$$\text{and} \quad \left[\mathbf{a}_{11} + \mathbf{a}_{12}\right]\left[\mathbf{q}_1\right] = \left[\mathbf{v}_1\right] \tag{3.40}$$

2, for sway, roll and yaw modes

$$\mathbf{v}_{n1} = -\mathbf{v}_{n2} \qquad \text{then} \qquad \mathbf{q}_1 = -\mathbf{q}_2$$

$$\text{and} \quad \left[\mathbf{a}_{11} - \mathbf{a}_{12}\right]\left[\mathbf{q}_1\right] = \left[\mathbf{v}_1\right] \tag{3.41}$$

For the diffraction boundary value, i.e. $-\partial\phi_0/\partial n$, ϕ_0 as well as $\partial\phi_0/\partial n$ can be split into symmetric and asymmetric parts. Then in a similar manner equations like Eqn.(3.40) and (3.41) can be used.

For the evaluation of the velocity potential, a similar scheme can be used for Eqn.(3.10) which is rewritten as

$$\begin{bmatrix}\phi_1\\ \phi_2\\ \phi_3\\ \phi_4\end{bmatrix} = \begin{bmatrix} b_{11} & b_{12} & b_{13} & b_{14}\\ b_{21} & b_{22} & b_{23} & b_{24}\\ b_{31} & b_{32} & b_{33} & b_{34}\\ b_{41} & b_{42} & b_{43} & b_{44}\end{bmatrix}\begin{bmatrix}q_1\\ q_2\\ q_3\\ q_4\end{bmatrix}. \tag{3.40}$$

or

$$\begin{bmatrix} \phi_1 \\ \phi_2 \end{bmatrix} = \begin{bmatrix} \mathbf{b}_{11} & \mathbf{b}_{12} \\ \mathbf{b}_{21} & \mathbf{b}_{22} \end{bmatrix} \begin{bmatrix} \mathbf{q}_1 \\ \mathbf{q}_2 \end{bmatrix} \tag{3.43}$$

where

$$\mathbf{b}_{11} = \begin{bmatrix} b_{11} & b_{12} \\ b_{21} & b_{22} \end{bmatrix}, \quad \mathbf{b}_{12} = \begin{bmatrix} b_{13} & b_{14} \\ b_{23} & b_{24} \end{bmatrix}, \quad \text{etc.}$$

$$\phi_1 = \begin{bmatrix} \phi_1 \\ \phi_2 \end{bmatrix}, \quad \phi_2 = \begin{bmatrix} \phi_3 \\ \phi_4 \end{bmatrix}$$

1, for surge, heave and pitch modes

$$\mathbf{q}_1 = \mathbf{q}_2 \quad \text{then} \quad \phi_1 = \phi_2$$

and $$\begin{bmatrix} \phi_1 \end{bmatrix} = \begin{bmatrix} \mathbf{b}_{11} + \mathbf{b}_{12} \end{bmatrix} \begin{bmatrix} \mathbf{q}_1 \end{bmatrix} \tag{3.44}$$

2, for sway, roll and yaw modes

$$\mathbf{q}_1 = -\mathbf{q}_2 \quad \text{then} \quad \phi_1 = -\phi_2$$

and $$\begin{bmatrix} \phi_1 \end{bmatrix} = \begin{bmatrix} \mathbf{b}_{11} - \mathbf{b}_{12} \end{bmatrix} \begin{bmatrix} \mathbf{q}_1 \end{bmatrix} \tag{3.45}$$

Because the matrices $\mathbf{a}_{11}$, $\mathbf{a}_{12}$, $\mathbf{b}_{11}$ and $\mathbf{b}_{12}$ are all N/2 x N/2, the use of above scheme does not need to evaluate the G and $\partial G/\partial n$ for N x N times to form the matrices **a** and **b** in Eqn.(3.5) and (3.10). It only needs to evaluate the G and $\partial G/\partial n$ for 2[N/2 x N/2] times, that means 50% of computing time is saved on creating the matrices.

Solving for the source densities using Eqn.(3.40) and (3.41) involves a matrix which is only one quarter the size (N/2 x N/2) of the matrix in Eqn.(3.5) (N x N), but to

find all the hydrodynamic coefficients the matrix must be inverted twice. The time saving depends on the method of inversion. If the time for the inversion increases as N^2, the time saving is 50%. In practice, the solution of Eqn.(3.40) and (3.41) is obtained by the elimination method whose computing time usually increases as N^3, that means the more computing time can be saved on the inversion of the matrix, but it should be keeping in mind that the main CPU time is spent on creating the matrices $\mathbf{a}_{11}$, $\mathbf{a}_{12}$, $\mathbf{b}_{11}$ and $\mathbf{b}_{12}$. The memory space saving is 50%.

Using a similar scheme, the amount of computation can be further reduced if the body geometry has two planes of geometry, say o-xz and o-xy planes. But advantage of this has not been taken in the present work.

This scheme of use of symmetry of the body geometry to reduce the computation effort can be found in many papers, such as Hogben and Standing[7], Inglis[3]. The composite source distribution (c.s.d) method recently introduced by Wu[24] is equivalent to the above scheme. But in present study the above scheme is used because it has simpler form than c.s.d. method and is physically easier to understand. When the body is not symmetric , the program based on c.s.d. method apparently does not work, but the present scheme is fully compatible. This situation is important for the research into the behaviour of damaged structures.

3.5 Use of Properties of Green's Function

3.5.1 Properties of Green's function

A list of Green's functions for different boundary conditions is presented in Table 2.1. Some of their properties which are well behavioured may be benefit to the computation. By denoting any two point in the field domain

$\mathbf{x}_i = (x_i, y_i, z_i)$; $\mathbf{x}_j = (x_j, y_j, z_j)$,

these properties are outline in following.

1, $G(\mathbf{x}_i, \mathbf{x}_j) = G(\mathbf{x}_j, \mathbf{x}_i)$

2, $$\frac{\partial}{\partial x_i} G(\mathbf{x}_i, \mathbf{x}_j) = -\frac{\partial}{\partial x_j} G(\mathbf{x}_j, \mathbf{x}_i)$$

$$\frac{\partial}{\partial y_i} G(\mathbf{x}_i, \mathbf{x}_j) = -\frac{\partial}{\partial y_j} G(\mathbf{x}_j, \mathbf{x}_i)$$

the two corresponding symmetric points of $\mathbf{x}_i$ and $\mathbf{x}_j$ with respect to the o-xz plane are denoted as

$$\mathbf{x}'_i = (x_i, -y_i, z_i), \qquad \mathbf{x}'_j = (x_j, -y_j, z_j)$$

Other properties of symmetry are given as

3, $$G(\mathbf{x}_i, \mathbf{x}_j) = G(\mathbf{x}'_i, \mathbf{x}'_j); \qquad G(\mathbf{x}_i, \mathbf{x}'_j) = G(\mathbf{x}'_i, \mathbf{x}_j)$$

$$\frac{\partial}{\partial x_i} G(\mathbf{x}_i, \mathbf{x}_j) = \frac{\partial}{\partial x_i} G(\mathbf{x}'_i, \mathbf{x}'_j); \qquad \frac{\partial}{\partial x_j} G(\mathbf{x}_i, \mathbf{x}_j) = \frac{\partial}{\partial x_j} G(\mathbf{x}'_i, \mathbf{x}'_j)$$

$$\frac{\partial}{\partial x_i} G(\mathbf{x}_i, \mathbf{x}'_j) = \frac{\partial}{\partial x_i} G(\mathbf{x}'_i, \mathbf{x}_j); \qquad \frac{\partial}{\partial x_j} G(\mathbf{x}_i, \mathbf{x}'_j) = \frac{\partial}{\partial x_j} G(\mathbf{x}'_i, \mathbf{x}_j)$$

$$\frac{\partial}{\partial y_i} G(\mathbf{x}_i, \mathbf{x}_j) = \frac{\partial}{\partial y_i} G(\mathbf{x}'_i, \mathbf{x}'_j); \qquad \frac{\partial}{\partial y_j} G(\mathbf{x}_i, \mathbf{x}_j) = \frac{\partial}{\partial y_j} G(\mathbf{x}'_i, \mathbf{x}'_j)$$

$$\frac{\partial}{\partial y_i} G(\mathbf{x}_i, \mathbf{x}'_j) = \frac{\partial}{\partial y_i} G(\mathbf{x}'_i, \mathbf{x}_j); \qquad \frac{\partial}{\partial y_j} G(\mathbf{x}_i, \mathbf{x}'_j) = \frac{\partial}{\partial y_j} G(\mathbf{x}'_i, \mathbf{x}_j)$$

$$\frac{\partial}{\partial z_i} G(\mathbf{x}_i, \mathbf{x}_j) = \frac{\partial}{\partial z_i} G(\mathbf{x}'_i, \mathbf{x}'_j); \qquad \frac{\partial}{\partial z_j} G(\mathbf{x}_i, \mathbf{x}_j) = \frac{\partial}{\partial z_j} G(\mathbf{x}'_i, \mathbf{x}'_j)$$

$$\frac{\partial}{\partial z_i} G(\mathbf{x}_i, \mathbf{x}'_j) = \frac{\partial}{\partial z_i} G(\mathbf{x}'_i, \mathbf{x}_j); \qquad \frac{\partial}{\partial z_j} G(\mathbf{x}_i, \mathbf{x}'_j) = \frac{\partial}{\partial z_j} G(\mathbf{x}'_i, \mathbf{x}_j).$$

These properties are attributable to the Green's function itself and can be derived from its definition.

If the body has the port-starboard symmetry with respect to o-xz plane, the symmetric and asymmetric boundary values can be written as follows

$$\mathbf{n}_i(\mathbf{x}_i) = (n_{1i}, n_{2i}, n_{3i}); \quad \mathbf{n}'_i(\mathbf{x}'_i) = (n'_{1i}, n'_{2i}, n'_{3i})$$

and $$n_{1i} = n'_{1i}, \quad n_{2i} = -n'_{2i}, \quad n_{3i} = n'_{3i}. \tag{3.46}$$

By means of the Equation

$$\frac{\partial G}{\partial n_i} = n_{1i}\frac{\partial G}{\partial x_i} + n_{2i}\frac{\partial G}{\partial y_i} + n_{3i}\frac{\partial G}{\partial z_i} \tag{3.47}$$

and the property 3, the following properties can be obtained for o-xz plane symmetric body.

$$\begin{aligned} \frac{\partial}{\partial n_i} G(\mathbf{x}_i, \mathbf{x}_j) &= \frac{\partial}{\partial n_i} G(\mathbf{x}'_i, \mathbf{x}'_j) \\ \frac{\partial}{\partial n_i} G(\mathbf{x}_i, \mathbf{x}'_j) &= \frac{\partial}{\partial n_i} G(\mathbf{x}'_i, \mathbf{x}_j) \end{aligned} \tag{3.48}$$

This property is due to the symmetry of the body which has been used in Eqn.(3.40) and (3.41).

The proof of these properties follows the symmetry of the source potential (Green's function) with respect to its arguments and the properties of the derivatives with respect to its arguments as well.

For the convenience of the discussion, the Green's function can be divided into singular and regular parts as Eqn.(2.44)

$$G = 1/R + G^*.$$

The singular part (1/R) satisfies all the properties 1, 2 and 3. There is an additional part to Property 2, i.e.

2, $$\frac{\partial}{\partial z_i}\left(\frac{1}{|\mathbf{x}_i - \mathbf{x}_j|}\right) = -\frac{\partial}{\partial z_j}\left(\frac{1}{|\mathbf{x}_i - \mathbf{x}_j|}\right).$$

Similarly, the regular part, $G^*(\mathbf{x}_i, \mathbf{x}_j)$, satisfies the all the properties 1, 2 and 3, and also has an addition to Property 2, i.e.

2, $$\frac{\partial}{\partial z_i} G^*(\mathbf{x}_i, \mathbf{x}_j) = \frac{\partial}{\partial z_j} G^*(\mathbf{x}_j, \mathbf{x}_i)$$

These properties will be very useful in the discussion of following section, use of the properties of Green's function to saving the computation effort.

3.5.2 Use of Properties of Green's Function

Generally speaking, the elements a_{ij} and b_{ij} in Eqn.(3.5) and (3.10) are neither symmetric nor asymmetric about the diagonal of the matrices.. If the body is symmetric, making use of the body symmetry and the Properties 1 and 3 in Section 3.5.1 the computing time can save nearly 50% as discussed above. Furthermore, if the Properties of the Green's function themselves are used together with the suitable numerical integral manner , the computing effort in creating the matrices **a** and **b** in Eqn.(3.5) and (3.10) can be further reduced by almost another half.

As mentioned in Section 3.2, the integration over one single panel is treated by either exact integral formula or point source approximation, Because the a_{ij} and b_{ij} are generally neither symmetric nor asymmetric, the exact integral formula cannot simply make of the properties of the Green's function, so it will not be discussed here. The exact integral formula is only used for the integral of the singular part of Green's function in the situation of the field point near the source panel, i.e. $R \leq Rc$. Otherwise, when $R > Rc$ the point source approximation formula are used. For the regular part of Green's function the point source approximation is always used in the present numerical procedure. As discussed, the singular part of Green's function has a much simpler form than its regular part and independent of the frequency. Once the singular part is calculated and will be stored for the use of all the calculations. Therefore, the computing time on this part is very limited compared with that on the regular part. In this section, the use of the properties of Green's function for the regular part will be discussed.

From the Eqn.(3.3)-(3.6), (3.25) and (3.26), the integration of the regular part of Green's function, G*, can be written in terms of $\mathbf{x}_i = (x_i, y_i, z_i)$ and $\mathbf{x}_j = (x_j, y_j, z_j)$, i.e.

$$a'_{ij} = [\ \Delta S_j + n_{1j}\ \delta_j\ ] \left[n_{1i} \frac{\partial}{\partial x_i} + n_{2i} \frac{\partial}{\partial y_i} + n_{3i} \frac{\partial}{\partial z_i} \right] G^*(\mathbf{x}_i, \mathbf{x}_j)$$

$$b'_{ij} = [\ \Delta S_j + n_{1j}\ \delta_j\ ]\ G^*(\mathbf{x}_i, \mathbf{x}_j)$$

for i=1,2...N, j=1,2,...M

and

$$a'_{ij} = \Delta\ S_j \left[n_{1i} \frac{\partial}{\partial x_i} + n_{2i} \frac{\partial}{\partial y_i} + n_{3i} \frac{\partial}{\partial z_i} \right] G^*(\mathbf{x}_i, \mathbf{x}_j)$$

$$b'_{ij} = \Delta S_j\ G^*(\mathbf{x}_i, \mathbf{x}_j)$$

for i=1,2,...N, j=M+1,...N, (3.49)

where a'_{ij} and b'_{ij} denote the integration of the regular part of Green's function, G*, involved in the elements a_{ij} and b_{ij} respectively. Introducing the Properties 1 and 2 in Section 3.5 for the G* gives

$$a'_{ji} = [\ \Delta S_i + n_{1i}\ \delta_i\ ] \left[-\ n_{1j} \frac{\partial}{\partial x_i} - n_{2j} \frac{\partial}{\partial y_i} + n_{3j} \frac{\partial}{\partial z_i} \right] G^*(\mathbf{x}_i, \mathbf{x}_j)$$

$$b'_{ji} = [\ \Delta S_i + n_{1i}\ \delta_i\ ]\ G^*(\mathbf{x}_i, \mathbf{x}_j)$$

for j=1,2,...N, i=1,2,...M

and

$$a'_{ji} = \Delta S_i \left[-\ n_{1j} \frac{\partial}{\partial x_i} - n_{2j} \frac{\partial}{\partial y_i} + n_{3j} \frac{\partial}{\partial z_i} \right] G^*(\mathbf{x}_i, \mathbf{x}_j)$$

$$b'_{ji} = \Delta S_i\ G^*(\mathbf{x}_i, \mathbf{x}_j)$$

for j=1,2,...N, i=M+1,...N (3.50)

By means of Eqn.(3.49) and (3.50) to calculate the influence coefficients a'_{ij} and a'_{ji}, or b'_{ij} and b'_{ji}, the G* and its derivatives $\partial G^*/\partial x$, $\partial G^*/\partial y$ and $\partial G^*/\partial z$ are only calculated once. Owing to the complicated form and the frequency dependent nature of the G* and its derivatives, the over 90% of the computing time in creating the matrices **a** and **b**

is spent on their evaluation. The above method needs only one evaluation of the G* and its derivatives for the both symmetric elements with respect to the main diagonal, a'_{ij} and a'_{ji} or b'_{ij} and b'_{ji},. The use of this method, Eqn.(3.49) and (3.50), can reduces nearly 50% of the creating **a** and **b**.

If the symmetry property of the body is used in the calculation, the matrices **a** and **b** are divided into four sub-matrices, Eqn.(3.37) and (3.43), and only two of them are calculated. In such cases, one sub-matrix, for example, the $\mathbf{a}_{12}$ or $\mathbf{b}_{12}$, in Eqn.(3.37) or (3.43), is off the main diagonal, so the Eqn.(3.49) and (3.50) are no longer valid. In order to extend the above method to involve this case, the Property 3 of Green's function may be introduced by denoting

$$\mathbf{x}_i = (x_i, y_i, z_i), \qquad \mathbf{x}_j = (x_j, y_j, z_j)$$
$$\mathbf{x}'_i = (x_i, -y_i, z_i), \qquad \mathbf{x}'_j = (x_j, -y_j, z_j).$$

and assuming the same panel arrangement for both star to portboard sides of the body surface, i.e. $\Delta S_i = \Delta S'_i$ where $\Delta S'_i$ is the area of the panel with its centroid at $\mathbf{x}'_i$. From Eqn.(3.3)-(3.6) and (3.24)-(3.27), the following formula can be obtained.

$$a'_{ij} = [\, \Delta S_j + n_{1j}\, \delta_j \,] \left[n_{1i} \frac{\partial}{\partial x_i} + n_{2i} \frac{\partial}{\partial y_i} + n_{3i} \frac{\partial}{\partial z_i} \right] G^*(\mathbf{x}_i, \mathbf{x}_j)$$

$$b'_{ij} = [\, \Delta S_j + n_{1j}\, \delta_j \,]\, G^*(\mathbf{x}_i, \mathbf{x}_j) \qquad i=1,2,\ldots\frac{N}{2}, \quad j=\frac{N}{2}+1,\ldots\frac{N}{2}$$

and

$$a'_{ij} = \Delta S_j \left[n_{1i} \frac{\partial}{\partial x_i} + n_{2i} \frac{\partial}{\partial y_i} + n_{3i} \frac{\partial}{\partial z_i} \right] G^*(\mathbf{x}_i, \mathbf{x}_j)$$

$$b'_{ij} = \Delta S_j\, G^*(\mathbf{x}_i, \mathbf{x}_j) \qquad i=1,2,\ldots\frac{N}{2}, \quad j=\frac{N+M}{2}+1,\ldots N, \qquad (3.51)$$

where the elements a'_{ij} and b'_{ij} represent the influences from the source panel with its centroid af $\mathbf{x}'_j$ on the field point $\mathbf{x}_i$ which only involve the integral of G* and its derivatives.

By means of the Property 1, 2 and 3 for G*, another group of equations are obtained, i.e.

$$a'_{ji} = [\,\Delta S_i + n_{1i}\,\delta_i\,]\left[\,-n_{1j}\frac{\partial}{\partial x_i} + n_{2j}\frac{\partial}{\partial y_i} + n_{3j}\frac{\partial}{\partial z_i}\right] G^*(\mathbf{x}_i, \mathbf{x}_j)$$

$$b'_{ji} = [\,\Delta S_i + n_{1i}\,\delta_i\,]\, G^*(\mathbf{x}_i, \mathbf{x}_j) \qquad j=1,2,\ldots\frac{N}{2},\quad i'=\frac{N}{2}+1,\ \frac{N+M}{2}$$

and

$$a'_{ji'} = \Delta S_i\left[\,-n_{1j}\frac{\partial}{\partial x_i} - n_{2j}\frac{\partial}{\partial y_i} + n_{3j}\frac{\partial}{\partial z_i}\right] G^*(\mathbf{x}_i, \mathbf{x}_j)$$

$$b'_{ji'} = \Delta S_i\; G^*(\mathbf{x}_i, \mathbf{x}_j) \qquad j=1,2,\ldots\frac{N}{2},\quad i'=\frac{N+M}{2}+1,\ldots N, \qquad (3.52)$$

where a'_{ji} and b'_{ji} represent the influence from the source panel with the centroid at $\mathbf{x}'_i$ on the field point $\mathbf{x}'_j$ for the integral of the G* and its derivatives. In terms of Eqn.(4.49) and (3.50), the evaluation times of the G* and its derivatives for a port-starboard symmetric body with total N panels to present is are (N/2 x N/2), which is only a quarter of the size of matrices **a** or **b**, which is (N x N). For the arbitrary body, there is no symmetry can be used, the total evaluation times for G* and its derivatives are (1/2)(N x N), which is half of the size of the matrices **a** and **b**.

3.6 Efficiency Consideration

The computational effort involved in the obtaining the results of the hydrodynamic coefficients, wave exciting forces and motion responses is always a criterion for judgement of the practical value of the method and the program. For several models with different number of panels the CPU time taken on ICL 3980 machine is given in Table 3.2. The program now works on double precision in order to evaluate the Green's function with an absolute error smaller than 10^{-6} and also make use of the NAG routine software package in ICL 3980 system. The total CPU time involves the whole procedure from the mesh generation to the prediction of the motion responses and wave loads. The CPU time per frequency here is the average value of twenty five typical non-dimensional frequencies from $\omega_e\sqrt{(L/g)}$=0.5 - 5.3 with 0.2 interval because the CPU time varies from different

frequencies and the singular art of the Green's function is frequency independent once calculated it will be stored and used for all the frequency calculations.

Table 3.2 The Comparison of the CPU Time per Frequency (in Seconds)

Number of Panels	Model	Present Procedure	Ordinary Procedure	Time Saving %
120	Ship Shaped Crane Vessel	6.2	9.9	37.4
200	Twin Cylinder	18.7	28.3	34.0
252	Series 60 Model	35.1	51.5	31.9
352	SWATH 1	72.4	118.1	30.7

Table 3.2 show the comparison between the ordinary numerical procedure and the present procedure which make use of the properties of Green's function for the bodies with port-starboard symmetry. Both methods have made use of the symmetry of the body geometry. The present one savesover 30% of the total computing time. From the results in Table 3.2 it can be seen that the total CPU time increases nearly as the square of the number of panels.

CHAPTER FOUR

PREDICTION OF MOTION RESPONSES OF MONO AND TWIN HULL SHIPS IN REGULAR WAVES

In this chapter the hydrodynamic coefficients, wave exciting forces and motion responses of the mono and twin hull ships travelling in regular waves were analysed by the three dimensional theory described in previous chapters. The results have been compared with the other theoretical and experimental results. Because the twin hull ship is primary concern here, the hydrodynamic interaction effects in the form of 'standing waves' between the two hulls were studied in detail. The purposes of this chapter are

1- to demonstrate the validity of the theory and the modified numerical procedure with respect to physical reality,

2- to investigate the 'standing wave' phenomenon and its effect on the hydrodynamic coefficients, wave excitation and motion responses of the twin hull ships, and

3- to apply the theory to the prediction of the twin hull ship motion in regular waves for practical uses.

For these purposes a Series 60 model with C_b=0.70, twin cylinders and a SWATH (small waterplane twin hull) ship model were analysed and their main particulars are given in Table 4.1.

The computational results of a Series 60 model were compared with other theoretical and experimental data to validate the method and the numerical procedure.

The standing waves phenomenon and its effect on the hydrodynamic coefficients, wave excitation of the twin hull body was systematically studied by varying the distance between the two hulls of the twin cylinders for several values. The frequencies at which the

Table 4.1 Main particulars and stability data

Designation	Symbol	Unit	Series 60	Twin cylinders	SWATH 1
Length (between perpendiculars)	L	m	3.048	2.0	1.5
Breadth	B_0	m	0.435	0.813,1.219,2.203	0.8092
Hull spacing between the central lines	B	m	---	0.61, 1.016, 2.0	0.72
Beam of each hull at W.L.	b_0	m	---	0.127	0.05
Draught	T	m	0.174	0.294	0.1984
Displacement	∇	m^3	0.1616	0.171	0.0218
Block coef.	C_b		0.700	---	---
Vertical centre of gravity above base	KG	m	0.179	---	0.1763
Transverse metacentric height	GM_T	m	0.030	---	0.191
Longitudinal metacentric height	GM_L	m	3.46	---	0.232
Inertia in pitch*	I_{55}	kg m^2	96.2	---	4.01
Inertia in roll*	I_{44}	kg m^2	3.48	---	3.30
Inertia in yaw*	I_{66}	kg m^2	96.2	---	6.36
Inertia conduct roll-yaw*	I_{46}	kg m^2	0.40	---	0.0
Waterplane area	A_W	m^2	0.1042	---	0.054
L.C.B. after F.P.		m	1.509	1.0	0.9725
Centre of floatation after F.P		m	1.575	1.0	0.972

* = relative to origin above centre of gravity in waveplane

standing waves occur, so called 'standing wave frequencies' were also discussed.

Finally, the present theory was used to predict the motion responses of a SWATH ship travelling in regular waves. A semi-empirical iterative method was introduced to estimate the viscous effects. This method is generally suitable for not only SWATH ships and also other type of semisubmersibles whose demi hull may not be as slender as SWATH ships. The results were compared with the 2D strip theory results and experimental data for different wave headings, with and without forward speed.

4.1 Series 60 Model

In order to provide the validation of the method and the numerical procedure, a Todd series 60 model with C_b=0.70 was firstly calculated with the model travelling at forward speed associated with F_n=0.0 and F_n=0.2. This typical model has been extensively studied by a number of previous authors. The available experimental and theoretical results are very convenient for the present purpose of validation. In this section the computational results have been compared with the experimental and the other theoretical results. The comparison with the other three dimensional results can be used to check the validity of the present numerical procedure which is modified to make using the symmetric properties of the Green's function and the body geometry. This numerical procedure provides the basis of the following studies including the predictions of the motion responses, wave loading of ships, and the random sea process. On the other hand the comparison with the strip theory and the experimental results can show the general validity of the present three dimensional theory to ship motion problem and the improvement from the simple two dimensional approximation.

The principal particulars of the Series 60 model are given in the Table 4.1. The hull form is represented by 252 panel elements as shown in Fig.4.1. The calculation was made by the modified numerical procedure described in the previous chapters. Because of the symmetric feature of the model about its centre plane, the method utilizes the symmetry of the body geometry and considers the half of the hull form only. Consequently considerable saving on both computing time and storage space is attained.

For the comparison the results obtained by some previous authors for the same model were used in this study which are listed as following:

Theoretical results

1, Strip theory: The results are given by Inglis [1] who used the Lewis-form method by dividing the hull into 20 segments each of which was modelled using a Lewis section.

2, Three dimensional theory: The results are also given by Inglis [2] using three dimensional source distribution method.

Experimental results

1, Gerritsma and Beukelman [3] give the measured results for whole and segmented models at F_n=0.2 for heave and pitch. Their model was 2.258 m long, so the results have been scaled up to the same length as present model;

2, Vugts [4] gives the experimental results measured on the model of length 3.048m for both whole and segmented hull at F_n=0.0 and F_n=0.2;

3, Van Leeuwen [5] measured the results for the whole model of length 2.258m at Fn=0.2 both with and without rudder in sway and yaw modes. The results are presented in stability axes and so they have been transformed and scaled for the present comparison.

4.1.1 Motion Induced Coefficients

The motion induced coefficients, i.e.added mass and damping, were computed over a wide range of frequencies of $0.8970 \leq \omega_e \leq 9.867$ or $0.5 \leq \omega_e\sqrt{(L/g)} \leq 5.5$ in non-dimensional frequencies. The coefficients were calculated for all six modes (i.e. surge, sway, heave, roll, pitch and yaw) including coupled motion induced coefficients.

The coefficients are presented in Fig.4.2-4.11. In all figures the abscissa is a non-dimensional frequency $\omega_e\sqrt{(L/g)}$. The added mass and damping are also represented as non-dimensional values, A'_{ij} and B'_{ij}. The non-dimensional products are described in the nomenclature.

Generally the very good correlations have been found between the present three dimensional results and Inglis 3D results which shows the validity of the present modified numerical procedure. The two approaches use similar basic theory but different numerical procedures, so the results should be very close to each other.

The distinct feature of the discontinuities in the coefficients of the vertical oscillations at $\omega_e \cong 9.13$ is considered to be caused by irregular frequencies. From the geometric properties of the model, i.e. L/B=7.0 and B/T=2.5, one would except an irregular frequency at $\omega_e \cong 9.16$ (corresponding λ/L=0.24) by means of Eqn. 2.92, and out of the frequency range of practical interesting for rigid body motion. However it is not true if the ship has a high speed and consequently a high encounter frequency. On other hand, when hydroelastic theory is used where the body is assumed flexible these irregular frequencies would become a very serious restriction since they occur in the region of resonances of the distortional mode (see reference [6]). The strategies to avoid irregular frequencies have discussed in the Chapter 2. The simplest way is to forecast them prior to setting the frequencies to be calculated and avoid them. The range of the effect of each irregular frequency is often very narrow, so the results laying in this range can be approximated by interpolation. The Eqn. 2.92 can be used to forecast.

For better understanding the theory, the two dimensional and the experimental results are also shown in the Fig.4.2-4.11. The discussion of the results are made in two groups, vertical mode of oscillation and lateral mode of oscillation which are assumed independent each other in the present theory.

I, Vertical mode of oscillation

Surge and Surge-Pitch

There is no measured data available for these modes. The strip theory neglects them by the assumption of the theory. Therefore no comparison can be made with experimental and two dimensional results. On other hand the two 3D results agree well with each other.

Heave

At higher frequencies both three dimensional and strip theory agree well with the measured data for F_n=0.0 and F_n=0.2 but in the low frequency range the strip theory deficiencies are apparent. This is due to the basic assumption in strip theory that the high oscillation frequency is required. In the present three dimensional theory the heave coefficients are speed independent and it certainly appears from the experiments that the speed effects on added mass are small.

Pitch

As with heave, the three dimensional results and strip theory results agree well in high frequency range, but at lower frequencies there is large difference between them. For zero speed damping coefficients three dimensional theory improved the results significantly, but at non-zero speed the agreement with measured data is only fair.

When the encounter frequency approaches zero, the A_{55} at F_n=0.2 as predicted by three dimensional theory become infinite. From the Table 3.2 it is clear that the A_{55} has an order of ω_e^{-2} . In the motion equation the A_{55} will be multiplied by ω_e^2 which means the contribution of A_{55} to the motion equation is only finite, whereas the A_{55} predicted by strip theory will gives an infinite contribution. Therefore, near the zero encounter frequencies in the cases of following and stern quatering seas must be avoided with strip theory.

Heave-Pitch

It is obvious that the added mass A_{35} of present results at zero speed, Fig.4.6, is different from the other three dimensional and strip theory results. The present one agrees with the experiments much better than the others. The reason is not clear, but it is confirmed by the calculations of three different panel arrangements for the same model from coarser to finer (only one result is shown here).

For the forward speed case the results show similar behaviour to that found in the zero speed case. The differences between present results and the others are caused by the zero speed A_{35} values. The present one lies close to measured data as well. Another

important fact can be found is the three dimensional results satisfies the Timman-Newman[7] symmetry relationship, but the strip theory results does not.

II, Lateral modes of oscillations

Sway

The predictions by all theories are close each other at both speeds and all of them underpredict the damping. This is believed to be the influence of viscosity as has been demonstrated by Vugts[8]. He used the strip theory to predict sway and roll damping of two dimensional rectangular cylinders with different B/T. In his results the theoretical predictions and the experiments coincide for larger ratio of B/T and get more inaccurate for smaller B/T. It can be understood that the flow pattern about the deep immersed sections is more influenced by separation than the shallow one. The sway added masses predicted by all the theory agree well with each other for both speed, but all of them are higher than the experimental results at Fn=0.2 which is due to the limitation of both 3D and 2D theories, i.e. A_{22} and B_{22} are speed independent.

Sway-Roll

The damping coefficients for this coupling mode, Fig.4.8, show the same tendencies as those in the sway mode. The underpredictions are caused by viscosity. The experiments show the damping coefficients are changed with forward motion but the theoretical results is independent of forward speed.

Roll

The added mass at both speeds are nearly constant which is experimentally confirmed by Vugts[8]. It is clear that the theory gives the inadequate results for the roll damping. Unlike other modes for the mono hull ship the viscosity gives a significant contribution to the roll damping. This will be discussed later. However both of the theories fail to predict satisfactorily the influence of forward speed. The hydrodynamic coefficients in roll mode are speed independent due to the limitation of the theory.

Yaw

At zero speed, the Fig.4.10 shows that all the theories predict satisfactorily the added mass. In the case of F_n=0.2, the three dimensional results lies close to the measurements, but they still can not simulate the trend of the added mass at the middle frequency range. The limitation of strip theory is obvious since it is speed independent in this mode. The agreement between the predictions by all the theories with experiments for the damping is not good at lower frequencies.

Sway-Yaw

For sway-yaw coupling, Fig.4.11 shows the present results of damping coefficients agree with the experiments better than the three dimensional results given by Inglis[1]. This is similar as that found in heave-pitch coupling mode and the reason is not clear either. For the zero speed the added mass the strip theory seems to be giving better results, but at Fn=0.2 the predictions of three dimensional theory are closer to the measurements.

4.1.2 Viscous roll damping

Potential theories, such as those under discussion, are based on the ideal flow assumptions, and so attributes all damping effects to wave damping. For most modes of oscillation of mono hull ships this gives adequate results but for roll motion the viscous effects must be considered.

The viscous effects on roll damping can be divided into two parts, i.e. skin friction and eddymaking.

(1) Skin friction

Skin friction is due to the existence of boundary layer in real fluid and causes a contribution to roll damping which is Reynolds number dependent. This contribution to the roll damping is quite important in the model test, but it has been shown by Myrhaug and Sand[9] to be negligible for real ship.

(2) Eddymaking

The eddymaking damping was studied by Tanaka[10]. It was found that this contribution is dependent on the roll velocity and independent of Reynolds number.

The different components of the roll damping on Series 60 were measured and compared with the prediction from the empirical formulae by Ikeda, Himena and Tanaka[11]. Their results are shown in Fig.4.12. Their results were used here. Fig.4.13 shows that the agreement of the prediction with experiments is improved significantly by introducing the viscous effect.

4.1.3 Wave Exciting Coefficients

The wave exciting forces and moments acting on the submerged hull of the model have been calculated with the model travelling at the speed associated with Fn=0.0 and Fn=0.2 in head sea ($\beta=180^0$), Fn=0.0 in bow quartering sea ($\beta=120^0$) and Fn=0.2 in beam sea ($\beta=90^0$). The results against the non-dimensional wave frequency, $\omega_e\sqrt{(L/g)}$, are presented in Fig.4.14-4.22. The contributions of Froude-Krylov force are also shown in the figures.

The experimental results are only available for heave and pitch modes in head sea at F_n=0.2, sway, heave, roll and pitch in bow quatering sea at Fn=0.0. Therefore the comparisons are only made for these modes.

All the results show the present predictions agree with the other 3D results very well which further confirms the present numerical procedure. The discussion of the comparisons with experiments and other theoretical results follows.

Head seas

From Fig.4.14-4.16 it can be seen that the diffraction components reduce the wave excitation in all the vertical modes, i.e. surge, heave and pitch. The Froude-Krylov forces dominates the total wave excitations in surge and heave modes, but the diffraction forces give the most important contribution to the pitch moments since the diffraction pressure at

the two ends is more sensitive to the pitch moments rather than surge and heave forces.

Fig.4.15 and 4.16 show the exciting force and moment predicted by 3D theory are closer to the measured values in the range of low frequencies at Fn=0.0, but at higher frequencies the strip theory results appear better. In fact, in spite of these differences and those found in hydrodynamic coefficients both 3D and strip theory predict similar heave and pitch responses, as shown in Fig. 4.24 and 4.25. At F_n=0.2 the 3D theory gives better results than strip theory.

Bow quartering seas

The bow quartering sea results are represented from Fig.4.17-4.19 for Fn=0.0. Comparing the results for vertical modes (surge, heave and pitch) with lateral modes (sway, roll and yaw), it can be found that the diffraction effects on the lateral modes are much more significant than those on the vertical modes. Unlike in the head sea the Froude-Krylov predictions are clearly inadequate and the results show the diffraction effect is important even in the vertical modes.

At zero speed, the 3D theory predicts heave and pitch excitation better at all frequencies. For the sway force, the 3D results agree well with the measurements. For the rolling moments the 3D predictions are significantly closer to the measurements than those obtained by strip theory but the level of agreement is not as good as those in the other modes. For the yaw moments their is little to choose between 3D and strip theory.

Beam seas

The beam sea results are shown in Fig.4.20-4.22 for sway, heave and roll at F_n=0.2. It can be seen that the Froude-Krylov forces predictions are inadequate. For the roll moments the diffraction force gives the largest contribution.

Two 3D results agree well each other but are much higher than the predictions by strip theory. The difference increases as the frequency increases just like was found in the bow quartering sea but more markedly. This is caused by the underprediction of diffraction

in strip theory. Diffraction increases in effect as the frequency increases.

4.1.4 Motion Responses

The theoretical results of hydrodynamic coefficients and wave excitation calculated previously were used in the coupled motion equation described in the Chapter 2 to predict the coupled responses of the model in six degrees of freedom. The viscous effect in roll damping has been taken into account. The results of the responses are shown in Fig.4.23-4.31. The comparisons among different theories and experiments are made for different wave heading, with and without forward speed.

Head seas

The results for Fn=0.0 and Fn=0.2 are shown in Fig.4.23-4.25. The surge responses get the minimum value near $\omega_e\sqrt{(L/g)}=2.75$ at Fn=0.0 and $\omega_e\sqrt{(L/g)}=3.75$ at $F_n=0.2$ where the surge excitations had their the minimum value. When the frequency approaches to zero the surge responses should theoretically approach to infinity due the zero stiffness in the surge mode of the motion equation but this limiting value is not shown in Fig.4.23. At the lowest frequency calculated, $\omega_e\sqrt{(L/g)}=0.5$, the surge responses still give the reasonable values. The non-dimensional heave responses approach to 1.0 while the frequency approaches to zero because the the heave wave exciting force equals to the heave stiffness, $C_{33}=\rho g A_W$, at zero frequency. The natural frequency of heave is about $\omega_e\sqrt{(L/g)}=3.25$, the natural period is about 1.08 sec.. The non-dimensional pitch response approaches to 1.0 at zero frequency. The reason is similar to the heave response. The pitch stiffness C_{55} equals to the pitch wave excitation when the frequency approaches to zero and the coupling coefficients of stiffness and wave excitation for heave-pitch cancel each other. The pitch natural frequency is about $\omega_e\sqrt{(L/g)}=3.75$ and its effect is not as obvious as heave natural frequency because the wave exciting moment is small at this frequency.

Bow quartering seas

The responses in six degrees of freedom with Fn=0.0 are shown from Fig.4.26-4.28. In the bow quartering seas, all the non-dimensional responses in vertical modes, i.e. surge, heave and pitch are less than those in head sea. For the lateral motions, the roll natural frequency is near $\omega_e\sqrt{(L/g)}=2.25$ which gives obvious coupling effect on sway

responses.

Beam seas

The sway, heave and roll responses are represented in Fig.4.29-4.31 These are the worst cases for sway and roll motions. The sway responses should theoretically become infinite due to the stiffness is zero, but this does not appear at the lowest frequency calculated. The roll response changes the phases by 180^0 when the frequency is changed from lower than its natural frequency to higher than it. The coupling effect between sway and roll is significant.The predictions by all the theories agree well each other in sway and roll modes but there is no experimental data available.

4.2 Standing wave phenomenon

4.2.1 Twin Cylinders

The panel method has been modified by using the symmetric properties of Green's function and the body geometry, so it is necessary to validate it for the twin or multi-hull bodies. Here a simple twin hull cylinder is first considered.

At the early stage of the SWATH program in DTNSRDC, the experimental studies on a forced oscillation of twin cylinders with small water plane area were carried out by Gerzina. The forced oscillation was made independently in heave, sway and roll modes and several amplitude of oscillations were used to check the linearity. Later Lee, Jones and Bedel[12] calculated the added mass and damping coefficients for those modes by 2D strip theory, the Frank close-fit method[13] was employed.

The model is shown in Fig.4.32 with the length of 2.0m, the radius of one hull of 0.1015m and the distance between the centre lines of the two hulls varies for three values, i.e. 0.61m, 1.016m and 2.0m. The first two distances were used by Gerzina and also employed in present calculations. The 164 panel elements were used to present the hull form as shown in Fig.4.32. The results given by Gerzina have been scaled to compare with the present non-dimensional values .

In this section the present predictions of added mass and damping in sway and heave modes were first compared with the 2D and experimental results to validate the theory for twin hull bodies. Then the results based on the twin hulls approach were compared with the demi hull results to investigate the hydrodynamic interaction between the two hulls.

I. Hydrodynamic coefficients

The added mass and damping coefficients of the twin cylinders with B=0.61m and B=1.016m were calculated by 3D theory and are shown in Fig.4.33. The present 3D results are compared with both experimental and 2D results for added mass and damping coefficients for sway and heave modes. The comparison shows that both theories correlate with the measured data well for this special model ('2D' model), but the 3D results still show the relatively better correlation in heave added mass prediction than the 2D results. It is also clear that the damping coefficients predicted by both theories are lower than experimental values this is considered to be caused by the viscous effect. As explained in the Section 4.3.3, the damping coefficients involved in the vertical plane modes play a sensitive role in prediction of heave and pitch motions. The damping obtained by the potential theory for a small amplitude of oscillation produce exaggerated peak amplitudes of motion at the natural frequencies, compared with the magnitude measured in motion experiments in regular waves. Therefore the viscous effect must be taken into account for predicting the motion of the SWATH type of ships.

The most strike feature of the results in Fig.4.33(a) is the discontinuity at non-dimensional frequency $\omega^2(r_0/g)=0.65$, where $\lambda/B_i\approx2.0$ (B_i is the distance between the inner boards of the twin hulls) for the sway mode, which is due to the effect of the asymmetric mode of standing waves between the two hulls. It is interesting to note that the dip in A_{33} at $\omega^2r_0/g\approx0.18$, where $\lambda/B_i\approx4.0$, was stated by Lee and Curphey[14] to be caused by the mutual blockage effect between the twin hulls. However the present studies show this dip is caused by the symmetric standing waves, such a dip has been experimentally confirmed by Lee, Jones and Curphey[15] for a conventional catamaran. In

Fig.4.33(b) there is a peak in heave added mass at $\omega^2 r_0/g \approx 0.7$, where $\lambda/B_i \approx 1.0$, which is caused by the second vertical standing waves. Generally the two theories underpredict the heave damping B_{33} because of the viscous effect. At lower frequencies the strip theory does better than 3D theory.

II. Hydrodynamic interaction between the two hulls

For better understanding the hydrodynamic interaction between the twin hulls, the comparison of the hydrodynamic coefficients between demi and twin hull approaches are presented in Fig. 4.34. The demi hull results are obtained under the assumption that the hydrodynamic interaction between two hulls are neglected, so the results are simply obtained by two times the results of the single hull. In heave mode, the two results agree well except at those at the frequencies where the standing waves occur. This means the hydrodynamic interaction is weak in the heave mode. Similar features were also found in the other vertical modes, i.e. surge and pitch. Whereas the differences in sway mode are much clear. The effect of the standing waves at $\omega^2 r_0/g \approx 0.65$ can not be seen in the demi hull results. The sway damping B_{22} predicted by demi hull theory is nearly as twice as those by the twin hull theory. The comparison shows that the demi hull theory is inadequate to predict the added mass and damping for sway mode, and the other transverse modes, roll and yaw. The results are not shown here.

4.2.2 The Standing Waves

When a twin hull surface piercing vessel oscillates in the free surface or in the incident waves, the radiation or diffraction waves generated on the one hull will transfer to and reflect back from the other. At certain combination of the frequencies and the distance between the inner boards of the twin hulls, the waves transformed and reflected in the vicinity of the twin hull have the same phase which causes the so called 'resonant wave' or 'standing wave'. This fluid interaction is verified the experiments on the SWATH model by McGregor[16]. The experiment shows that the standing wave can makes the wave amplitude in the vicinity of the two hulls 3-4 times the incident wave amplitude, and at same time it produces the maximum wave loads on the hull structure and large motion responses. It significantly effects the hydrodynamic feature of twin hull ships. In order to

investigate the hydrodynamic effect of the standing waves, the twin cylinders, as shown in Fig.4.32, was systematically analysed by varying the spacing between the twin hulls using 3D diffraction theory. The distance between the twin hulls, B, was varied for three different values B=0.61m, 1.016m and 2.0m, i.e. B/L=0.305, 0.508 and 1.0. The results are shown in Fig.4.35-4.50. In order to discuss it is appropriate to divide the standing waves into two different types since they have different features.

I. Symmetric standing waves

The symmetric standing waves are generated at certain frequencies by the oscillation of the twin hull in the vertical modes or under the action of the symmetric incident waves (or symmetric part of the incident waves). In these cases, the radiation and diffraction standing waves between the twin hulls are symmetric about the centre line with the maximum amplitude on it.

II. Asymmetric standing waves

The asymmetric standing waves are generated at certain frequencies by the oscillation of the twin hulls in the transverse modes or under the action of the asymmetric incident waves (or asymmetric part of the incident waves). The both radiation and diffraction standing waves are asymmetric about the centre line with zero amplitude on it.

4.2.3 The Influence of the Standing Waves

Generally, the standing waves influence the hydrodynamic features of twin hull ships in three different ways.

- introducing rapid changes in the curves of added mass from maximum to minimum, sometimes negative added mass,
- producing the peak values on damping coefficients, and
- producing the peak values on the wave exciting forces.

The influences result the maximum wave loads on the twin hull ship structure, large motion responses and serious upwelling phenomenon.

The influences of the symmetric and asymmetric standing waves are clear in the

results shown in the Fig.4.35-4.50. From the results, it can be seen that the effects of standing waves generally decreases as the spacing between the two hulls increases. Theoretically there are infinite number of standing waves could occur, but in present calculation only the first two symmetric and asymmetric waves can be seen. The results also show that the effect of standing waves decrease significantly as the standing wave frequency increases, so in practice only first few standing waves with low frequencies are of interest. The discussion will be made in detail in following text. The corresponding frequencies of the symmetric and asymmetric standing waves are indicated by ω_{e1} and ω_{e2} respectively. The values of ω_{e1} and ω_{e2} for varying B/L are listed in the Table 4.2.

I, Effect of standing waves on hydrodynamic coefficients

When the twin hull body oscillates at the frequencies ω_{e1}, the symmetric radiation standing waves occurs and it only effects in the hydrodynamic coefficients in the vertical modes, which is clearest in heave mode. The heave added mass A_{33} attains a minimum at first symmetric standing wave and has a jump at the second one. There are corresponding peaks on the curves of the heave damping B_{33} (see Fig.4.36).Generally this effect decreases as the B/L value increases. For the most separated case of B/L=1.0, the influence of the second vertical standing waves is much less than those in the other two cases.

The asymmetric radiation standing waves at ω_{e2} introduce peak values in the added mass curves in all the transverse modes, i.e. A_{22}, A_{44}, A_{66} and A_{24}. these are rapidly changed from the positive maximum to the minimum values (possibly negative). The standing wave frequencies, ω_{e2}, appear to be the turning point. The corresponding effect on the damping coefficients, B_{22}, B_{44}, B_{66} and B_{24}, results in peak values of all the transverse modes, as shown in Fig.4.38-4.41.

The peak values of the damping caused by symmetric and asymmetric standing waves are physically reliable since the dissipation of the energy through surface waves dispersion is partially prevented when standing waves occur.

II. Effect of standing waves on wave excitation

Head sea

In the head sea, the incident waves are symmetric about the centre line, so only the symmetric diffraction standing waves could occur. In the Fig.4.42, the symmetric standing wave at ω_{e1} produces peaks on the curves of wave exciting forces F_2^p and F_2^s acting on the port and starboard sides of the vessel. these are 180^0 out of phase each other and tend to split the twin hulls. A similar influence can be seen on the curves of F_4^p and F_4^s as well (Fig. 4.43)

Beam sea

In beam seas, the results are more interesting. The incident waves in this case are neither symmetric nor asymmetric about the centre line. From Fig.4.47, it is clear that both symmetric and asymmetric diffraction standing waves at ω_{e1} and ω_{e2} influence the wave exciting forces F_2^p significantly. The first peak on the curve F_2^p is introduced by the symmetric diffraction standing waves at ω_{e1} This produces the maximum side force and bending moment on the cross-deck structure, and the second peak by the asymmetric diffraction standing waves at ω_{e2} which produces the maximum wave exciting forces contributing to the motion responses. In order to understand the features of these two different diffraction standing waves, it is appropriate to divide the incident wave and the diffraction wave potentials into symmetric(even) and asymmetric(odd) parts. The incident wave potential is given in Eqn. 2.7, i.e.

$$\begin{aligned}\phi_0 &= -\frac{iga}{\omega}\exp\left[kz + ik\left(x\cos\beta + y\sin\beta\right)\right] \\ &= \phi_0^e + \phi_0^o\end{aligned} \tag{4.1}$$

where

$$\phi_0^e = -\frac{iga}{\omega}\exp\left[kz + ikx\cos\beta\right]\cos\left(ky\sin\beta\right)$$

and

$$\phi_0^o = -\frac{iga}{\omega}\exp\left[kz + ikx\cos\beta\right]\sin\left(ky\sin\beta\right).$$

The diffraction potential is defined by the boundary conditions

$$\frac{\partial \phi_D}{\partial n} = -\frac{\partial \phi_0}{\partial n} \qquad \text{on S}$$

Since $\phi_D = \phi_D^e + \phi_D^o$,

$$\frac{\partial \phi_D^e}{\partial n} = -\frac{\partial \phi_O^e}{\partial n}$$

$$\frac{\partial \phi_D^o}{\partial n} = -\frac{\partial \phi_O^o}{\partial n} \qquad \text{on S} \qquad (4.2)$$

The part of the incident wave associated with the potential ϕ_D^e is called the even part of incident wave, and associated with ϕ_D^o the odd part.In head sea only ϕ_D^e remains, so only symmetric diffraction standing wave could occur. In beam sea or other heading, both ϕ_D^e and ϕ_D^o are generally non-zero. The two boundary conditions in Eqn.(4.2) could make the diffraction waves which are generated on the one hull transfer and reflected back from the other have the same phase in the vicinity of the twin hulls at certain frequencies, This means that both symmetric and asymmetric standing waves could occur. The prediction of the force F_2^p in Fig.4.47 has confirmed this phenomenon.

The F_i^e(even part of the force F_i) has the same amplitude and sign (same phase) acting on the port and starboard sides of the vessel, whereas F_i^o(the odd part of the force F_i) has the same amplitude but opposite sign acting on the port and starboard sides of the vessel. The F_i^e and F_i^o on the right side hull can be obtained from following formulae.

$$F_i^e = \begin{cases} \int_{S_R} (\phi_0^e + \phi_D^e)\, n_i \, ds & i=1,3,5 \\ \int_{S_R} (\phi_0^o + \phi_D^o) n_i \, ds & i=2,4,6 \end{cases} \qquad (4.3a)$$

$$F_i^o = \begin{cases} \int_{S_R} (\phi_0^o + \phi_D^o)\, n_i\, ds & i=1,3,5 \\ \int_{S_R} (\phi_0^e + \phi_D^e)\, n_i\, ds & i=2,4,6 \end{cases} \qquad (4.3b)$$

where S_R is the wetted surface area of the right hull.

The symmetric standing waves at ω_{e1} are only associated with the even part of the diffraction potential ϕ_D^e, so they produce peak values on the curves of F_3^e, F_2^o, F_4^o and F_6^o, as shown in Fig.4.48-4.49. Specially, F_2^o is the force tending to split the hulls and produces the maximum bending moment at cross deck structure at ω_{e1}. The asymmetric standing waves at ω_{e2} associate with the odd part of the diffraction potential ϕ_D^o, so they produce the peak values on the curves of F_2^e, F_4^e, F_6^e and F_3^o etc., as shown in Fig.4.48-4.49. The F_2^e gives the maximum total exciting force contributing to its motion.

It is interest to note that all the even forces F_i^e, for i=1-6, only contribute to the motion responses of the ship, whereas all the odd forces F_i^o, for i=1-6, only contribute to wave loads on the ship structure. In this section, the results have shown the important effect of standing waves on the hydrodynamic coefficients, wave excitations of the twin hull body. In the next section and Chapter 6, the investigation will be made on its effects on the motion responses and waves loads respectively.

4.2.4 Standing wave frequency

It has been suggested that the standing wave frequencies for two parallel surface piercing cylinders with infinite length may be obtained by following formula[17]

$$\frac{\lambda}{B_j} = \frac{1}{n} \begin{cases} n=1, 2, 3, \ldots & \text{for symmetric standing waves} \\ n=0.5, 1.5, 2.5, \ldots & \text{for assymmtric standing waves} \end{cases} \qquad (4.4a)$$

or

$$\omega = \left[g \frac{2\pi n}{B_i} \right]^{\frac{1}{2}} \begin{cases} n = 1, 2, 3, \ldots & \text{for symmetric standing waves} \\ n = 0.5, 1.5, 2.5, \ldots & \text{for asymmetric standing waves} \end{cases}$$

(4.4b)

This formula based on the assumption that 'the wave generated between two cylinders is symmetric or asymmetric and that at each end the wave slope is zero.

The above conjecture for symmetric mode is drawn from the 2D interference studies conducted on simple sections primarily regarding the heave mode[12,17,18]. Data for surface piercing strut or column type bodies in asymmetric modes was found generally scarce[19]. This feature was confirmed by present study.

The standing waves frequencies of different spacing between the two hulls are listed in Table 4.2. The results show that when L/B value becomes large, the values for the second symmetric standing waves approach to 2.0, for the first asymmetric standing waves approach to 1.0 and for second asymmetric standing waves are around 0.67. This is close to that estimated by Eqn.(4.4).

On the other hand,the results in Table 4.2 also show the strong 3D effect on the first symmetric standing waves. For different L/B values, λ/B_i varies significantly from about 3.0 to 6.5. The concept of wave reflection between the two hulls in transverse direction is difficult to explain why the λ/B_i value of this standing wave is not integer. In order to understand this phenomenon the further discussions are made as follows.

4.2.5 Discussions on transverse and longitudinal standing waves

The above discussions on standing waves are based on the concept of wave reflection between the two hulls in transverse direction. This explanation was used in many papers of two dimensional theories in which only the transverse wave interaction between the two hulls can be considered, and also used by Price and Wu[23] to explain the three dimensional standing wave phenomenon in the vicinity of the twin hull semi-submersibles.

Table 4.2 Frequencies of standing waves of the twin cylinders

	B/L		1.0	0.508	0.305
	B(m)		2.0	1.016	0.61
	B_i(m)		1.873	0.889	0.483
Symmetric standing waves	1 (Long.)	ω_{e1}(rad./sec.)	3.322	4.153	4.429
		$\omega_{e1}\sqrt{(L/g)}$	1.5	1.875	2.0
		λ(m)	5.585	3.574	3.142
		λ/Bi	2.982	4.020	6.505
		λ/L_s	3.103	1.986	1.746
	2 (Trans.)	ω_{e1}(rad./sec.)	5.814	8.305	11.07
		$\omega_{e1}\sqrt{(L/g)}$	2.625	3.75	5.0
		λ(m)	1.823	0.894	0.503
		λ/Bi	0.973	1.006	1.041
Asymmetric standing waves	3 (Trans.)	ω_{e2}(rad./sec.)	4.983	6.090	8.028
		$\omega_{e2}\sqrt{(L/g)}$	2.25	2.75	3.625
		λ(m)	2.482	1.662	0.956
		λ/Bi	1.325	1.870	1.979
	4 (Trans.)	ω_{e2}(rad./sec.)		10.24	13.17
		$\omega_{e2}\sqrt{(L/g)}$		4.625	6.125
		λ(m)		0.587	0.335
		λ/Bi		0.660	0.694

From the computational results in this thesis, one can find that the λ/L_s values of the 'so called' first symmetric standing waves for different L/B are close to 2.0, where L_s is the length of the strut. Eatock Taylor and Hung[24] also confirmed this by investigating upwelling in the vicinity of SWATH ships with both single and tandem struts. Their results are given in Fig.4.50. The characteristic of the antinode at the centre and a node fore and aft near the strut extremes. This condition is physically realistic for two reasons: Firstly the λ/L_s is close to 2.0, and then the locations of node and antinodes at these points will satisfy the expected symmetric flow conditions. This behavior is reminiscent of a channel with

open ends, in which resonant modes exist at

$$\frac{\lambda}{2L_s} = \frac{1}{n}, \quad n = 1, 2, \ldots\ldots . \tag{4.4c}$$

This type of standing waves are termed 'longitudinal standing waves' here.

The present study suggests that the wave interaction in the vicinities of the twin hull ships could occur in both transverse and longitudinal direction. At the lowest frequency the longitudinal standing waves usually occur and cause the most serious upwelling and side force acting on the twin hull structures. While at higher frequencies the wave interactions in transverse direction are often dominant, so the transverse standing waves are usually seen. Theoretically there are infinite number of standing waves, but their effect decreases significantly as the standing wave frequency increases. Therefore only the first few standing waves with the lowest frequencies have serious effect and are of primary interest.

Above conclusions are made primarily based on the results of the computations, they still need systematic experiments to confirm. If the conclusions are true, the longitudinal standing waves, which usually produce the most serious upwelling and side forces on the structure, are purely three dimensional effect and difficult to be predicted by any two dimensional theory.

4.3 A SWATH SHIP

The SWATH (Small Waterplane Area Twin Hull) ships have attracted increasing interesting since the last decade and now receiving considerable attention. Among many advantages over conventional mono hull vessels, a major attraction is superior sea keeping performance at a seaway and little speed reduction in waves. A comprehensive review of SWATH ships has been made by McGregor[20].

In this section, the 3D hydrodynamic analysis is performed on a tandem strut SWATH ship. The different wave heading and forward speeds were considered. Parametric investigations include hydrodynamic coefficients, wave exciting forces and motion responses of the twin hulls. The effects of standing waves are specially discussed.

The viscous effects are taken into account by a semi empirical iterative method. The comparison has also been made with the results from 2D predictions and the experiments.

The model is shown in Fig.4.51 with the principal particulars listed in the Table 4.1. The model was represented by 356 panel elements.

4.3.1 Hydrodynamic Coefficients

The hydrodynamic coefficients calculated by 3D theory are shown in the Fig.4.52-4.63. The results are represented in two groups, vertical modes (surge, heave and pitch) and the transverse modes (sway, roll and yaw) including their coupling terms as well. In the present theory, the only speed dependent hydrodynamic coefficients are in pitch and yaw and their coupling modes. Therefore only these speed dependent coefficients are shown in two different cases associated with the Froude numbers of F_n=0.0 and F_n=0.261 (i.e. U=0.0m/s and U=1.0m/s). The others are all speed independent. From the Green's second identity, it can be proved that at zero speed $A_{ij}=A_{ji}$ and $B_{ij}=B_{ji}$, but in practical numerical calculation this can not be satisfied absolutely. The double curves in the coupling coefficients at zero speed indicate the error of the calculations. One curve represents A_{ij} or B_{ij} and the other A_{ji} or B_{ji}.

I, Vertical oscillations

In the first group of results Fig.4.52-4.57, vertical mode coefficients are presented. The most distinct feature in those results are the effects of the symmetric standing waves at $\omega_e\sqrt{(L/g)}\approx 3.875$, the corresponding $\lambda_e/B_i\approx 0.937$ ($\lambda_e=2\pi g/\omega_e^2$). Since the twin hull of the SWATH model is quite separate and there also is a gap between the two struts on the same hull, the standing wave effect is not as strong as those in the case of the twin cylinders discussed in the Section 4.3 and the effect of the first vertical standing wave on hydrodynamic coefficients is not visible.

At F_n=0.0 the standing wave at $\omega_e\sqrt{(L/g)}\approx 3.875$ introduces the minimum values on the curves of A_{11}, A_{33}, A_{55} and A_{35} and the peak values on the corresponding damping terms B_{11}, B_{33}, B_{55} and B_{35}. For the A_{13}, A_{15}, B_{13} and B_{15} the influences of the vertical

standing waves are in different direction because the values of these coefficients seem up side down from the former.

It is interesting to note that the forward speed does not change the encounter frequencies of the standing waves which stay at $\omega_e\sqrt{(L/g)}\approx 3.875$ at $F_n=0.261$. This is expected (see Table 2.1) because the speed dependent terms of the coefficients are based on the corresponding zero speed coefficients which all have rapid changes at the frequency of the standing waves. The ways in which the standing wave exert an influence are also dependent on the speed dependent term of each coefficient. For example, the speed dependent terms of A_{35} and A_{53} are $-(U/\omega_e^2)B_{33}^0$ and $+(U/\omega_e^2)B_{33}^0$, where the B_{33}^0 indicates the corresponding value of B_{33} at zero speed, so the peak of B_{33}^0 at standing wave frequency results minimum or maximum values on the curves of A_{35} and A_{53} respectively.The result satisfies the Timman-Newman relationship.

The dashed lines in the damping coefficients indicate the damping coefficients including viscous effect. This is predicted by a semi-empirical iterative method presented in the Section 4.3.2. Because the viscous effect is motion dependent, the present results were obtained by assuming the SWATH model under the bow quartering sea ($\beta=135^0$) and the wave amplitude of 0.02m. In fact, if the wave heading and amplitude are changed the results do not change significantly except those near the motion natural frequencies. The damping coefficients show that the viscous damping gives a considerable contribution to the total damping except at the frequencies of the standing waves. As discussed previously, at frequencies of standing waves the standing waves can cause very large wave damping which dominates the total damping, so the viscous contribution is relatively small. In the lower and middle frequency range which is the range of practical interest, the viscous damping dominates the B_{33}, B_{55} and B_{35}. As shown in the motion responses for vertical modes, the viscous effect influences the motion responses significantly near the motion natural frequencies.

II, Transverse oscillations

The results of the transverse mode coefficients are shown in Fig.4.58-4.63. The

two asymmetric standing waves are evaluated to be at $\omega_e\sqrt{(L/g)}\approx 2.875$ and $\omega_e\sqrt{(L/g)}\approx 4.5$, corresponding to $\lambda_e/B_i\approx 1.425$ and 0.695. Comparing the B/L value of the present tandem strut model with those in Table 4.2, the corresponding value of λ_e/B_i for the standing waves are justifiable. The both standing waves in the present results produce rapid changes from the maximum values to the negative minimum on the curves of A_{22} and A_{66} and the ω_{e2} seems to be the turning point. The standing waves also produce peak values on the damping curves of B_{22} and B_{66} at F_n=0.0 and F_n=0.261. For all the A_{44}, A_{24}, B_{44} and B_{24}, the standing waves introduce maxima. The results show that the standing waves effect the hydrodynamic coefficients in transverse modes significantly.

The total damping including the viscous effect is also presented in the in the same figures. In contrast to those in the vertical modes, the viscous damping in transverse modes is much less significant. Although the viscous damping in transverse modes has the same order of magnitude as those in vertical modes , its contributions to the total damping is limited because the potential wave damping is an order higher than in the vertical modes. In Fig.4.61, it is seen that the wave damping in roll mode B_{44} is much less than B_{22} and B_{66}, so the viscous effect is clearer. At forward speed, the results predicted by present 3D theory satisfies the Timman-Newman relationship.

4.3.2 Viscous Effect

The viscous effect due to drag has been discussed in detail for SWATH ships by Lee and Curphey[14] in five degrees of freedom. Their method is based on the empirical formula given by Thwaites[21] from the crossflow approach to a slender body at a moderate angle of incidence in a uniform flow. In order to extend this approach to the six degrees of freedom for SWATH ships or other type of semi-submersibles (for example, the semi-submersible crane barge in the Chapter 5). The structure is divided into two sets of strips parallel to the x and z axes. Then suitable pointson each strip contour are chosen as representative point for evaluating the relative velocity. Based on the crossflow approach, a pseudo-steady-state assumption has to be made to apply the method to an oscillatory body and the viscous interaction between the twin hulls is neglected. Then the viscous forces and moments due to drag in six degrees may be approximated as

$$\Delta F_{D1} = 0.5\rho\Delta S_1 C_D \dot{\xi}_{r1}|\dot{\xi}_{r1}|$$
$$\Delta F_{D2} = 0.5\rho\Delta S_2 \left[U^2 a_0 \alpha_1(x) + C_D \dot{\xi}_{r2}|\dot{\xi}_{r2}| \right]$$
$$\Delta F_{D3} = 0.5\rho\Delta S_3 \left[U^2 a_0 \alpha_2(x) + C_D \dot{\xi}_{r3}|\dot{\xi}_{r3}| \right]$$
and (4.5)
$$F_{Di} = \Sigma\Delta F_{Di} \qquad \text{for} \quad i=1,2,3$$
$$F_{D4} = -\Sigma z\Delta F_{D2} + \Sigma y\Delta F_{D3}$$
$$F_{D5} = -\Sigma x\Delta F_{D3} + \Sigma z\Delta F_{D1}$$
$$F_{D6} = -\Sigma y\Delta F_{D1} + \Sigma x\Delta F_{D2}$$

where the two parts of the viscous effects involved in the crossflow approach are the viscous lift (associated with the viscous lift coefficient a_0) and the crossflow drag (associated with the crossflow drag coefficient C_D). The ΔS_1 is the projected area of the strip along z axis in x direction, and ΔS_2 and ΔS_3 are the projected area of the strip along x axis in y and z directions respectively, $\dot{\xi}_{r1}$, $\dot{\xi}_{r2}$ and $\dot{\xi}_{r3}$ are relative velocity components in the x, y and z directions. ΔF_{Di} indicates the element of viscous force in ith direction, and $\alpha_1(x)$ and $\alpha_2(x)$ are the angles of incidence of flow at the representative point of a strip in x-y plane and x-z plane.

It is clear the viscous lift forces only act on the body in y and z directions with the angles of incidence $\alpha_1(x)$ and $\alpha_2(x)$. Since $\alpha_1(x)$ and $\alpha_2(x)$ are small, the diffraction effect is neglected. The relative velocity components in x, y and z directions can be written as

$$\dot{\xi}_{r1} = -\dot{\xi}_1 - z\dot{\xi}_5 + y\dot{\xi}_6 + \zeta_x'$$
$$\dot{\xi}_{r2} = -\dot{\xi}_2 - x\dot{\xi}_6 + z\dot{\xi}_4 + \zeta_y' \qquad (4.6)$$
$$\dot{\xi}_{r3} = -\dot{\xi}_3 - y\dot{\xi}_4 + x\dot{\xi}_5 + \zeta_z'$$

where the velocity components of a wave particle in x, y and z directions are

$$\zeta_x' = \frac{\partial \phi_0}{\partial x} e^{-i\omega t}$$

$$\zeta_y' = \frac{\partial \phi_0}{\partial y} e^{-i\omega t} \qquad (4.7)$$

$$\zeta_z' = \frac{\partial \phi_0}{\partial z} e^{-i\omega t}$$

where

$$\begin{bmatrix} \frac{\partial \phi_0}{\partial x} \\ \frac{\partial \phi_0}{\partial y} \end{bmatrix} = \begin{bmatrix} \cos\beta \\ \sin\beta \end{bmatrix} a\,\omega \exp\left[ik\,(x\cos\beta + y\sin\beta) \right] \exp(kz)$$

$$\frac{\partial \phi_0}{\partial z} = -\,ia\omega \exp\left[ik\,(x\cos\beta + y\sin\beta) \right] \exp(kz)$$

$$\alpha_1(x) = \frac{\dot{\xi}_{r2}}{U} - \xi_6$$

$$\alpha_2(x) = \frac{\dot{\xi}_{r3}}{U} + \xi_5 \qquad (4.8)$$

In the foregoing expressions, Eqn.(4.6), the crossflow drag terms are nonlinear, hence, they can not be directly introduced into the linear motion equations. By using Fourier Series, it can be shown that

$$\cos\theta \left| \cos\theta \right| = \sum_{n=1}^{\infty} a_{2n-1} \cos(2n-1)\theta$$

where

$$a_n = 0 \qquad \text{for n even}$$

$$a_n = (-1)^{\frac{n+1}{2}} \frac{8}{n(n^2-4)\pi} \qquad \text{for n odd}$$

$$a_1 = \frac{8}{3\pi}, \quad a_3 = \frac{8}{15\pi}, \quad a_5 = \frac{8}{105\pi} \ \ldots\ \ldots\ .$$

Taking the first term yields an equivalent linear approximation

$$\cos\theta \,|\cos\theta| \approx \frac{8}{3\pi}\cos\theta$$

and for any harmonic motion given by $x = x_0\cos\omega t$, the approximation is

$$\dot{x}\,|\dot{x}| \approx \frac{8}{3\pi}\omega\dot{x}_0\dot{x}. \qquad (4.9)$$

Substituting (4.6) and (4.8) into (4.5) and applying the equivalent linearization procedure of equation (4.9) gives

$$\Delta F_{D1} = \frac{4}{3\pi}\rho\Delta S_1 C_D \dot{\xi}_{r10}\dot{\xi}_{r1}$$

$$\Delta F_{D2} = \frac{1}{2}\rho\Delta S_2\left[-a_0U^2\xi_6 + a_0U\dot{\xi}_{r2} + \frac{8}{3\pi}C_D\dot{\xi}_{r20}\dot{\xi}_{r2}\right] \qquad (4.10)$$

$$\Delta F_{D3} = \frac{1}{2}\rho\Delta S_3\left[-a_0U^2\xi_5 + a_0U\dot{\xi}_{r3} + \frac{8}{3\pi}C_D\dot{\xi}_{r30}\dot{\xi}_{r3}\right]$$

where $\dot{\xi}_{r10}$, $\dot{\xi}_{r20}$ and $\dot{\xi}_{r30}$ are amplitude of $\dot{\xi}_{r1}$, $\dot{\xi}_{r2}$ and $\dot{\xi}_{r3}$, and can be written as

$$\dot{\xi}_{r10} = \omega_e\left[\left[\mathrm{Re}(\xi_{r1})\right]^2 + \left[\mathrm{Im}(\xi_{r1})\right]^2\right]^{\frac{1}{2}}$$

$$\dot{\xi}_{r20} = \omega_e\left[\left[\mathrm{Re}(\xi_{r2})\right]^2 + \left[\mathrm{Im}(\xi_{r2})\right]^2\right]^{\frac{1}{2}} \qquad (4.11)$$

$$\dot{\xi}_{r30} = \omega_e\left[\left[\mathrm{Re}(\xi_{r3})\right]^2 + \left[\mathrm{Im}(\xi_{r3})\right]^2\right]^{\frac{1}{2}}.$$

Then the viscous force can be split into viscous damping, viscous restoring and viscous wave exciting force terms, i.e.

$$F_{Di} = -\sum_{j=1}^{6}\left[B_{vij}\,\dot{\xi}_j + C_{vij}\,\xi_j \right] + F_{vj} \quad \text{for } i=1,2...6, \tag{4.12}$$

where viscous wave exciting forces may be expressed as

$$\begin{aligned}
F_{v1} &= \sum a_x\,\dot{\xi}_{r10}\,\zeta'_x \\
F_{v2} &= \sum a_y\,\dot{\xi}_{r20}\,\zeta'_y \\
F_{v3} &= \sum a_z\,\dot{\xi}_{r30}\,\zeta'_z \\
F_{v4} &= \sum y\,a_z\,\dot{\xi}_{r30}\,\zeta'_z - \sum z\,a_y\,\dot{\xi}_{r20}\,\zeta'_y \\
F_{v5} &= \sum z\,a_x\,\dot{\xi}_{r10}\,\zeta'_x - \sum x\,a_z\,\dot{\xi}_{r30}\,\zeta'_z \\
F_{v6} &= \sum x\,a_y\,\dot{\xi}_{r20}\,\zeta'_y - \sum y\,a_x\,\dot{\xi}_{r10}\,\zeta'_x
\end{aligned} \tag{4.13}$$

with

$$(a_x, a_y, a_z) = -\frac{4}{3\pi}\,\rho\, C_D\,(\Delta S_1, \Delta S_2, \Delta S_3)\,.$$

All these viscous terms are dependent on the motion amplitude, therefore they will be determined simultaneously with the solution of the motion equation by an iterative procedure.

For the present SWATH model to two hull are treated separately. The representative points of the strips are chosen at the middle of the strip along z axis for ΔS_1, the one-half draught of the strip along the x axis for ΔS_2 and the centre of the sub-hull for the strip along x axis for ΔS_3. All of them are on the centre line of the demi-hull.

4.3.3 Wave exciting forces

The wave exciting forces and moments are calculated for three different heading, head sea ($\beta=180^0$), bow quartering sea ($\beta=135^0$) and beam sea ($\beta=90^0$). at $F_n=0.0$ and $F_n=0.261$ (i.e. U=0.0m/s and U=1.0m/s). The components of Froude-Krylov force and diffraction force are also shown in the results. The abscissa is non-dimensional wave frequency.

Head sea

Fig.4.64-4.66 present the wave exciting forces in head sea with Fn=0.0 and Fn=0.261. In surge forces, the Froude-Krylov force dominates the total wave excitation, but in heave and pitch, the effect of diffraction component is obvious. At $\omega\sqrt{(L/g)}\approx3.875$ (or $\omega\sqrt{(L/g)}\approx2.338$ at $F_n=0.261$), there are peaks on all the curves of surge, heave and pitch forces which are caused by the symmetric standing waves.

Bow quartering sea

As shown in Fig.4.67-4.72, the diffraction in this heading is more significant than those in the head sea case. In the vertical modes, it is clear that the vertical diffraction standing wave at $\omega\sqrt{(L/g)}\approx3.875$ ($\omega\sqrt{(L/g)}\approx2.615$ for Fn=0.261) introduces peak values in surge, heave and pitch forces. In the transverse modes, the diffraction component contributes the largest part of the total excitation. At zero speed, the two transverse standing waves at $\omega\sqrt{(L/g)}\approx2.875$ and at $\omega\sqrt{(L/g)}\approx4.5$ produce peak values on the sway and yaw forces (F_2 and F_6). For roll mode F_4, this effect is smaller, but its influence on the diffraction components is still clear in the results.At $F_n=0.261$, it is interesting to note that the first asymmetric standing wave at $\omega\sqrt{(L/g)}\approx2.079$ (corresponding encounter wave frequency $\omega_e\sqrt{(L/g)}\approx2.875$) influences a greater influence on F_2, F_4 and F_6 than at zero speed. The effect of the second asymmetric standing wave at $\omega\sqrt{(L/g)}\approx2.934$ (corresponding encounter wave frequency $\omega_e\sqrt{(L/g)}\approx4.5$) is much less significant than at zero speed.

Beam sea

The wave exciting forces at zero speed are shown from Fig.4.73-4.75. Because the

model is nearly fore-aft body symmetric, the surge, pitch and yaw forces are much smaller than the other forces, so only the forces in sway, heave and roll modes are shown here. The diffraction effects are more important in sway and roll than those in the heave. The symmetric standing wave produces a peak in heave exciting force at $\omega\sqrt{(L/g)}\approx 3.975$. The asymmetric standing waves at $\omega\sqrt{(L/g)}\approx 2.875$ and $\omega\sqrt{(L/g)}\approx 4.5$ cause the peak excitation values in the curves of F_2 and F_4.

4.3.4 Motion responses

The hydrodynamic coefficients and wave exciting forces/moments calculated in previous sections were introduced into the coupled motion equations in six degrees freedom. The results of motion responses in head seas(180^0), bow quartering seas(135^0) and beam seas(90^0) were compared with experimental and 2D strip theory results which were obtained from the strip theory program, SWATH L, developed by Atlar[22]. The results are shown in Fig.4.76-4.82. The comparison was also made for the forward speed cases in head seas associated with F_n=0.13 (0.5m/s) and F_n=0.26 (1m/s). The 3D theory has considered the viscous effects by the method described in section 4.3.2, but 2D results are without the viscous effects.

Due to small waterplane area and deep submerged main hull, the SWATH ships usually have small wave damping comparing with mono conventional mono hull, consequently the contribution from viscous damping is very large. The viscous effects on motion responses are shown in Fig.4.76. The results show that the viscous effects influence the motion responses significantly near the motion resonant frequencies. When the viscous effects are considered the results are significantly improved and agree well with experiments even in the range of motion resonances.

Head seas

The head seas results for different forward speeds are presented in Fig.4.77-4.79 for surge , heave and pitch respectively. The surge responses predicted by 3D theory generally agree well with experimental results, but it fail to predict the peak near $\omega_e\sqrt{(L/g)}=1.0$ satisfactorily. This peak is caused by the coupling effect from pitch

resonance. It can be seen the pitch resonance is underpredicted as well. If the viscous effect is reduced, both pitch and surge responses near $\omega_e\sqrt{(L/g)}=1.0$ can be improved. The 2D theory neglects the surge motion, so no results can be predicted.

At zero speed, the heave and pitch responses from both 2D and 3D theories agree well with the experiments,but 3D results are better than 2D. The predictions by 2D theory near the heave and pitch resonant frequencies are too high. These can be reduced by introducing the viscous effects. For forward speed cases, the difference between 2D and 3D theories is clear. In the case of $F_n=0.13$, the 2D results are clearly unsatisfactory. These results may be improved by including viscosity, but the 3D effect on this tandem strut model is another reason.The 2D results of pitch responses near its resonant frequency at $F_n=0.13$ may be improved by including viscosity, but the heave responses are already lower than the experimental values and will be further reduced if viscosity is taken into account.

Bow quartering seas

3D results for surge responses generally agree well with experiments and are underpredicted near $\omega_e\sqrt{(L/g)}=1.0$ where the peak is caused by coupling effect from pitch resonance. The pitch responses predicted by 3D theory are lower than experiments near its resonance. This is due to the too large viscous correcting term. Reducing viscous effects, the responses of both pitch and surge can be improved.The agreement between 3D results and experiments for heave responses is good, but 2D results are poor in the important medium frequency range. The peak near $\omega_e\sqrt{(L/g)}=1.0$ can be improved by including viscosity, but this will further reduce the peak near $\omega_e\sqrt{(L/g)}=1.5$ which is already underpredicted. The pitch responses predicted by 2D theory are too high at lower frequencies. at higher frequencies the 2D prediction agree well with the experiments.

In sway and yaw modes, it is clear that 2D theory does not predict the motion responses satisfactorily, but 3D theory does well. the 3D results for roll mode agree with the experiment better than 2D results. The 2D results are too high at heave resonance and also in the range of $\omega_e\sqrt{(L/g)}=1.5$-2.5.

Beam seas

The results from the both 2D and 3D agree well with the experiments except for the 2D results near the roll resonant frequency. The overprediction by 2D theory on sway and roll responses near roll resonance is due to the lack of viscous effect.

It is interest to note that the sway responses in beam seas. The first peak near $\omega_e\sqrt{(L/g)}=1.0$ is caused by coupling effect from roll resonance. The second peak from $\omega_e\sqrt{(L/g)}=2.5\text{-}4.0$ is the result of asymmetric standing waves. On the curve of sway wave exciting forces in beam sea (Fig.4.73) there also is a peak in the same frequency range. This is produced by the standing waves and causes the second peak in sway responses. The experiments have shown the this peak and the predictions agree well with the experiments.

Generally, both 2D and 3D theories produce satisfactory results in head and beam seas. The 3D results are better than 2D. The difference between the two theories occurs in quartering seas. In bow quartering seas, the 2D results are generally poor, specially for sway, heave and roll modes (at least for present model), but 3D results agree well with the experiments.

4.4 Conclusions

On validating the theory

1, From the very good agreement between the present 3D theory and the other 3D theory on hydrodynamic coefficients, wave exciting forces and motion responses of Series 60 model, it can be concluded that the modified numerical procedure is identical to the original one, but it increases the computational efficiency considerably.

2, The 3D method gives more realistic values for the low frequency hydrodynamic coefficients unlike 2D theory which is restricted to high frequencies of oscillation. In spite of these differences both 3D and 2D method predict motion responses which agree quite closely. This is due to the fact that at lower frequencies, where 2D and 3D theory differ most, the equations of motion are dominated by the stiffness and wave exciting terms.

On standing waves

1, Standing waves occur at certain combinations of wave frequencies and the spacing between the twin hulls. Its effect on the hydrodynamic features of twin hull ships is significant and can be predicted by present theory satisfactorily.

2, Two types of standing waves with different natures may occur in the vicinity of the twin hull ships, i.e. longitudinal and transverse standing waves. The longitudinal standing waves occur at $2L_s/\lambda=n$ and transverse standing waves occur at $2B_i/\lambda=n$, where L_s is length of strut, B_i is inner distance of the twin hulls, λ is the wave length and n is any integer number.

3, Theoretically there are infinite number of standing waves could occur, but their effect decreases significantly as the standing wave frequency increases. Therefore only the first few standing waves with the lowest frequencies have serious effect and are of primary interest. The first longitudinal standing wave usually has the lowest frequency and can therefore cause the most serious effects which may produce the maximum upwelling and side forces on the structures.

4, The conclusions made for longitudinal standing waves are mainly based on the theoretical calculations. Therefore, systematic experiments are needed to support the present finding. If the finding is true, those longitudinal standing waves are three dimensional effects and subsequently the three dimensional method should be used in the predictions.

On SWATH ships

1, Both 3D and 2D strip theory can be applied for predicting motion responses of SWATH ships in waves, but the 3D theory is more reliable. If only head and beam seas cases are interesting, the 2D theory is acceptable. Otherwise if oblique seas are also need to be predicted, the 3D theory is recommended.

2, The viscous effect on SWATH ships can be predicted by combining the crossflow approach with present theory. This effect must be included in prediction the motion responses of SWATH ships.

CHAPTER FIVE

PREDICTION OF MOTION AND SLING TENSION RESPONSES OF CRANE VESSELS DURING HEAVY LIFT OPERATION IN REGULAR WAVES

The motion of a crane vessel during heavy lift operation is quite different from that in its free floating condition since it is significantly influenced by the coupling between the motions of the vessel and the load being lifted. Consequently it is important in the design of such a vessel that an appropriate method which takes the coupled motion effect into consideration is used to predict the motion responses and sling tension force.

In the past, many theoretical methods[1,2] have been used to calculate the wave load and motion responses of mono and twin hull ships, but very few papers have dealt with the crane vessel with the coupled motion effect. In this chapter the theoretical method is modified to include the effect of the coupled motion in 8 degrees freedom using a similar approach as[3], but additionally the viscous effect is taken into account. The results show that the viscous effect plays a sensitive role in the prediction of the motion response when the coupled motion effect is included, especially for the semi-submersible type of crane vessels. Two typesof crane vessels, ship shaped and semi-submersible, are analysed in this study, so 3D diffraction theory is the most suitable method.

In contrast to the the SWATH ship or ordinary semi submersible, the semi submersible crane vessel has the columns which relatively short and the cross section dimension are similar in size to the hull separation and the column submergence. The three dimensional effect between the pontoon and the columns as well as the twin hulls are dominated in this case, so the strip theory and the Morison approach are inadequate to use due to their limitations, and the three dimensional diffraction theory is believed to be the most suitable method and used here to predict the hydrodynamic forces on the submerged

part of the vessels.

Both motion responses, with and without the coupled motion effect of the load being lifted and the sling tension force, are calculated. Some of the results have been compared with the experiments. The agreement is generally very good. The results show that such coupled motion effects on the motion performance of the crane vessel are great. It is therefore considered necessary in the design of crane vessels that the coupled motion effect is taken into account when predicting the motion response.

5.1 Motion Prediction Method

5.1.1 Motion of vessel

In order to describe the motion of the vessel and the load being lifted, it is appropriate to divide the entire system into two parts, the vessel and the load alone. Both of them satisfy Newton's second law. Small wave and motion amplitudes are assumed in order to apply linear theory. A right handed Cartesian coordinate system o-xyz with x-y plane in still water surface and z positive upward through the centre of the gravity is used. For the vessel, the six-degree-motion equations with viscous effect may be written as

$$\sum_{j=1}^{6}\left[(M_{ij} + A_{ij})\ddot{\xi}_j + (B_{ij} + B_{vij})\dot{\xi}_j + C_{ij}\,\xi_j \right] = F_i + F_{vi} + f_i$$

$$i=1,\ 2,\ \ldots 6 \qquad (5.1)$$

where M_{ij} is generalized inertia matrix of the vessel alone. A_{ij}, B_{ij} and C_{ij} are added mass, wave damping and hydrostatic restoring coefficients, F_i is wave exciting force, B_{vij} and F_{vi} are viscous damping and viscous wave exciting force due to drag, i, j = 1,6 denote the motion modes of surge, sway, heave, roll, pitch and yaw respectively, $\xi_i = \xi_{i0}\, e^{-i\omega t}$ is the displacement of motion in ith mode with the amplitude of ξ_{i0}, and f_i is the component of the tension force on the sling cable, f, in ith direction about the origin.

5.1.2 Motion of load

To describe the motion of the load relative to the coordinate system o-xyz, two additional variables φ_1 and φ_2, the swing angles of the load about x, y axes, are introduced. If small swing angles are assumed, the motion equation of the load alone can

be derived in x, y and z directions respectively, as

$$
\begin{aligned}
f\varphi_2 + ml\ddot{\varphi}_2 &= m\,(\ddot{\xi}_1 + \chi_3\ddot{\xi}_5 - \chi_2\ddot{\xi}_6) \\
-f\varphi_1 - ml\ddot{\varphi}_1 &= m\,(\ddot{\xi}_2 - \chi_3\ddot{\xi}_4 + \chi_1\ddot{\xi}_6) \\
f - mg &= m\,(\ddot{\xi}_3 + \chi_2\ddot{\xi}_4 - \chi_1\ddot{\xi}_5)
\end{aligned}
\qquad (5.2)
$$

where l is the cable length, χ_1, χ_2 and χ_3 are coordinates of the jib extremity in x, y and z directions and m is the mass of the load. The dynamic tension on the cable is $f_d = f - mg$.

5.1.3 Motion of coupled system

Substituting eqn. (5.2) into (5.1) and taking account of different direction of the tension force f acting on the jib and the load gives

$$
\sum_{j=1}^{6} \left[(\bar{M}_{ij} + A_{ij})\,\ddot{\xi}_j + (B_{ij} + B_{vij})\,\dot{\xi}_j + \bar{C}_{ij}\,\xi_j \right] - m\,\ddot{\xi}_{Ri} = F_i + F_{vi}
$$

$$
i = 1, 2, \ldots 6 \qquad (5.3)
$$

where $\ddot{\xi}_{Ri}$ is the relative acceleration of the load to the o-xyz in ith direction with

$$
\ddot{\xi}_{Ri} = l\,(\ddot{\varphi}_2, \ddot{\varphi}_1, 0) \qquad \text{for } i = 1, 2, 3
$$

and

$$
\ddot{\xi}_{Ri} = l\,(\chi_1, \chi_2, \chi_3) \times (\ddot{\varphi}_2, \ddot{\varphi}_1, 0) \qquad \text{for } i = 4, 5, 6.
$$

The exact relative acceleration in z direction, $\ddot{\xi}_{R3} = l\,(\dot{\varphi}_1^2 + \dot{\varphi}_2^2)$, is a higher order term which has already been neglected in the formula. $\bar{M}_{ij}$ and $\bar{C}_{ij}$ are the inertia and restoring coefficient matrices of the entire system when the load is located at the top of the jib respectively.

The system of equation (5.2) and (5.3) is solvable and also applicable for any type of crane vessels. In this chapter both ship shaped and semi-submersible type of crane vessels are analysed, so 3D diffraction theory is adopted to yield the potential terms such as A_{ij}, B_{ij} and F_i. The 3D source-doublet distribution method is used. There are several

detailed papers[1,2] available for this method, so no description of it is represented here.

5.1.4 Dynamic sling tension

If the motion responses are known, the dynamic sling tension can be obtained by the last equation of Eqn.(5.2).

5.1.5 Viscous effect

The viscous terms, B_{vij} and F_{vi} play the sensitive role when the coupling effect between the vessel and the load is taken into account and must be considered. Two different empirical methods are used for ship shaped and semi-submersible types of vessels separately.

For the ship shaped crane vessel the experiments show that the peak values at resonant frequency in roll model is not predicted correctly when the coupling effect is considered, therefore the viscous effect must be included in the prediction. In this study it was found that the rolling viscous damping B_{v44} is the most important term and the other may be neglected. The B_{v44} can be estimated by the method of Ikeda, Himena and Tanaka[4] which is common in prediction of viscous damping for mono hull ships.

The viscous effect on the semi-submersible type of crane vessel is more sensitive in the vertical modes than those on the ship shaped one, because its small waterplane area makes it have small wave damping especially in the vertical modes of motion (heave and pitch) and the contribution of the viscous effect to the total damping becomes more important. The viscous effect due to drag has been discussed in detail for SWATH ships by Lee and Curphey[5] and McGregor, et.al.[6] in five degrees of freedom. Their estimating method is based on the empirical formula given by Thwaites[7] from crossflow approach to a slender body. This approach has extended to the six degrees of freedom in order to be applied to the semi-submersible crane vessel. The detail description has already given in section 4.3.2. For the present problem the general equation in section 4.3.2 will be set for special case that forward speed U = 0.0 and $C_D = 0.5$

5.2 Multi resonant frequencies

The resonant frequencies on the curves of motion responses of a crane vessel with the effect of the load being lifted do not coincide with those without such an effect and the natural frequency of the pendulum. The multi resonant frequencies may occur on one single mode of motion, therefore in practice it is important to predict such resonant frequencies.

To simplify the problem, the coupling effects between surge and pitch, heave and pitch are neglected. The resonant frequencies of the the coupled motion system can be obtained from equation (5.2) and (5.3), that is,

$$\omega_{1,2} = \frac{(\omega_P^2 + \omega_L^2) + \sqrt{(\omega_p^2 - \omega_L^2)^2 + 4\frac{m_{55}}{\bar{M}_{55} + A_{55}}\omega_P^2\omega_L^2}}{2\left(1 - \frac{m_{55}}{\bar{M}_{55} + A_{55}}\right)} \qquad (5.4)$$

where $\omega_P^2 = \frac{\bar{C}_{55}}{\bar{M}_{55} + A_{55}}$, $\omega_L^2 = \frac{g}{L}$ and $m_{55} = m\,l_3^2$, and ω_P is the resonant frequency of the pitch motion, ω_L is the resonant frequency of the pendulum, $\bar{M}_{55}$ and $\bar{C}_{55}$ are the pitch inertia and restoring coefficient of the entire system respectively, and m_{55} the pitch intertia of the load alone.

When $m_{55}/(\bar{M}_{55}+A_{55}) \approx 0.0$, the ω_1 and ω_2 equal to ω_P and ω_L respectively, that means the load effect is too small to effect the motion responses of the entire system. The greater value of $m_{55}/(\bar{M}_{55}+A_{55})$, the greater differences between ω_1, ω_2 and ω_P, ω_L will be. One simple relationship can be adopted, i.e.

$\omega_1 \le \omega_P$ and $\omega_L \le \omega_2$.

For the roll motion, a similar relationship can be found

$$\omega_{1,2} = \frac{(\omega_R^2 + \omega_L^2) + \sqrt{(\omega_R^2 - \omega_L^2)^2 + 4\frac{m_{44}}{\bar{M}_{44} + A_{44}}\omega_R^2\omega_L^2}}{2\left(1 - \frac{m_{44}}{\bar{M}_{44} + A_{44}}\right)} \qquad (5.5)$$

where $\omega_R^2 = \frac{\overline{C}_{44}}{\overline{M}_{44} + A_{44}}$, $\omega_L^2 = \frac{g}{L}$ and $m_{44} = m\, l_3^2$, and ω_R is resonant frequency of the roll motion, $\overline{M}_{44}$ and $\overline{C}_{44}$ are the roll inertia and restoring coefficient of the entire system respectively, and m_{44} is the roll inertia of the load alone. There is a similar relationship.

$\omega_1 \leq \omega_R$ and $\omega_L \leq \omega_2$.

In the computation, the coupling effect between different modes of motions is included and the results are different from the simplified prediction formula. In some cases the coupling effect is not very strong, for example the load is small compared with the total displacement (say less than 5%) or abaft lifting in head sea, the above formula can be used to roughly predict the multi resonant frequencies. This is often its case and so the prediction formula is valuable. Some examples are given in Table 2. In the table the calculated values are read from the computation and the estimated values are obtained from the formula (5.4) and (5.5).

5.3 Numerical results

Two types of crane vessels, ship shaped and semi-submersible as shown in Fig.5.1 and Fig.5.2, are analysed. The semi-submersible crane vessel is examined for free floating (without the load) and two lifting conditions, abaft (A) and athwartship (B). The principal particulars of the vessels are listed in the Table 5.1. The models are represented by 120 panel elements for the ship shaped vessel and 272 for semi- submersible.

Table 5.1 Principal Particulars of Crane vessels

	Ship Shaped	Semi-sub (Free floating)	Semi-sub (Cond. A)	Semi-sub (Cond. B)
L, B, d (m)	2.0, 0.76, 0.0974	1.82, 1.164, 0.318	1.82, 1.164, 0.350	1.82, 1.164, 0.33
▽(kg)	135.1	249.2	261.66	254.18
KG (m)	0.381	0.242	0.270	0.255
GM_L, GM_T (m)	0.208, 3.416	0.145, 0.538	[illegible]	0.132, 0.523
K_{xx}, K_{yy}, K_{zz} (m)	0.481, 0.977, 0.882	0.407, 0.525, 0.66[illegible]	[illegible]	0.453, 0.550, 0.66[illegible]
K_{xy}, K_{yz}, K_{zx} (m)	0.0, 0.0, -0.54	0.0, 0.0, 0.0	0.0, 0.0, 0.26	-0.062, 0.139, 0.078
Load (kg)	19.5	0.0	12.46	4.98

The results for the ship shaped vessel are shown in Fig.5.3 against the non-dimensional frequency $\omega\sqrt{(L/g)}$. The most distinct feature of the results is that the coupling motion effects introduce the multi resonant frequencies on the curves of the motion responses and the dynamic sling tension, unlike the motion responses of the vessel without the load which usually have only one resonant frequency on each mode of motion. As discussed previously, the resonant frequencies are closely related to the resonant frequencies of uncoupled vessel and the load, but usually do not coincide with them. For the ship shaped vessel, the multi resonant frequencies of pitch and roll in head and beam seas are listed in the Table 5.2. The estimated values of pitch resonant frequencies in the head sea agree well with the calculated values, whereas for the roll motion in the beam sea the agreement is not good. The reason may be attributed to the roll-yaw coupling effect. If the coupling term K_{xz} is set to zero, the agreement is good (not presented). In this case the mass of the load is about 15% of the total displacement of the vessel and the K_{xz} is even bigger than K_{xx}, so the roll-yaw coupling effect is very strong. It is also clear that the differences between the multi resonant frequencies of the entire system and the individual frequencies in roll is greater than those in the pitch because the influence fact $m_{44}/(\overline{M}_{44}+A_{44})$ is bigger than $m_{55}/(\overline{M}_{55}+A_{55})$.

Table 5.2 **Multi Resonant Frequencies**

		Ship Shaped		Semi-sub (cond. A)		Semi-sub (Cond. B)	
		Cal.	Est.	Cal.	Est.	Cal.	Est.
Pitch	$\omega_1\sqrt{(L/g)}$	1.50	1.40	1.05	1.08		
	$\omega_2\sqrt{(L/g)}$	2.05	2.12	1.75	1.69		
	$\omega_L\sqrt{(L/g)}$		1.49		1.55		
	$\omega_P\sqrt{(L/g)}$		1.87		1.12		
	$A_{55}/(\Delta L^2)$		0.25		0.08		
Roll	$\omega_1\sqrt{(L/g)}$	1.25	0.95	0.65	0.70	0.70	0.70
	$\omega_2\sqrt{(L/g)}$	2.90	3.24	1.75	1.68	1.65	1.63
	$\omega_L\sqrt{(L/g)}$		1.49		1.55		1.57
	$\omega_R\sqrt{(L/g)}$		1.15		0.63		0.70
	$A_{44}/(\Delta B^2)$		0.15		0.25		0.25

The viscous effect influences the roll response near the resonant frequencies significantly, but for pitch response it is negligible. Generally, the very good agreement

between theoretical and experimental results have been achieved. The experimental data for ship shaped vessel is taken from[3].

The results of the semi-submersible type of vessel are presented in Fig.5.4-5.6 for free floating condition, lifting condition A and B. The results of the free floating condition have been compared with the results for heave and roll in beam sea[8] and the agreements are good.

In the lifting condition A, it can be found that the coupled motion effect on the heave is negligible, whereas on the roll response it is quite clear. On the roll response curve, the coupled motion effect seems to reduce the peak value at the resonant frequencies. The second resonant frequency effect is barely observable when the viscosity is included.

In the head sea, the coupling effect is not as great as those in the beam sea because the $\overline{M}_{55}$ and $\overline{C}_{55}$ are greater than $\overline{M}_{44}$ and $\overline{C}_{44}$. The viscous effect in pitch motion is more sensitive than those in pitch of the ship shaped vessel. This is caused by the relative small pitch wave damping of semi-submersibles comparing with the total damping.

In the lifting condition B, such an effect on the roll motion response is obvious, although the load is less than 2% of the total displacement of the vessel in weight. The viscous effect is important in order to predict correctly the peak value at the second resomant frequency correctly which is usually near the frequency of the peak of the wave spectrum.

The multi resonant frequencies of the entire system for both lifting conditions are listed in the Table 5.2. Generally, the agreements between calculated and estimated values are good because the loads in the both cases are not very heavy comparing with the total displacement (5% for condition A and 2% for B).

5.4 Conclusions

From the present study the following conclusions may be drawn.

1, The coupled motion effects between the vessel and the load being lifted influence the motion response of both ship shaped and semi-submersible crane vessels significantly and must be taken into account in predicting the motion responses.

2, The viscous effect may be neglected in the prediction of the motion responses of the vessel alone, but when the coupling effect of the load is considered it changes the peak values at resonant frequencies especially for the semi-submersible, so it should be included.

3, The estimation formula of resonant frequencies of the entire system may be used to roughly estimate the multi resonant frequencies when the coupling effect between different modes of motion is not so strong.

4, The motion behaviour of the semi-submersible type of crane vessels is generally better than that of the ship shaped one. The former has smaller motion responses and longer natural period of motion which may be beyond the peak of the wave spectrum.

The study presented here shows that the coupled motion effect should be considered in reasonable way in design of crane vessels. The present method may help to reduce the expensive experiments to a minimum in the primary design stage.

CHAPTER SIX

WAVE LOADING ON CROSS-DECK STRUCTURE OF TWIN HULL SHIPS IN REGULAR WAVES

In this chapter, the bending moment, vertical shear force, horizontal shear force and torsional moment acting on the cross-deck structure of SWATH ships in regular waves will be analysed by 3D theory. The hydrodynamic force distributions along the hulls of SWATH are also calculated. The standing wave effect on wave loads of twin hull ships will be discussed. In order to simplify the problem, port and starboard symmetry has been assumed.

In many previous 2D theories, the loading on the cross-deck structure of SWATH ships is calculated under the equivalent two dimensional hull form assumption, so only the beam sea case can be dealt with and the pitch and yaw motion effect is neglected. The torsional moment on the cross-deck is difficult to predict because it often has its maximum value in quartering seas. In the present study, the traditional 2D approach is extended to the 3D case to treat the wave loading on the cross-deck structure for any wave heading . The four major types of wave loads: bending moment, vertical shear, horizontal shear and torsional moment, can be predicted by the present method. Although the maximum torsional moments on cross deck of SWATH are usually much smaller than the maximum bending moments, the combination effect from both of them in oblique seas may produce the maximum local stress on the cross deck. Therefore, it will be necessary to check such kind of loading condition in the primary design stage if the proper prediction method is available.

On the other hand, the side forces and bending moments on cross deck of SWATH in pure beam seas were seen to be the worst wave loading conditions. The recent research[10] has found that the seas approaching from just forward or aft of beam give

biased load distributions which may cause the maximum local stress on the cross deck structure. Since strip theories are only valid in pure beam seas, they can not predict such load distributions along the hull. To overcome this problem the three dimensional theory has been applied in this chapter and the results have been presented.

In order to validate the method a SWATH ship has been analysed and compared with the experimental values. The 3D effect is taken into account in present 3D theory, so the mathematical model for SWATH ships is also applicable to conventional catamarans or semisubmersibles whose demi hull may not as slender as SWATH ships.

6.1 Formula for Wave Loading on Cross-Deck Structure of Twin Hull Ships

As the incident wave propagates past the body, a pressure distribution is established over the hull which tends to excite motion in six degrees of freedom. As motion is excited, additional forces and loads due to the motion itself are generated. The motion prediction method has been presented in the previous chapters. Once the motion is known, the loading may computed.

The first study of wave loads on the cross section of mono hull ships is credited to Jacobs[1] who extended the strip theory for heave and pitch motion in head waves of Korvin-Kroukovsky and Jacobs[2] to include the wave induced vertical shear forces and bending moments for a ship in regular head waves. Later Salvesen et al[3] presented an analysis of all mode loads on a mono hull ship running in oblique waves. The application of 2D theory to prediction of wave loads on the cross-deck structure of twin hull ships is pioneered by Lee and Curphey[4]. In their method an equivalent 2D hull assumption is made and the effects of pitch and yaw motion are neglected and only beam sea case can be dealt with. In the present study, the Lee and Curphey's approach is extended to 3D case including the effect of all six degrees freedom of motion, so the wave loading in oblique wave (any wave direction) can be predicted theoretically.

The maximum torsional moment on the cross-deck usually occurs in bow

quartering sea and is of primary importance in the structure design. In practical design the maximum torsional moment is usually approximated from the maximum side force on the hull in beam sea[5]. From the present study it is clear that there is no direct relationship between the side force and torsional moment. The torsional moment is actually caused by the odd pitch moment which acts on the two hull with opposite direction. Therefore such an approximate method for the maximum torsional moment is open to question. Consequently a proper way to predict this moment is of practical importance in the structure design of the twin hull ships.

Generally, the six components of the loads acting on the cross deck structure are:

1- vertical bending moment: the moment tending to roll the hulls relative to each other,

2- vertical shear force: the force tending to heave the hulls differentially,

3- torsional moment: the moment tending to pitch the hulls with respect to each other,

4- transverse force: the force tending to differentially translate the hulls athwartships (sway),

5- yawing moment: the moment tending to produce differential yawing, and

6- the force tending to produce differential surging.

The first four types of loads may be considered to be of great importance. The other loads are expected to produce stresses in the prototype cross structure about an order of magnitude smaller than the first four types. In this chapter, only the first four types of loads are analysed. The remaining two can be evaluated in the similar manner, but are not discussed here.

In order to formulate the problem, the structure loading may be resolved into following contributing effects.

1- Wave exciting force: This component of structural loading arises from the pressure distribution of the incident wave, when the body is restrained from moving. Based on the linear theory, this component can be further divided into incident wave

exciting force, or Froude-Krylov force, and the wave diffraction force.

2- Motion induced hydrodynamic force: This component arises from the hydrodynamic effect when the body moves in the calm water. The effect of such a force is normally represented as added mass and damping coefficients.

3- Hydrostatic restoring force: This component arises from the change of mean floating position of the body due to its excited motion in waves.

4- Mass inertia force: This component is due to the acceleration of the body when it is moving.

To find the loading at the mid-section of the cross-deck, a standard approach of the structural analysis would be to cut the body at the section where the loading is to be determined and consider all of the forces and moments (both inertia and hydrodynamic) acting on the free end.

If the portion to the right of the cut is taken to be the free end as shown in Fig. 6.1 the moments and shears are given by the mass inertia force minus the total external forces acting on the free portion in a sense which provide the moment or force in a given direction.

The loading at cross-deck mid-section of SWATH ships ($y=0$ and $z=h_0$) is then given.

$$M_b = M_{bI} - \int_{S_R} p \left[n_3 y + n_2 (h_0 - z) \right] ds$$

$$M_T = M_{TI} - \int_{S_R} p \left[n_5 \right] ds \qquad (6.1)$$

$$V_2 = V_{2I} - \int_{S_R} p \left[n_2 \right] ds$$

$$V_3 = V_{3I} - \int_{S_R} p \left[n_3 \right] ds$$

where M_b, M_T, V_2 and V_3 are bending moment, torsional moment, horizontal shear force and vertical shear force respectively, M_{bI}, M_{TI}, V_{2I} and V_{3I} are mass inertia forces of the free end portion and in general depend on all modes of motion, p is the hydrodynamic pressure, S_R denotes the integration over the submerged portion of the demi hull on the right. The same loading quantities must also be obtained if the left hull is taken as the free end and all forces and moments acting on the left hull are considered.

As mentioned in section 4.4.2, all the forces acting on the port and star board hulls of ship can be split into even and odd components. If the foregoing expressions of the loading on the left and right demi-hulls are added together with sign consistent with loading convention and then divided two as shown in Fig. 6.1, the loading at mid-section of cross-deck may be evaluated by using the symmetric and antisymmetric nature of the forces on the two hulls with respect to the centreline. This greatly simplifies the loading analysis.

The even vertical forces acting the the twin hulls in the same direction produce positive bending moments and opposite vertical shear forces on the both right and left free ends, so summation of the bending moments and vertical shear forces from each hull gives twice the bending moment but no vertical shear. In contrast, the odd vertical forces produce no bending moment but twice vertical shear force. An analogous argument can be made for the case of horizontal forces acting on each hull. An even horizontal force produce no bending moment or horizontal shear force but does tend to produce roll and sway responses. An odd horizontal forces produce both a bending moment and horizontal shear force at mid-section of cross-deck.

Similarly, the even pitch moment produces only pitch motion but no torsional moment. The odd pitch moment which acts on both hulls in different directions produces the torsional moment at mid-section of cross-deck. The pitch moment here also includes the mass inertia, hydrostatic and hydrodynamic forces.

Once the loading at mid-section of cross-deck structure is determined, the loading at any section above the waterline can be found. This can be done by subtracting the mass

inertia forces of the portion between the mid-section and the section calculated from the already known loading at the mid-section because the both hydrostatic and hydrodynamic forces acting only on the submerged part of the hull.

The formula of the structural loading at mid-section of cross deck may now be rewritten following the method of summation of the loading on the two free ends described above, i.e.

$$M_b = \frac{1}{2} m y_0 \ddot{\xi} - \frac{1}{2} \iint_S p \left[(n_3 | y |) + n_2 (h_0 - z) \, \mathrm{sgn}(y) \right] ds$$

$$M_T = -\frac{1}{2} \iint_S p \left[n_5 \, \mathrm{sgn}(y) \right] ds \qquad (6.2)$$

$$V_2 = -\frac{1}{2} \iint_S p \left[n_2 \, \mathrm{sgn}(y) \right] ds$$

$$V_3 = \frac{1}{2} M y_0 \ddot{\xi}_4 - \frac{1}{2} \iint_S p \left[n_3 \, \mathrm{sgn}(y) \right] ds$$

where y_0 is the y-coordinate of the centre of gravity, (x_0, y_0, z_0), of the demi hull, as shown in Fig. 6.2 .

It is clear that the heave mass inertia force only contributes to the bending moment, and the roll mass inertia force only to the vertical vertical shear force. Sway inertia force does not effect the horizontal shear because it is an even force. Pitch mass inertia force does not contribute to torsional moment and it is an even force too.

The hydrodynamic pressure p can be expressed as ,

$$p = -i\omega t \left[\Phi_0 + \Phi_D + \sum_{i=1}^{6} \Phi_i \xi_i \right] \rho g \left(\xi_3 + y \xi_4 - x \xi_5 \right) \qquad (6.3)$$

where the terms in the first bracket are the contributions from hydrodynamic effect and

those in the second bracket from the hydrostatic effect. As mentioned previously ϕ_i=1, 3, 5 are even functions and ϕ_i=2, 4, 6 are odd functions. The incident wave and diffraction wave potentials may also be resolved into even and odd components, and denoted by ϕ_0^e, ϕ_0^o, ϕ_D^e and ϕ_D^o respectively.

The dynamic loading at the mid-section of cross-deck, then can be expressed in the simple form listed in Table 6.1-6.4 which only includes the terms contributing to the certain type of loading. The formula of loading at any position of the cross-deck and vertical strut are also listed in the Tables 6.1-6.4.

In the Tables 6.1-6.4, the constant mass distribution over the cross-deck and the vertical strut are assumed. The m_d and m_s represent the mass density per unit span on the cross deck and unit height along the vertical strut respectively. (x_0,y_0,z_0) is the centre of gravity of a demi hull with respect to the coordinate system o-xyz and x_0=0.0. In the first row of Tables 6.1-6.4 , the terms contributing to the loads at the mid-section of the cross-deck given by Eqn.(6.2) are given. The second row of Tables 6.1-6.4 gives the addition contribution which must be included to determine a given load quantity at a location y along the cross-deck. The third row denotes the contributions which must be further included to obtain the load at a vertical location z along the strut. Terms in the third row below the dashed line must be included if z below the waterline ζ=0.0, S_C is the submerged area of the strut between the free surface ζ=0.0 and the cutting section ζ=z, (η,ζ) are dummy variables of the integration about S_C.

All the results of dynamic loading obtained from Table 6.1-6.4 are complex which can be expressed, for example, by $M = M_R + iM_I$

$$| M_b | = \sqrt{M_{bR}^2 + M_{bI}^2} \qquad (6.4)$$

$$\text{Phase} = \tan^{-1} (M_{bI}/M_{bR})$$

The similar relationship can be obtained for torsional moment M_T, vertical shear V_3 and horizontal shear V_2.

The amplitude of motion responses ξ_i, i=1,2,...6, contained in Table 6.1-6.4 can be solved by the method described in the previous chapters. Once the motion responses are known there is no difficulty in solving the loading equation.

6.2 Comparison between Computational and Experimental Results

The dynamic wave loads on the SWATH 1 shown in Fig.4.51 were analysed for three different wave heading, head sea (180^0), bow-quartering sea (135^0) and beam sea (90^0) at zero speed. The same panel arrangement on the hull as that in section 4.3 was used. The data of cross-deck and strut of SWATH 1 are also shown in Fig.4.51. Thirty two frequencies were carried out in the calculation.

In order to validate the theory, the computational results were compared with the experimental data for the bending moment at mid-section of cross deck in bow-quartering and beam seas, because only those experimental results were available. The experiment was carried out by Djatmiko[6]. All the results are shown in Fig.6.3-6.6. The discussions are made for four major wave loads respectively in the following sections.

6.2.1 Bending moment

From the results that the maximum bending moment is seen to occur in beam seas. The most prominent feature of bending moment response is the large peak occurring at λ/B_0=2.1 equivalent to λ/L_S=1.5. This peak is associated with the effect of the first longitudinal standing wave. As mentioned in section 4.2.2, the first longitudinal standing wave may introduce the maximum wave loading on the cross-deck structure. This is confirmed here. The theoretical results agree well with the experimental data on both the frequencies at which the maximum bending moment (or first longitudinal standing waves) occurs and the amplitude of the bending moment. The first longitudinal standing wave does not effect the added mass and damping coefficients as mentioned in section 4.3.1, but its effect on the loads is obvious. The other peak on the bending moment is at about λ/B_0=1.0. It is associated with the second symmetric standing wave (transverse). This peak also appears in the experiment. In bow quartering sea case, the theoretical predictions agree also well with experiments which confirm the two peaks caused by the standing

waves at λ/B_0=2.1 and 1.0 respectively.

In Fig.6.3 and 6.4, the motion responses of SWATH 1 in sway, heave and roll in beam sea are also shown against the abscissa of ratio of wave length to maximum beam (λ/B_0) in order to compare with the loading results. Comparing the loads and motion results, it can be found that roll resonance at low frequency has virtually no influence at mid-section bending moment. The experiments have confirmed this feature.

The components of the bending moment in the beam seas are presented in Fig. 6.7(a). The large contribution of wave diffraction is apparent. This kind of influence is purely hydrodynamic effect associated with the standing waves and would not be predicted by simple theories based on the 'static' approach or diffraction theory with the fluid interaction between the twin hulls neglected.

In addition, the transverse bending moment of SWATH 1 in regular beam waves at cross deck strut juncture and strut at waterline were also calculated by the formulae in Table 6.2 and presented together with those at cross deck mid-section in Fig.6.8. It is noted that the roll resonance occuring at λ/B_0=9.2 has no effect on the moment at mid-section. Moving along the cross deck to the juncture with the strut, a secondary peak due to roll resonance occurs, with the primary peak nearly unaffected. On the strut, the moment is reduced but the secondary peak remains unchanged. Although the peak bending moment is greatest at the mid-section, the appearance of the secondary peak at other location on the cross deck means that in irregular waves the statistical amplitude of the bending moment could be slightly greater away from the mid-section, if the roll resonant frequency is in the vicinity of the wave spectrum.

6.2.2 Horizontal shear force

The horizontal shear force response has almost identical shape with the bending moment. The maximum value occurs in beam seas. The two peaks on the each response curve of three different heading are at λ/B_0=2.1 and λ/B_0=1.0 coinciding with those of bending moment response curves. This suggests the bending moment on the cross-deck

structure of SWATH ships is primarily a result of the action of horizontal forces applied on the hull with some equivalent vertical moment arm. The present results show that for SWATH ships which have narrow beam and large draft the horizontal side load is one order higher than the vertical load in short wavelengths (near the peak), so the bending moment is dominated by the contribution from the side loads. Consequently, this suggests an approximate formula for the bending moment calculation if the horizontal side load is known, i.e.

$$M=(h_0+D/2)*V_2 \qquad (6.5)$$

The difference between the maximum bending moment calculated by Eqn.(6.5) and actual theoretical prediction is about 5% for present model. In the early design stage , the maximum side load can be roughly evaluated from the semi empirical formulae[7], the maximum bending moment can then be obtained by Eqn.(6.5).

In contrast the conventional catamaran has large beam-draft ratio, and the relative magnitudes of the vertical and horizontal loads are roughly the same order of amplitude. This feature was shown in the theoretical and experimental work by Wahab, et al.[8] and Jones and Gerzina[9].

6.2.3 Vertical shear force

The vertical shear force is an order smaller than the horizontal force. It has its maximum value in the beam sea case. The theory predicts the roll resonance should contribute to the vertical shear force.In Fig. 6.4, the peak in the vertical shear response does occur at roll resonant frequency. The other peak at $\lambda/B_0=2.0$ is believed to be caused by the asymmetric standing wave, but is it less significant than the one induced by the roll motion resonance.

6.2.4 Torsional moment

In contrast to the bending moment, horizontal and vertical shear force, the maximum torsional moment occurs in a quartering sea. The results show that the

torsional moment has the peak values at λ/B_0=2.1 and λ/B_0=1.0 which coincide with the peaks of bending moment and horizontal shear force. This is expected because the theory predicts the peak torsional moment be should associated with the symmetric standing waves as is the bending moment.

The Fig.6.7(b) presents the different components of the torsional moment in bow-quartering sea. The contribution from the diffraction component is apparently dominant over the maximum torsional moment which associated with the first longitudinal standing wave at λ/B_0=2.1, i.e. λ/L_s=1.5. This is purely hydrodynamic effect and can not be predicted by simple methods based on the 'static' approach, or by the diffraction theory with the fluid interference between the twin hull neglected. For the present model, the contribution from incident wave (Froude-Krylov force) is only about 18% of the maximum torsional moment. On the other hand, the maximum torsional moment is about 10% of the maximum bending moment, but its prediction still provides important information for the structure design.

6.3 Wave Load Distributions over the Hull of SWATH

The wave loads, e.g. side forces and bending moments, on cross deck structure in pure beam seas were seen to be the worst wave loading conditions. The recent research[10] has found that the seas approaching from just forward or aft of beam give biased load distributions which may cause the maximum local stress on the cross deck structure. The present computational results have confirmed this. The side force distributions along a tandem strut model (SWATH 1) and a single strut model (same geometry as SWATH 1, but only a single strut on each hull) were calculated. The calculation were carried out from 45^0 to 135^0 with 2.5^0 intervals. For present two models the most serious conditions is 82.5^0 and 97.5^0 (7.5^0 forward and aft of beam) at the frequency where the maximum side force occurs. The results are presented in Fig.6.9. In this condition the total side force acting on the hull is nearly equal to that in beam seas, but the biased load distributions produce the maximum local side force at the position forward or aft of middle of the strut. This kind of load may cause the serious local stress which is worse than that in case of beam seas. Since the present strip theories for wave load calculation on SWATH are

only valid in pure beam seas, they can not predict such load distributions along the hull. To overcome this problem the three dimensional theory should be applied.

On the other hand, the advanced structural analyses for SWATH or other twin hull ships are mainly based on three dimensional methods. If the strip theory is used for hydrodynamic load calculation, a rough approximation of load distribution along the hull must be employed. The three dimensional theory has ability to calculate the wave load distribution directly and so can provide more accurate wave load input for the structural analyses not only for beam sea case but also for any wave heading.

6.4 Conclusions

On theory

1, Dynamic load prediction based on present 3D diffraction theory agreeswell with available experimental data in both beam and bow quartering waves, confirming the basic validity of the the present method. Because the 3D effect is taken into account, the present method can predict the wave load in any wave direction and also theoretically has potential to predict the wave load on semi-submersible crane vessels or similar type of vessels on which the 3D effect is significant, but these still need more experimental work to validate.

2, The Experiments confirm that the first longitudinal standing wave produces the maximum bending moments at cross deck of the SWATH ship. This effect can be predicted by the present theory.

3, The major improvement of the present method is its ability to predict the wave loads and its distribution over the hull at any wave heading. This ability gives designers much more flexibility to investigate the different loading conditions during primary design stage in contrast the tradition 2D theory is only adequate in beam seas conditions.

4, It is believed that the present three dimensional method can produce the more accurate load distribution over the wetted hull surface of a vessel than two dimensional theory. Those predictions are important for structural analysis. More experimental data is

still needed to validate the predictions of force distribution from the present theory.

On the features of the dynamic load on the SWATH

1, The horizontal acting loads on the SWATH ships are an order of amplitude larger than vertical acting loads. The transverse bending moment acting on the cross deck is primarily a result of the side loads at a point near mid draft.

2, The most prominent feature of the side load and bending moment responses on the cross deck is a large peak due to the effect of the first longitudinal standing waves which usually occur at wavelength close to twice of the length of the strut.

3, The maximum torsional moment occurs quartering waves at the same frequency at which the maximum bending moment occur, but the former is an order smaller than the latter in amplitude. This effect is necessary to be considered if the proper prediction method is available, since the local combined stress between bending and torsional effects on the cross deck may be very large.

4, The analytical results show that the sea approaching just forward or aft of the beam can produce the biased load distributions which may introduce the maximum local stress on the structure. It is difficult to predict this kind of load distribution by any two dimensional theory, but the prediction from three dimensional theory still need to be justified by experiments.

CHAPTER SEVEN

RANDOM SEA PROCEDURE

As indicated in Chapter 1, the principle of superposition introduced by St. Denis and Pierson reduces the complex problem of ship motions and wave loads in seaway, which behaves random in nature, to two problems:

1, the prediction of the ship motions and wave loads in regular waves and

2, the prediction of the statistical responses in irregular waves using the regular wave results.

In previous chapters all the discussion is concentrated in the first problem since it is the major task of the seakeeping study and also the main objective of this thesis. The results have shown that the predictions from the present theory agree well with the experimental data for various type of mono and twin hull ships.

In this chapter the second problem is dealt with. The wave energy spectrum method is used for determining the statistical responses of the ship motion, wave loads in irregular waves. The seakeeping criteria for both monohulls and SWATH are discussed. In practice, a ship designer not only needs to know the motion and wave load responses of a ship to be designed in the extreme sea condition, but is also interested in the seakeeping qualities of such a ship, for example the seakeeping effectiveness i.e. the percentage of time that ship may be expected to operate in a given ocean environment with safe and prudent operation of the ship and with an effective ship's crew and equipment. For above reason, the method to evaluate the seakeeping qualities of a ship is introduced in the chapter. Based on this method, if the regular wave responses of a ship, the seakeeping criteria and the statistical probability of specific sea conditions (i.e. certain wave height, modal period etc.) in given ocean environment are known, the seakeeping qualities of the ship can be predicted.

Finally, the motion response results of the prototype SWATH 1 in irregular waves are calculated as a numerical example. The results of its seakeeping effectiveness in the North Atlantic are represented and compared with a selection of monohulls. The wave loads on the cross-deck structure of the SWATH 1 in irregular waves are given as well.

7.1 General Considerations and Formulae

In principle, the time history of the system responses of the ship motion and wave loads to any random single can be obtained for a linear system by a convolution integral of the product of the signal and the inverse Fourier transform of the transfer function[1,2]. Here, the transfer function, or called frequency response function, is the ratio of the complex amplitudes of any motion or wave load quantity to the amplitude of the incident wave. A correct approach to ship motion and wave loads in the time domain, however, is not so straightforward as described previously as has been pointed out by Cummins[3]. As is well recognized, a unique representation of the time history of sea waves is impossible. Hence, representation of the sea waves has been made through energy spectra from which various statistical averages of the wave condition can be obtained.

The application of the sea energy spectra in conjunction with the transfer function to obtain various statistical averages of ship motion and loads responses was first introduced by St. Denis and Pierson[4]. Since then, statistical averages have been used almost as a standard tool for investigation of ship motions and wave loads in an irregular seaway. To simplify the problem, the three major assumptions were made in this approach, i.e.

1, the relationship between the wave exciting and ship responses is linear,

2, the ship motions are stationary and normal random processes with zero mean and

3, the sea energy spectral density function of waves and ship motion are narrow banded.

Following the spectral method of St. Denis and Pierson, the variance of the absolute value of a transfer function, say $|\xi_i|/a$, can be obtained by

$$E = \int_0^\infty \left[\frac{|\xi_i|}{a} \right]^2 S(\omega)\, d\omega = m_0 \qquad (7.1)$$

where $[\ |\xi_i|/a\ ]^2$ is often called the response amplitude operator (RAO), $S(\omega)$ is sea energy spectral density function, which has the dimensional unit of $[L^2T]$ or $[m^2s]$. The variances for velocity and acceleration of ith mode of motion can also be obtained by

$$E_v = \int_0^\infty \omega^2 \left[\frac{|\xi_i|}{a} \right]^2 S(\omega)\, d\omega = m_2 \qquad (7.2)$$

and

$$E_a = \int_0^\infty \omega^4 \left[\frac{|\xi_i|}{a} \right]^2 S(\omega)\, d\omega = m_4 \qquad (7.3)$$

Since the sea energy spectral density function of waves and ship motion are assumed narrow banded, the distribution of motions or wave loads may be described by a Rayleigh probability density function, although this may not be quite true in some cases[11]. Under this assumption, the statistical averages of ship responses can be expressed in the form

$$\text{'Average' amplitude} = C\sqrt{(E\ )} \qquad (7.4)$$

Here $\sqrt{(E\ )}$ is called Root Mean Square (RMS) of a particular motion amplitude; C=1.253 gives the average; C=2.0 gives the one-third highest average or significant value; C=2.546 gives the one-tenth highest average.

If the absolute motion amplitude $|\xi_i|$ is replaced by the absolute load amplitudes $|V_2|$, $|V_3|$, $|M_b|$ or $|M_T|$, the Eqn.(7.1)-(7.4) can be used to predict the statistical averages of horizontal forces, vertical shear forces, Bending moments or torsional moments on the ship structure respectively.

For a design or operational criterion, it is also interest to know the probable extreme value a ship may encounter in given sea environments. From the property of the Rayleigh distribution function, this can be shown as[5]

$$\gamma_n(\varepsilon) = \sqrt{2 \ln\left[\frac{3600\,H}{2\pi\varepsilon}\sqrt{\frac{m_2}{m_0}}\right]}\sqrt{E} \qquad \text{for small } \varepsilon \qquad (7.5)$$

where H is the time in hours during which an extreme sea environment may persist. ε is a probability factor. For ε=0.01, the Eqn.(7.5) gives a 99% assurance that the maximum amplitude $\gamma_n(0.01)$ will not be exceeded. Whereas for ε=1.0, $\gamma_n(1)$ represents the 'most probable maximum amplitude'. For large number of observations, the probability that the maximum value will exceed $\gamma_n(1)$ is 63.2%.

The problem of the cross-structure slamming of a SWATH ship is a serious concern for the designer. This phenomenon results when the cross structure hits the surface of the water at small or moderate angles giving rise to dynamic pressures and loads which can reach extremely high levels. The probability of this impact occurring and the expected number of impacts per unit time acting on the cross-structure can be estimated by the method of Ochi and Motter[6,7]. The requirement for an impact of the cross-structure of a SWATH ship is that the vertical relative motion of the hull is greater than the cross - structure clearance above the calm water level[8,9]. The formula is

$$N_S = \frac{n}{2\pi}\sqrt{\frac{E_v^{(R)}}{E^{(R)}}}\exp\left[-\frac{C_d^2}{2E^{(R)}} - \frac{V_T^2}{2E_v^{(R)}}\right] \qquad (7.6)$$

where superscript (R) denotes the relative motion at the location of interest. C_d is the vertical distances above the calm water level to bottom of either the main hull or the cross-deck in the same dimensional unit used for $\sqrt{(E^{(R)})}$, V_T is the threshold velocity that incites slamming. The value of V_T can differ from case to case and should be given in the same dimensional unit as $\sqrt{(E_V{}^{(R)})}$. In many cases the value of V_T is unknown, and if V_T is set to zero, the Eqn.(7.6) then gives either the number of hull bottom emergencies or water contacts of cross-deck bottom per n seconds. If V_T is set to zero and C_d is set to be the deck height, then Eqn.(7.6) provides the probable number of occurrences of deck wetness

by green water per n seconds.

The complex relative vertical motion of a point (x,y,z) on the ship is given by

$$\xi_V^{(R)} = \xi_V^{(A)} - \zeta_0 \qquad (7.7)$$

and

$$\xi_V^{(A)} = \xi_3 + y\xi_4 - x\xi_5 \qquad (7.8)$$

where $\xi_V^{(A)}$ is complex absolute vertical motion and ζ_0 is complex amplitude of incident waves given by

$$\zeta_0 = a\, e^{ik\,(x\cos\beta - y\sin\beta)}. \qquad (7.9)$$

7.2 Wave energy spectra

Common mathematical expressions which are frequently used by ship investigators are the so called Pierson-Moskowitz spectrum[10] and 17th ITTC spectrum[11].

The Pierson-Moskowitz spectrum is obtained semi-empirically by analysis of extensive wave data relating to fully developed sea condition in North Atlantic. This spectrum was recommended by 11th ITTC conference (1966) for ship motion computations when information on typical (i.e. locally derived) sea spectrum is not available[12]. It has the form of

$$S(\omega) = \frac{C_1}{\omega^5} \exp\left[-\frac{C_2}{\omega^4} \right] \qquad [m^2\text{-sec}] \qquad (7.10)$$

where

$C_1 = 0.78$

$C_2 = 3.12/H_{1/3}^2$

where $H_{1/3}$ is the significant wave height in metres. If the only information available is the significant wave height, this spectrum may be used. Note that Pierson-Moskowitz spectrum is a single parameter spectrum, i.e. uniquely determined by a single parameter, e.g significant wave height or wind speed. This limits the flexibility of the spectral description because of the fixed relationship between wave height and modal wave period. T_0, where the wave period of maximum wave energy(i.e the peak of the spectral

distribution) is:

$$T_0 \approx 5.0\sqrt{(H_{1/3})}$$

with the maximum value of wave spectrum, $S(\omega)=0.25e^{-5/4}H_{1/3}^{5/2}$. The Pierson-Moskowitz spectrum is illustrated in Fig.7.1.

If further information is available on the modal wave period, the 17th ITTC wave spectrum can be used, i.e.

$$s(\omega) = 320 \frac{H_{1/3}^2}{T_0^4 \omega^5} \exp\left[\frac{-1951}{T_0^4 \omega^4} \right] (3.3)^Y \qquad (7.11)$$

where

$$Y = \exp\left[- \frac{0.766\ \omega\ T_0 - 1.0}{\sqrt{2}\,\sigma} \right]^2$$

and

$$\sigma = 0.07 \quad \text{for } \omega \le 6.28/T_0$$

$$\sigma = 0.09 \quad \text{for } \omega > 6.28/T_0$$

where T_0 is the modal wave period. The other characteristic wave period can be used as well, such as the average wave period T_1, by means of

$$T_1 = 0.834 T_0$$

Of the two spectra discussed above, a more recent trend indicates a preference for two parameter spectrum because it is not constrained by the assumption of a fully developed sea. Pierson-Moskowitz spectrum, on other hand, is a less complex spectrum and appears to be quite reasonable, where its limitations are accepted.

The flexibility of two parameter spectrum is attractive when used in conjunction with data reflecting observations of both wave height and modal period for a specific ocean area. The data of this type is available for the North Atlantic[14,15] and other ocean area. It provides some keys as the frequency of occurrence of wave conditions throughout the world. Thus the specifications of the two parameters of 17th ITTC spectrum

can be made with some intelligence and regard of the operating area of the ship under evaluation.

In this chapter, the seakeeping effectiveness of the SWATH 1 will be evaluated in terms of the average probability of occurrence of specific ocean condition (i.e. certain wave height and modal period), therefore the 17th ITTC spectrum is used to determine the seakeeping qualities. The wave loads on the SWATH 1, on other hand, are only evaluated in the most serious condition (beam and quartering seas), so the Pierson-Moskowitz spectrum is used because of its simplicity.

7.3 Spectral Transformation

If a ship is in transit at speed U at an angle β to the predominant direction of the waves, then it will 'encounter' the waves at a frequency different from that which it would meet if it were at rest. The encounter frequency is rewritten here

$$\omega_e = \omega - \frac{U\,\omega^2}{g}\cos\beta$$

The energy of the wave is the same whether it is expressed in term of ω or ω_e, so that

$$E_W[\,\zeta^2\,] = \int_0^\infty S(\omega)\,d\omega = \int_0^\infty S(\omega_e)\,d\omega_e \qquad (7.12)$$

where

$$S(\omega_e) = \frac{S(\omega)}{|\,d\omega_e/d\omega\,|} \qquad (7.13)$$

The modulus of $d\omega_e/d\omega$ is used because $S(\omega_e)$ must always be positive.[see ref.[11]]. By deriving the definition of encounter frequency, one can obtain

$$S(\omega_e) = \frac{S(\omega)}{\left|\,1 - \frac{2\,U\,\omega}{g}\cos\beta\,\right|} \qquad (7.14)$$

Given the wave spectrum $S(\omega)$, it is thus possible to find the 'wave encounter spectrum', $S(\omega_e)$. Its effect is to distort the spectrum as shown in Fig.7.1 for Pierson-Moskowitz spectrum. It should be noted that the area under the curves represents the energy of the waves, and is thus constant. This formula only applies in deep water. In shallow water, the spectrum would need modified since wave speed also depends on the depth of water.

7.4 Seakeeping Criteria

The U.S. Navy seakeeping criteria, which include a set of 12 criteria with which one can assess the seakeeping quality of candidate design, are chosen in the study. These criteria are shown in Table 7.1. The establishment of these criteria were primarily of interest in Anti-Submarine-Warfare (ASW) missions of a naval combatant. The discussion of the establishment of those criteria was given in detail by Olsen[15]. Four seakeeping categories were considered as listed in Table 7.2. The first, general category, identifies seakeeping considerations that are essential to effective operations regardless of the mission. The seakeeping criteria in this category are concerned with the safe and prudent operation of the ship with the effectiveness of ship crew. This category includes criteria 1-6 for monohulls; criteria 1-3, 11 and 12 for SWATH. The second category addresses the ability of ship to support embarked ASW helicopters and includes criteria 7-9, as well as the appropriate general criteria for both monohulls and SWATH. The third category addresses the impact of ship motion on the performance of hullmounted sonars on the monohulls. Thus it includes criteria 1-6 and 10. Because of the SWATH configuration, a sonar dome emergence criterion was inappropriate for SWATH. The fourth category (all criteria) combines both the helicopter and sonar categories and reflects a composite seakeeping assessment.

The criterion 11 based on the occurrence of wave impact on the SWATH cross-structure limits the relative motion of the 1/10th highest displacement between the SWATH and waves to maximum of 6.1 metres. The 6.1 metres figure is simply the design clearance between the bottom of the cross structure and the waterline of the prototype SWATH 1. As discussed by Olsen[15], this roughly equates to one wave contact every 2 to 5 minutes. The

Table 7.1 Selected Seakeeping Criteria and Categories[15]

General Criteria

Monohulls and SWATH

(1) 12^0 single amplitude average roll (personnel effectiveness)

(2) 3^0 single amplitude average pitch (personnel and equipment effectiveness)

(3) Motion sickness indicator (20 percent of laboratory subjects experience emesis within 2 hours)

Monohulls only

(4) Bottom plate damage

(5) Three slams in 100 motion cycles

(6) One deck wetness every 2 minutes

SWATH only

(11) 6.1-metre average of highest 1/10th relative bow motions (slamming)

(12) 4.2-metre significant relative motion at the propeller (propeller emergence)

Helicopter Operating Criteria for Monohulls and SWATH

(7) 12.80 double amplitude significant roll

(8) 2.54-metre double amplitude significant vertical displacement at the flight deck

(9) 2.13-metre-per-second significant vertical velocity at the flight deck

Hull-Mounted Sonar Criterion for Monohulls Only

(10) Sonar dome emergence criterion (three-out-five detection opportunities)

Table 7.2 Principle Dimensions of the Ships

	Sample	Unit	SWATH 1	FFG 7	FF 1052	DD 963
Full load displacement	∇	m^3	1395	3578	4246	7822
Length between Perpendiculars	L	m	60.0[1]	124.0	127.0	161.0
Beam	B	m	32.4	14.0	14.0	17.0
Draft	T	m	7.1	4.5	4.7	5.9

Note: (1) The length shown for SWATH is the length of the main sub-hull

(2) The clearance between the bottom of the SWATH cross deck structure and mean free surface is 6.1 metres.

(3) The distance between the mean free surface and the 25% blade tip of the SWATH propellers in vertical position is 4.2 metres

(4) The co-ordinates of the centre of the fight deck is (-15.0, 0.0, 8.1)

criterion 12 is based upon the phenomenon of propeller emergence. The criterion limits the relative vertical displacement at the SWATH propeller to maximum of 4.20 metres. This is equivalent to an exposure of 25% of the blade tip in the vertical position which can result in 9% loss of total thrust[15].

The data of the prototype SWATH 1 and the other three monohull designs are listed in Table 7.2.

7.5 Seakeeping Assessment

In the foregoing discussion, the method of evaluating ship responses in irregular waves and the twelve seakeeping criteria were identified. Here, those method and criteria will be used to evaluate the seakeeping qualities of a candidate ship design. SWATH 1 was used as an example. By means of the method discussed in Section 7.1, there are four major steps to assess the seakeeping quality of a ship in given ocean environment:

1, calculate the motion spectra of a ship in irregular waves by using its motion response results in regular waves and the wave spectra,

2, evaluate the statistical averages of the ship responses in irregular waves from its motion spectra,

3, compare the irregular wave results with the seakeeping criteria for all possible wave headings, forward speeds and modal wave periods, and

4, estimate the seakeeping effectiveness of the ship design in given ocean environment by using the data of the average probability of occurrence of specific ocean conditions.

7.5.1 Motion spectra of a ship

The motion spectrum is the integrand of Eqn.(7.1), i.e.

$$S_{mi}(\omega_e) = \left[\frac{|\xi_i(\omega_e)|}{a} \right]^2 S(\omega_e) \qquad (7.15)$$

where $S_{mi}(\omega_e)$ is the motion spectrum in ith mode of motion, the RAO is the function of encounter frequency and the wave spectrum is also corrected for encounter frequency by

Eqn.(7.14). Similar process can also apply to velocity and acceleration of the motion in Eqn.(7.2) and (7.3), i.e.

$$S_{vi}(\omega_e) = \omega_e^2 \left[\frac{|\xi_i(\omega_e)|}{a} \right]^2 S(\omega_e) \qquad (7.16)$$

and

$$S_{ai}(\omega_e) = \omega_e^4 \left[\frac{|\xi_i(\omega_e)|}{a} \right]^2 S(\omega_e) \qquad (7.17)$$

where $S_{vi}(\omega_e)$ and $S_{ai}(\omega_e)$ are velocity and acceleration spectra in ith mode of motion respectively.

The Fig.7.2-7.4 show the motion spectra of prototype SWATH 1 in irregular waves for head, bow quartering and beam seas at 15 knots. The 17th ITTC spectrum was used. Only one special case is shown in the figures, i.e. significant wave height $H_{1/3}$=3.25 metre and wave modal period T_0=12.3 seconds. The wave spectrum and the the RAO curves are also shown in the figures. It is obvious that when the peak of of wave spectrum is close to the resonance of the motion response in particular mode, the motion spectrum gives the maximum value. To reduce the motion responses of a ship in seaway, it is important to avoid this situation occurring.

7.5.2 Statistical averages of ship responses

The statistical averages of ship responses in irregular waves can be obtained by integrating the motion spectra over whole of the encounter frequency range, i.e. Eqn.(7.1)-(7.3). Then Eqn.(7.4) and the different statistical constants can give the different statistical values. If the 17th ITTC spectrum is used, the motion spectrum is different for each wave modal period. Consequently, the integral of Eqn.(7.1)-(7.3) must be carried out for different modal wave period. Because the Root Mean Square (RMS), i.e. $\sqrt{E}$ in Eqn.(7.4), obtained by 17th ITTC spectrum is linear with respect to significant wave height, the dependence can be treated as independent to the significant wave height.

The results of SWATH 1 in irregular waves for different modal periods, wave

headings and forward speeds are calculated in this study. Some important figures of them are shown in Fig.7.5-7.10. those include the significant amplitudes of heave, roll, pitch, relative bow motion, relative vertical motion at the propeller and vertical velocity at the flight deck in head, bow quartering or beam and at 0 to 25 knots forward speeds with 5 knots increment. The results of relative motion amplitudes were calculated by means of Eqn.(7.1) and (7.7).

7.5.3. Comparing the irregular wave results with the seakeeping criteria

To evaluate the seakeeping quality of a ship, the ship responses in irregular waves should be compared with the specific seakeeping criteria for all possible wave headings and forward speeds. This can be easily conceptualized by viewing the seakeeping matrix of Fig.7.11. The ship is represented at the centre of the matrix and is proceeding from left to right. The concentric bands of the matrix represent different ship speeds while the radials represent the wave heading. The centre of the matrix represent zero speed. Each cell of the seakeeping matrix addresses a specific condition, where the ship motion spectra, whether it be for roll, pitch, heave or whatever, will be varied. For the present study, the calculation consists of estimates of ship motion spectra and statistical averages of motion responses in modal period of 7.0, 8.5, 9.5 and 12.0 seconds, for heading angles from 0^0 to 180^0 in 15^0 increments, and at speeds from 0 to 25 knots in 5 knots increments. Although the seakeeping matrix is symmetric about the port and star board of a ship, it still consists of 78 cells in the present case and each of them should be evaluated for four different wave modal periods.

The results of above calculations are shown in Table 7.3-7.6. The upper matrices in those tables identify the seakeeping criterion that is first exceeded for each combination of ship speed and heading angle. Those criteria are listed in Table 7.1. The lower matrix of each table identifies the significant wave heights (in metres) at which the limiting criteria are exceeded. Thus the two matrices in each table are complementary.

Among the 12 criteria listed in Table 7.1, the criterion 3 was not considered in above evaluations because of the lack of detailed information for such criterion, and the

Table 7.3 SWATH Seakeeping Criteria (1-2, 7-9, 11-12)
7.0 Second Modal Wave Period

Ship Speed (Knots)	Head Sea 180	165	150	135	120	105	Beam Sea 90	75	60	45	30	Following Sea 15	0
0	12	11	0	0	12	12	12	12	12	12	12	12	12
5	12	12	0	0	12	12	12	12	12	12	12	12	12
10	12	12	0	0	12	0	12	12	12	12	8	2	2
15	12	0	0	0	12	12	12	12	2	2	2	2	2
20	0	0	0	0	12	12	12	12	12	2	2	2	2
25	0	0	0	0	12	12	12	8	2	2	2	2	8

Limiting Seakeeping Factors

0 No seakeeping threshold exceeded for wave with significant heights up to 9.75 metres

1-12 The indicated SWATH seakeeping criteria is exceeded
(Criteria 1-12 are listed in Table 7.1)

Note: Criterion 8 used here is 2.54 metres double amplitude of significant vertical displacement at flight deck due to pitch only.

Acceptable Significant Wave Height (metres)

Ship Speed (Knots)	Head Sea 180	165	150	135	120	105	Beam Sea 90	75	60	45	30	Following Sea 15	0
0	8.5	9.4	9.75	9.75	8.2	7.0	6.7	6.9	7.6	7.6	7.6	7.9	8.5
5	8.5	9.4	9.75	9.75	8.5	7.3	6.7	7.0	7.3	7.9	6.4	5.2	4.9
10	8.8	9.4	9.75	9.75	8.8	9.75	6.7	6.9	5.8	3.7	3.4	1.5	1.5
15	9.4	9.75	9.75	9.75	9.1	7.9	6.7	6.9	7.6	6.8	1.2	1.5	2.1
20	9.75	9.75	9.75	9.75	9.4	7.9	6.7	6.7	3.0	1.5	0.9	0.9	1.2
25	9.75	9.75	9.75	9.75	9.4	8.2	6.7	4.9	3.4	3.0	3.4	3.7	7.3

Table 7.4 SWATH Seakeeping Criteria (1-2, 7-9, 11-12)
8.5 Second Modal Wave Period

Ship Speed (Knots)	Head Sea 180	165	150	135	120	105	Beam Sea 90	75	60	45	30	15	Following Sea 0
0	12	0	0	0	12	12	12	12	12	12	12	12	12
5	12	12	0	12	12	12	12	12	12	12	8	8	8
10	12	12	12	12	12	12	12	12	12	8	8	2	8
15	12	12	12	12	12	12	12	12	12	8	2	2	2
20	12	12	12	12	12	12	12	12	12	2	2	2	8
25	12	12	12	12	12	12	12	12	2	2	2	2	0

Limiting Seakeeping Factors:

0 No seakeeping threshold exceeded for wave with significant heights up to 9.75 metres

1-12 The indicated SWATH seakeeping criteria is exceeded
(Criteria 1-12 are listed in Table 7.1)

Note: Criterion 8 used here is 2.54 metres double amplitude of significant vertical displacement at flight deck due to pitch only.

Acceptable Significant Wave Height (metres)

Ship Speed (Knots)	Head Sea 180	165	150	135	120	105	Beam Sea 90	75	60	45	30	15	Following Sea 0
0	9.75	9.75	9.75	9.75	8.2	7.3	6.7	7.0	7.3	7.3	7.6	7.9	8.5
5	8.8	9.75	9.75	9.75	8.2	7.3	7.0	7.0	7.6	7.9	7.9	7.0	6.7
10	8.5	9.1	9.4	9.1	8.2	7.3	7.3	7.6	8.5	5.2	3.4	1.5	1.5
15	8.8	9.1	9.4	9.1	7.9	7.3	7.0	7.6	9.4	2.1	1.2	0.9	0.9
20	9.1	9.4	9.7	9.4	8.2	7.3	6.7	7.6	4.2	1.8	0.9	0.9	0.9
25	9.4	9.7	9.7	9.4	8.5	7.3	6.4	7.0	2.1	2.4	2.7	2.7	9.75

Table 7.5 SWATH Seakeeping Criteria (1-2, 7-9, 11-12)
9.5 Second Modal Wave Period

Ship Speed (Knots)	Head Sea 180	165	150	135	120	105	Beam Sea 90	75	60	45	30	Following Sea 15	0
0	12	12	12	12	12	12	12	12	12	12	12	12	12
5	12	12	12	12	12	12	12	12	12	12	8	8	8
10	12	12	12	12	12	12	12	12	12	8	2	2	2
15	12	12	12	12	12	12	12	12	2	2	2	2	2
20	12	12	12	12	12	12	12	12	12	2	2	2	2
25	12	12	12	12	12	12	12	12	2	2	2	2	0

Limiting Seakeeping Factors:

0 No seakeeping threshold exceeded for wave with significant heights up to 9.75 metres

1-12 The indicated SWATH seakeeping criteria is exceeded
(Criteria 1-12 are listed in Table 7.1)

Note: Criterion 8 used here is 2.54 metres double amplitude of significant vertical displacement at flight deck due to pitch only.

Acceptable Significant Wave Height (metres)

Ship Speed (Knots)	Head Sea 180	165	150	135	120	105	Beam Sea 90	75	60	45	30	Following Sea 15	0
0	9.4	9.75	9.4	8.5	7.0	9.4	5.8	6.1	6.1	6.1	6.4	6.7	7.0
5	8.2	8.5	8.8	8.2	7.3	7.3	7.0	6.1	6.7	8.2	8.2	7.6	7.3
10	7.6	7.9	8.2	7.6	7.3	6.7	6.4	7.0	9.1	5.2	3.0	1.8	2.1
15	7.6	7.9	7.9	7.6	7.0	7.3	6.1	7.6	6.7	2.1	1.5	0.9	1.2
20	7.9	8.2	8.2	7.6	7.0	6.1	5.5	8.2	5.2	1.8	0.9	0.9	0.9
25	8.2	8.5	8.5	7.9	7.0	6.1	5.5	8.2	2.7	2.1	2.7	2.7	9.75

Table 7.6 SWATH Seakeeping Criteria (1-2, 7-9, 11-12)
12.0 Second Modal Wave Period

Ship Speed (Knots)	Head Sea 180	165	150	135	120	105	Beam Sea 90	75	60	45	30	Following Sea 15	0
0	8	2	8	12	12	12	12	12	12	12	12	12	12
5	9	9	9	9	9	12	12	12	12	8	8	8	
10	12	12	12	12	12	12	12	12	12	8	8	8	8
15	12	12	12	12	12	12	12	12	8	8	8	8	8
20	12	12	12	12	12	12	12	12	8	8	8	8	8
25	12	12	12	12	12	12	12	12	8	8	8	8	0

Limiting Seakeeping Factors:

0 No seakeeping threshold exceeded for wave with significant heights up to 9.75 metres

1-12 The indicated SWATH seakeeping criteria is exceeded
(Criteria 1-12 are listed in Table 7.1)

Note: Criterion 8 used here is 2.54 metres double amplitude of significant vertical displacement at flight deck due to pitch only.

Acceptable Significant Wave Height (metres)

Ship Speed (Knots)	Head Sea 180	165	150	135	120	105	Beam Sea 90	75	60	45	30	Following Sea 15	0
0	6.1	6.1	7.0	7.3	7.0	7.0	6.7	6.4	6.4	6.1	5.8	5.8	5.8
5	5.2	5.2	5.5	5.8	6.1	6.4	6.4	7.9	8.8	7.9	7.9	7.6	7.3
10	4.8	4.8	4.6	4.9	5.2	6.1	7.3	8.5	9.1	6.1	3.7	2.4	2.4
15	4.6	4.6	4.3	4.3	4.3	5.5	7.6	9.1	7.3	3.4	1.8	1.5	1.8
20	4.9	4.9	4.6	4.3	4.0	5.2	7.6	9.6	6.7	2.4	0.6	0.9	0.9
25	5.2	5.2	4.9	4.6	4.0	4.6	7.6	9.4	3.9	1.5	3.0	3.3	9.75

criterion 8 used here is the 2.54 metres double amplitude of significant vertical displacement at flight deck due to pitch only. The criterion 8 was discussed by Olsen[15] in detail. The above treatment of the criterion 8 follows the practice of Olsen.

From the results in Table 7.3-7.6, it can be seen that the criteria 2, 8 and 12 are most seriously concerned. All those criteria are closely related to the pitch motion of the SWATH. If the pitch response can be reduced, the seakeeping quality of the SWATH will be improved considerably, specially for following and stern oblique sea cases. The SWATH 1 model used here has no fin control system. The use of passive or active fins can reduce the pitch response considerably, and consequently improve the seakeeping quality of SWATH. The detailed discussion about fin control on SWATH ships were given by Caldeira-Savaiva and Clarke[16] and McGregor, et al.[17], but this is beyond of the scope of the present study.

The results in Table 7.3-7.6 also show that the SWATH performance is very good in head, bow quartering and beam seas, but appears to suffer in following and stern quartering seas because of pitching. The pitch spectrum in following sea at 20 knots is represented in Fig.7.12 against the wave frequency. At ω=0.476, the denominator in Eqn.7.14 becomes zero, the encounter wave spectrum is therefore approaches to infinity. In this case the area under the wave spectral curve remains finite[1]. The peak on the encounter wave spectrum contributes a large peak on the pitch spectral curve which results large pitch response of the SWATH in irregular following waves. Furthermore, with the information of Table 7.3-7.6, the seakeeping effectiveness of a ship in given ocean environment can be evaluated as follows.

7.5.4 Seakeeping effectiveness evaluation

Seakeeping effectiveness is the percentage of time that a ship could expect to operate in given ocean environment without violating any of the specified criteria. The data in Table 7.3-7.6 were derived based on the 17th ITTC spectrum (two parameters), it is then possible to take the observed wave heights for a specified ocean environment and evaluate

the seakeeping effectiveness of the SWATH 1. The average probability of occurrence of specific ocean conditions in the North Atlantic are listed in Table 7.7[14,15]. By means of the probability data in Table 7.7 and the data in Table 7.3-7.6, the seakeeping effectiveness of SWATH 1 in the North Atlantic can be estimated. To do this two assumptions should be made as follows:

1, the probability of the encountering a sea at a specific heading angle relative to the ship is equally likely for all headings, and

2, the speed at which the ship desired to operate is equally distributed at 0, 5, 10, 15, 20 and 25 knots.

Table 7.7 Wave Height Distributions[15]

Significant Wave Height	North Atlantic Summer (June, July) Wave Period (T, seconds)			
(Z, metres)	T≤7	8<T≤9	10<T≤11	12≤T
Z≤0.75	.12	.00	.00	.00
0.75<Z≤1.75	.37	.06	.01	.01
1.75<Z≤2.75	.15	.09	.03	.01
2.75<Z≤3.75	.04	.03	.02	.01
3.75<Z≤5.75	.01	.02	.01	.01
5.75<Z≤7.75	.00	.00	.00	.00
7.75<Z≤9.75	.00	.00	.00	.00
Significant Wave Height	North Atlantic Winter (December, January) Wave Period (T, seconds)			
(Z, metres)	T≤7	8<T≤9	10<T≤11	12≤T
Z≤0.75	.03	.00	.00	.00
0.75<Z≤1.75	.15	.03	.00	.01
1.75<Z≤2.75	.13	.10	.04	.02
2.75<Z≤3.75	.06	.07	.05	.03
3.75<Z≤5.75	.02	.05	.06	.04
5.75<Z≤7.75	.01	.02	.02	.02
7.75<Z≤9.75	.00	.01	.01	.02

Table 7.8 Seakeeping Effectiveness of SWATH 1 and the Speed Effect on it in the North Atlantic (Criteria 1-2, 7-9, 11-12)

Speed (knots)	All	0	5	10	15	20	25
Summer	0.87	1.00	0.98	0.85	0.78	0.73	0.91
Winter	0.78	0.92	0.91	0.73	0.70	0.66	0.73
General	0.82	0.96	0.94	0.79	0.74	0.69	0.82

Table 7.9 Comparison of Seakeeping Effectiveness Between SWATH and Monohulls

Season	SWATH 1	FFG 7	FF 1052	DD 963
Summer	0.87	0.78	0.84	0.92
Winter	0.78	0.48	0.58	0.71
General	0.825	0.63	0.71	0.815

Note: The criteria 1-10 for monohulls and the criteria 1, 2, 7-9, 11, 12 for SWATH

The results for prototype SWATH 1 in the North Atlantic for different seasons are shown in Table 7.8. The effect of forward speed on seakeeping effectiveness is also presented in the table. The seakeeping effectiveness of the SWATH 1 decreases as the speed increases from 0 to 20 knots. The poorest case is 20 knots. At 25 knots seakeeping effectiveness becomes better. The results at 30 knots have also been calculated (but not presented) and are even better than the 25 knots case.

In comparing with the monohulls, the seakeeping effectiveness of three other monohull frigates are shown together with SWATH 1 results in Table 7.9. Those results for the monohulls were given by Olsen[15]. Their main dimensions are also listed in Table 7.1. The comparison show that 1397 tons SWATH 1 provides better seakeeping effectiveness

than 3578 tons FFG7 and 4246 tones FF1052. It would appear that the monohulls, especially the smaller FF1052 and FFG7 Classes without fin stabilization, poorly satisfy the roll criterion. On the other hand, the fin control system can also increase the seakeeping effectiveness of the SWATH ship considerably.

7.6 Wave Loads in Irregular Waves

The wave loads on the ship in irregular waves can be calculated in a similar way as the motion response evaluation in irregular waves. The Eqn.(7.1) and (7.4) can also be used if the motion response in Eqn.(7.1) is replaced by the wave load response. For the wave loads on the cross-deck structure of SWATH ships the Eqn.(7.1) becomes

$$E = \int_0^\infty \left[\frac{|V_2(\omega_e)|}{a} \right]^2 S(\omega_e)\, d\omega_e \qquad (7.18)$$

where $|V_2(\omega_e)|$ is the amplitude of horizontal force acting on the cross-deck structure of the SWATH and can be replaced by the other type of wave loads, $|V_3(\omega_e)|$, $|M_b(\omega_e)|$ or $|M_T(\omega_e)|$. When the value of E in Eqn.(7.18) is calculated, Eqn.(7.4) could give the different statistical average of the specific wave load in irregular waves.

The Pierson-Moskowitz spectrum was used in wave load calculation. The results of significant horizontal force, vertical shear, bending moment and torsional moment on the cross-deck structure of the SWATH 1 in irregular beam and bow quartering waves are shown in Fig.7.13-7.14. The results are given against significant wave heights. It is obvious that the maximum bending moment occurs at beam sea, while the maximum torsional moment occurs at quartering sea.

7.7 Conclusions

On theory

1. The method presented in this chapter together with the singularity distribution method described in previous chapters can be used to predict the seakeeping qualities of a ship in the certain ocean environment when its hull form is given. The predictions include not only the motion response of a ship in given sea state or the extreme sea condition, but

also the seakeeping effectiveness of the ship in certain ocean environments. This method provides a useful and economic tool to estimate the seakeeping qualities of a ship at early design stage.

2, The method described here can also predict the statistical wave load responses on the structure of a ship in given sea state in arbitrary wave heading. With some modification, the method can be further used to estimate the extreme wave loads on a ship in given ocean environment and certain period.

On SWATH

3, The method for evaluating the seakeeping effectiveness concerns that the accuracy of the motion response prediction of a ship in regular wave at any possible wave heading and forward speed is equally important for evaluating the seakeeping effectiveness, while for evaluating the most serious motion conditions the head, following (pitching) and beam (rolling) seas are more important than the others. Considering the conclusions made in chapter 4, both 3D and 2D theories give reasonable prediction for head and beam sea cases, but for oblique seas the 3D theory is more reliable than 2D theory. Therefore, it may be concluded that if only the most serious motion condition of SWATH in a seaway is needed the both 3D and 2D theories are acceptable, while if the seakeeping effectiveness is to be predicted the 3D theory will provide more reliable results than the 2D theory.

4, Because of the theoretical limitations of the present 3D and the 2D theories, both of them are unable to accurately predict the motion responses of a ship in regular following and stern oblique waves near the range of zero encounter frequency. The predictions in above situation are important for seakeeping quality prediction, so a more reliable method for predicting the motion response in regular following and stern oblique waves near the zero encounter frequency range is necessary for future development.

5, To improve the seakeeping quality of SWATH, it is important to reduce its pitch response especially in following and stern oblique sea cases. The use of a fin control system is necessary for higher speed operations.

6, If one is primarily concerned with the seakeeping performance of a ship, the SWATH can offer a major improvement vis-a-vis similar size conventional monohull designs.

CHAPTER EIGHT

CONCLUSIONS AND PROPOSALS FOR FUTURE DEVELOPMENT

8.1 Conclusions

As the results of the investigations presented in this thesis the following conclusions can be drawn.

1) The existing three dimensional panel method has been modified in two ways in order to improve its computational efficiency.

a) *By using of symmetric properties of Green's function:* This approach has saved over 30% of total computing time for the examples used in this thesis and it is applicable for both symmetric or non-symmetric bodies. The modification made in this approach is simple and easy to merge with ordinary three dimensional panel method program. It may, therefore, suggest a practical way to improve existing three dimensional panel methods (Chapter 3).

b) *By introducing two types of high order panel methods:* The T.C.method is marginally more efficient than the ordinary panel method for the present numerical examples where only a few hundred of panels are employed, but this improvement will be more significant when a more complex body or a multihull body is calculated and consequently more panels are needed to approximate the body geometry. The T.G. method is computationally less efficient than ordinary panel method although it can minimize the effect from irregular frequencies (Appendix A).

2) The predictions from modified panel method (a) agree well with experimental and other theoretical results for the Series 60 model, confirming basic validity of the present modification. The results also show that the three dimensional theory gives more realistic value for the low frequency hydrodynamic coefficients than the two

dimensional theory which is restricted to high frequency oscillation. In spite of these differences both two and three dimensional theories predict motion responses which agree quite closely for the monohull model. This is due to the fact that at lower frequencies, where two and three dimensional theories differ most, the equations of motion are dominated by the stiffness and wave exciting forces (Chapter 4).

3) Both two and three dimensional theories are acceptable in predicting motions of SWATH ships in head and beam seas, while in oblique seas three dimensional theory produces more realistic predictions at least for the present tandem strut model. The relatively poor predictions by the two dimensional approach are due to its inability to treat the hydrodynamic interaction between twin hulls properly because it only take such interactions in transverse direction into account (Chapter 4).

4) The viscous damping effects motions of SWATH ships significantly and must be considered in the motion predictions. The viscous damping on SWATH motion can be predicted by combining the crossflow approach with present three dimensional theory. In a strict theoretical sense, an extension of the equilinearization method for predicting motion in irregular waves cannot be justified. However, the present approach is recommended until a more rigorous and practical means is developed (Chapter 4).

5) The standing waves can significantly effect the hydrodynamic coefficients of twin hull ships by introducing rapid changes in the curves of added masses from maximum value to minimum value (sometime negative) and peaks on the curves of damping coefficients. These effects can be predicted by the present three dimensional theory (Chapter 4).

6) Two types of standing waves with different natures may occur in the vicinity of the twin hull ships, i.e. longitudinal and transverse standing waves. The

longitudinal standing waves occur at $2L_s/\lambda=n$ and transverse standing waves occur at $2B_i/\lambda=n$, where L_s is length of strut, B_i is inner distance of the twin hulls, λ is the wave length and n is any integer number (Chapter 4).

7) The first longitudinal standing wave with the lowest frequency, i.e. $2L_s/\lambda=1$, usually produces the maximum side force and bending moment on the cross deck structure of twin hull ships and its induced bending moments on the cross deck structure of SWATH can be predicted by the present three dimensional theory with reasonable accuracy in beam and quartering seas (Chapter 4 and 6).

8) The conclusions made for longitudinal standing waves are mainly based on the theoretical calculations. Therefore, systematic experiments are needed to support the present finding. If the finding is true, those longitudinal standing waves must have very strong three dimensional effects and subsequently the three dimensional method should be used in the predictions (Chapter 4).

9) The theoretical method introduced in this thesis is acceptable for predicting motion and sling tension of crane vessels during heavy lifting operations. The results confirm that both the coupling motion effect between the vessel and the load being lifted and the viscous damping effect on the motion are significant. The present method includes these effects in the prediction and the results agree well with available experimental data (Chapter 5).

10) A general three dimensional method for predicting wave loads on cross deck of twin hull vessels is presented and it is suitable for arbitrary wave heading unlike the widely used strip theory approach which is only valid in pure beam sea. The three dimensional predictions agree closely with available experimental data in both beam and quartering seas which can be used to validate the present method (Chapter 6).

11) The analytical results show that the sea approaching just forward or aft of the beam can produce the biased load distribution which may introduce the maximum

local stress on the structure. It is difficult to predict this kind of load distribution by two dimensional theory, but the prediction from three dimensional theory still need to be justified by experiments. It is believed that the present three dimensional method can produce the more accurate load distribution over the wetted hull surface of a vessel than two dimensional theory. Those predictions are important for structural analysis (Chapter 6).

12) The method for predicting statistic responses of motion and wave load of a ship in irregular waves based on wave energy spectrum is presented. This method is then extended to predict the seakeeping quality of a specific ship design in given ocean environment. By means of this method, if the ship hull form and the ocean environmental data for certain area are known, the seakeeping quality of the design can be evaluated analytically. Therefore, it provides a useful tool for practical ship designers (Chapter 7).

13) If only the most serious motion condition of SWATH in a seaway is needed the both 3D and 2D theories are acceptable, while if the seakeeping effectiveness is to be predicted the 3D theory will provide more reliable results than the 2D theory (Chapter 7).

14) Prediction of ship motion in following waves or at high forward speed is an area that needs further improvement of theory. This is particularly important for SWATH if future developments call for equipping with controllable fins to maintain good seakeeping quality in following waves (Chapter 4 and 7).

8.2 Proposals for Future Developments

The three dimensional theory presented in this thesis has been shown to be a powerful tool in the solution of ship motions and wave loads in regular and irregular waves. It has been successfully applied to a number of engineering problems with good prediction accuracy. Furthermore, the work in this thesis has also provided an important basis which can be a stepping stone towards further developments. As

extensions of the present work, a number of other problems can be dealt with by means of the direct application or minor modification of the present theory and program. These problems are briefly listed as follows.

1) *Relative bow motion and slamming*: The usual approach to predict the relative bow motion of a ship is to simplify the problem by neglecting the effect from disturbance of the ship to the local free surface elevation near the bow. This results in generally poor prediction, especially for the twin hull vessels since the hydrodynamic effect is very significant in this condition. Both experimental and theoretical results have shown that at certain frequencies the amplitude of wave elevation in the vicinity of twin hulls can be three or four times higher than the amplitude of the incident waves, so this contribution to the relative bow motions can not be simply neglected. The present theory and the program have the ability to predict such an effect even near the bow region where the three dimensional effect is significant. It is worth while to investigate the application of the present theory to predict the relative bow motion of twin hull ship by taking the local elevation into account. With better predictions of relative bow motions, the prediction of the occurrences of slamming and the slamming forces acting on the cross deck structures of twin hull ships, which are difficult to predict correctly by traditional strip theory approach instead some empirical correction terms must be used, will also be improved.

2) *Upwelling*: The upwelling phenomenon in the vicinity of twin or multi hull bodies, such as SWATH, semi-submersible and TLP, can be predicted by the present theory in both frequency and time domain. This approach can directly deal with three dimensional problem in a much cheaper way than the finite differences and finite element method. By means of the theoretical and experimental investigations into upwelling, the standing wave phenomenon and its effect on the wave loading can also be systematically studied. This is still an area which is not well understood.

3) *Predicting motion and forces between two ships closely advancing in waves*: This is equivalent to the problem of ships fueling in a seaway and is of interest to either naval or merchant ships. By slightly modifing of present theory this problem can be predicted.

The applications of the present theory is now restricted to the first order force and motion problems. With the further modification of the present theory and program, the study can be carried out in the second order force and motion problems in both frequency and time domains, i.e.

4) *Second order wave drifting forces and motions*: Based on the first order potential provided by the present program, it is possible to calculate the second order wave drifting forces and motions by using the near field approach. The second order forces are primarily important in the motion prediction of mooring systems and for TLPs. This approach can also extended to the time domain solution for the problem of so called 'low frequency second order motions' by applying Fourier transformation to the frequency domain solution.

5) *Wave added resistance*: The wave added resistance is equivalent to the prediction of the second order wave drifting forces acting on the moving bodies in surge direction. The forward speed effect can be considered in two different ways: firstly, by simplified three dimensional approach as described in this thesis in terms of the forward speed correction terms, or by full three dimensional theory in terms of the translating and pulsating source which satisfies the forward speed dependent free surface condition. The second approach is much more computationally time consuming than the first one.

So far the discussions have shown that the present theory and program have been successfully applied or have the ability to apply to wide range of motion and wave load problems for both ships and offshore structures. However, it should always be keept in mind that this application is only valid for the problem in which the basic assumptions of the

theory are acceptable. In other words, the present theory can only apply to the problems with linear free surface, small motion amplitude and an open free surface region, and for a moving body the Froude number must be low and the oscillation frequency must be high. Removing all of these limitations is, at least at present, impossible, but modifying some of them for a specific purpose do can form a reasonable proposal for future development.

6) *Introducing the translating and pulsating source*: When a ship moves a quite high Froude number, the forward speed effect on the free surface condition is not negligible. Therefore, the Green's function which satisfies the forward speed dependent free surface condition, i.e. translating and pulsating source, should be employed in the present program. The hydrodynamic effect from the steady state potential may also considered if necessary. This approach may be extended to the second order problem to calculate the wave added resistance as mentioned in the Proposal 5.

7) *Large amplitude motions*: The large amplitude motions in serious ocean environments are of primary concern in the design practice for either ships or offshore structures. The removal of the linear assumption on the free surface condition and the body surface condition which is derived from the mean wetted surface becomes necessary. The use of fundamental sources (1/R) distribution over whole body, free surface and a control surface at infinity is one of the possible approaches. In terms of this approach the introduction of non-linear free surface boundary condition is relatively easy. If the frequency domain solution is further transferred to the time domain there even exists a way to solve the problem for the body surface kinetic boundary conditions over instantaneously submerged body surface. Unfortunately, the non-linear radiation condition at infinity is still a difficult task. There are two possible ways to do it. Firstly, by setting the control surface, on which the radiation condition must be satisfied, far away from the body, so that the non-linear radiation effect is negligible. But this will increase the total number of panels required on the free surface and consequently the computational effort will increase dramatically. Secondly, by applying the solutions

for the non-linear radiation condition on the control surface. This may lead a efficient way for the present problem, but is a mathematical problem.

Apart from the foregoing discussion, there is a more practical method to solve this problem. In this method, the present frequency solution is firstly transferred to the time domain, then the hydrostatic and hydrodynamic terms in the motion equations can be derived on the instantaneously wetted body surface at every time step by using the present program, and finally the motion equation can be solved at each time step. This method is not theoretically rigorous since the linear free surface condition and linear body surface condition are still kept in the solution. However, it is simpler and more straightforward than the first suggested approach, and it can improve the solution over the original three dimensional theory.

8) *Ship motions in following seas*: The solution of this problem is an area that needs further improvement both theoretically and experimentally. The use of translating and pulsating source can improve the solution near the zero encounter in following seas since this approach does not assume the high oscillation frequency at forward speed case. But the experiments have shown that the coupling effect between the surge and pitch on the motion responses in the following seas is significant. This kind of coupling effect may not be small enough to be considered by the linear assumption. The prediction of the motion responses in the following seas, especially for the SWATH with fin control system, is an important task for the future research.

9) *Solution of a problem with restricted free surface region*: The oil sloshing in a tank at a seaway is such kind of problem. The combination of the present theory and the fundamental source distribution method (Proposal 7) for the fluid region outside and inside the tank respectively may suggest a way for the solution.

The three dimensional theory is still computationally expensive, especially when translating and pulsating sources are used. Clearly another important area is to improve

computational efficiency which leads to the following tasks.

10) To find a efficient way to evaluate the double integral in the translating and pulsating source is a key point to make the full three dimensional theory for ship motion problem computationally more efficient.

11) *High order panel method*: As discussed in Appendix A the high order panel method has potential to improve the computational efficiency of three dimensional panel method when more panels are required to approximate a complex body or a multi hull body. Even for simple mono hulls, if the translating and pulsating source is employed and the steady state potential is taken into account the high order panel method may become computational efficient. As next step of the development of high order panel method the quadrilateral curvilinear panels with constant or higher order source density distribution may be introduced. The major advantage of such panels is that they fit the body surface more closely than the present triangular plan panels used in Appendix A.

REFERENCES

CHAPTER ONE

[1] Euler, L.:'Scientia Navalis, sev Tractatus de Construendis ac Dirigendis Navibus', St. Petersburg, 1749

[2] Bernoulli, D.:'Principles Hydrostatiques et Mecaniques, ou Memoire sur la Maniere de Diminuer le Roulis et le Tangage d'un Navire sans qu'il Perde Sensiblement Aucune des Bonnes Qualities que sa Construction Doit Lui Donner', Prix de l'Academie des Sciences, Paris, 1757

[3] St. Denis, M. and Pierson, W.J.:'On the Motion of Ships in Confused Seas', Trans. SNAME 61, 1953, pp 280-357

[4] Korvin-Kroukovsky, V.B. and Jacobs, W.R.:'Pitching and Heaving Motions of a Ship in Regular Waves', Trans. SNAME 65, 1957, pp 590-632

[5] Jacobs, W.R.:'The Analytical Calculation of Ship Bending Moments in Regular Waves', Journal of Ship Research, Vol.2, No.1, 1958

[6] Gerritsma, J. and Beukelman, W.:'Analysis of the Modified Strip Theory for the Calculation of Ship Motions and Wave Bending Moments', Int. Shipbuilding Progress 14, 1967, pp 319-337

[7] Smith, W.E.:'Computation of Pitch and Heaving Motions for Arbitrary Ship Forms', Int. Shipbuilding Progress, Vol.14, No.155, 1967

[8] Ursell, F.:'On the Heaving Motion of a Circular Cylinder in the Surface of a Fluid', Quart J. Mech. Appl. Maths. 2, 1949, pp 218-231

[9] Thorne, R.C.:'Multipole Expansions in the Theory of Surface Waves', Proc. Camb. Phil. Soc. 49, 1953, pp 707-716

[10] Porter, W.:'Pressure Distributions, Added Mass and Damping Coefficients for Cylinders Oscillating in a Free Surface', Univ. of California Eng. Publ. Series 82-16, 1960

[11] Tasai, F.:' On the Damping Force and Added Mass of Ships Heaving and Pitching', Report of Research Institute for Applied Mechanics, Kyushu University, 1960

[12] Frank, W.:'Oscillations of Cylinders in or below the Free Surface of Deep Fluids', NSRDC Report 2375, 1967

[13] Smith, W.E. and Salvesen, N.:'Comparison of Ship-Motion Theory and Experiment for Destroyer with Large Bulb', J. Ship Research, Vol.14, No.1, 1970

[14] Timman, R. and Newman, J.N.:'The Coupled Damping Coefficients of Symmetric Ships', J. Ship Research, 5, 1962, pp 1-7

[15] Ogilvie, T.F. and Tuck, E.O.:'A Rational Strip Theory of Ship Motions-Part 1', Department Naval Arch. and Marine Eng., Michigan Univ., Report 013, 1969

[16] Salvesen, N., Tuck, E.O. and Faltinsen, O.:'Ship Motions and Sea Loads', Trans. SNAME 79, 1970, pp 250-287

[17] Vugts, J.H.:'The Hydrodynamic Forces and Ship Motions in Oblique Waves', Neth Res Centre TNO Report 150S, 1971

[18] Kim, C.H., Chou, F.S. and Tien, D.:'Motions and Hydrodynamic LOads of a Ship Advancing in Oblique Waves', Trans. SNAME, Vol.88, 1980, pp 225-256

[19] Newman, J.N.:'The Theory of Ship Motions', Advances in Applies Mechanics 18, 1978, pp 221-283

[20] Troesch, A.W.:'The Diffraction Potential for a Slender Ship Moving through Oblique Waves', The Department of Naval Arch. and Marine Eng., Univ. of Michigan, Report No.176, 1975

[21] Haskind, M.D.:'The Exciting Forces and Wetting of Ships in Waves', Published in Russian in Izvestia Akademii Nauk, SSSR, Otdelenie Tekhnicheskikh Nauk, No.7, 1957, pp 65-79; English Translation in David Taylor Model Basin Translation No.307, March 1962

[22] Ogilvie, T.F.:'Fundamental Assumptions in Ship-Motion Theory', Proc. Int. Symposium on the Dynamics of Marine Vehicles and Structures in Waves, Meth. Eng. Publ., London, 1975, pp 135-145

[23] Faltinsen, O.:'A Rational Strip-Theory of Ship Motions-Part 2', Dept. Naval Arch. and Marine Eng., Michigan Univ. Report 013, 1971

[24] Maruo, H.:'On the Wave Pressure on the Surface of a Slender Ship Fixed in Head Seas', Proc. 14th ITTC, 1975, pp 322-331

[25] Ursell, F.:'Note on the Refraction of Head Seas by Long Ships', 10th Symposium on Naval Hydrodynamics, 1974, pp 17-20

[26] Moeyes, G. Measurement of Exciting Forces in Short Waves', Delft Progress Report 2, 1976

[27] Kim, C.H.:'The Hydrodynamic Interaction between Two Cylindrical Bodies Floating in Beam seas', SIT-OE-72-10, Ocean Engineering Department, Stevens Institute of Technology, Oct. 1972

[28] Kim, C.H.:'Motion and Loads of a Catamaran Ship of Arbitrary Shape in a Seaway', J. Hydronautics, Vol.10, No.1, Jan. 1976, pp 8-17

[29] Lee, C.M., Jones, H.D. and Curphey, R.M.:'Prediction of Motion and Hydrodynamic Loads of Catamarans', Marine Technology, Vol.10, No.4, Oct. 1973

[30] Lee, C.M. and Curphey, R.M.:'Prediction of Motion, stability, and Wave Load of Small-Waterplane-Area, Twin-Hull Ships', Trans. SNAME, Vol.85, 1977, pp 94-130

[31] Fein, A.J. and Lamb, G.R.:'The Developing Technology of SWATH Ship Dynamics', OTC Paper 4432, Houston, May, 1983

[32] Newman, J.N. and Sclavounos, P.:'The Unified Theory of Ship Motion', Proc. 13th Symp. on Naval Hydrodynamics, Tokyo, Oct. 1980, p 373

[33] Hong, Y.S.:'Heave and Pitch Motions of SWATH Ships', J Ship Research, Vol.30, 1986, pp 12-25

[34] Takagi, M.:'An Examination of the Ship Motion Theory as Compared with Experiment', Int. Symp. on the Dynamics of Marine Vehicles and Structures in Waves, Mech. Eng. Publ., London, 1975, pp 161-169

[35] Eatock Taylor, R. and Hung, M.:'Some Wave Load Effects in the Design of SWATH Ships', Proc. 3rd Int. Symp. on Practical Design of Ships and Mobile Units,

Trondheim, June 1987

[36] Djatmiko, E., 'Experimental Investigation of SWATH Ship Motion and Wave Loading', M.Sc. Thesis, Department of Naval Architecture and Marine Engineering, University of Glasgow, Dec. 1987

[37] Olsen, S.R.:'An Evaluation of the Seakeeping Qualities of Naval Combatants', Naval Engineers Journal, Feb. 1978, pp 23-38

[38] Kennel, C., White, B. and Constock, A.:'Innovative Naval Design for North Atlantic Operation', SNAME Annual Meeting, 1985

[39] Wu, Y.S.'Hydroelasticity of Floating Bodies', Ph.D. Thesis, Brunel University, U.K., 1984

[40] McGregor, R.C. (Univ. of Glasgow): Private Cammunacation on Wave Loads of SWATH Ships, Dec. 1987

[41] Hess, J.H. and Smith, A.M.O.:'Calculation of Non-Lifting Potential Flow about Arbitrary Three-Dimensional Bodies', Douglas Aircraft Co., Report No.ES40622, 1962

[42] Garrison, C.J.:'Hydrodynamic Of Large Objects in the Sea. Part 1-Hydrodynamic Analyses', J. Hydronautics, Vol.8, 1974, pp 5-12

[43] Garrison, C.J.:'Hydrodynamic Of Large Objects in the Sea. Part 2-Motion of Free-Floating Bodies', J. Hydronautics, Vol.9, 1975, pp 58-63

[44] Faltinsen, O.M. and Michelsen, F.C.:'Motions of Large Structures in Waves at Zero Froud Number', Int. Symp. Dynamics of Marine Vehicles and Structures in Waves, University College, London, 1974, pp 99-114

[45] Hogben, N. and Standing, R.G.:'Wave Loads on Large Body', Int. Symp. Dynamics of Marine Vehicles and Structures in Waves, University College, London, 1974, pp 258-277

[46] Bai, K.J. and Yeung, R.W.:'Numerical Solutions to Free Surface Flow Problem', Proc. 10th Symposium of Naval Hydrodynamics, Cambridge, Mass., 1974, pp 609-647

[47] Yeung, W.:'Numerical Methods in Free Surface Flows', Annual Review of Fluid Mechanics, Vol.14, 1982, pp 395-442

[48] Zienkiewicz, O.C., Kelly, D.W. and Bettess, P.:'Marriage a la Mode-the Best of Both Worlds (Finite Element and Boundary Integrals)', Chapter 5, Energy Methods in Finite Analysis, (ed. Glowinski, R., Roding, E.Y. and Zienkiewicz, O.C.) Willey, Chichester, 1979

[49] Eatock Taylor, R. and Zietsman, J.:'Hydrodynamic Loading on Multicomponent Bodies', Proc. Int. Conf. on Behaviour of Offshore Structures, MIT, 1982, pp 424-446

[50] Chang, M.S.:'Computations of Three Dimensional Ship Motions with Forward Speed', Proc. 2nd Int. Conf. on Numerical Ship Hydrodynamics, Washington D.C., 1977, pp 124-135

[51] Inglis, R.B., 'Three-dimensional Analysis of the Motion of a Rigid Ship in Waves', Ph.D. Thesis, Dept. of Mechanical Engineering, University College of London, 1980

[52] Chen, H.H., Torng, J.M. and Shin, Y.S.:'Progress Report Task 1 of Hydrodynamic Pressure Project for NSMB Cooperative Research Sea Loads Working Group', American Bureau of Shipping, May, 1985

[53] Price, W.G. and Wu, Y.S.:'Hydrodynamic Coefficients and Responses of Semisubmersibles in Waves.', 2nd Int. Symp. on Ocean Eng. and Ship Handing, SSPA Gothenbury, 1982, pp 393-416

CHAPTER TWO

[1] Haskind, W.D.,:'The Exciting Forces and Wetting of Ships in Waves', DTMB (Translation) No.307, 1962, (Originally Published 1957)

[2] Salvesen, N., Tuck, E.O. and Faltinsen, O.:'Ship Motion and Sea Loads', Trans. SNAME Vol.78, 1970

[3] John, F.:'On the Motion of Floating Bodies: Part II', Commun. on Pure Appl. Math., Vol.3, 1950, pp45-101

[4] Newman, J.N.:'The Theory of Ship Motions', Adv. Appl. Mech, Vol.18, 1978

[5] Wehausen, J.Y. and Laitone, E.V.:'Surface Waves', Handbuch der Physik, Vlo.9, Springer Verlag, Berlin 1960

[6] Shen, S.F.:'Finite Element Methods in Fluid Mechanics', Annual Review of Fluid Mechanics, Vol.9, 1977, pp421-445

[7] Mei, C.C.:'Numerical Methods in Water Waves Diffraction and Radiation', Annual Review of Fluid Mechanics Vol.10, 1978, pp393-416

[8] Yeung, W.:'Numerical Methods in Free Surface Flows', Annual Review of Fluid Mechanics Vol.14, 1982, pp395-442

[9] Bai, K.J. and Yeung, R.W.:'Numerical Solutions to Free Surface Flow Problem', Proc. 10th Symposium of Naval Hydrodynamics, Cambridge, Mass., 1974, pp609-647

[10] Bettess, P.:'Finite and Infinite Elements for Fluid Loading on Offshore Structures - An Assessment of Accuracy', Integrity of Offshore Structure - 3 (ed. Faulkner, D., Cowling, M.J. and Incecik, A.), Elsevier Applied Science, London and New York, 1987

[11] Zienkiewicz, O.C., Kelly, D.W. and Bettess, P.:'Marriage a la Mode - the Best of Both Worlds (Finite Element and Boundary Integrals)', Chapter 5, Energy Methods in Finite Analysis, (ed. Glowinski, R., Roding, E.Y. and Zienkiewicz, O.C.) Willey, Chichester, 1979

[12] Frank, W.:'Oscillation of Cylinders in or below the Free Surface of Deep Fluids', Naval Ship Res. Dev. Centre Report 2375, vit 40pp 1967

[13] Garrison, C.J., Seethara Rao, V.:'Interaction of Waves with Submerged Objects', Proc. ASCE J. Waterway, Harbors, Coastal Engrg. Div. Vol97, 1971, pp259-277

[14] Faltinsen, O.M. and Michelsen, F.C.:'Motions of Large Structures in Waves at Zero Froud Number', Int. Symp. Dynamics of Marine Vehicles and Structures in

Waves, University College, London, 1974, pp99-114

[15] Inglis, R.B. and Price. W.G.:'Three-Dimensional Ship Motion Theory - Comparison between Theoretical Predictions and Experimental Data of the Hydrodynamic Coefficients with Forward Speed', RINA Paper W2, 1981

[16] Pien, P.C.:'Calculation of Non-Lifting Potential Flow about Arbitrary Three-Dimensional Bodies Based on Doublet Distributions', DTNSRDC, Bethesda, Rep. No SPD 601-01, 1975

[17] Chang, M.S. and Pien, P.C.:'Hydrodynamic Forces on a Body Moving beneath a Free Surface', Proc. 1st Conf. on Numerical Ship Hydrodynamics, Gaitherbury, 1975

[18] Brard, R.:'The Representation of a Given Ship Form by Singularity Distribution When the Boundary Condition on the Free Surface is Linear', Journal of Ship Research, 1972

[19] Chang, M.S.:'Computations of Three Dimensional Ship Motions with Forward Speed', Proc. 2nd Int. Conf. on Numerical Ship Hydrodynamics, Washington D.C. 1977, pp124-135

[20] Eatock Taylor, R.'Techniques for Wave Diffraction and Radiation Problems', University College London, Marine Technology Centre Report, 1979

[21] Wu, X.J. and Price, W.G.:'Appearance and Disappearance of Irregular Frequencies in Wave-Structure Interaction Problems:, Proc. 1st Workshop on Water Waves and Floating Bodies, MIT, 1985

[22] Shin. Y.S.:'Three Dimensional Effects on the Hydrodynamic Coefficients and Wave Exciting Forces Used in Prediction of Ship Motion', Ph.D. Thesis, Dept. of Naval Architecture and Ocean Eng., University of Michigan, 1979

[23] Delves, L.M. and Walsh, J.:'Numerical Solution of Integral Equations', Oxford Clarendon 1974,

[24] Chertock, G.:'Integral Equation Method in Sound Radiation and Scattering From Arbitrary Surface', Nav. Ship Res. Dev. Centre Report 3538, 1971

[25] Ursell, F.:'Short Surface Waves due to an Oscillating Immersed Bodies', Proc. Roy. Soc., A220, 1953, pp90-103

[26] Ursell, F.:'Irregular Frequencies and the Motion of Floating bodies in a Free Surface', J. Fluid Mech., Vol.105, 1982, pp143-156

[27] Faltinsen, O.:'A Study of Two Dimensional Added Mass and Damping Coefficients by the Frank's Close Fit Method', Det. Norske Veritas Report 69-10-S, 1969

[28] Ohmatsu, S.:'On the Irregular Frequencies in the Theory of Oscillating Bodies in a Free Surface', Ship Res. Inst., Tokyo, Japan, Paper 48, 1975

[29] Soding, H.'The Flow around Ship Section in Waves', Schiffstechnik 20, 1973, pp9-15

[30] Soding. H. and Lee, K.Y.:'The Two Dimensional Potential Flow Excited by a Body Oscillating at a Free Surface (description of Accompanying Program ASYM 1)', Technische University, Hannover Report 12, 1975

[31] Ogilvie, T.F. and Shin, Y.S.:'Integral Equation Solutions for Time Dependent Free Surface Problem', J. Soc. Naval Architecture, Japan, Vol.143, 1978

[32] Salavounos, D. and Lee. C.H.:'Topic on Boundary-Element Solutions of Wave Radiation-Diffraction Problem', Proc. 4th Int. Conf. on Numerical Ship Hydrodynamics, Washington D.C., 1985

[33] Burton, A.J. and Miller, G.F.:'The Application of Integral Equation Method to the Numerical Solution of Some Exterior Boundary-Value Problems', Proc. Royal Soc. London A323, 1971, pp.201-220

[34] Inglis, R.B. and Price, W.G.:'Calculation of the Velocity Potential of a Translating Pulsating Source', Trans. RINA, Paper W2, 1980

[35] Guevel, P. and Bougis, J.:'Ship-Motion with Forward Speed in Finite Depth', International Shipbuilding Progress, Vol.29, 1982, pp103-117

[36] Wu, G.X. and Eatock Taylor, R.:'A Green's Function Form for Ship Motion at Forward Speed', Int. Shipbuilding Progress, Vol.34, 1987, pp189-196

CHAPTER THREE

[1] Faltinsen, O.M. and Michelsen, F.C.:'Motions of Large Structures in Waves at Zero Froude Number', Int. Symp. Dynamics of Marine Vehicles and Structures in Waves, University College, London, 1974, pp99-114

[2] Shin. Y.S.:'Three Dimensional Effects on the Hydrodynamic Coefficients and Wave Exciting Forces Used in Prediction of Ship Motion', Ph.D. Thesis, Dept. of Naval Architecture and Ocean Eng., University of Michigan, 1979

[3] Inglis. R.B.:'Three-Dimensional Analysis of the Motion of a Rigid Ship in Waves', Ph.D. Thesis, Dept. of Mechanical Engineering, University College London, 1980

[4] Hess, J.H. and Smith, A.M.O.:'Calculation of Non-Lifting Potential Flow about Arbitrary Three-Dimensional Bodies', Douglas Aircraft Co., Report No.ES40622, 1962

[5] Wilikinson, J.H. and Reinsch, C.:'Handbook for Automatic Computation, Vol.II, Linear Algebra, pp.93-110, Springer Verlag, 1971

[6] 'NAG Library Manual', Numerical Algorithms Group, Oxford, 1982

[7] Hogben, H. and Standing, R.G.:'Wave Loads on Large Bodies', Int. Symposium on the Dynamics of Marine Vehicles and Structures in Waves, London, 1975

[8] Kochin, N.E.:'The Theory of Wave Generated by Oscillations of a Body under the Free Surface of a Heavy incompressible Fluid', Translated in Soc. Nav. Archit. Marine Eng. Tech. Res. Hull, No.1-10, 1952

[9] Havelock, T.H.:'The Damping of the Heaving and Pitching Motion of a Ship', Philosophical Magazine, Vol.33, Series 7, 1942, pp666-673

[10] Haskind, M. D.:'The Oscillation of a Body immersed in Heavy Fluid', Prikl. Mat. ekh, 8, 1944, pp287-300

[11] Thorne, R.C.'Multiple expansions in the Theory of Surface Waves', Proc. Cambridge Philos. Soc. 49, 1953, pp707-716

[12] Zienkiewicz, O.C., Kelly, D.W. and Bettess, P.:'Marriage a la Mode - the

Best of Both Worlds (Finite Element and Boundary Integrals)', Chapter 5, Energy Methods in Finite Analysis, (ed. Glowinski, R., Roding, E.Y. and Zienkiewicz, O.C.) Willey, Chichester, 1979

[13] Ursell, F.:'The Periodic Heaving Motion of a Half-immersed Sphere', Manchester University, Dept. of Mech., Report to U.S. Office of Naval Research, 1963

[14] Kim. W.D.:'On the Harmonic Oscillations of a Rigid Body on Green Surface', J. Fluid Mech. Vol.21, 1965, pp427-451

[15] Yeung, R.W.:'A Singularity Distribution Method for Free Surface Flow Problems with on Oscillating Body', University of Calif., Berkeley, Report NA 73-6, 1973

[16] Hearn, G.E.:'Alternative Methods of Evaluating Green's Function in Three-Dimensional Ship Wave Problems', J Ship Research, Vol.21, 1977, pp89-93

[17] Newman, J.N.:'Double-precision Evaluation of the Oscillatory Source Potential', J. Ship Research, Vol.28, No.3, 1984, pp151-154

[18] Guevel, P. and Doubisse, J.C.:'Oscillations d'un Flotteur Soumis a L'action de la Haule', Lecture notes E.N.S.M. Nantes, France, 1978

[19] Martin, M.:'Resolution numerique due Probleme Linearise de la Lenue a la mer, Trans, Assoc. Tech. Maritime Aeronautique, 1980

[20] Noblesse, F.:'The Green Function in the Theory of Radiation and Diffraction of Regular Water Waves by a Body', J Eng. Math., Vol.16, 1982, pp137-169

[21] Newman, J.N.:'The Evaluation of Free Surface Green Functions', Proc. of 4th Int. Conf. on Ship Hydrodynamics, Washington D.C., 1985

[22] Abramowitz, M. and Stegun, I.A.:'Handhhok of Mathematical Functions with Formulas, Graphs and Mathematical Tables', Government Printing Office, Washington and Dover, New York, 1964

[23] Monecella, V.J.:'The disturbance due to a Slender Ship Oscillating in Waves in a Fluid of Finite Depth', J Ship Research, Vol.10, 1966

[24] Wu, Y.S.'Hydroelasticity of Floating Bodies', Ph.D. Thesis, Brunel University, U.K., 1984

CHAPTER FOUR

[1] Inglis, R.B., 'Three-dimensional Analysis of the Motion of a Rigid Ship in Waves', Ph.D. Thesis, Dept. of Mechanical Engineering, University College of London, 1980

[2] Inglis, R.B. and Price, W.G., 'Three-dimensional Ship Motion Theory - Comparison between Theoretical Predictions and Experimental Data of the Hydrodynamic Coefficients with forward speed', RINA Paper, No. W2, 1981

[3] Gerristma, J. and Beukelman, W., 'The Distribution of the Hydrodynamic Forces on a Heaving and Pitching Ship Model in Still Water', Int. Ship Building Progress, Vol.11, No.123, Nov. 1964, pp.506-522

[4] Vugts, J.H., 'The Hydrodynamic Forces and Ship Motions in Oblique Waves', Neth. Res. Centre, TNO Report 150S, 1971

[5] Van Leeuwen, G., 'The Lateral Damping and Added Mass of a Horizontally Oscillating Ship Model', Neth. Ship Res. Centre, TNO Report 65S Dec. 1964

[6] Bishop, R.E.D. and Price, W.G., 'Hydroelasticity of Ships', Cambridge University Press, 1979

[7] Timman, R. and Newman, J.H., 'The Coupled Damping Coefficients of Symmetric Ships', J. of Ship Research, Vol.5, No.1 1962, pp.1-7

[8] Vugts, J.H., 'The Hydrodynamic Coefficients for Swaying, Heaving and Rolling Cylinders in a Free Surface', Neth. Ship Research Centre TNO, Report No.112S, May, 1968

[9] Myrhaug, D. and Sand, L.O., 'On the Frictional Damping to the Rolling of a Circular Cylinder', Division of Ship Hydrodynamics, Norwegian Institute of Technology, Trondheim, 1978

[10] Tanaka, N., 'A Study on the Bilge Keels, Part 4, On the Eddy Making Resistance to the Rolling of a Ship Hull', Japan Society of Naval Architects, No.109, 1960, pp.205-212

[11] Ikeda, Y., Himena, Y. and Tanaka, N., 'Components of Rolling Damping of a Ship at Forward Speed', J. Soc. Naval Architecture of Japan, 143, 1978, pp.113-125

[12] Lee, C.M., Jones, H. and Bedel, J.W., 'Added Mass and Damping Coefficients of Heaving Twin Cylinders in a Free Surface', NSRDC Report 3695, 1971

[13] Lee, C.M. and Curphey, R.M., 'Prediction of Motion, Stability and Wave Loads of Small-Waterplane-Area, Twin-Hull Ships', SNAME Transactions, Vol.85, 1977, pp.94-130

[14] Frank, W., 'Oscillation of Cylinders in or below the Free Surface of Deep Fluid', NSRDC Report 2375, 1967

[15] Lee, C.M., Jones, H.D. and Curphey, R.M., 'Prediction of Motion and Hydrodynamic Loads of Catamaran', Marine Technology, Vol.10, No.4, Oct. 1973

[16] McGregor, R.C., 'Experimental Staudy of Upwelling of SWATH 1 in Beam Seas: Compliant Systems Cohesive Program, Report No.NAOE-87-37, University of Glasgow, 1987

[17] Wang, S. and Wahab, R., 'Heaving Oscillations of Twin Cylinders in a Free Surface', J. Ship Research, Vol.15, No.1, March 1971, pp.33-48

[18] Wang, S., 'On the Hydrodynamic Forces of Twin-Hull Vessels', Proc. 12th Coastal Engineering Conf., Vol.3, Washington D.C., 1970, pp.1701-1721

[19] Atlar, M. and Lai, P.S.K., 'A Two-Dimensional Method Estimating Hydrodynamic Loads and Motion of a Twin-Hull Semi-Submersible Associated with Some Hydrodynamic Aspects in Regular Beam Seas', Report NAOE-85-34, Dept. of Naval Architecture and Ocean Eng., University of Glasgow, 1985

[20] McGregor, R.C., 'An Illustration of Some SWATH Vessel Characteristics', 4th High Speed Craft Conf., London, 1983

[21] Thwaites, B., Ed., 'Incompressible Aerodynamics', Oxford University Press, 1960, pp.405-421

[22] Atlar, M., 'SWATH Wave Load Program - Method of Solution for 5 Degree of Freedom Coupled Equations of Motion of a SWATH Ship', Report No.NAOE-86-36, University of Glasgow, 1986

[23] Price, W.G. and Wu, Y.S.:'Hydrodynamic Coefficients and Responses of Semisubmersibles in Waves.', 2nd Int. Symp. on Ocean Eng. and Ship Handing, SSPA Gothenbury, 1982, pp 393-416

[24] Eatock Taylor, R. and Hung, M.:'Some Wave Load Effects in the Design of SWATH Ships', Proc. 3rd Int. Symp. on Practical Design of Ships and Mobile Units, Trondheim, June 1987

CHAPTER FIVE

[1] Faltinsen, O. and Michelsen, F.C.: 'Motion of Large Structures in Waves at Zero Froude Number ', International Symposium on the Dynamics of Marine Vehicles and Structures in Waves, London, 1974

[2] Zheng, X.: 'Calculation of Potential Flow about Arbitrary Three Dimensional Bodies, Part 2 - Free Surface Flow ' Report NAOE-85-54, University of Glasgow, 1985

[3] Nojiri, N. and Sasaki, T.: 'Motion Characteristics of Crane Vessels in Lifting Operation ', Paper no. 4603, OTC, Houston, 1983

[4] Ikeda, Y., Himena, Y. and Tanaka, N., 'Components of Rolling Damping of a Ship at Forward Speed', J. Soc. Naval Architecture of Japan, 143, 1978, pp.113-125

[5] Lee, C.M. and Curphey, R.M.: 'Prediction of Motion, Stability and Wave Load of Small-Waterplane-Area, Twin-Hull Ships ', Trans. SNAME, Vol. 85, 1977, pp. 94-130

[6] McGregor, R.C., Drysdale, L.H. and Wu, J-Y,: 'On the Response of SWATH Ship in the Presence of Control Fins ', 8th Ship Control Systems Symposium, The Hague, 1987

[7] Thwaites, B., Ed.: ' Incompressible Aerodynamics ', Oxford University Press,

1960, pp. 404-421

[8] Bassiouny, A.: 'The Stabilization of Semi-Submersibles', Ph.D Thesis, Dept. of Naval Architecture and Ocean Eng., University of Glasgow, April 1980

CHAPTER SIX

[1] Jacobs, W.R. 'The Analytical Calculation of Ship Bending Moments in Regular Waves', J. Ship Research, Vol. 2, No. 1, 1958

[2] Korvin-Kroukovsky, B.V. and Jacobs, W.R., 'Pitching and Heaving Motions of a Ship in Regular Waves', Trans. SNAME, Vol. 65, 1957

[3] Salvesen, N., Tuck, E.O. and Faltinsen, O., 'Ship Motion and Sea loads', Trans. SNAME, Vol. 78, 1970

[4] Lee, C.M. and Curphey, R.M. 'Prediction of Motion, Stability, and Wave load of Small-Waterplane, Twin-Hull ships', Trans. SNAME, Vol. 85, 1977, pp. 94-150

[5] Kennel, C., Lecture in the Department of Naval Architecture and Marine Engineering of Glasgow University, 1987

[6] Djatmiko, E., 'Experimental Investigation of SWATH Ship Motion and Wave Loading', M.Sc. Thesis, Department of Naval Architecture and Marine Engineering of Glasgow University, 1987

[7] Sikora, J., Dinsenbacher, A. and Beach, J.E., 'A Method for Estimating Lifetime loads and Fatigue lives for SWATH and Conventional Monohull Ships', Naval Engineers Journal, May, 1983

[8] Wahab, R., Pritchett, C. and Ruth, L.C., 'On the Behavior of the ASR Catamaran in Waves', Marine Technology, Vol. 8, No. 3, July, 1971

[9] Jones, H.D. and Gerzina, D.M., 'Motions and Hull-induced Bridging Structure loads for a Small Waterplane Area, Twin-Hulled Attack Aircraft Carrier in Waves', DTNSRDC Report 3819, Aug. 1973

[10] McGregor, R.C. (Univ. of Glasgow): Private Cammunacation on Wave Loads

of SWATH Ships, Dec. 1987

CHAPTER SEVEN

[1] Price, W.G. and Bishop, R.E.D.:'Probabilistic Theory of Ship Dynamics', Chapman Hall, 1974

[2] Pinkster, J.A.:'Low Frequency Second Order Wave-Exciting Forces on Floating Structures', Ph.D. Thesis, NSMB Publication No.650, Wageningen, 1980

[3] Cummins, W.E.:'The Impulse Response Function and Ship Motion ', Schiffstecknik, Vol.9, 1962, pp.101-109, Reprinted as DTMB Report 1661

[4] St. Denis, M. and Pierson, W.J.:'On the Motion of Ship in Confused Seas', Trans. SNAME, Vol.61, 1953, pp.280-357

[5] Ochi, M.K.:'On the Prediction of Extreme Values', Journal of Ship Research, Vol.17, No.1, 1973, pp29-37

[6] Ochi, M.K. and Motter, L.E.:'Prediction of Extreme Values of Impact Pressure Associated with Ship Slamming', Journal of Ship Research, Vol.13, No.2, June 1969

[7] Ochi, M.K. and Motter, L.E.:'Prediction of Slamming Characteristics and Hull Responses for Ship Design', Paper Presented at the Annual Meeting of SNAME, Nov., 1973

[8] Lee, C.M., Jones, H.D. and Curphy, R.M.:'Prediction of Motion and Hydrodynamic Loads of Catamarans', Marine Technology Journal, Oct. 1973

[9] Lee, C.M. and Curphy, R.M.:'Prediction of Motion, Stability, and Wave Load of Small-Waterplane-Area, Twin-Hull Ships', Trans. SNAME Vol.83, 1977, pp.94-130

[10] Pierson, W.J. and Moskowitz, L.:'A Proposed Spectral Form for Fully Developed Wind Seas, Based on the Similarity Theory of S.A. Kitaigarodskii', Journal of Geophysical Research, Vol.69, No.24, 1964, pp5181-5190

[11] Report of the Seakeeping Committee, 17th International Towing Tank Conference, 1984, p.531

[12] Michel, W.H.:'Sea Spectra Simplified', Marine Technology (Jan. 1968).

pp.17-30

[13] Bretschneider, C.L.:'Wave Variability and Wave Spectra for Wind-Generated Gravity Waves', Beach Erosion Board, U.S. Navy Corps of Engineers TM118, 1959

[14] Commander Naval Weather Service Command, U.S. Navy Marine Climatic Atlas of the World-Vol.1:'North Atlantic Ocean (Revised 1974)', NAVAIR 50-IC-528, Dec. 1974

[15] Olsen, S.R.:'An Evaluation of the Seakeeping Qualities of Naval Combatants', Naval Engineers Journal, Feb. 1978, pp.23-38

[16] Caldeira-Savaiva, F.L.A. and Clarke, D.:'Application of Multivariable Control Techniques to the Active Motion Control of SWATH Craft', Int. Conf. on SWATH ships and Advanced Multi-Hulled Vessels, London, April 1985

[17] McGregor, R.C., Drysdale, L.H. and Wu, J-Y:'On the Response of SWATH ship in Presence of Control Fins', 8th Ship Control Systems Symposium, The Hague, 1987

APPENDIX A

HIGHER ORDER PANEL METHODS

Abstract

Triangular panels with linear source density distribution are employed in the 3D panel method for the radiation and diffraction problem. Both the collocation and 'Galerkin' techniques have been used in the solution of the boundary integral equation. Extensive computations were made for the hydrodynamic coefficients of a spheroid and a Series 60 model. Comparisons on accuracy, efficiency and the behaviours in the vicinity of the first irregular frequency have been made between the present approaches and the ordinary panel method which uses quadrilateral panels with constant source distribution on each panel. The results show that the triangular panel method with the 'Galerkin' solution can minimize the effect from irregular frequencies, but it is computational inefficient, and the triangular panel method with the collocation solution is more efficient than the ordinary quadrilateral panel method.

1. Introduction

The 3D boundary integral method (or panel method) was pioneered by Hess and Smith (1964) in the context of infinite fluid flow. In their method the body surface is replaced by plane quadrilateral panels and a constant source density is assumed on each panel. In terms of Green's theorem, a Fredholm integral equation can be derived from the body surface boundary condition and then solved by the collocation technique for the velocity potential on each panel. Based on their work, numerous others, such as Garrison (1974), Faltinsen and Michelsen (1974), have extended this approach to the radiation and diffraction problem of linear surface waves by introducing the free surface potential or Green's function.

Nowadays, this approach which uses quadrilateral panels with constant source density

and collocation technique for its solution (called ordinary panel method in the following) has already used in most of 3D panel method programs, but there are two limitations which are worthy of noting here.

1. The composite source surface is discontinuous. For an arbitrary body it is not possible to arrange the trapezoids so that all four corners of each panel match the corners of adjacent panel. In other words, the source surface has leaks (see Fig.1).

2. The source distribution is discontinuous. The source density is constant over each panel and therefore jumps stepwise at boundary of two panels.

To avoid these limitations, one can either increase the number of panels used to approximate the body surface or improve the accuracy of each panel (changing the shape of panels or using higher order distribution of source density over each panel). In some cases, the latter approach is effective and has already been used successfully in some panel programs, for example Breit, Newman and Sclavounos (1985) and Breit (1985). In this study, an alternative way using triangular panels with linear source density distribution was employed in the 3D panel method. It is clear that this kind of panel can eliminate the two limitations mentioned above and improve the accuracy of panel description.

Two alternative methods based on the triangular panel approach were used in this paper. One of them uses the 'collocation' technique to solve the boundary integral equation (called T.C. method) and another uses 'Galerkin' technique (called T.G. method). The comparisons were made among the three methods, T.C., T.G. and ordinary panel method with the collocation solution, for heave added mass and damping coefficients of a spheroid, and the heave added mass and damping coefficient distribution along the hull of a Series 60 model. The results show that the T.G. method is computational inefficient, but it can minimize the effect from the irregular frequencies. The T.C. method is shown to be more efficient than the ordinary panel method. In the present numerical examples for which only a few hundred or less panels were used, the improvement of computational efficiency of the T.C. method is not significant. If a more complex geometry or multi-hull body is considered and more panels are

required, the advantage of the T.C. method will be more apparent. Finally, the possible directions for future work on the computation of wave-body effect using boundary integral method have been discussed.

2. Formulation of the Problem

The formulation considers a rigid body floating on a free surface. A right handed coordinate system o-xyz fixed with respect to the mean position of the body is used, with positive z vertically upwards through the centre of gravity of the body and origin in the plane of undisturbed free surface. Assuming the fluid to be idealized, the linearised problem describing the hydrodynamics associated with a body in sinusoidal waves may be expressed in terms of the velocity potential, $\phi(x,y,z)$. The complex time dependence $e^{-i\omega t}$, where ω is circular frequency and t is time, has already been factored out. After making the linear decomposition, the total potential can be rewritten as

$$\phi = \phi_0 + \phi_7 + \sum_{i=1}^{6} \phi_i \xi_i \qquad (1)$$

where ϕ_i, i=1,2,...6, are the velocity potential arising from the motion of the body and ξ_i, i=1,2,...6, are the amplitude of motion in each of six degrees freedom. The modes i=1,2,3 correspond to translation in the x, y, z directions and modes i=4,5,6 to rotation about the same axes respectively. ϕ_0 is the incident wave potential, i.e.

$$\phi_0 = \frac{iga}{\omega} \exp(kz + ikx\cos\beta - iky\sin\beta) \qquad (2)$$

where a is the wave amplitude, β the direction of wave propagation relative to x-axis and $k=\omega^2/g$ is the wave number. ϕ_7 is the diffraction potential. All potentials ϕ_i, i=1,2,...7, are governed by Laplace equation, the linear free surface condition, seabed condition, the body surface condition and the radiation condition.

Substituting the Green's function and one of the potentials ϕ_i, i=1,2,...7, into Green's theorem leads to the boundary integral equation

$$- \Omega \phi_i (\mathbf{x}) + \int_S d\xi \, \phi_i (\xi) \frac{\partial G (\mathbf{x}, \xi)}{\partial n_\xi} = \int_S d\xi \, V_n (\xi) \, G (\xi, \mathbf{x}) \qquad (3)$$

where $\mathbf{x}=(x,y,z)$ and $\xi=(\xi,\eta,\zeta)$ are two points on the body surface, $\mathbf{n}=(n_1,n_2,n_3)$ is the unit outward normal and $\mathbf{x}\times\mathbf{n}=(n_4,n_5,n_6)$, V_n is the normal component of the velocity on the body surface and is equal to $-i\omega n_j$ for j=1,2,...6 or $-\partial\phi_0/\partial n$, j=7. In general, $\Omega(>0)$ takes a value of 2π if $\mathbf{x}$ is on a plane surface, but otherwise is the solid angle inside the fluid in the neighbourhood of point $\mathbf{x}$, if $\mathbf{x}$ happens to be a vertex point, then $G(\mathbf{x},\xi)$ is the Green's function, which has different form in different boundary conditions. A good collection of Greens functions can be found in [Wehausen and Laitone, 1960].Since V_n is known, the unique solution of the Eqn.(3) always exists except at a set of discrete frequencies known as 'irregular frequencies'.

The integral Eqn.(3) may be solved numerically beginning with the subdivision of body surface S into N panels. Let S_j be the surface area of jth panel (j=1,2...N). After discretising, the Eqn.(3) can be written as

$$- \Omega \phi (\mathbf{x}) + \sum_{j=1}^{N} \int_{S_j} d\xi \, \phi \, (\xi) \frac{\partial G (\mathbf{x}, \xi)}{\partial n_\xi} = \sum_{j=1}^{N} \int_{S_j} d\xi \, V_n (\xi) \, G (\xi, \mathbf{x}) \qquad (4)$$

where the subscript i is omitted from ϕ. Generally, ϕ is variable in each panel. For different assumptions on the source density distribution over each panel, one can choose different collocation points $\mathbf{x}$ and make a linear system of equations with equal number of unknowns. This system of equations can then be solved directly for velocity potential. This is so called 'collocation method'. In an alternative way, the 'Galerkin' technique may be used where Eqn.(3) is satisfied in an averaged sense by integration over ith panel, i.e.

$$- \Omega \int_{S_i} d\mathbf{x} \, \phi \, (\mathbf{x}) + \sum_{j=1}^{N} \int_{S_i} d\mathbf{x} \int_{S_j} d\xi \, \phi \, (\xi) \frac{\partial G (\mathbf{x}, \xi)}{\partial n_\xi}$$

$$= \sum_{j=1}^{N} \int_{S_i} d\mathbf{x} \int_{S_j} d\xi \, V_n (\xi) \, G (\xi, \mathbf{x}) \qquad (5)$$

The numerical solution of Eqn.(4) and (5) involves evaluation of the indicated integrals over each panel and solution of resulting linear system. In the ordinary panel method, the source density over a panel is assumed constant. The singular part of Green function is integrated analytically [Hess and Smith, 1964], and the integral of the regular part is simply obtained by $\phi_j S_j$, where ϕ_j is the source density in jth panel. In alternative, the source distribution can be assumed to have a higher order approximation and the integral is then performed by analytical method or numerical procedure to a certain accuracy. This leads to the higher order panel method. In present study the triangular panel with linear source density distribution is employed. This kind of panel can eliminate the two limitations of the ordinary panel method as mentioned above.

3. Numerical Solution Using Triangular Panel with Linear Source Density Distribution

3.1 Collocation method (T.C. method)

To solve Eqn.(4) numerically, N flat triangular panels are used to approximate the body surface and there are N_T grid points on the body surface. Each panel has linear distribution of velocity potential over it, so the source density function ϕ within each panel can be approximated by some convenient linear distribution function as follows

$$\phi(\xi)\,|_{S_j} = [g_1(\xi), g_2(\xi), g_3(\xi)]\,[\phi_{\beta_1}, \phi_{\beta_2}, \phi_{\beta_3}]^T = g \cdot \phi_{\beta(j)} \qquad (6)$$

where $\phi_{\beta(j)}$ is a three components vector and denotes the values of ϕ at three vertices of jth triangular panel and integers β_i, i=1,2,3, are evidently depend on the jth panel. Combining Eqn.(6) and (4) gives

$$-\Omega\,\phi(x) + \sum_{j=1}^{N} Q_j\,\phi_{\beta(j)} = \sum_{j=1}^{N} P_j\,v_{\beta(j)} \qquad (7)$$

where P_j and Q_j are source and normal-dipole distribution integrals over jth panel and $v_{\beta(j)}$ is the normal vector on the three vertices of the jth panel.

$$P_j = \int_{S_j} [g_1, g_2, g_3]\, G(\mathbf{x}, \xi)\, d\xi$$

$$Q_j = \int_{S_j} [g_1, g_2, g_3] \frac{\partial}{\partial n} G(\mathbf{x}, \xi)\, d\mathbf{x} \qquad (8)$$

The Greens function can be written as

$$G = \frac{1}{\mathbf{r}} + G^*(\mathbf{x}, \xi)$$

where $\mathbf{r} = |\mathbf{x}-\xi|$, $1/\mathbf{r}$ is defined as the singular part of Green function and $G^*(\mathbf{x}, \xi)$ is the regular part. It is more convenient to integrate the Eqn.(8) by treating the singular and regular parts of Greens function separately.

3.1.1. Integration of the singular part over a panel

The singular part, $1/\mathbf{r}$, is not slowly vary when the point $\mathbf{x}$ is near the panel over which the integration is to be carried out and are, in fact, singular as $\mathbf{r} \to 0$. Thus, the integral of Eqn.(8) for singular part was carried out analytically in this study. The analytical formula for such integration was derived by Webster(1975) in terms of the local coordinate system. Since the detail of the formula can be found in [Webster, 1975], it is not given here.

3.1.2. Integration of the regular part over a panel

The regular part of Green's function, G*, is much more complex than the singular part and consequently, it is impossible for it to be integrated analytically. The regular part and its normal derivative, G* and $\partial G^*/\partial n$, are regular throughout the fluid domain and oscillate with a wavelength of approximately λ. In practice, λ is generally large, so G* and $\partial G^*/\partial n$ vary slowly over S_j. Thus a valid and convenient approximation to the integration for G* and $\partial G^*/\partial n$ is to evaluate the integration by the discrete source approximation. The final formulae are as follows

$$P_j^T = S_j \begin{bmatrix} \frac{1}{4} G^*(x, x_{\beta 0}) + \frac{1}{12} G^*(x, x_{\beta 1}) \\ \frac{1}{4} G^*(x, x_{\beta 0}) + \frac{1}{12} G^*(x, x_{\beta 2}) \\ \frac{1}{4} G^*(x, x_{\beta 0}) + \frac{1}{12} G^*(x, x_{\beta 3}) \end{bmatrix} \qquad (9)$$

where $x_{\beta 0}$ is coordinates of the centroid of jth triangular panel. $x_{\beta i}$, i=1,2,3, are coordinates of the three vertices of jth triangular panel. $\phi_{\beta 1}$,$\phi_{\beta 2}$ and $\phi_{\beta 3}$ in Eqn.(7) are the potentials at $x_{\beta 1}$, $x_{\beta 2}$ and $x_{\beta 3}$ respectively. Simply replacing G* in Eqn.(9) by $\partial G^*/\partial n$ gives

$$Q_j^T = S_j \begin{bmatrix} \frac{1}{4} \frac{\partial}{\partial n} G^*(x, x_{\beta 0}) + \frac{1}{12} \frac{\partial}{\partial n} G^*(x, x_{\beta 1}) \\ \frac{1}{4} \frac{\partial}{\partial n} G^*(x, x_{\beta 0}) + \frac{1}{12} \frac{\partial}{\partial n} G^*(x, x_{\beta 2}) \\ \frac{1}{4} \frac{\partial}{\partial n} G^*(x, x_{\beta 0}) + \frac{1}{12} \frac{\partial}{\partial n} G^*(x, x_{\beta 3}) \end{bmatrix} \qquad (10)$$

and

$$\frac{\partial G^*}{\partial n} = n_1 \frac{\partial G^*}{\partial x} + n_2 \frac{\partial G^*}{\partial y} + n_3 \frac{\partial G^*}{\partial z}$$

3.1.3. Solution of the boundary integral equation

Substituting Eqn.(9) and (10) together with the integral results of the singular part over each panel into Eqn.(7), a set of the equations with N_T unknowns is obtained. So far, the point x in Eqn.(7) is undecided. If the x is chosen to be at each grid point, it leads immediately to a linear system of N_T algebraic equations with the same number of unknowns. This linear system can be solved directly for the velocity potential at each grid point in terms of standard computer subroutine.

3.2 'Galerkin' method (T.G. method)

The triangular panels with linear source density distribution are again employed, but the boundary integral equation from 'Galerkin' approach, Eqn.(5), is used here. Substituting Eqn.(6) into (5), a similar discrete integral equation to Eqn.(7) is obtained. The integrations

over each panel with respect to the ξ-variable in Eqn.(5) are treated in the same way as those in collocation method for both the singular and regular part. That is, the singular part of Green's function is analytically integrated, and the regular part is integrated by making use of Eqn.(9) and (10). On other hand, all the integrations with respect to x-variable in Eqn.(5) are carried out by the discrete sources approximation method which is similar to the way used to derive Eqn.(9) and(10). Then, the x in Eqn.(5) is chosen as each of N_T grid points. The system of N_T equation is solved directly.

4. Numerical Results

In order to compare the present numerical schemes with the ordinary panel method, the extensive computations have been performed for heave and pitch added mass and damping coefficients of a semi submerged prolate spheroid (beam/length=1/4) and the added mass and damping coefficient distribution along the hull of a Series 60 model (C_b=0.70) in infinite depth. The added mass and damping coefficient are defined in the conventional manner, as the factors which multiply the acceleration and velocity of the body respectively, in the equation for the radiation force.

The comparison between the three different methods for added mass and damping coefficients of the spheroid are presented in Fig.2 and 3 in heave and pitch modes respectively. The hydrodynamic coefficients are plotted against the parameter $1/\sqrt{(M_K)}$, where M_K is the total numbers of evaluations of Green's function and its derivatives or the total numbers of the elements of the main matrix in discrete boundary integral equation (Eqn.(4) or (5)). The same M_K value means the about same CPU time consumed in creating such a matrix.

For ordinary panel method

$$M_K=N^2 \tag{11}$$

For T.C. method

$$M_K=(N+N_T)*N_T \tag{12}$$

For T.G. method

$$M_K=4*(N+N_T)*N_T \tag{13}$$

The inversion of such a matrix takes times like N^3 for ordinary panel method and N_T^3 for T.C. and T.G. methods. The different panel arrangements for each kind of method are listed in the Table 1. The finest panel arrangement is for the ordinary panel method and has 162 panels on half of the body.

In the results shown in Fig.2 and 3, the values from three different methods fall nearly on a straight line, specially for the ordinary panel method, and have the same tendency. It is therefore reasonable to assume the error of the results reduces as $1/\sqrt{(M_K)}$ approaches zero and the 'most accurate' results are obtained from the finest panel arrangement for the ordinary panel method. Because the accurate results are unknown, the comparisons are made based on the 'most accurate' results.

From the Fig.2 and 3, it can be seen that the results obtained by the T.C. method converge to the 'most accurate' results more quickly than those by the ordinary panel method. For the same $1/\sqrt{(M_K)}$ value, the results from the T.C. method are closer to the 'most accurate' results except the coarest panel arrangement. In other words, for the same accuracy, the former is computationally more efficient than the latter. In contrast, for the same $1/\sqrt{(M_K)}$ value the T.G. method produces worse results than the other two, this means the T.G. method is less efficient than the others for the present numerical example. For the same panel arrangement it is found that the T.G. method hardly gives the improvement on the accuracy over the T.C. method, but its M_K value is four times higher the that of T.C. method. Its large increase on computational effort and little improvement in accuracy make it computational inefficient.

The improvement in the accuracy by T.C. method is more significant at higher frequency than that at lower frequency, because the shape error between actual body surface and composite panel surface dominates the total error of the results at lower frequency, but at higher frequency the error caused by rough approximation of source distribution plays a more important role. Similarly, the improvement of the T.C. method is more obvious in pitch mode than that in the heave mode because the velocity potential distribution is more variable in the pitch motion.

Perhaps the major shortcoming of boundary integral method for free surface problems is the presence of 'irregular frequencies' which correspond to the eigenfrequencies of the interior homogeneous Dirichlet problem. The behaviour of the different panel methods have been investigated in the vicinity of the first irregular frequency. The results according to the four models with different number of quadrilateral panels with constant source density distribution are shown in Fig.4. The amplitude and bandwidth of the irregular frequency disturbance decrease with more panels. Fig.5 shows the comparison among different panel methods in the vicinity of the first irregular frequency. For the same number of panels, the disturbance of irregular frequency on the results obtained by the T.G. method is less than that on the results by the T.C. method, but both of the triangular approaches show the better behaviour than the ordinary panel approach.

The comparison between the ordinary panel method and the T.C. method has been further made for the added mass and damping coefficient distribution along the hull of a Series 60 model with C_b=0.7 at F_n=0.2. The 104 panels were used in the ordinary panel program to approximate the half of the hull form, otherwise the 104 panels (N) with 75 grid points (N_T) were used in the T.C.method program. $A_{33}(x)$ and $B_{33}(x)$ are added mass and damping coefficient per unit length at x position along the hull. The $\sqrt{(M_K)}$ value for ordinary panel method is 104 and for the T.C. method is 116. The CPU time required to invert the matrix is normally dependent on N^3 for the ordinary panel program and N_T^3 for triangular panel program respectively, so the total CPU time consumed on the two programs are nearly same. The Fig.6 shows the comparisons of the two kinds of the results with the experimental data given by Vugts (1971). The T.C. method gives more accurate results.

5. Conclusion and Future Directions

Two alternative approaches to 3D panel method for the radiation and diffraction problem have been presented. For present numerical examples the T.C. method is shown to be more efficient than the ordinary panel method, in other words the former produces more accurate results than the latter without increasing the computational effort, but the T.G. method is computational inefficient.

The investigation of the irregular frequencies shows that both amplitude and bandwidth of irregular frequency disturbance dimishes as the number of panels increases. If the same number of panels are used, the T.G. method shows the better behaviour than the T.C. method, but both of them perform better than ordinary panel method.

In the panel method, the solution involves the two main CPU time consuming steps, (1) creating the N*N matrix (or N_T*N_T for triangular panel approach) by evaluating the Green function and its derivatives and (2) inverting this matrix. The CPU time required on the first step increases as the order of N^2 (or N_T^2), but the second step takes times like the order of N^3 (or N_T^3). Tuck (1974) suggested 'any computing problem involving inversion of a dense matrix is optimized by making the time taking to invert the matrix about equal to that required to evaluate its elements'. In the present programs the time required on the two steps is about same if a few hundred panels are used. Otherwise, for the more complex geometry or multi hull body it will be necessary either to increase the number of panels, shifting the burden almost entirely to the matrix inversion or else to improve the panel description. In order to balance the CPU time required on the two steps to optimize the calculation, the higher order panel approach may be valuable.

In the present numerical examples in which only a hundred or less panels were used, the improvement by using triangular panel approach with collocation solution over the ordinary panel method is not significant. The consideration should be made on the potential efficiency of the present approach when large number of panels are required in the calculation. In such a case, the use of higher accurate panels may reduce the total number of panels required in the calculation and save CPU time on the inversion of the main matrix.

Finally,it is noted that the combination of the present triangular panel approach with ordinary quadrilateral panel approach to match the different places of a ship hull and reduce the total number of required panels is one possible future direction for the present work. Introducing the curvilinear panel instead of present plane-panel to fit the body surface more closely is another possible future direction.

Acknowledgements

The authors would like to thank the Chinese Government and British Council for their financial support for the first author during his study at the University of Glasgow.

References

Breit, S.R., Newman, J.N. and Sclavounos, P.D. (1985), 'A New Generation of Panel Programs for Radiation-Diffraction Problems', Proc. of 4th Int. Conf. on the Behavior of Offshore Structures, pp.531-544

Breit, S.R. (1985), 'A Higher-Order Panel Method for Surface Wave Radiation and Diffraction by a Spheroid', 4th Int. Conf. on Numerical Ship Hydrodynamics, Washington D.C., pp.200-215

Faltinsen, O.M. and Michelsen, F.C. (1974), 'Motions of Large Structures in Waves at Zero Froude Number', Int. Symp. on the Dynamics of Marine Vehicles and Structures in Waves, Univ. College, London, pp.99-114

Garrison, C.J. (1974), 'Hydrodynamics of Large Objects in the Sea', J. Hydronautics, Vol.8, No.5

Hess, J.L. and Smith, A.M.O. (1964), 'Calculation of Nonlifting Potential Flow about Arbitrary Three-Dimensional Bodies', J. Ship Research, Vol.8, No.2, pp.22-44

Tuck, F.C. (1974), 'Discussion to 'Numerical Solutions to Free-Surface Flow Problems', by Bai, K.J. and Yeung, R.W., Proc. of 10th Naval Hydrodynamics Symp., pp.644-645

Vugts, J.H. (1971), 'The Hydrodynamic Forces and Ship Motions in Oblique Waves', Neth Res Centre TNO Report 150S

Webster, W.C., (1975), 'The Flow about Arbitrary, Three-Dimensional Smooth Bodies', J. Ship Research, Vol.19, No.4, pp.206-218

Wehausen, J.V. and Laitone, E.V. (1960), 'Surface Waves', Handbuch der Physic (S. Flugge, ed.) Vol.9, pp446-778

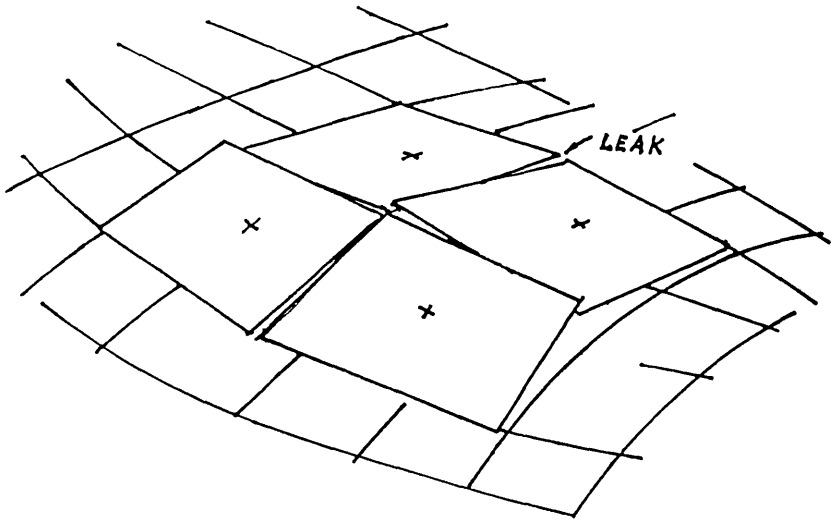

Fig. 1 Quadrilateral panels on irregular surface

Table 1 Different panel arrangements on the submerged surface of a spheroid (ε=1/4) for the three different panel methods. N is the number of panels on the half of the submerged surface and N_T is the number of grid points (for triangular panel method). The parametre M_K is defined by Eqn.(11), (12) and (13)

	quadrilateral panel method		triangular panel method (collocation)			triangular panel method ('Galerkin')		
	N	$\sqrt{(M_K)}$	N	N_T	$\sqrt{(M_K)}$	N	N_T	$\sqrt{(M_K)}$
1	18	18	18	16	23.3	18	16	26.6
2	32	32	32	25	37.7	32	25	75.4
3	50	50	50	36	55.6	50	36	111.2
4	72	72	72	49	77.0	72	49	144.0
5	98	98	98	64	101.8	98	64	203.6
6	128	128						
7	164	164						

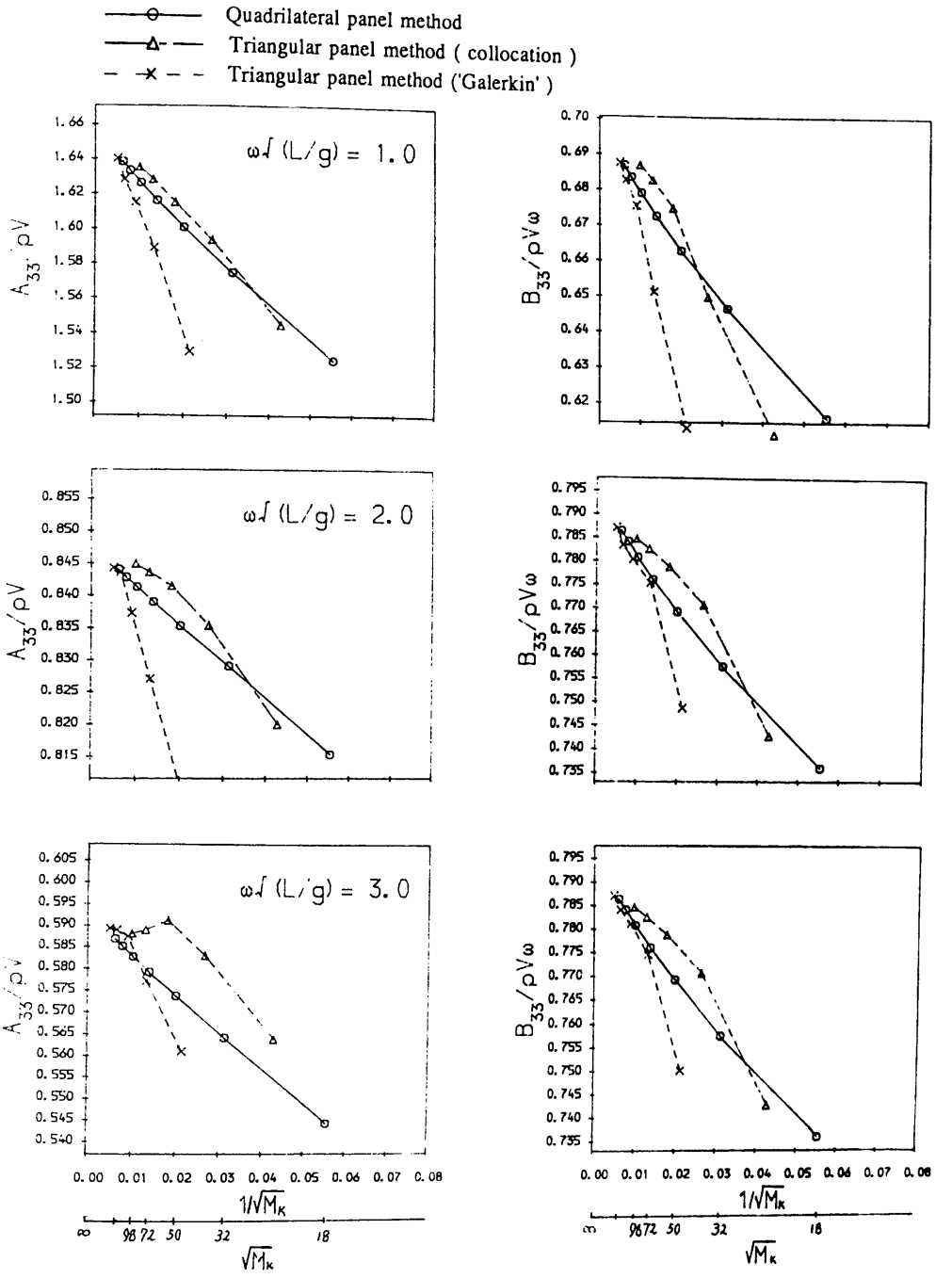

Fig. 2 Comparisons of the heave added mass and damping coefficients of a spheroid (ε=1/4) obtained by the three different panel methods versus reciprocal of the parametre $\sqrt{(M_K)}$. M_K is defined by Eqn. (11), (12) and (13)

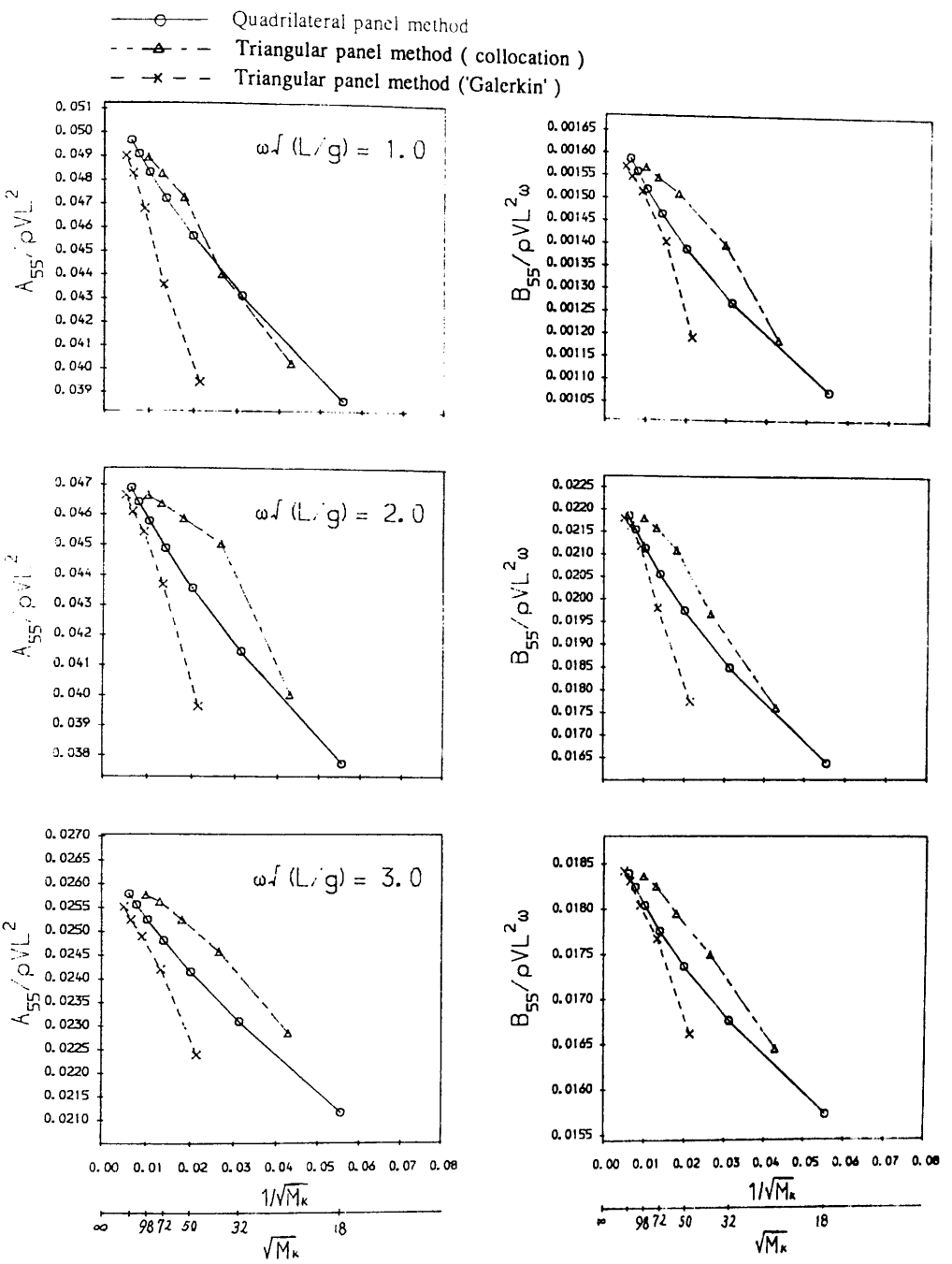

Fig. 3 Comparisons of the pitch added inertia and damping coefficients of a spheroid (ε=1/4) obtained by the three different panel methods versus reciprocal of the parametre $\sqrt{(M_K)}$. M_K is defined by Eqn. (11), (12) and (13)

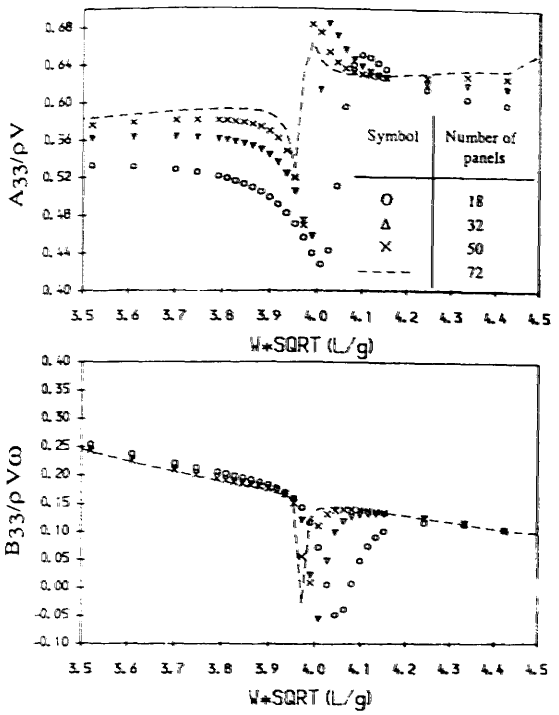

Fig. 4 Behaviors of spheroid coefficients obtained by the ordinary panel method according to four models with different numbers of quadrilateral panels in the vicinity of the first irregular frequency.

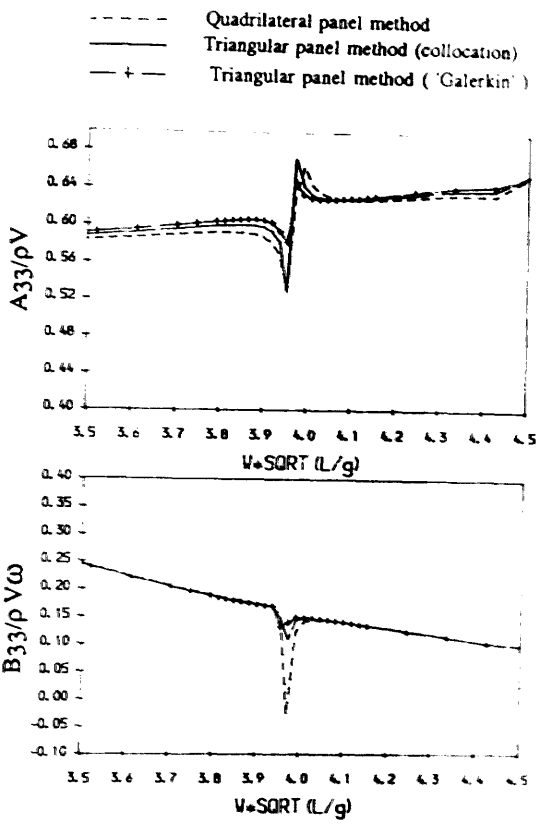

Fig. 5 Comparisons of the spheroid coefficients from different panel methods in the vicinity of the first irregular frequency. The results from the ordinary panel method are based on 72 panels and from triangular panel methods are based on the 72 panels with 49 grid points on the half of the hull.

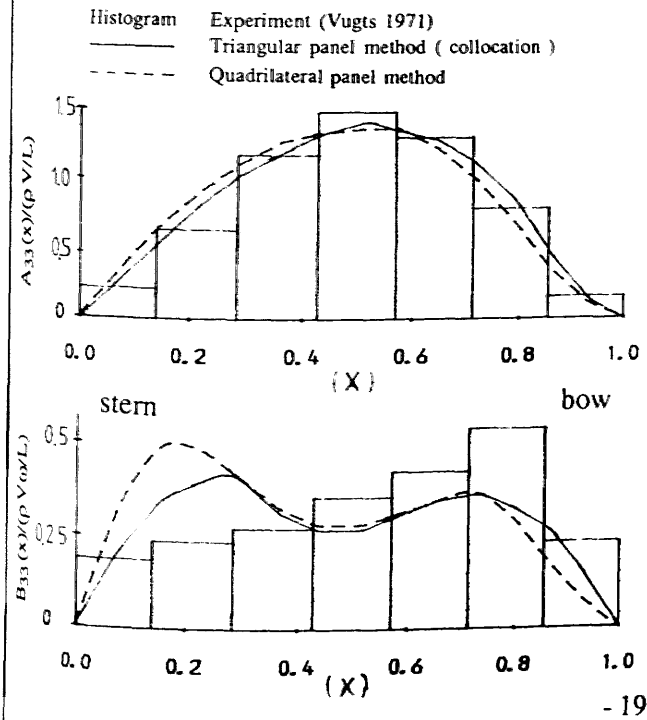

Fig. 6 Heave added mass and damping coefficients distribution along the hull of a Series 60 model (C_b=0.7) with ω_e=7.0 and F_n=0.2.

APPENDIX B

LINEARIZATION OF THE FREE SURFACE CONDITIONS

The condition for free surface is as follow

$$\frac{D}{Dt}(\zeta - z_0) = 0 \qquad \text{(B.1)}$$

where $z_0=\zeta(x_0,y_0,t)$ represents the free surface elevation. $(D/Dt)=\partial/\partial t+\nabla\cdot\nabla$.and dynamic condition is obtained from Bernoulli's equation by assuming the pressure at the free surface be constant equal to atmospheric pressure.

$$\Phi_t + \frac{1}{2}\nabla\Phi\cdot\nabla\Phi + g\zeta = 0. \qquad \text{(B.2)}$$

It is clear those conditions involve the unknown of the free surface elevation, ζ. To obtain the single boundary condition for the potential which does not explicitly involve the wave elevation, the substantial derivative of Eqn.(B.2) and the fact of

$$\frac{D\zeta}{Dt} = (\Phi_{Z_0})_{Z_0} = \zeta$$

from Eqn.(B.1) gives the new linear free surface boundary condition

$$\Phi_{tt} + 2\nabla\Phi_t\cdot\nabla\Phi_t + \frac{1}{2}\nabla\Phi\cdot\nabla(\nabla\Phi\cdot\nabla\Phi) + g\Phi_{Z_0} = 0\,, \quad z=\zeta. \qquad \text{(B.3)}$$

The potential here involves both steady and unsteady components. According to the assumptions of the incident wave and the resulting motion responses of the body are small, the linearization of Eqn.(B.3) can be made by introducing Eqn.(2.4) to Eqn.(B.3) and neglecting only the second order of the unsteady potential ϕ, that is

$$\phi_{tt} + 2\mathbf{W}\cdot\nabla\phi_t + \mathbf{W}\cdot\nabla(\mathbf{W}\cdot\nabla\Phi) + g\phi_Z + \frac{1}{2}(\mathbf{W}+\nabla\phi)\cdot\nabla(\mathbf{W}\cdot\mathbf{W}) + gU\overline{\phi}_Z = 0 \qquad \text{on } z=\zeta \qquad \text{(B.4)}$$

where $\mathbf{W}$ is the velocity vector of steady flow relative to the moving reference frame

$$\mathbf{W} = U \nabla \left[\bar{\phi}(x,y,z) - x \right] \tag{B.5}$$

and there is no restriction on steady potential. Newman argued that directly applying the Eqn.(B.3) on the steady free surface elevation, $z=\bar{\zeta}$, by assuming the difference between ζ and $\bar{\zeta}$ is higher order quantity and used the Taylor series expansion in Eqn.(B.2) showed

$$\zeta - \bar{\zeta} = -\left[(\phi_t + \mathbf{W}\cdot\nabla\phi) / (g + \mathbf{W}\cdot\mathbf{W}_Z) \right]_{Z=\bar{\zeta}} \tag{B.6}$$

which is of the order $0(\phi)$.

Hence expanding all the terms in Eqn.(B.4) from ζ to $\bar{\zeta}$ and neglecting the second order quantity $0(\phi^2)$, it follows that

$$\phi_{tt} + 2\,\mathbf{W}\cdot\nabla\phi_t + \mathbf{W}\cdot\nabla(\mathbf{W}\cdot\nabla\phi) + g\,\phi_Z + \frac{1}{2}\nabla\phi\cdot\nabla(\mathbf{W}\cdot\mathbf{W})$$
$$+ \frac{1}{2}\frac{\partial}{\partial z}\left[\mathbf{W}\cdot\nabla(\mathbf{W}\cdot\mathbf{W}) + g\,U\,\bar{\phi}_Z \right](\zeta - \bar{\zeta}) = 0 \qquad \text{on } z=\bar{\zeta}. \tag{B.7}$$

This equation governs the unsteady potential provided by the velocity of the steady flow W is known. Since the steady flow depends not only on the steady forward speed but also on the body geometry, the linearization of the steady potential can be adopted only when suitable geometric restrictions are placed on the shape of the body surface. If further assume that the body geometry is thin or flat or steady forward speed motion is small, the higher order quantities $0(\phi\bar{\phi})$ and $0(\bar{\phi}^2)$ can be neglected from Eqn.(B.7) due to $\bar{\phi}$ is small. the Eqn.(B.7) reduces to

$$\Phi_{tt} - 2\,U\,\Phi_{xt} + U^2\,\Phi_{xx} + g\,\Phi_z = 0 \qquad \text{on } z=\bar{\zeta}. \tag{B.8}$$

For the steady forward motion the boundary condition can be obtained by letting unsteady potential ϕ to be zero in Eqn.(B.4), that is

$$\frac{1}{2}\mathbf{W}\cdot\nabla(\mathbf{W}\cdot\mathbf{W}) + g\,U\,\bar{\phi}_z = 0 \qquad \text{on } z=\bar{\zeta} \tag{B.9}$$

where the steady state free surface elevation $\bar{\zeta}$ is given by

$$\bar{\zeta} = -\frac{1}{2g}(\mathbf{W}\cdot\mathbf{W} - U^2)_{z=\bar{\zeta}}$$
$$= -\frac{U^2}{2g}\left[\nabla\bar{\phi}\cdot\nabla\phi - 2\bar{\phi}_x\right]_{z=\bar{\zeta}} \qquad \text{(B.10)}$$

which states the steady wave elevation $\bar{\zeta}$ is of the order $0(\bar{\phi}^2)$. Therefore, applying Eqn.(B.8) on z=0 instead of $z=\bar{\zeta}$ has the error of order $0(\bar{\phi}^2)$. Thus the linear free surface boundary condition can be written as

$$\Phi_{tt} - 2U\Phi_{xt} + U^2\Phi_{xx} + g\Phi_z = 0 \qquad \text{on } z=0 \qquad \text{(B.11)}$$

For the case of a body in steady forward motion the time dependent terms in Eqn.(B.11) go out and the steady potential $\bar{\phi}$ satisfies the linear boundary condition

$$U^2\bar{\phi}_{xx} + g\bar{\phi}_z = 0 \qquad \text{on } z=0 \qquad \text{(B.12)}$$

Alternatively for a body without forward speed the speed dependent terms are vanished and Eqn.(B.11) becomes

$$\phi_{tt} + g\phi_z = 0 \qquad \text{on } z=0 \qquad \text{(B.13)}$$

For the time harmonic problem introducing Eqn.(B.2) to Eqn.(B.11) and (B.13) gives

$$(i\omega + U\frac{\partial}{\partial x})^2\phi + g\frac{\partial}{\partial z}\phi = 0 \qquad \text{on } z=0 \qquad \text{(B.14)}$$

for forward speed case and

$$-\omega^2\phi + g\frac{\partial}{\partial z}\phi = 0 \qquad \text{on } z=0 \qquad \text{(B.15)}$$

for zero speed case.

APPENDIX C

SIMPLIFICATION OF THE BODY BOUNDARY CONDITION

The boundary condition on the body surface can be written as

$$\frac{\partial \Phi}{\partial \mathbf{n}} = \mathbf{v}_{S_t} \quad \mathbf{n} \qquad \text{on } S_t \qquad \text{(C.1)}$$

where S_t is the instantaneous wetted surface of the body and $\mathbf{n}$ is the unit normal vector pointing outward of S_t. This condition states that the relative velocity between the fluid and body surface in the direction normal to body surface be zero. Generally, this condition has to be satisfied at the instantaneous position of the body wetted surface. Since the oscillation of the body is small, the local velocity of the fluid can be represented in terms of Eqn.(2.4) and (B.5), i.e.

$$\mathbf{v}_{S_t} = \mathbf{W}|_{S_t} + \nabla \phi \qquad \text{(C.2)}$$

where $\mathbf{W}|_{S_t}$ is the steady velocity due to forward motion of the body which is evaluated on the instantaneous surface S_t.

For convenience, an oscillatory co-ordinate system fixed on the body should be employed, that is

$$\mathbf{r}' = \mathbf{r} - \alpha$$

and

$$\alpha = \eta + \Omega \times \mathbf{r}'$$

where α is an infinite small vector of the oscillatory displacement, η and Ω are the translation and rotation components of α respectively. By means of α the unit normal vector $\mathbf{n}$ of the body surface in its instantaneous position S_t can be expressed by the body surface in its steady state position S, S is the mean wetted body surface, through the first order contribution, as

$$\mathbf{n}|_{S_t} = \mathbf{n}|_S + \Omega \times \mathbf{n}|_S \qquad \text{(C.2)}$$

The $\mathbf{W}|_{S_t}$ can be expressed by the velocity on the steady state body surface taking the differentiation of it in α direction into account, that is

$$\mathbf{W}|_{S_t} = \mathbf{W}|_S + \alpha \nabla \mathbf{W}|_S . \qquad \text{(C.3)}$$

Substituting Eqn.(C.1)-(C.3) in Eqn.(B.5) and the fact that

$$\phi_n \, \mathbf{n}|_{S_t} = \dot{\alpha}\mathbf{n}|_{S_t}$$

gives that

$$(\mathbf{W} + \nabla \phi) \mathbf{n} = \dot{\alpha}\mathbf{n} \qquad \text{on } S_t. \qquad \text{(C.4)}$$

Hereafter the overdot signifies the time differentiation in the reference frame of axes, or

$$\left[\mathbf{W} + (\alpha \nabla) \mathbf{W} + \nabla \phi \right] (\mathbf{n} + \Omega \times \mathbf{n}) = \dot{\alpha} (\mathbf{n} + \Omega \times \mathbf{n}).$$

Neglecting the second order terms in ϕ, α and Ω the following expression is obtained

$$\phi_n = \left[\dot{\alpha} + \Omega \times \mathbf{W} - (\alpha \nabla) \mathbf{W} \right] \cdot \mathbf{n} \qquad \text{on S.}$$

The first two terms give the rate of change of α in a frame of reference moving with steady flow. By means of the vector identity, the Eqn.(C.2) and the fact of $\nabla \mathbf{W} = \nabla^2 \bar{\phi} = 0$ (incompressibility), a more compact results can be obtained

$$\phi_n = \left[\dot{\alpha} + \nabla \times (\alpha \times \mathbf{W}) \right] \cdot \mathbf{n} \qquad \text{on S} \qquad \text{(C.5)}$$

This formula was first derived by Timman and Newman. Furthermore, from the definition of α, the assumptions about the diffraction and radiation problems, the harmonic motion problem can be expressed

$$\eta = (\eta_1, \eta_2, \eta_3) \, e^{-i\omega t}$$

$$\Omega = (\eta_4, \eta_5, \eta_6) \, e^{-i\omega t}$$

The boundary condition for the radiation potential ϕ_j (j=1,2,...6) can be presented

in terms of Eqn.(C.5) as

$$\frac{\partial}{\partial n}\phi_j = -i\omega n_j + U m_j \qquad j=1,2,...6 \qquad \text{on S} \qquad \text{(C.6)}$$

where

$$(n_1, n_2, n_3) = \mathbf{n}$$
$$(n_4, n_5, n_6) = \mathbf{r} \times \mathbf{n} \qquad \text{(C.7)}$$
$$(m_1, m_2, m_3) = -(\mathbf{n}\cdot\nabla)\,\mathbf{W}/U$$
$$(m_4, m_5, m_6) = -(\mathbf{n}\cdot\nabla)(\mathbf{r} \times \mathbf{W})/U \qquad \text{(C.8)}$$

This formulations were introduced by Oglivie and Tuck. If the assumption $\mathbf{W} = -(U, 0, 0)$ is made by neglecting the perturbation of steady velocity potential in the case of the body shape is assumed thin or flat, the relationship in Eqn.(C.8) reduces to

$$(m_1, m_2, m_3) = 0$$
$$(m_4, m_5, m_6) = (0, n_3, -n_2). \qquad \text{(C.9)}$$

For the diffraction problem, the governing Eqn.(2.14) is rewritten here as a boundary condition

$$\frac{\partial \phi_I}{\partial n} = -\frac{\partial \phi_D}{\partial n} \qquad \text{on S.} \qquad \text{(C.10)}$$

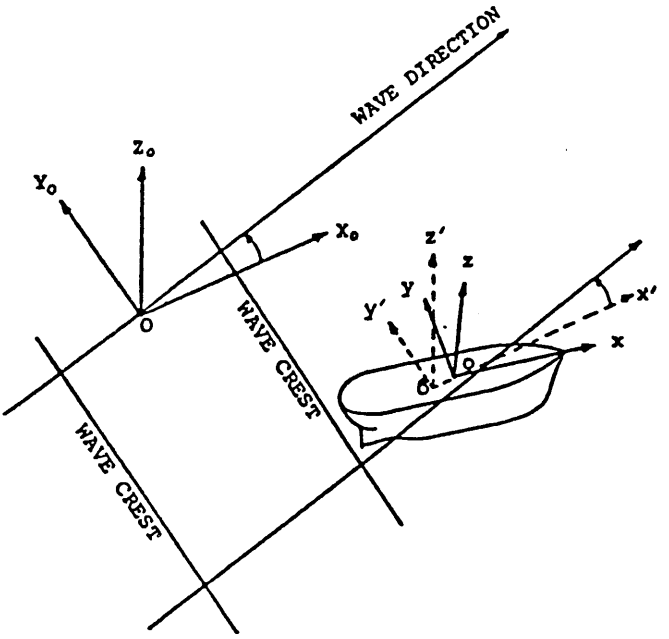

Fig. 2.1a The Co-ordinate Systems

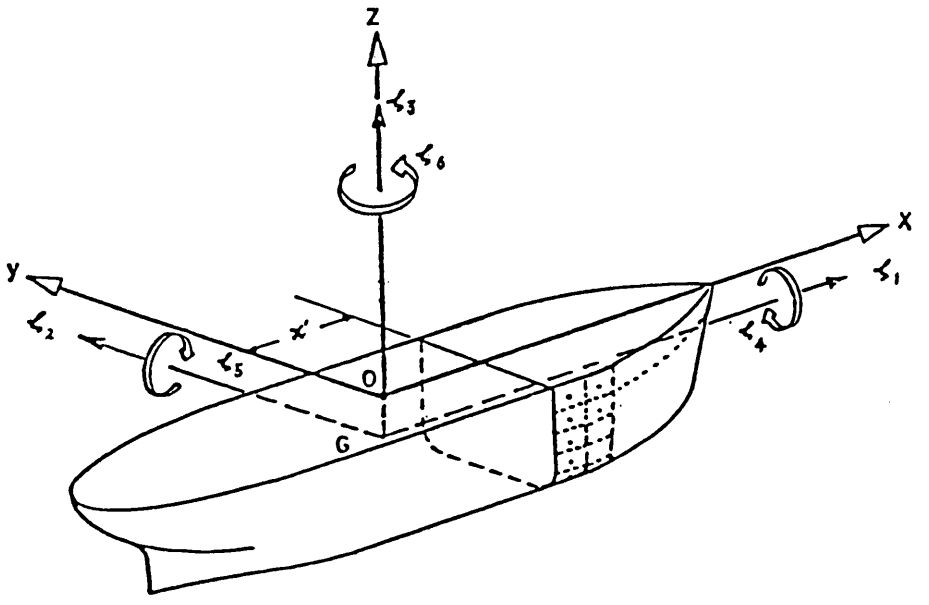

Fig. 2.1b Definition of Motions

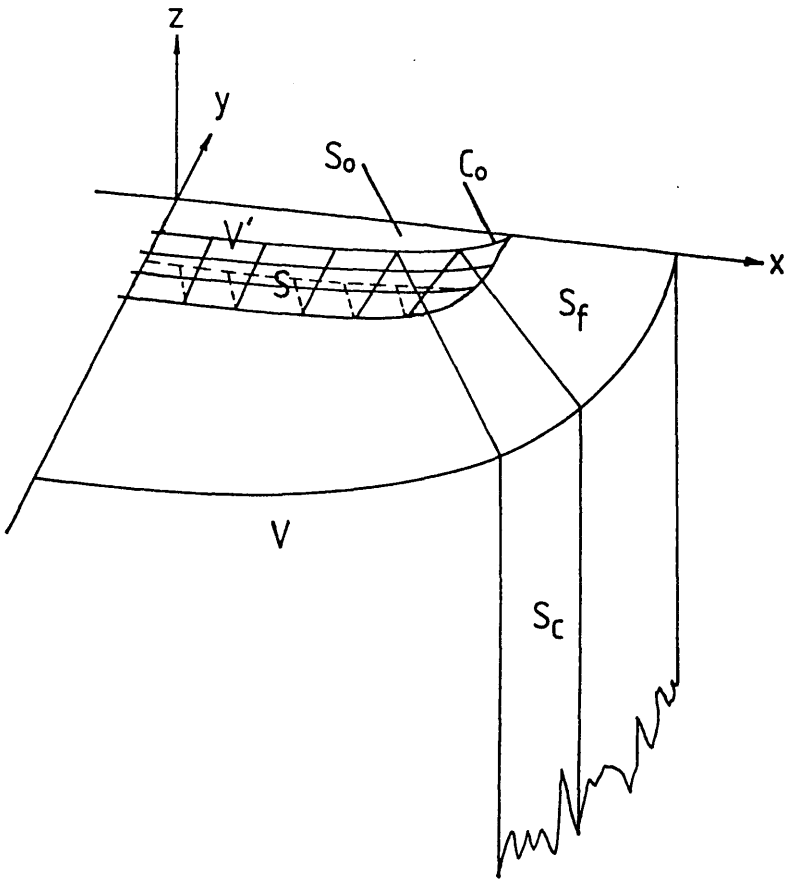

Fig. 2.2 Definition of Integral Surfaces and Volumes

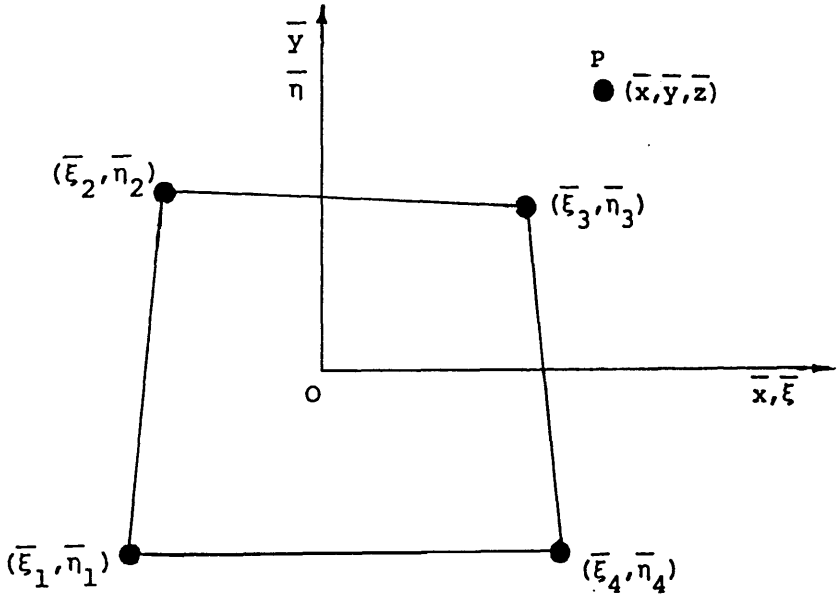

Fig. 3.1 Local Co-ordinate System

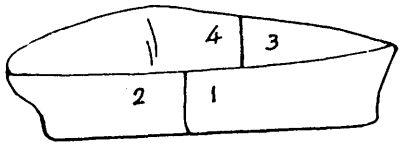

Fig. 3.2 Typical Partitioning of o-xz Plane Symmetric Body

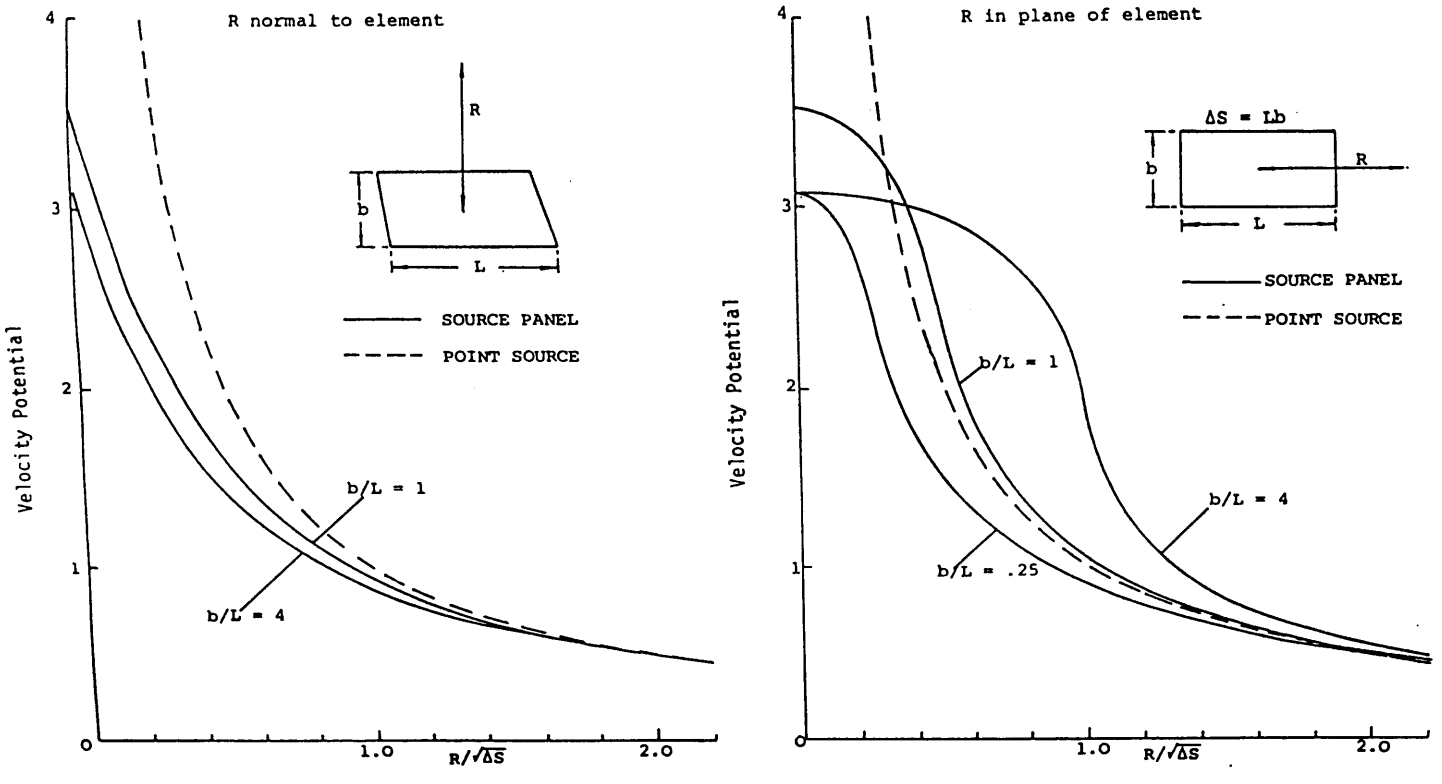

Fig. 3.3 Comparison between Exact Integral and Point Source Approximation for Singular Part of Green's Function

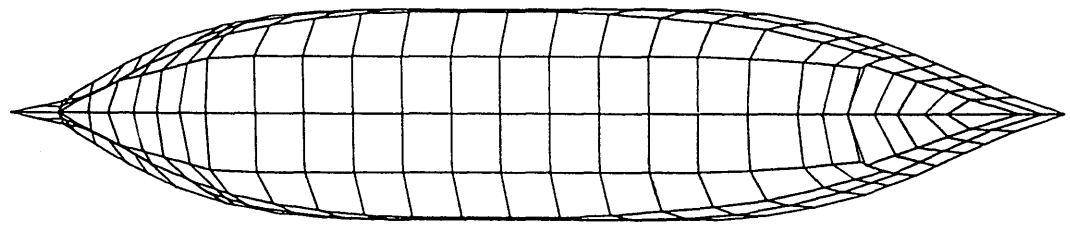

Fig. 4.1 Series 60 Hull form represented by 252 panel elements

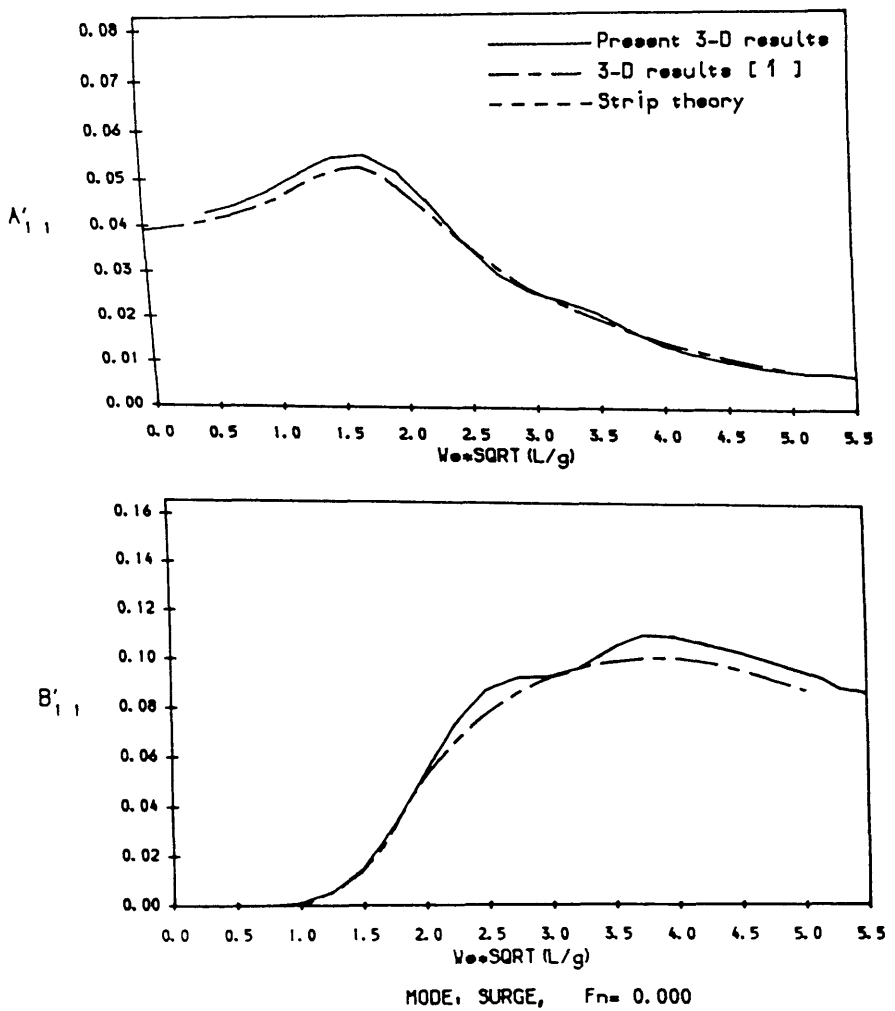

Fig. 4.2 Surge added mass and damping coefficients of Series 60 model

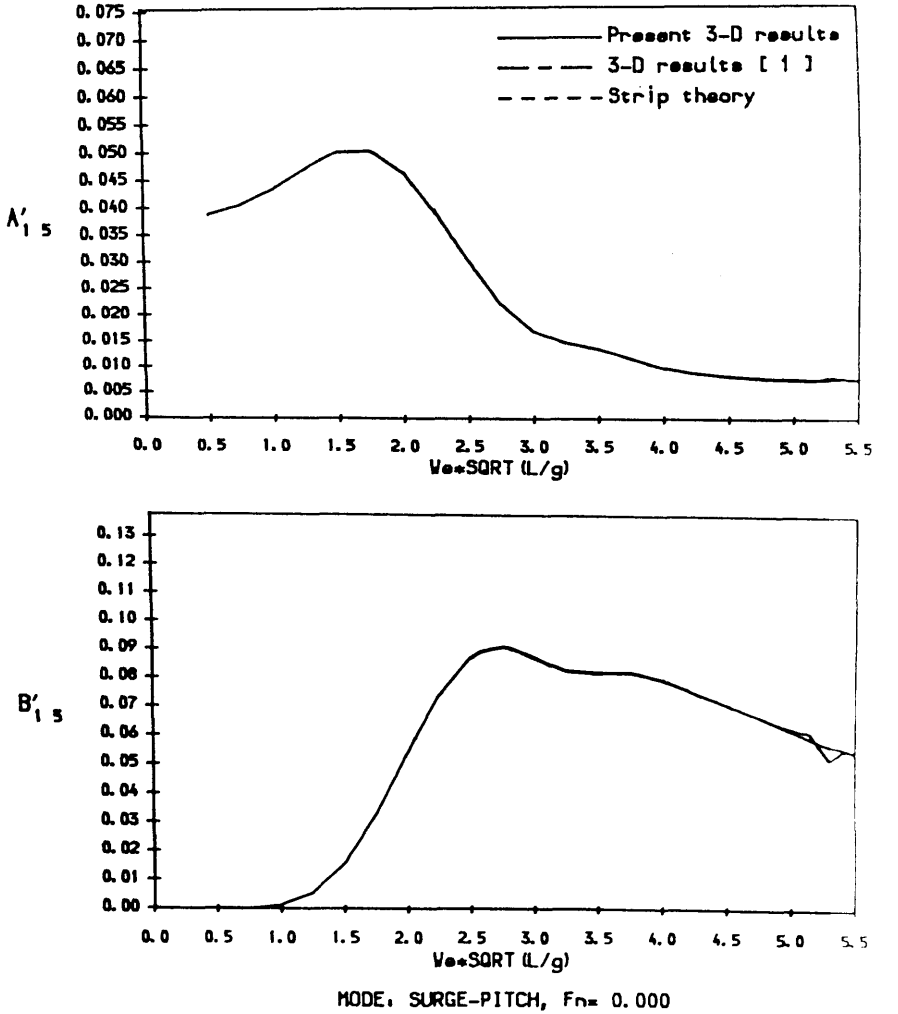

Fig. 4.3 Surge-pitch coupling added mass and damping coefficients of Series 60 model

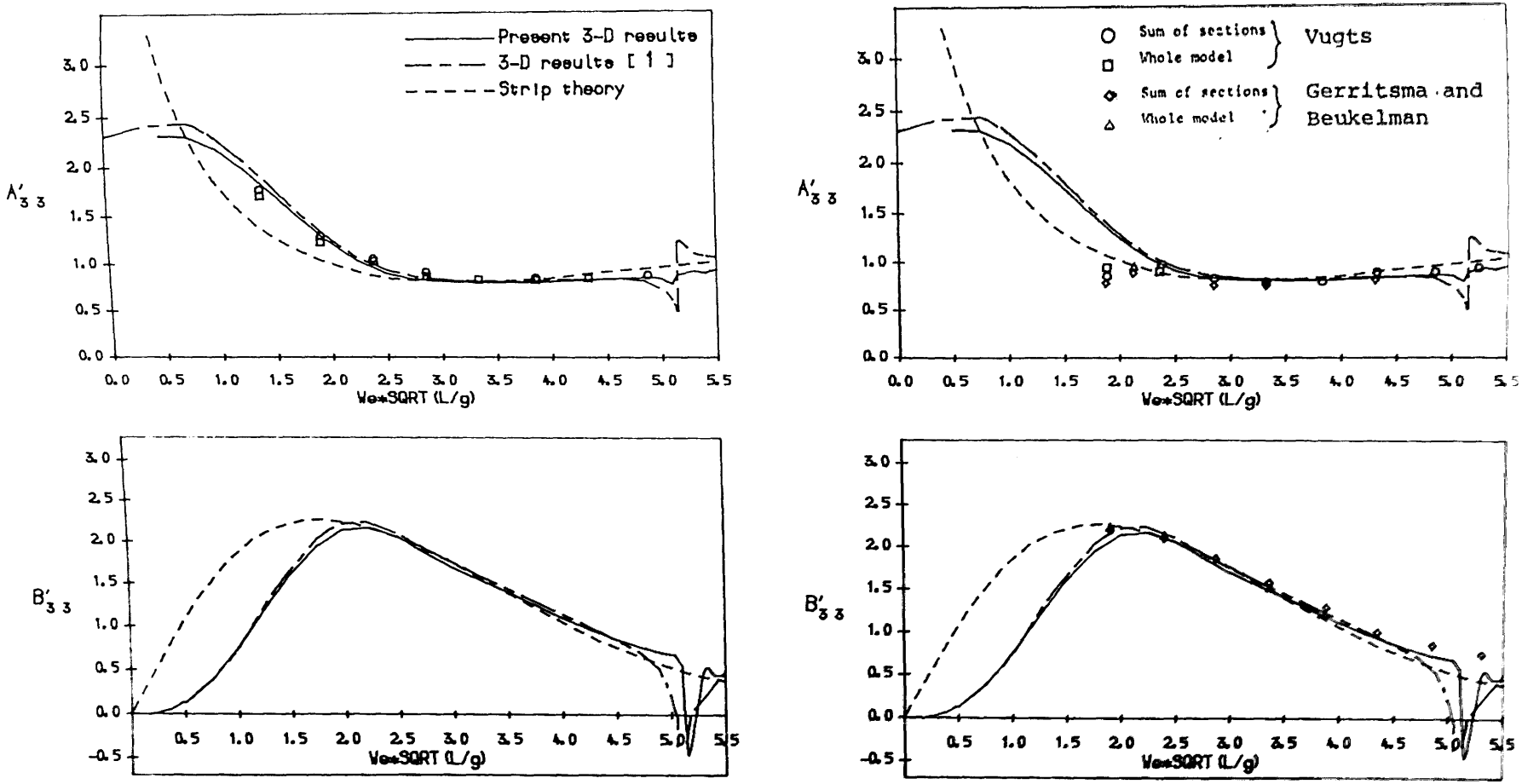

Fig. 4.4 Heave added mass and damping coefficients of Series 60 model at F_n=0.0 and F_n=0.2

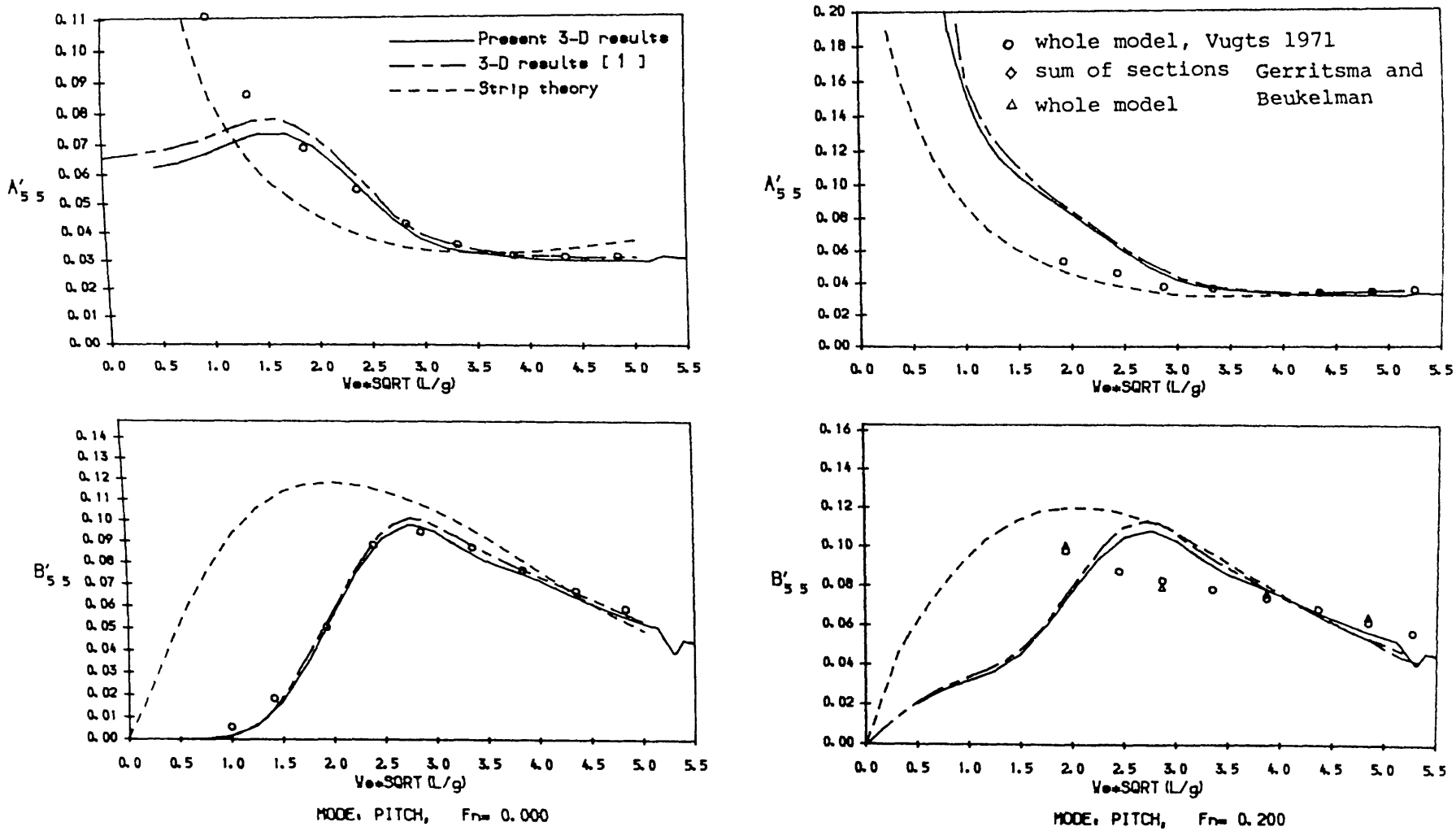

Fig. 4.5 Pitch added inertia and damping coefficients of Series 60 model at F_n=0.0 and F_n=0.2

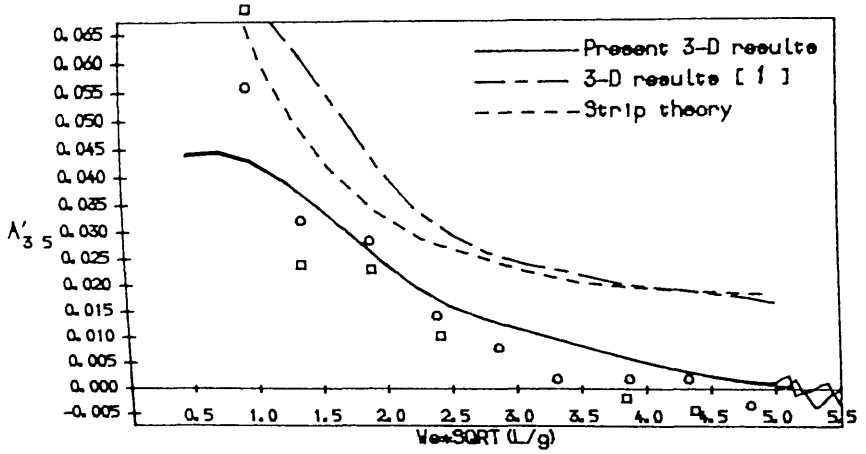

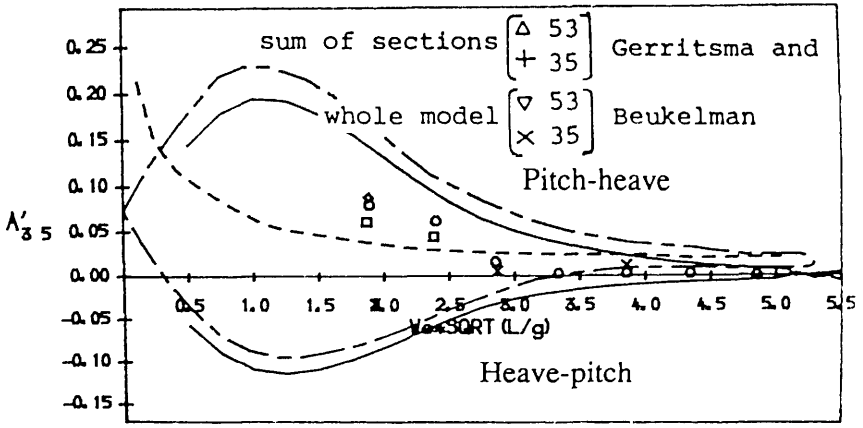

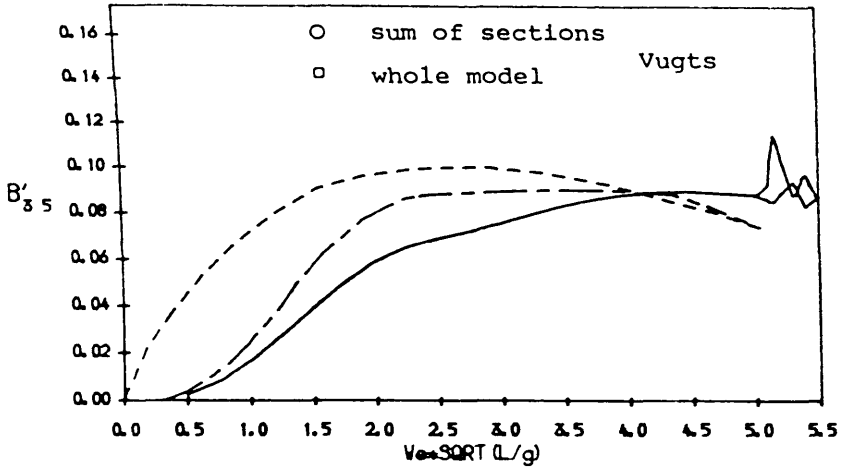

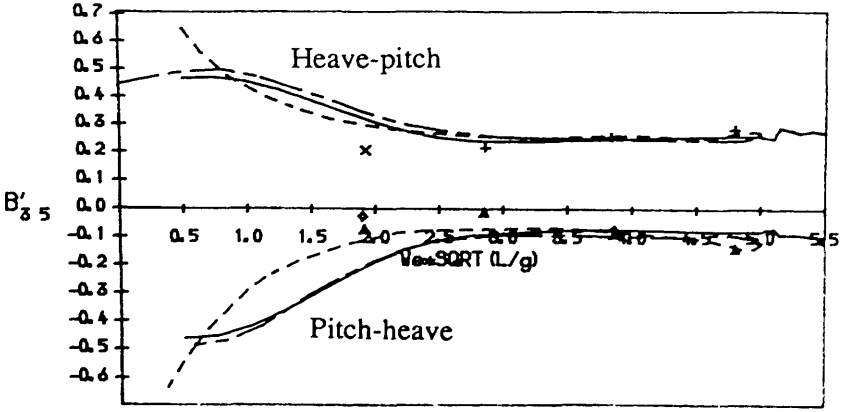

MODE: HEAVE-PITCH, Fn= 0.000

MODE: HEAVE-PITCH, Fn= 0.200

Fig. 4.6 Heave-pitch coupling added inertia and damping coefficients of Series 60 model at F_n=0.0 and F_n=0.2

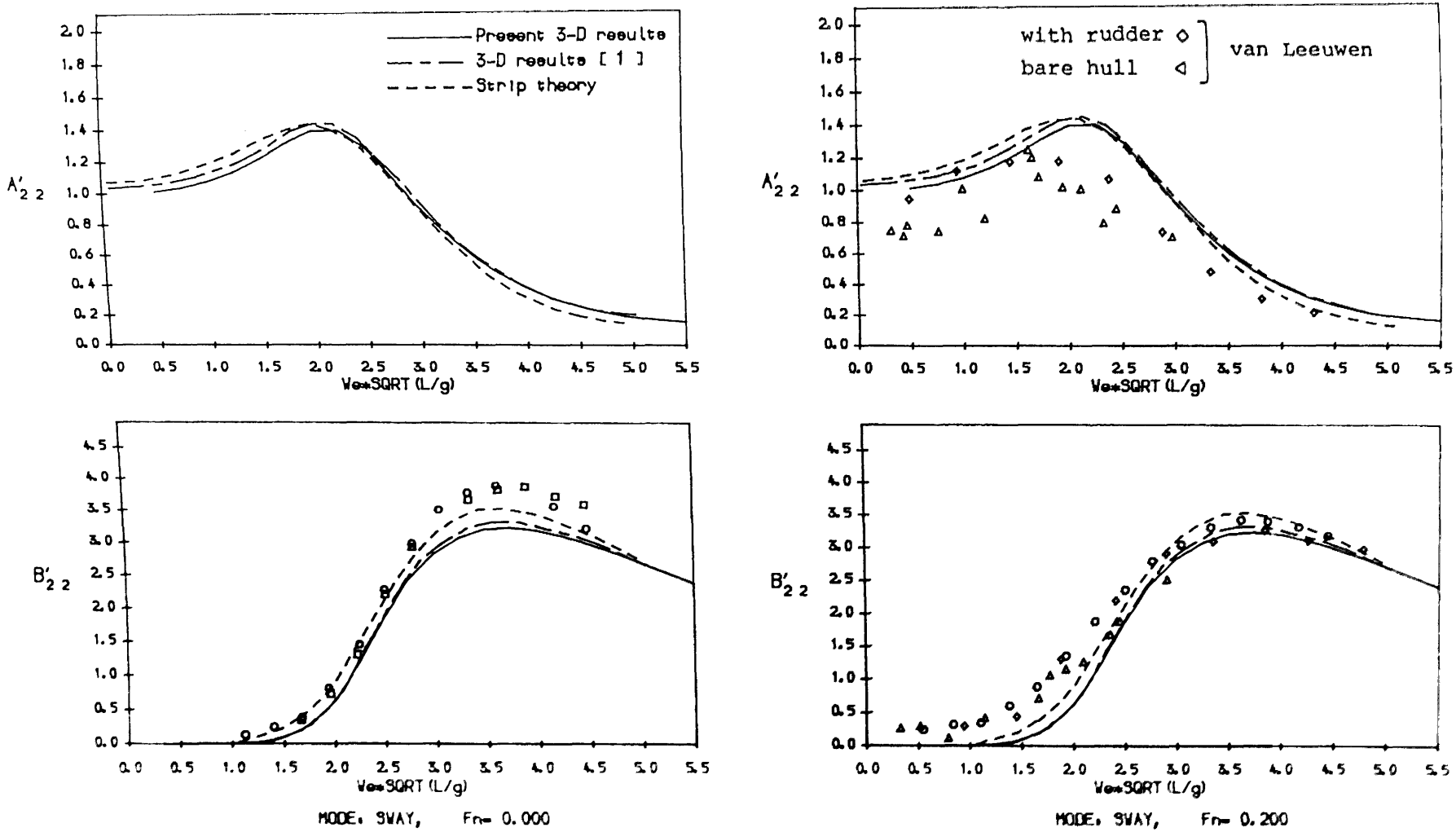

Fig. 4.7 Sway added mass and damping coefficients of Series 60 model

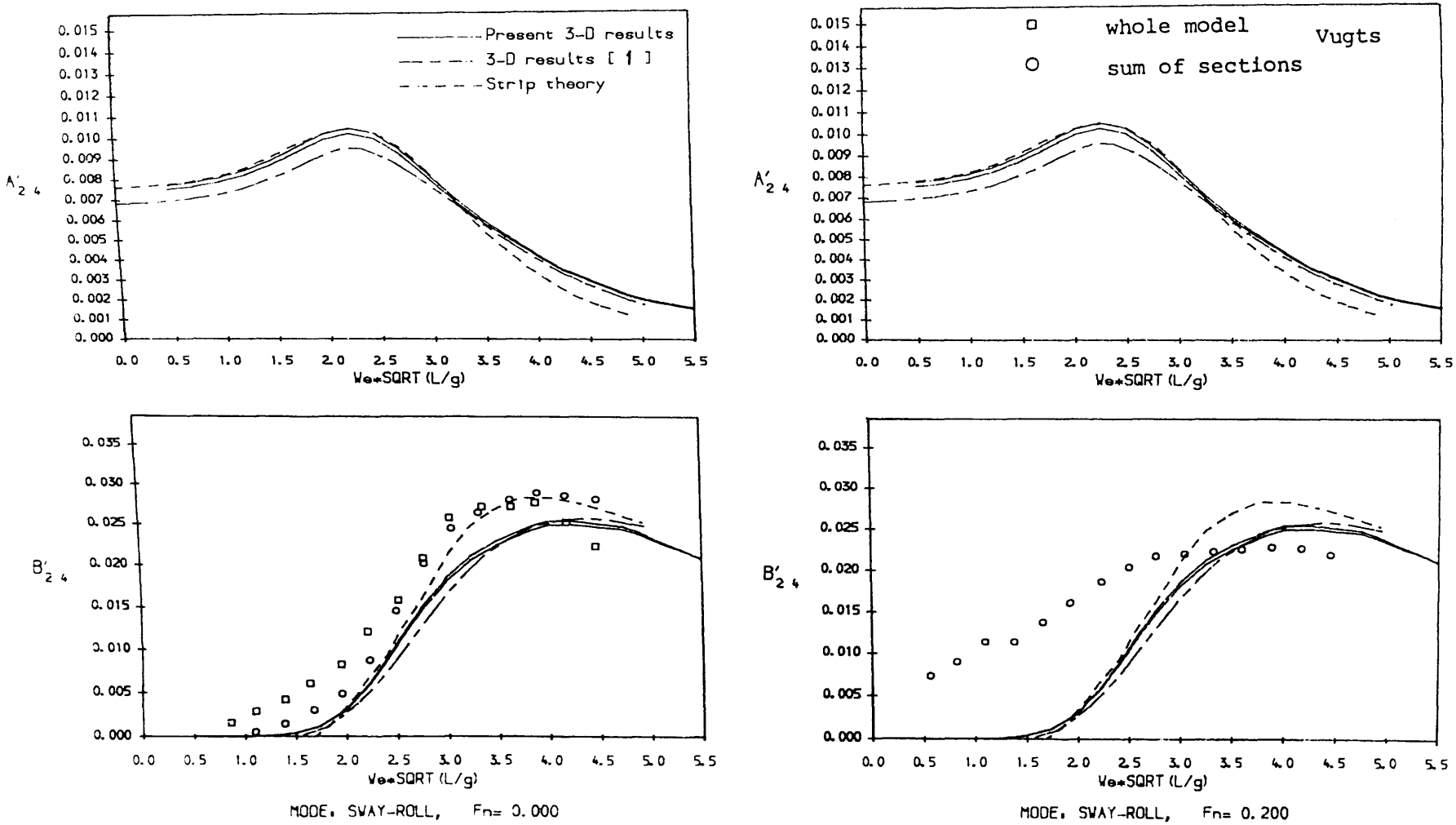

Fig. 4.8 Sway-roll coupling added inertia and damping coefficients of Series 60 model

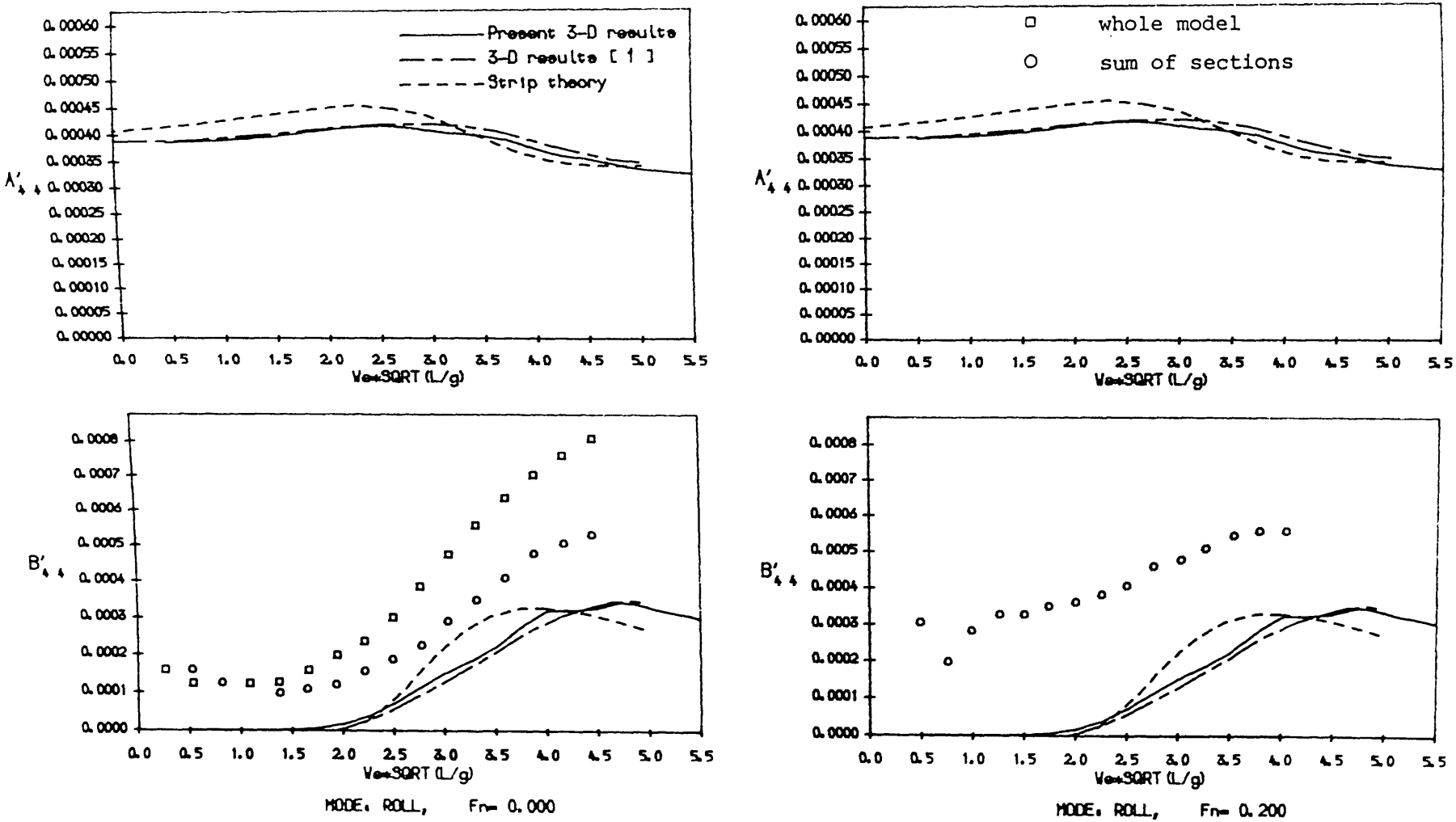

Fig. 4.9 Roll added inertia and damping coefficients of Series 60 model

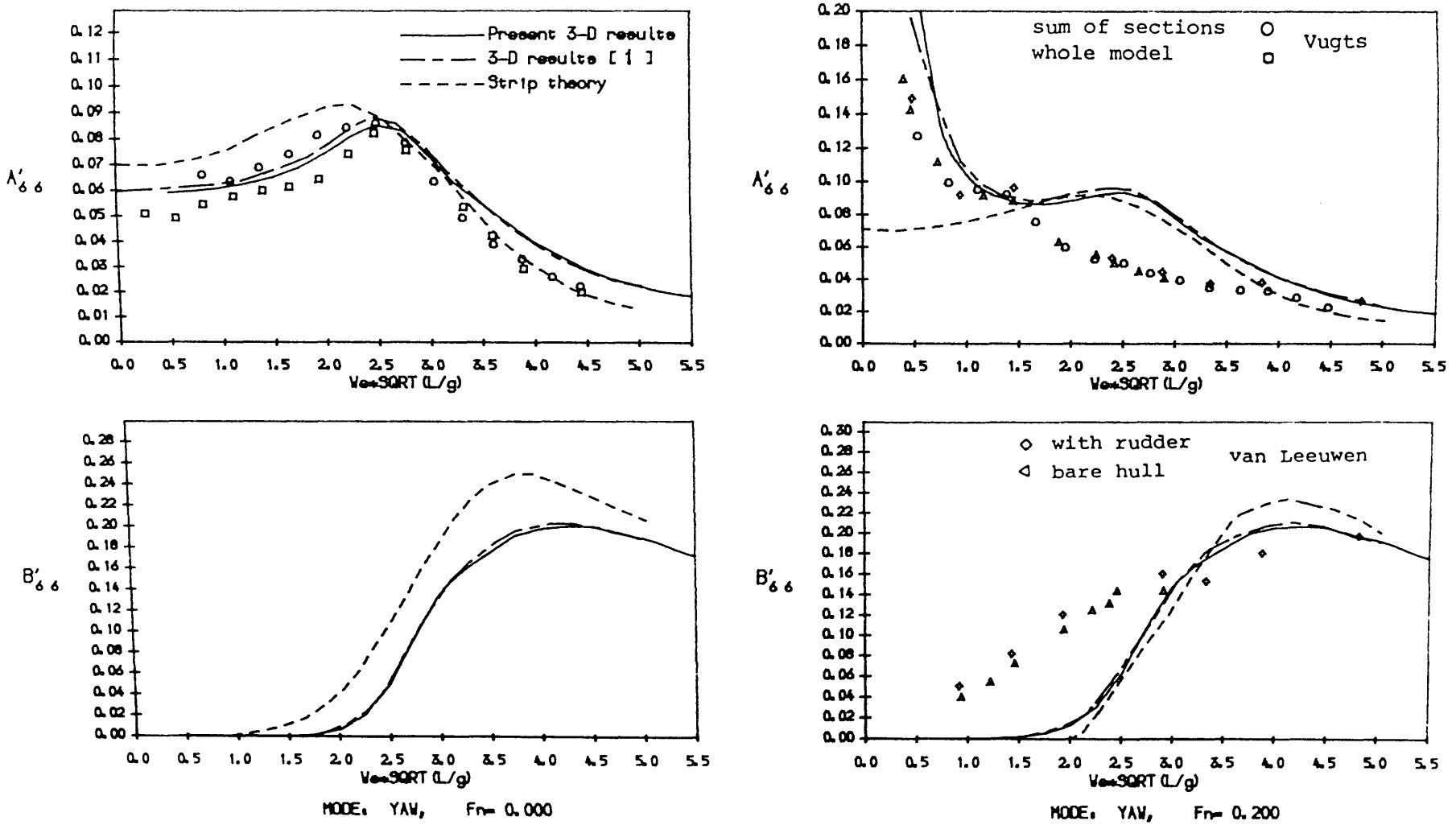

Fig. 4.10 Yaw added inertia and damping coefficients of Series 60 model at F_n=0.0 and F_n=0.2

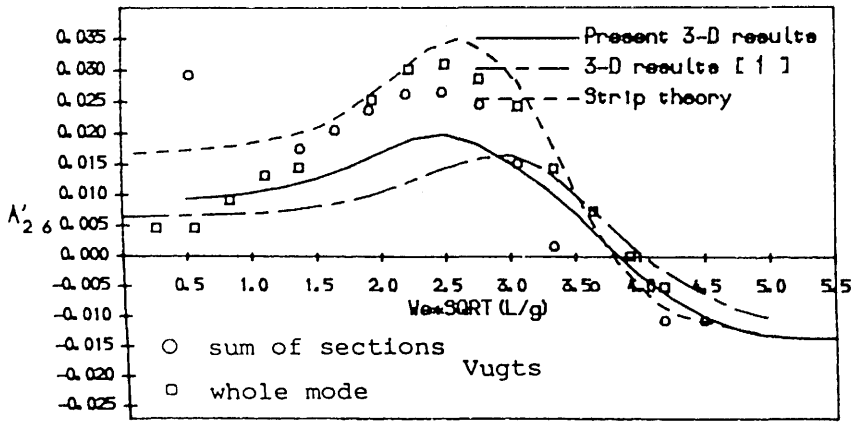

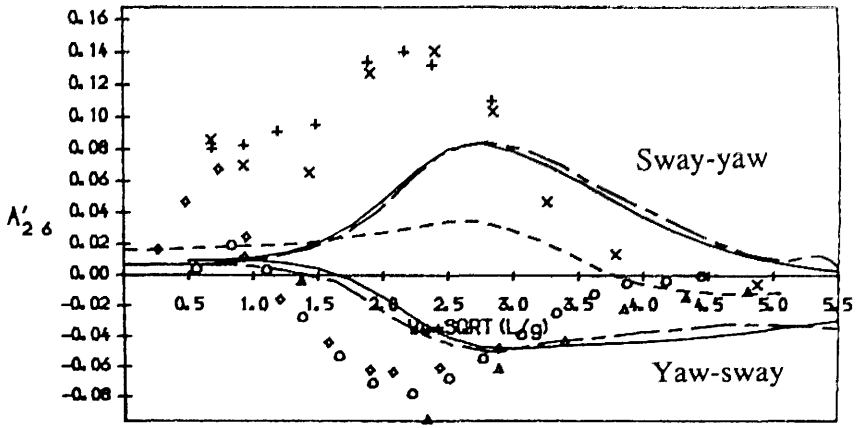

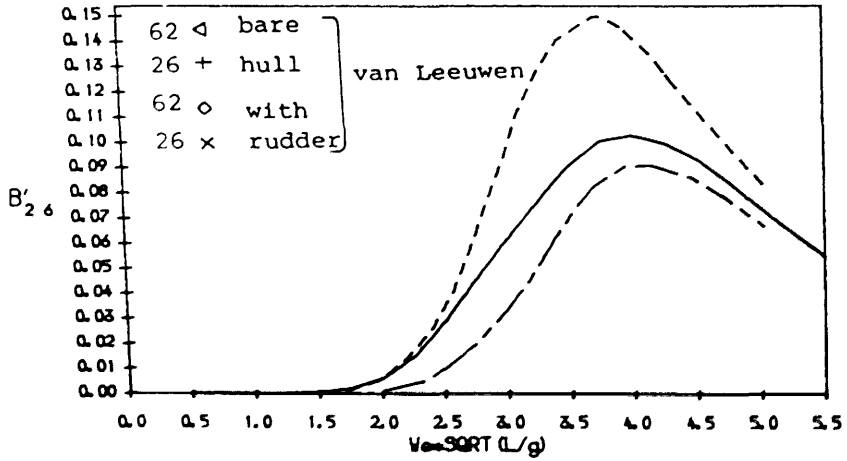

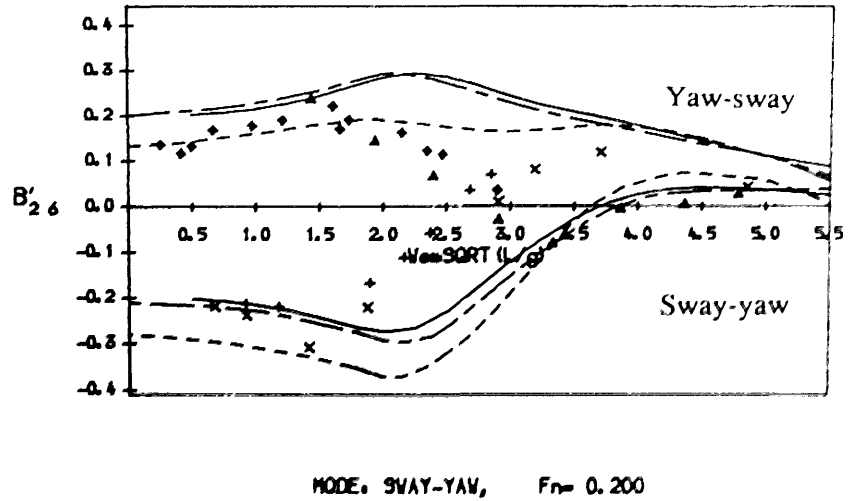

Fig. 4.11 Sway-yaw coupling added inertia and damping coefficients of Series 60 model at F_n=0.0 and F_n=0.2

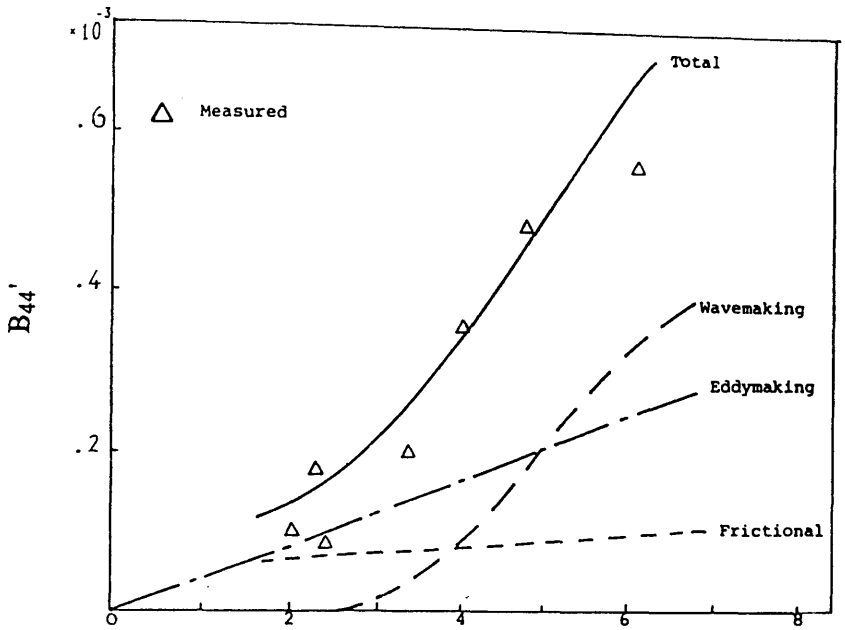

Fig. 4.12 Components of roll damping for Series 60 model at F_n=0.0 according to Ikeda, Himena and Tanaka [11]

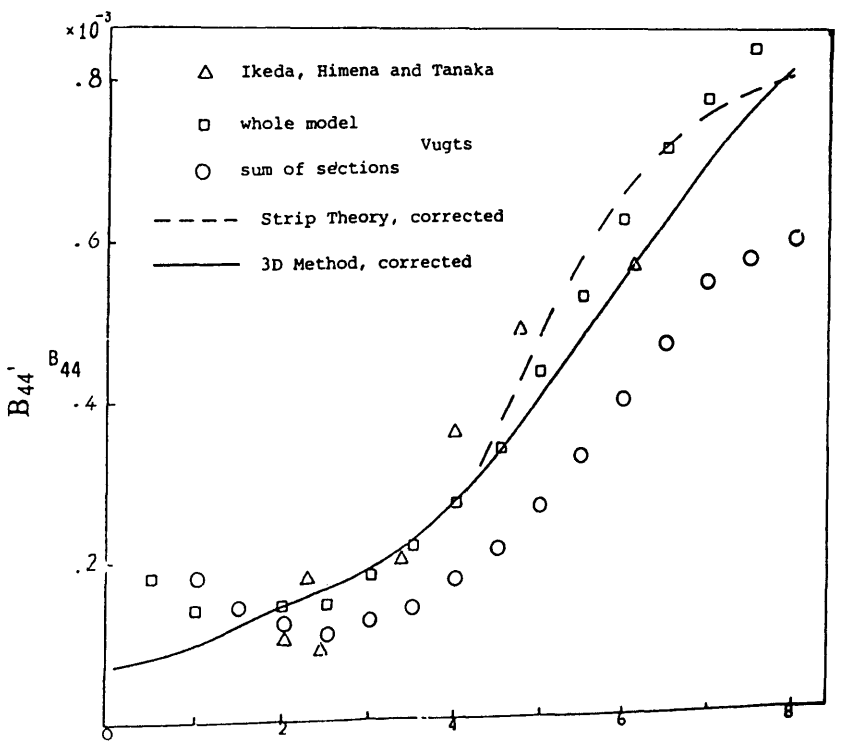

Fig. 4.13 Roll damping coefficients of Series 60 at F_n=0.0 including viscous effect

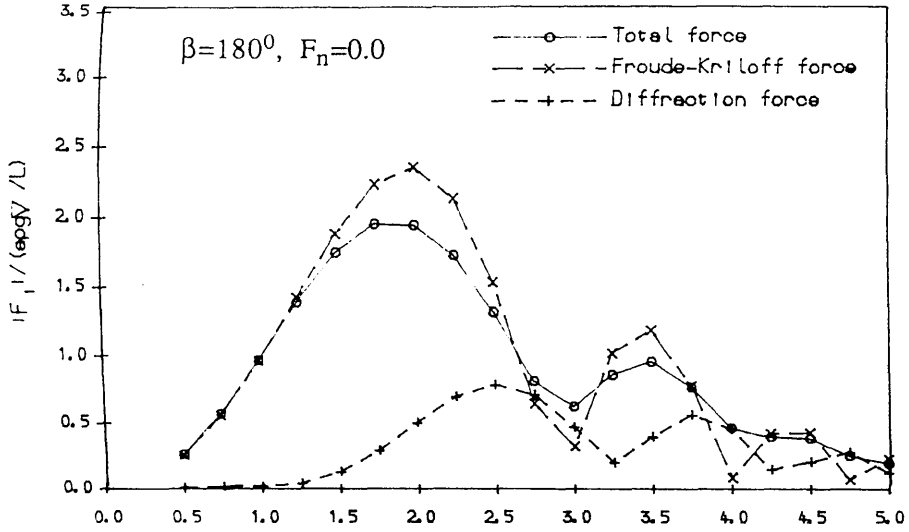

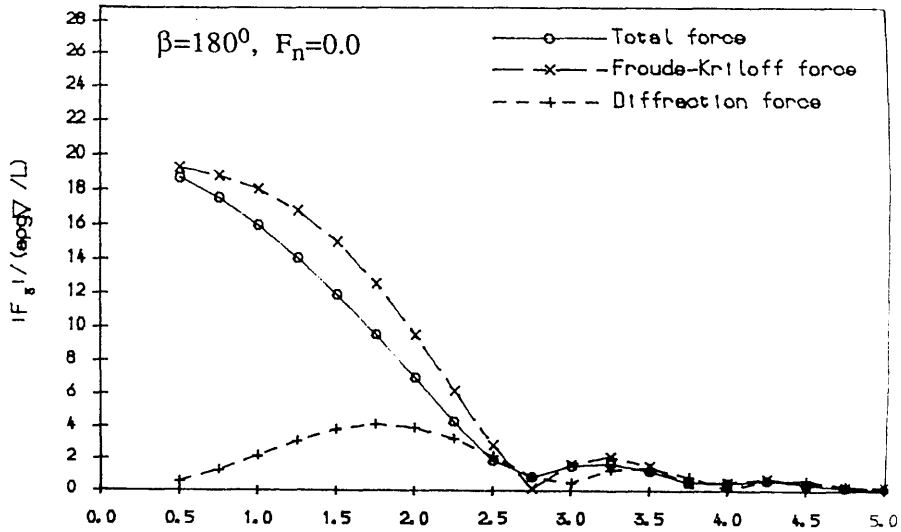

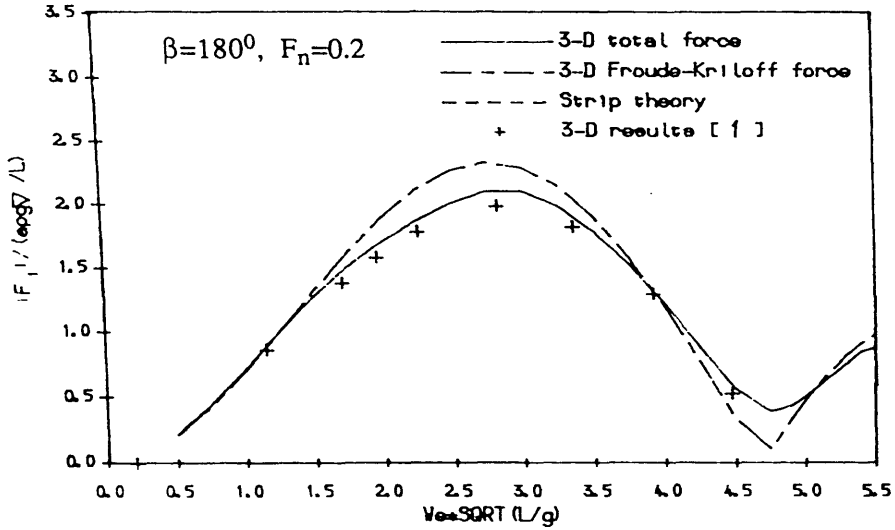

Fig. 4.14 Surge wave exciting forces on Series 60 in head sea at F_n=0.0 and F_n=0.2

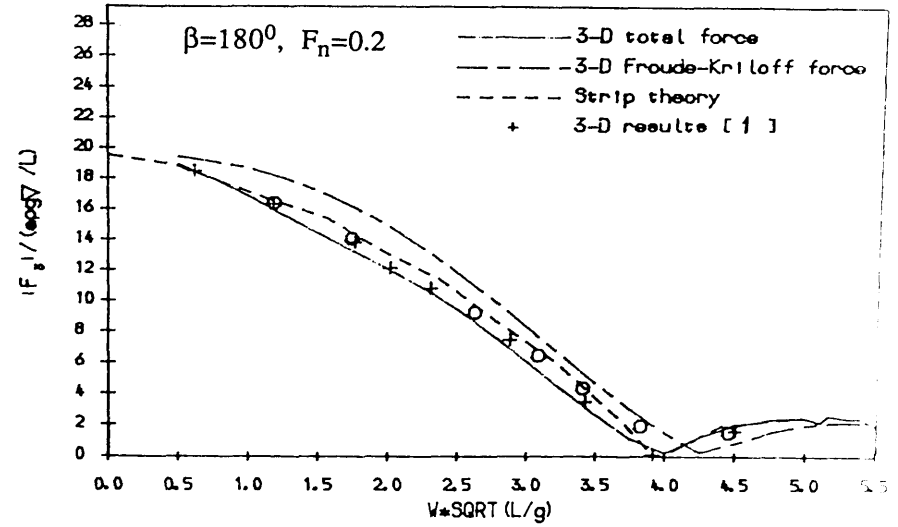

Fig. 4.15 Heave wave exciting forces on Series 60 in head sea at F_n=0.0 and F_n=0.2

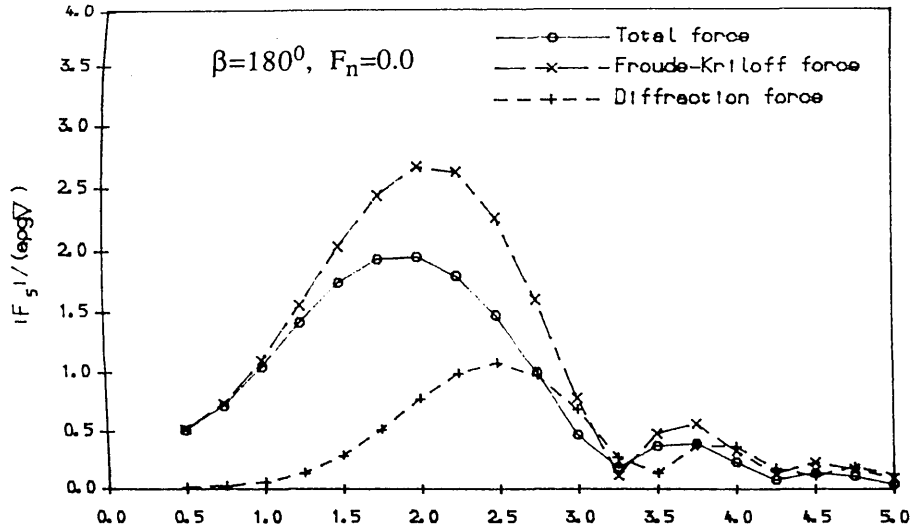

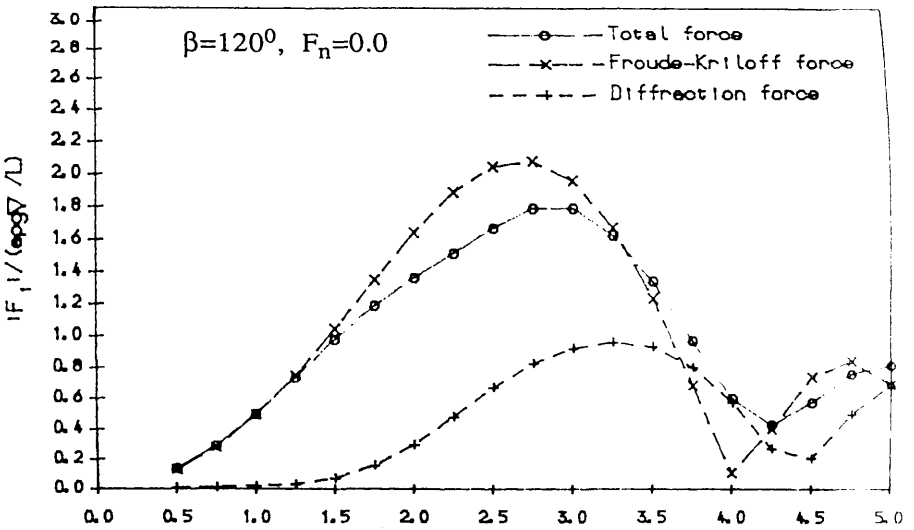

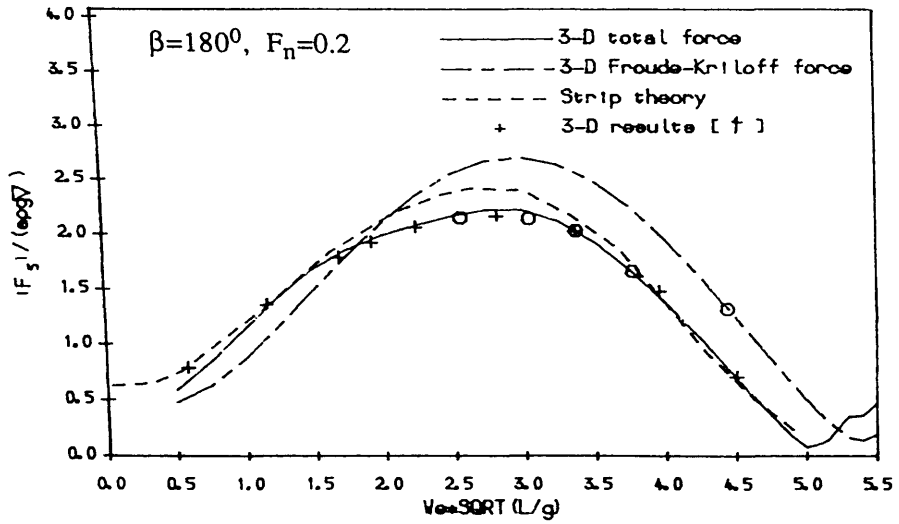

Fig. 4.16 Pitch wave exciting moments on Series 60 in head sea at F_n=0.0 and F_n=0.2

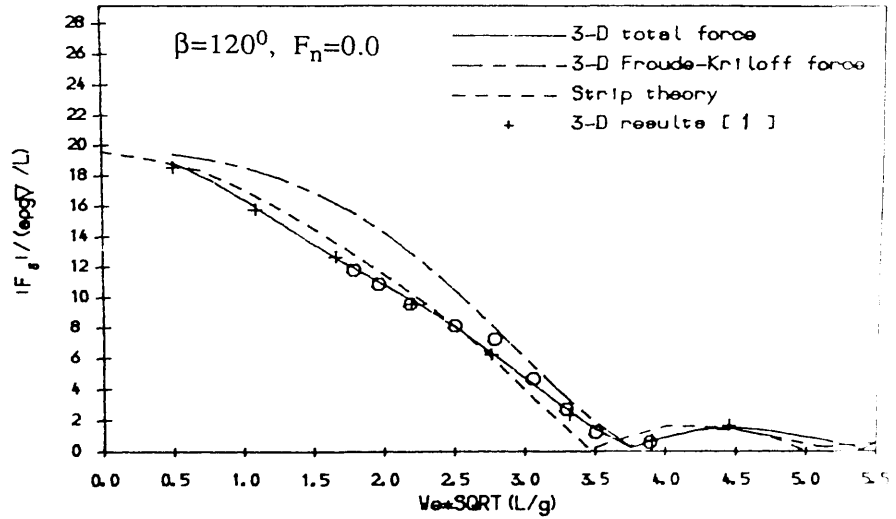

Fig. 4.17 Surge and heave wave exciting forces on Series 60 in bow quartering sea at F_n=0.0

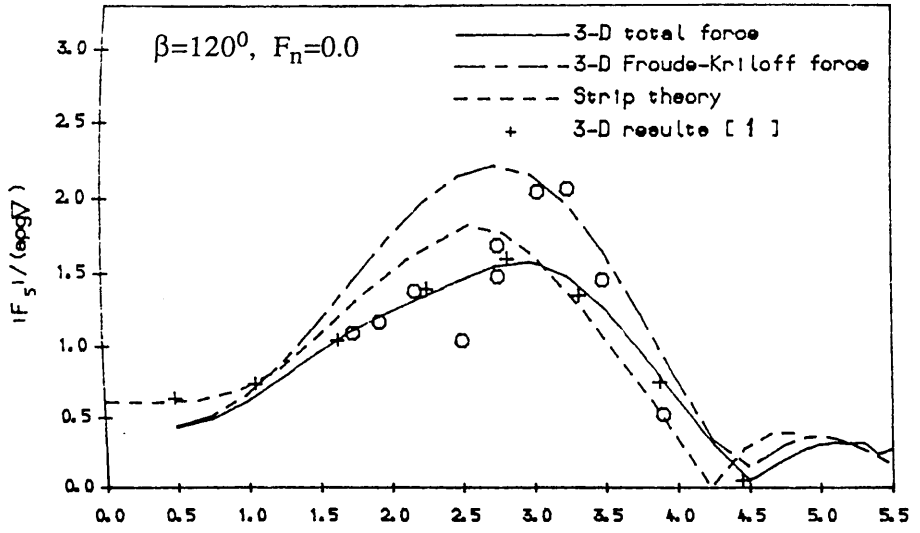

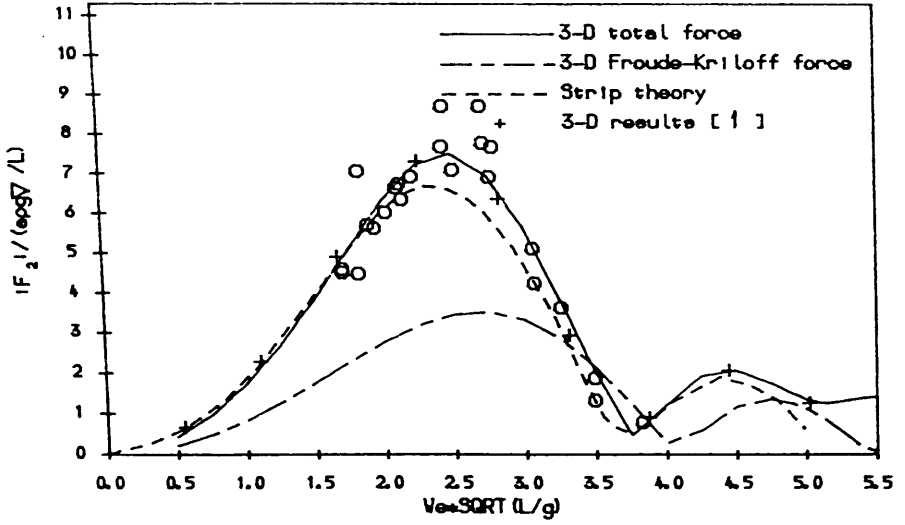

Fig. 4.18 Pitch and sway wave exciting moments/forces on Series 60 in bow quartering sea at F_n=0.0

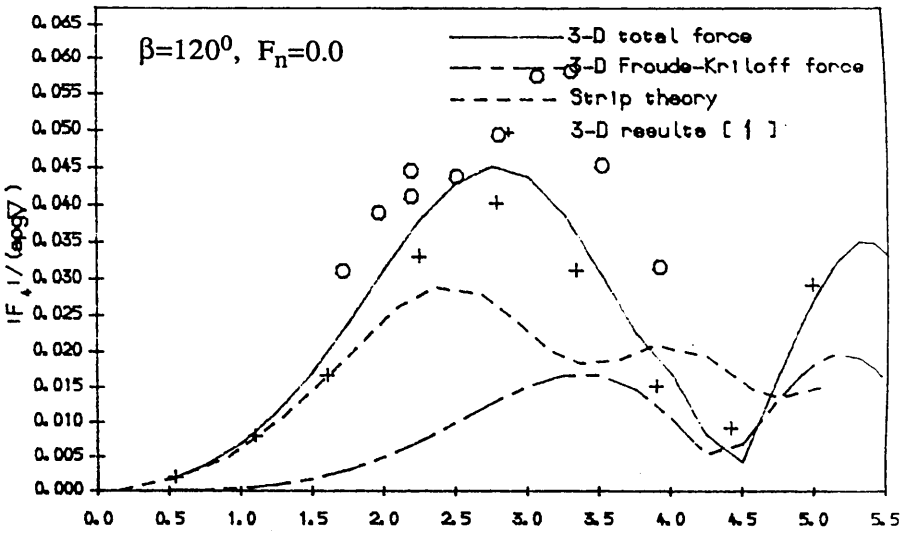

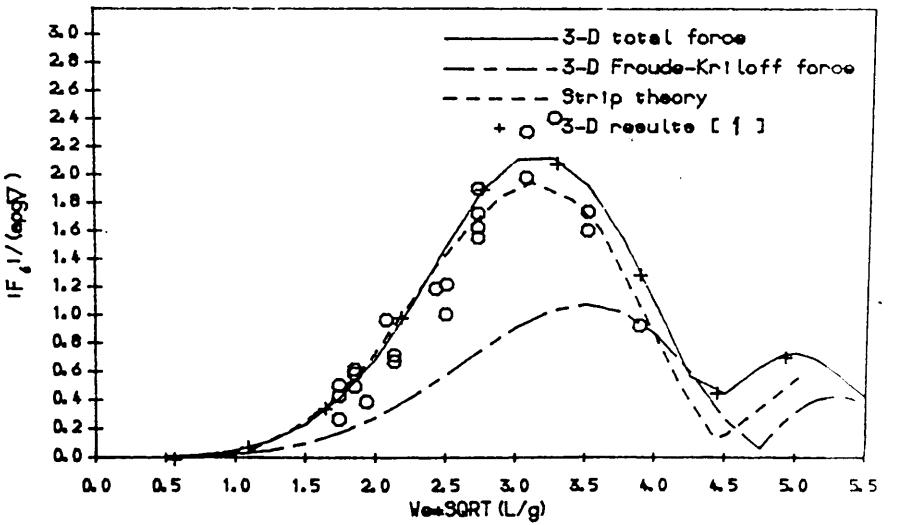

Fig. 4.19 Roll and yaw wave exciting moments on Series 60 in bow quartering sea at F_n=0.0

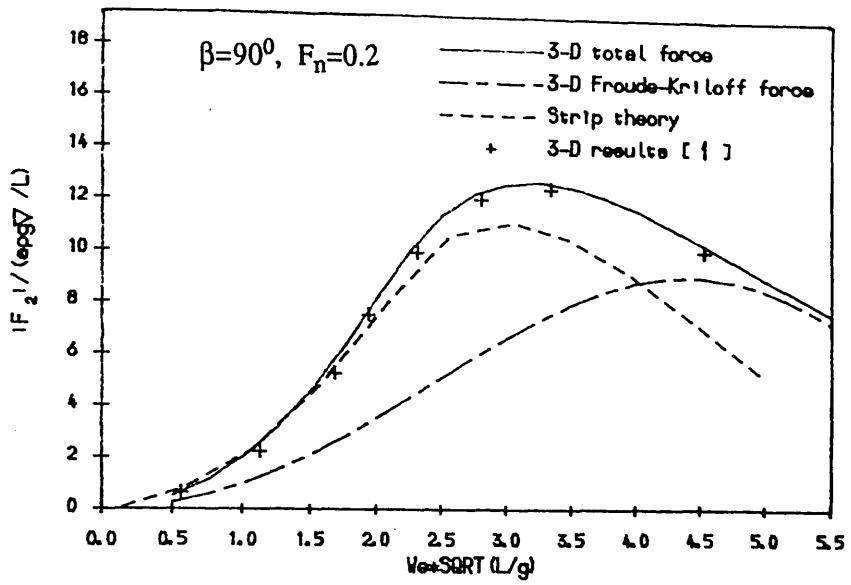

Fig. 4.20 Sway wave exciting forces on Series 60 in beam sea at F_n=0.2

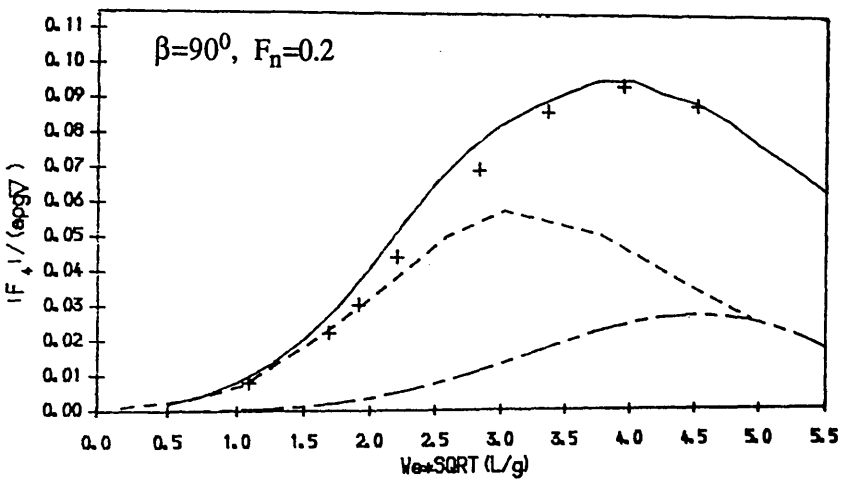

Fig. 4.21 Heave wave exciting forces on Series 60 in beam sea at F_n=0.2

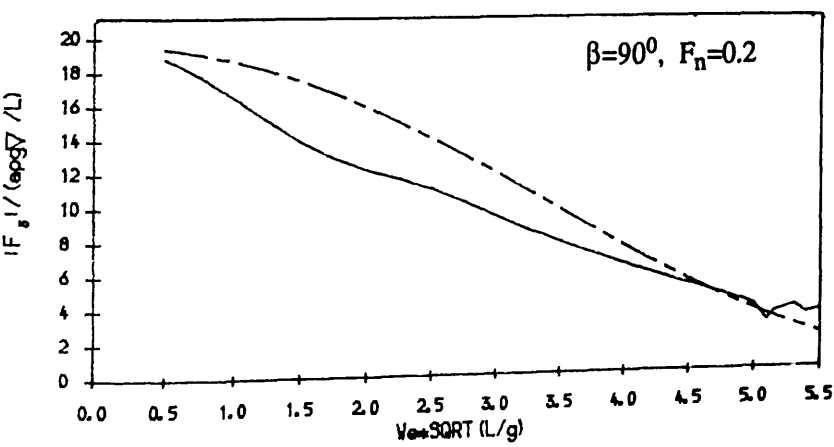

Fig. 4.22 Roll wave exciting moments on Series 60 in beam sea at F_n=0.2

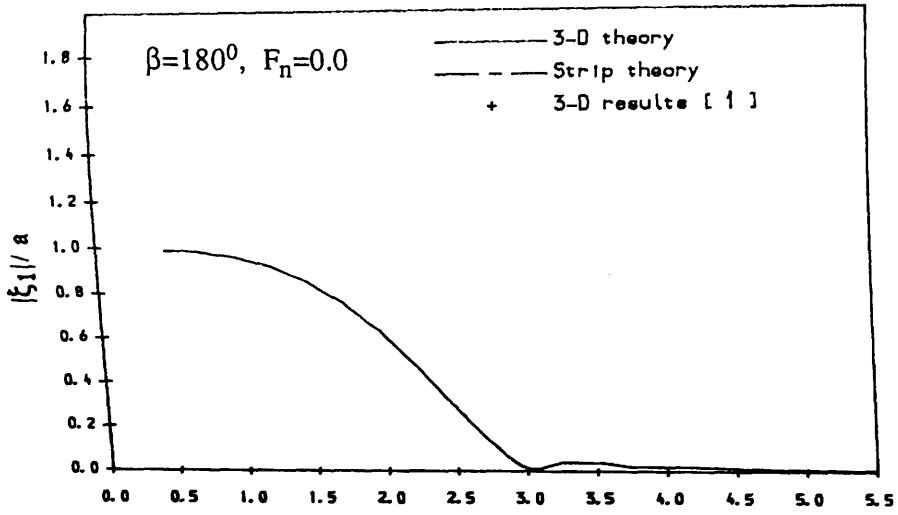

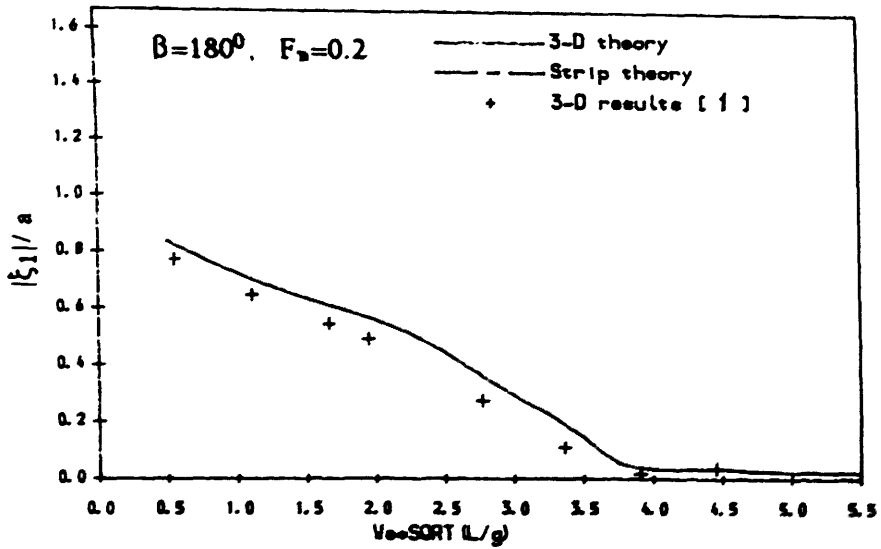

Fig. 4.23 Surge motion responses of Series 60 in head sea at F_n=0.0 and F_n=0.2

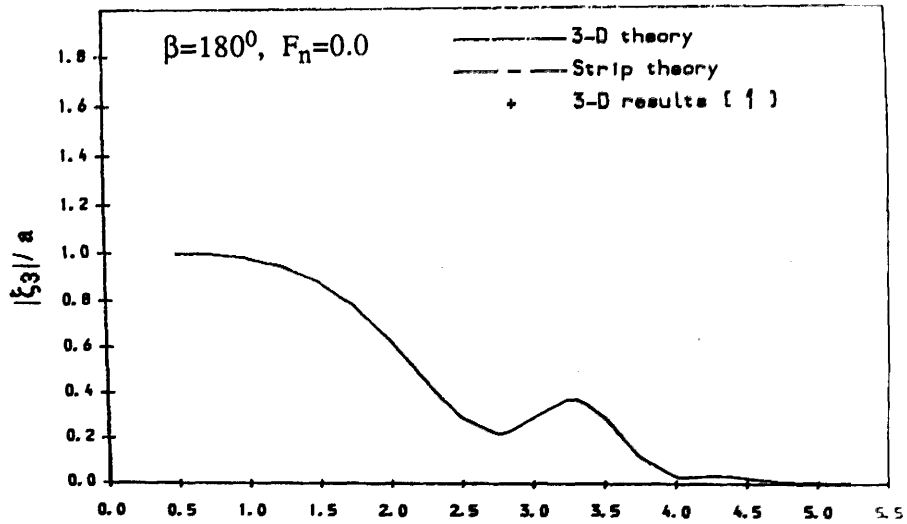

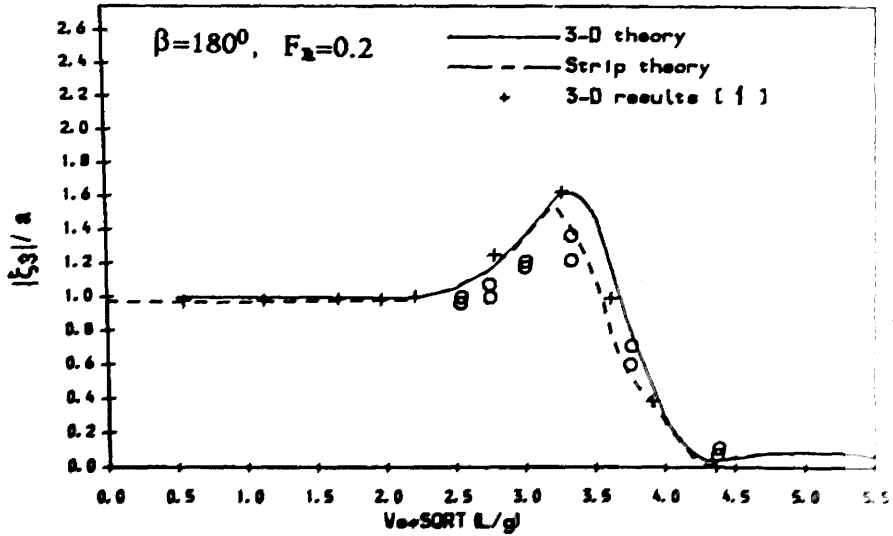

Fig. 4.24 Heave motion responses of Series 60 in head sea at F_n=0.0 and F_n=0.2

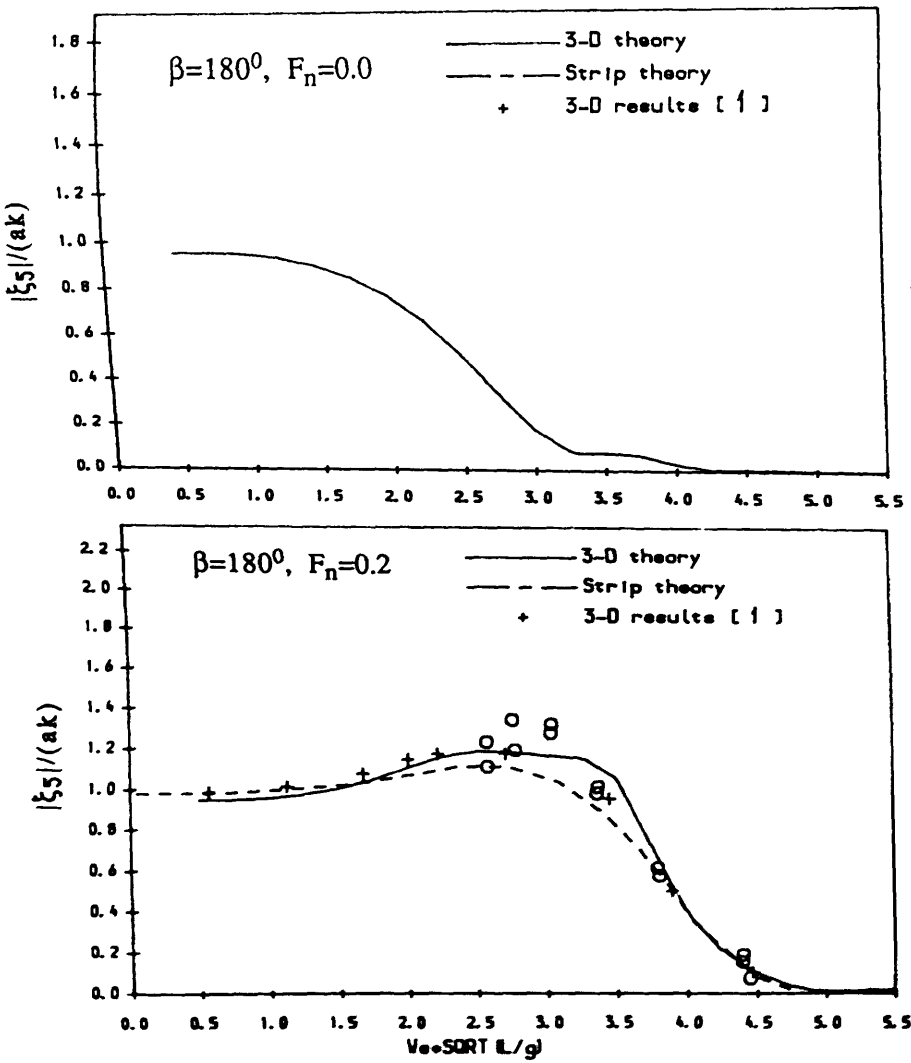

Fig. 4.25 Pitch motion responses of Series 60 in head sea at F_n=0.0 and F_n=0.2

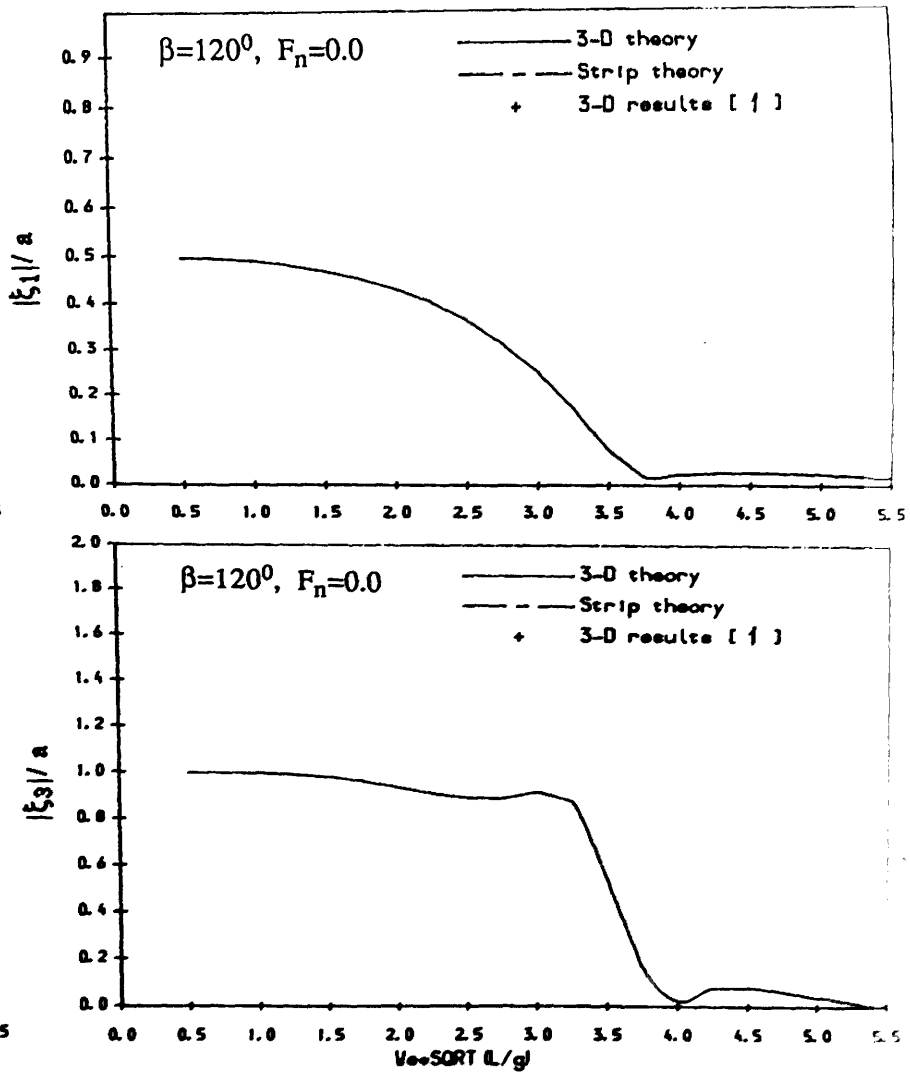

Fig. 4.26 Surge and heave motion responses of Series 60 in bow quartering sea at F_n=0.0

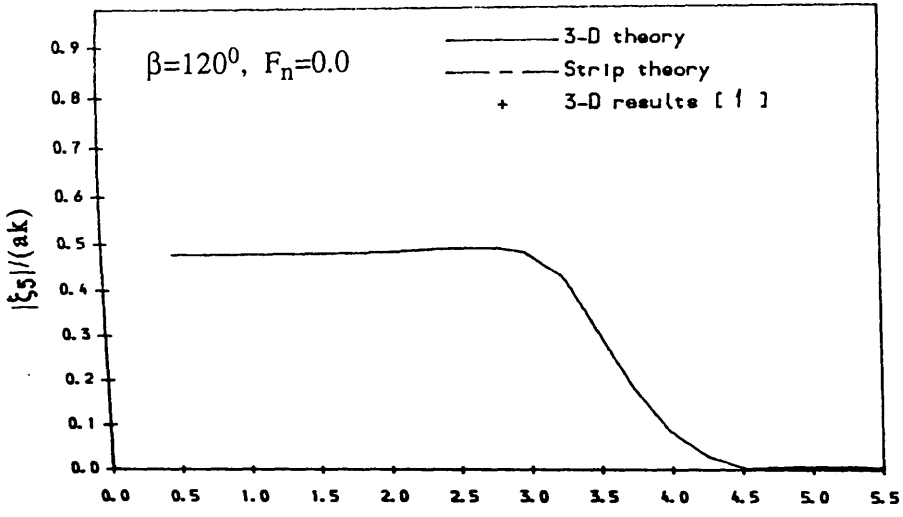

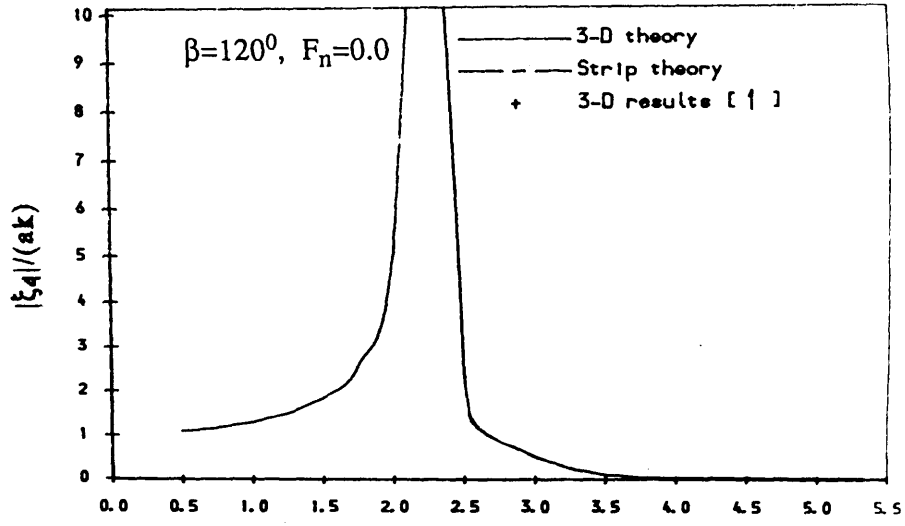

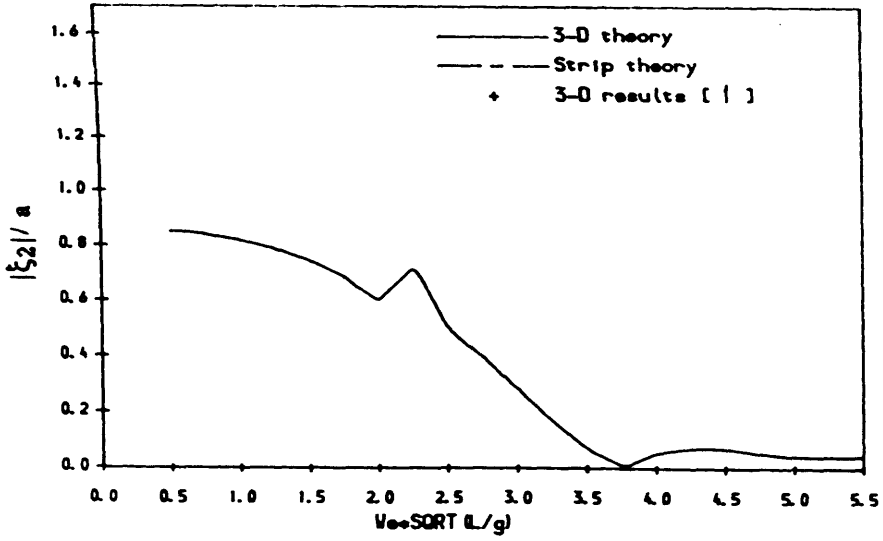

Fig. 4.27 Pitch and sway motion responses of Series 60 in bow quartering sea at F_n=0.0

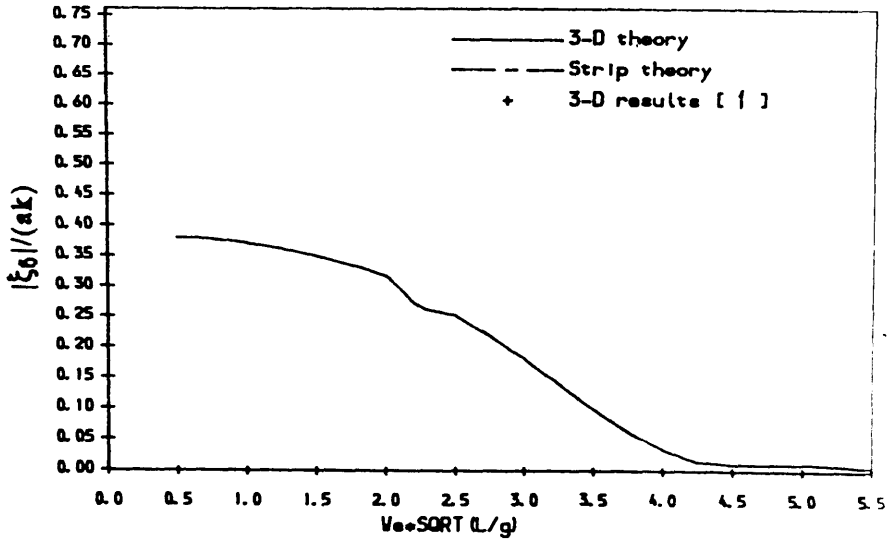

Fig. 4.28 Roll and yaw motion responses of Series 60 in bow quartering sea at F_n=0.0

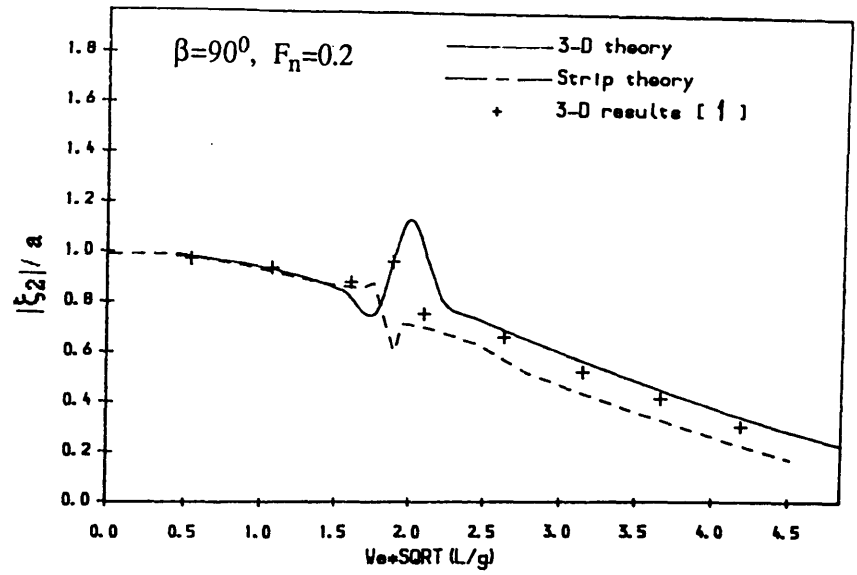

Fig. 4.29 Sway motion responses of Series 60 in beam sea at F_n=0.2

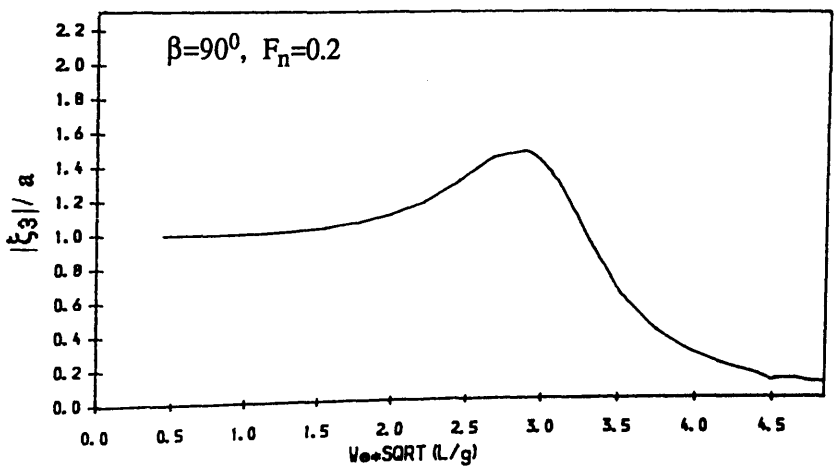

Fig. 4.30 Heave motion responses of Series 60 in beam sea at F_n=0.2

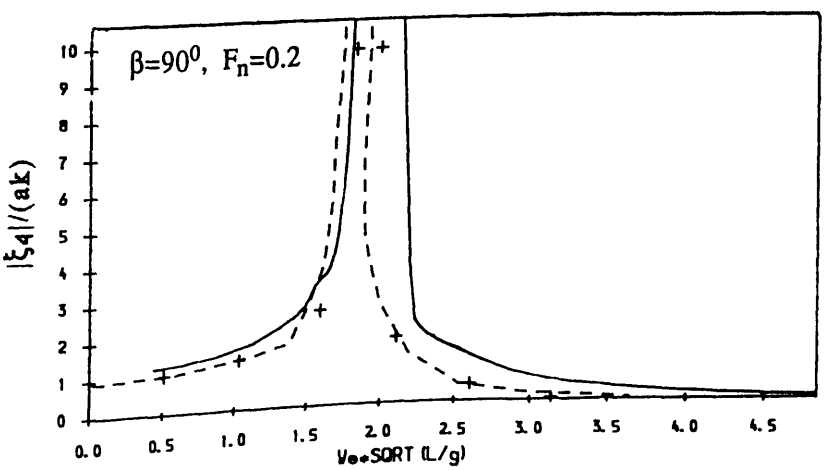

Fig. 4.31 Roll motion responses of Series 60 in beam sea at F_n=0.2

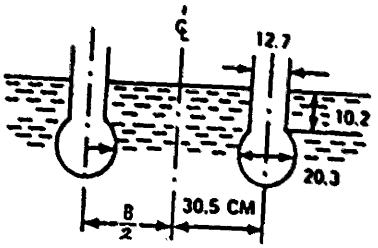

(a) B/L = 0.305

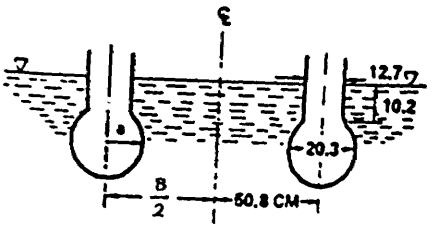

(b) B/L = 0.508

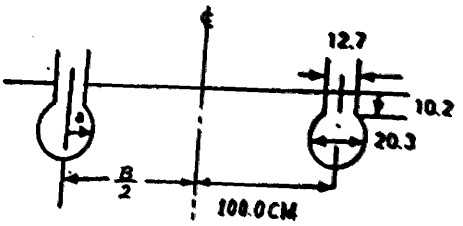

(c) B/L = 1.0

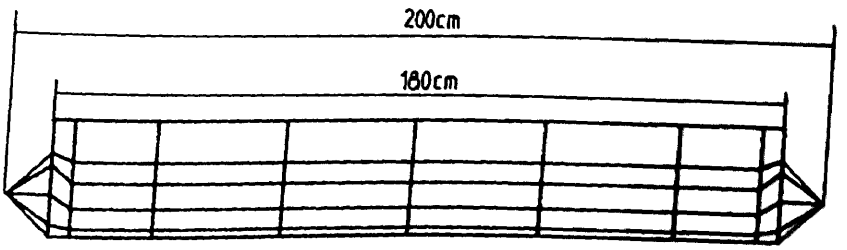

Fig. 4.32 Geometry of twin cylinders with the hull form represented by 192 panel elements

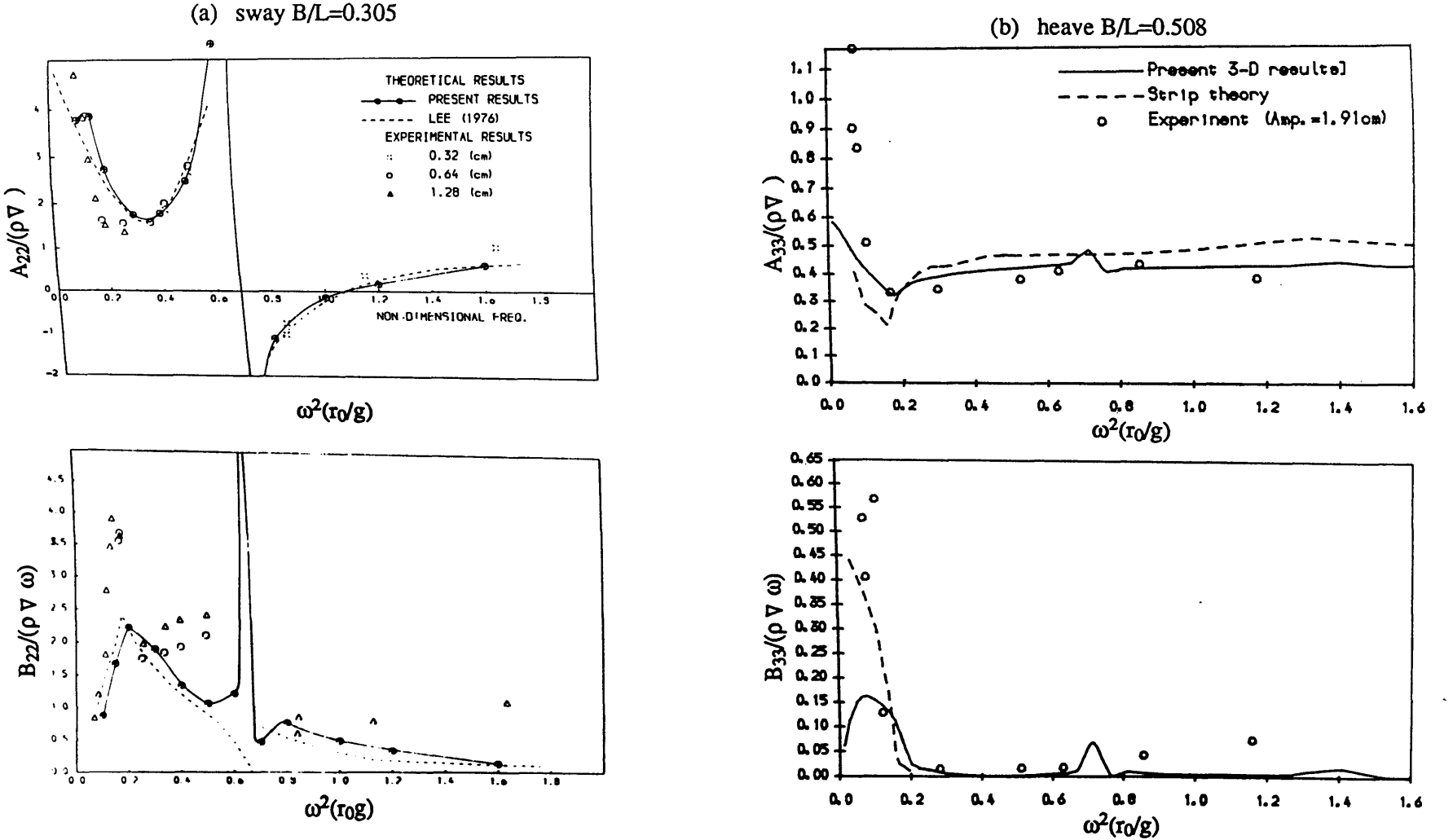

Fig. 4.33 Sway and heave added mass and damping coefficients of twin cylinders

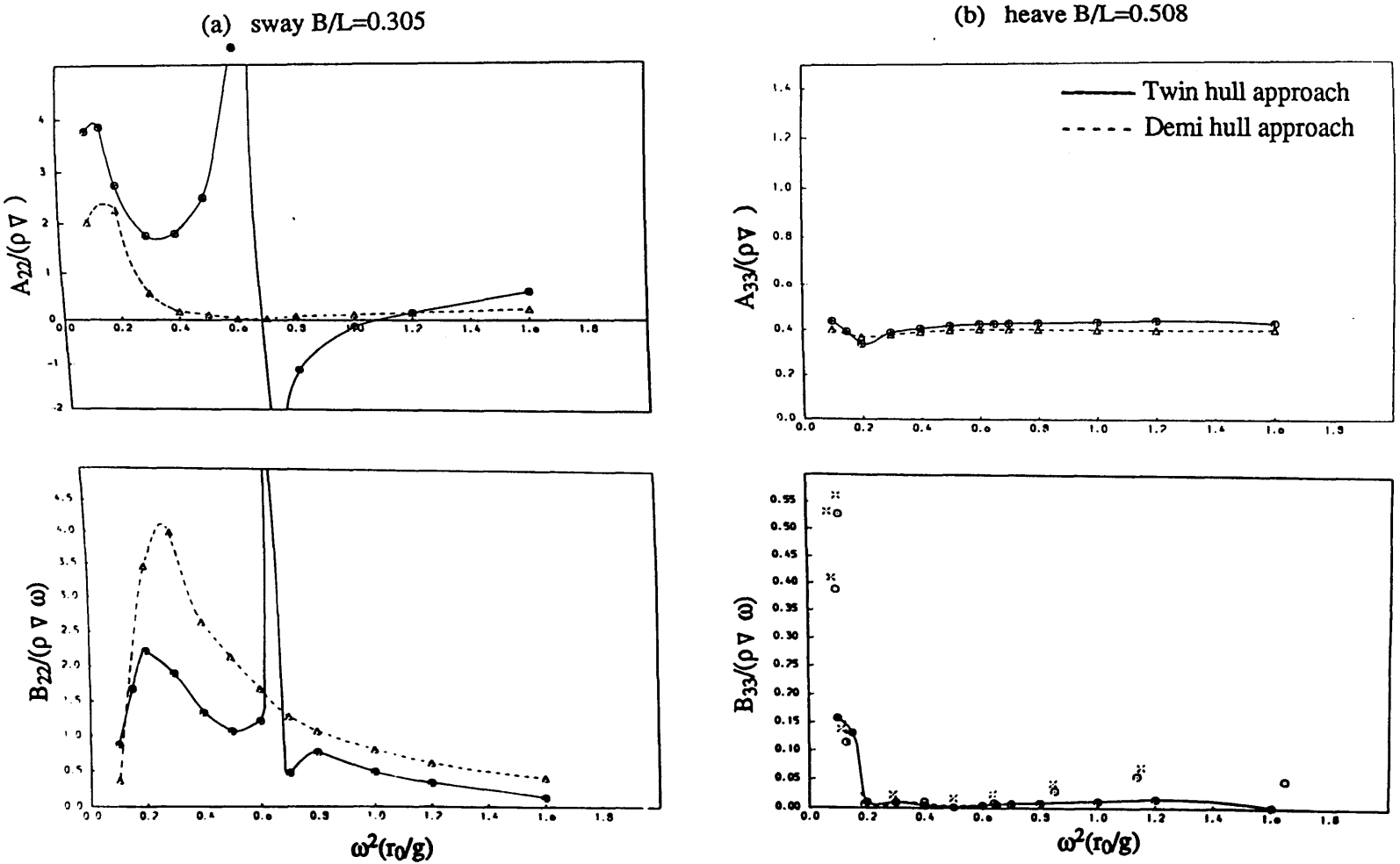

Fig. 4.34 Comparison between twin and demi hull approaches on twin cylinders

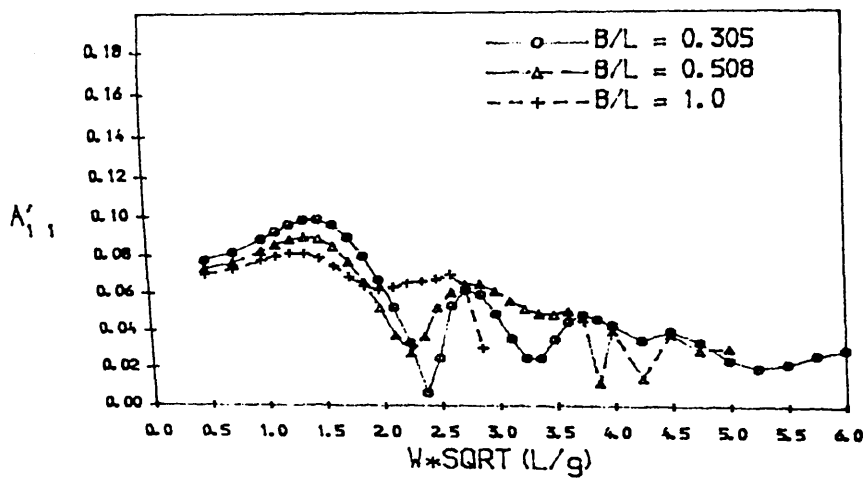

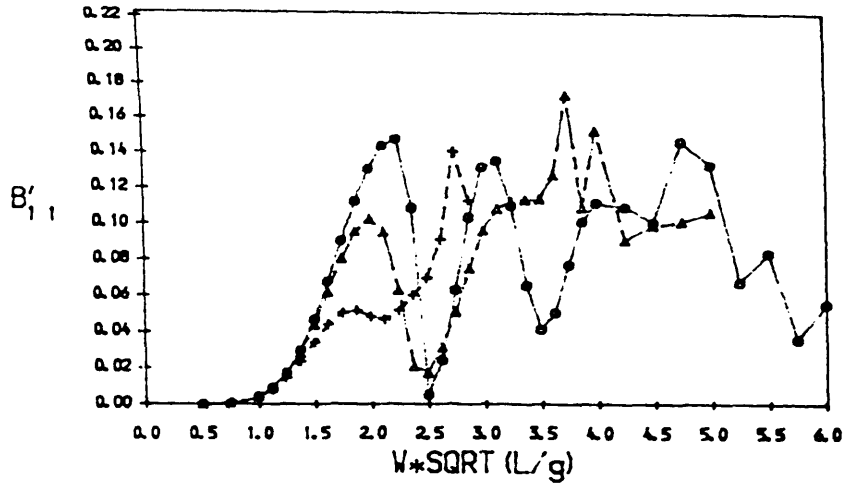

Fig. 4.35 Surge added mass and damping coef. of twin cylinders

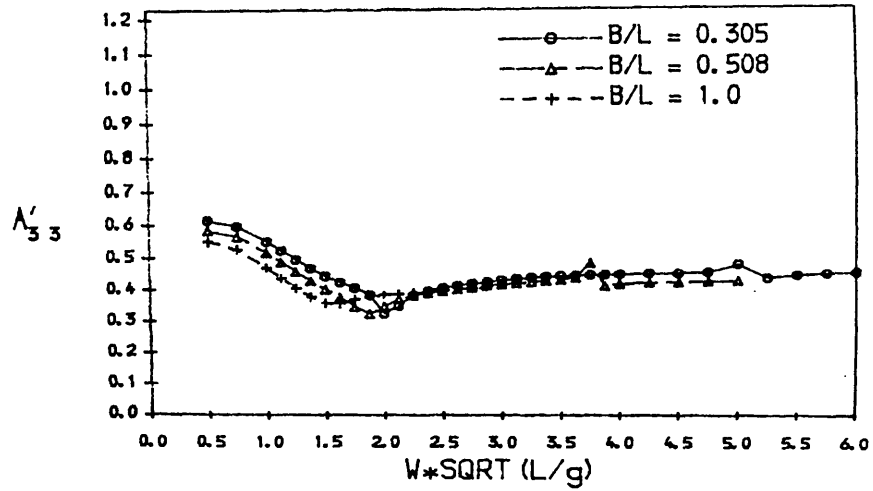

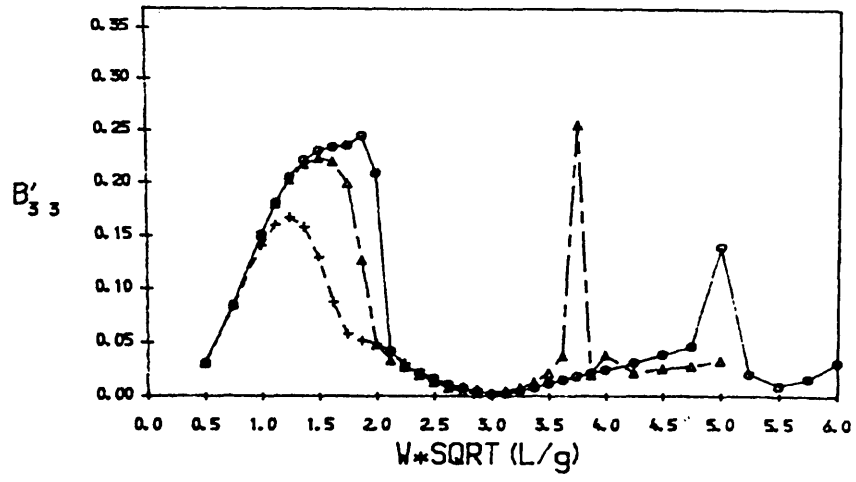

Fig. 4.36 Heave added mass and damping coef. of twin cylinders

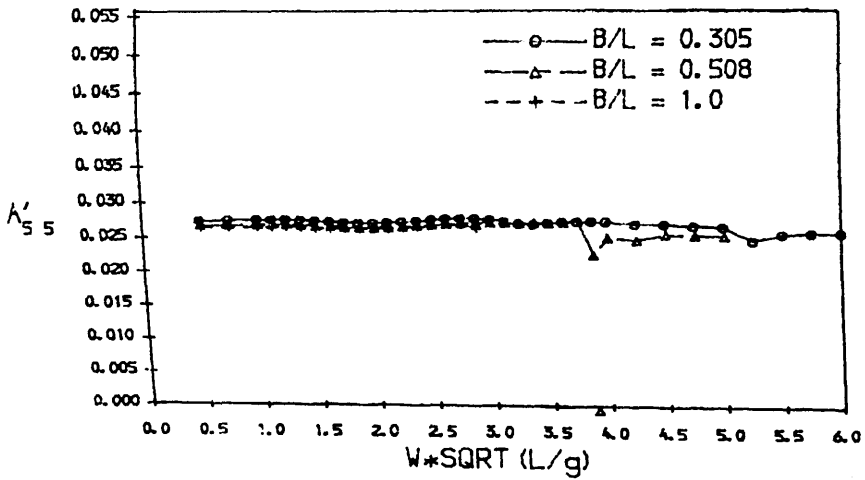

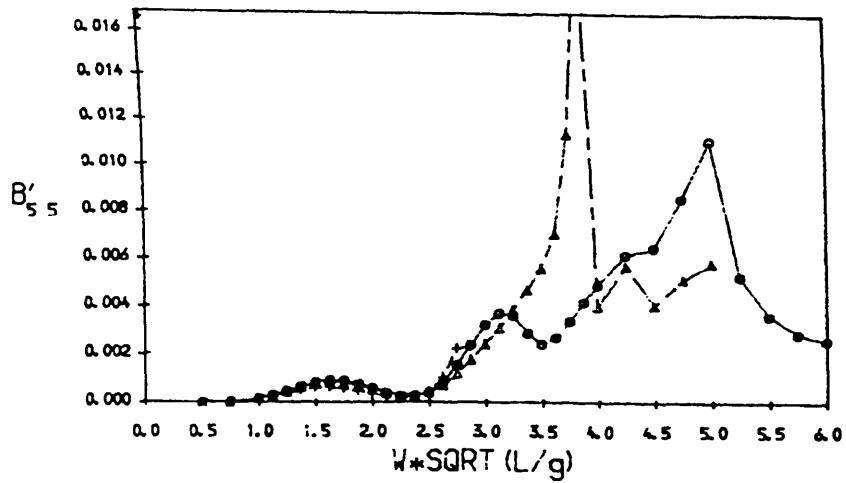

Fig. 4.37 Pitch added inertia and damping coef. of twin cylinders

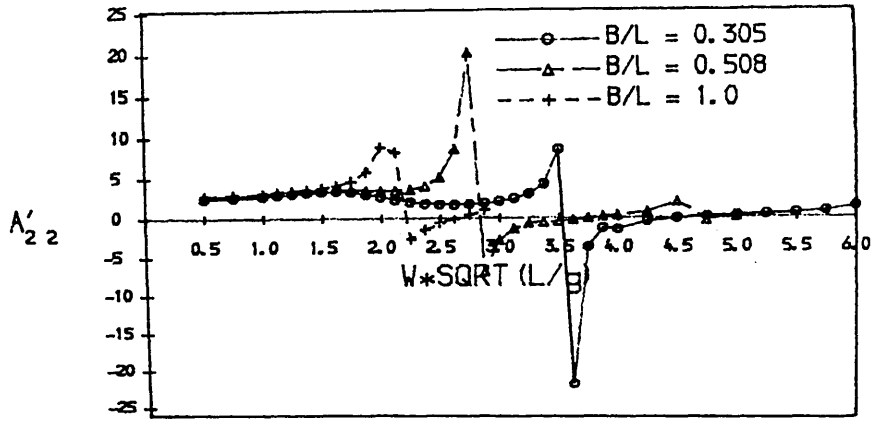

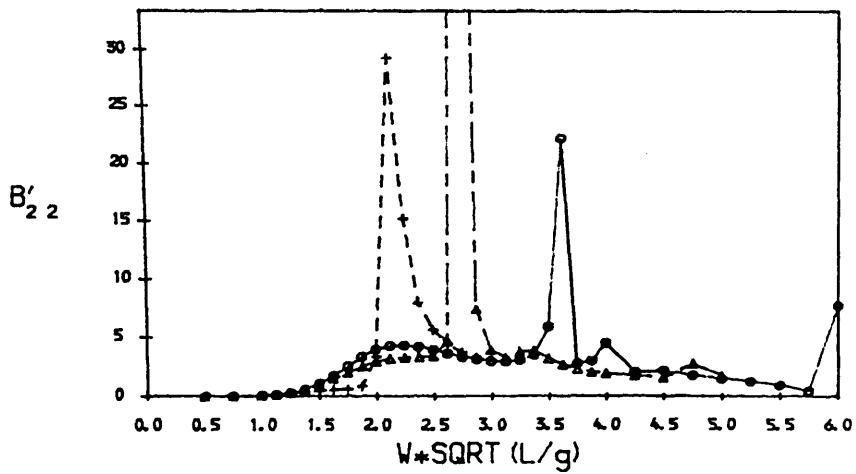

Fig. 4.38 Sway added mass and damping coef. of twin cylinders

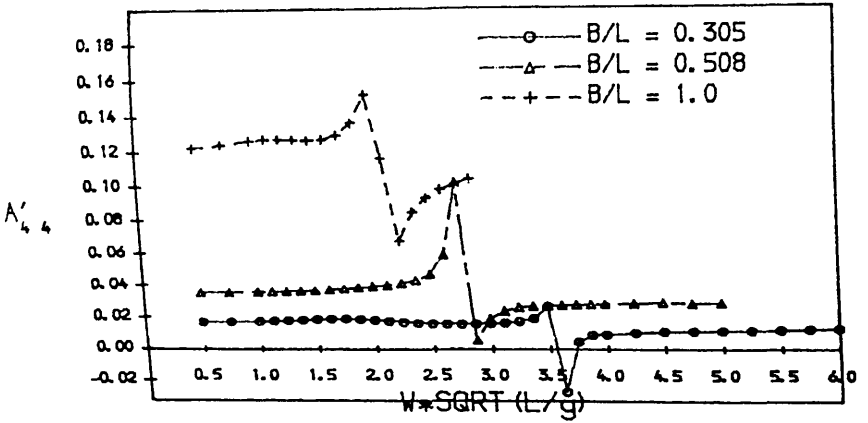

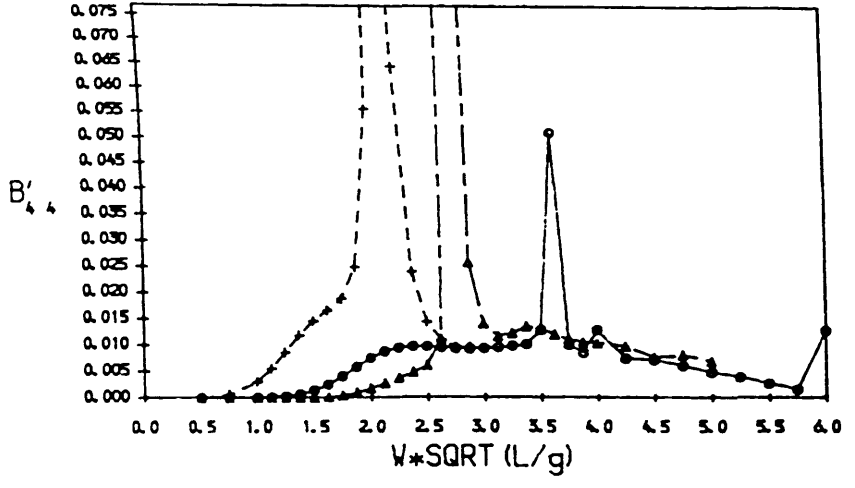

Fig. 4.39 Sway-roll coupling added inertia and damping coefficients of twin cylinders

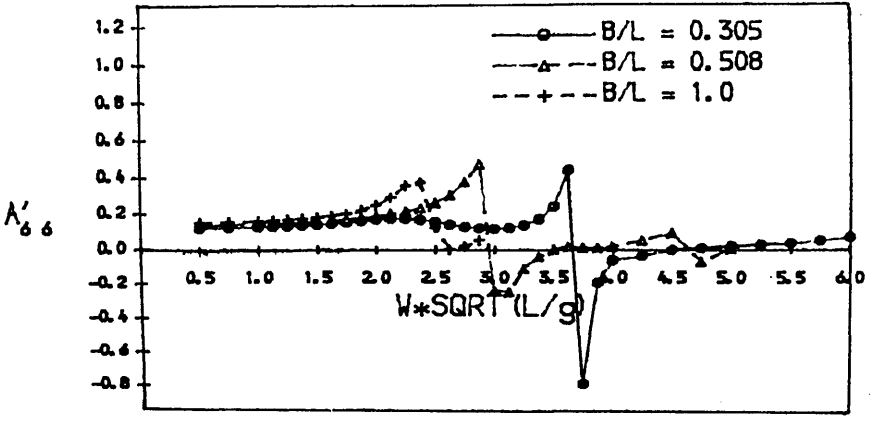

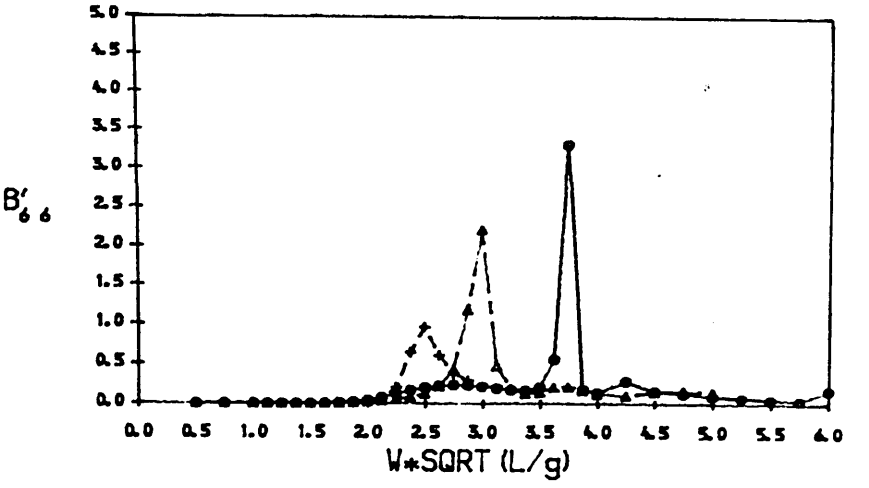

Fig. 4.40 Roll added inertia and damping coef. of twin cylinders

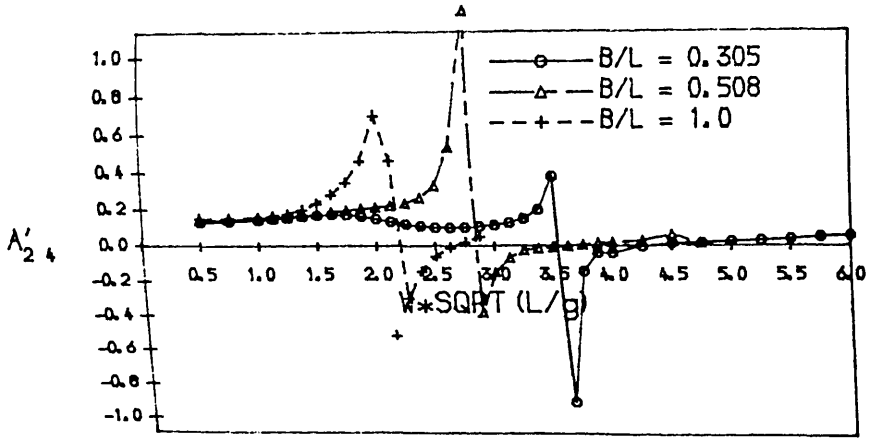

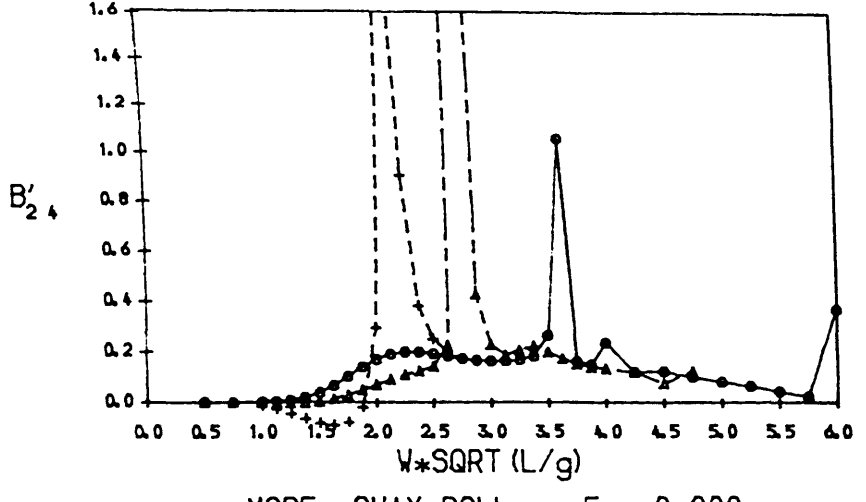

Fig. 4.41 Yaw added inertia and damping coef. of twin cylinders

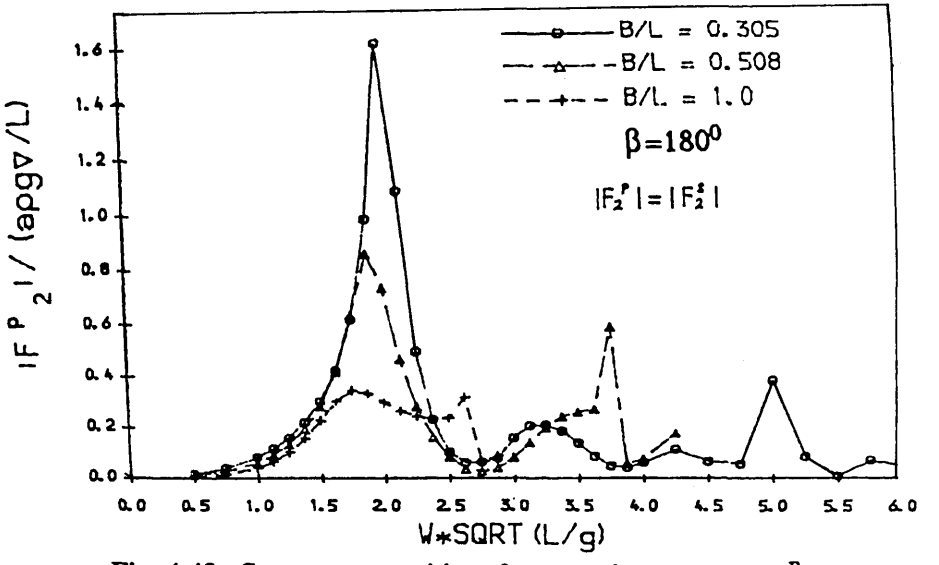

Fig. 4.42 Sway wave exciting forces acting on port (F_2^P) and star (F_2^S) board sides of twin cylinders in head sea

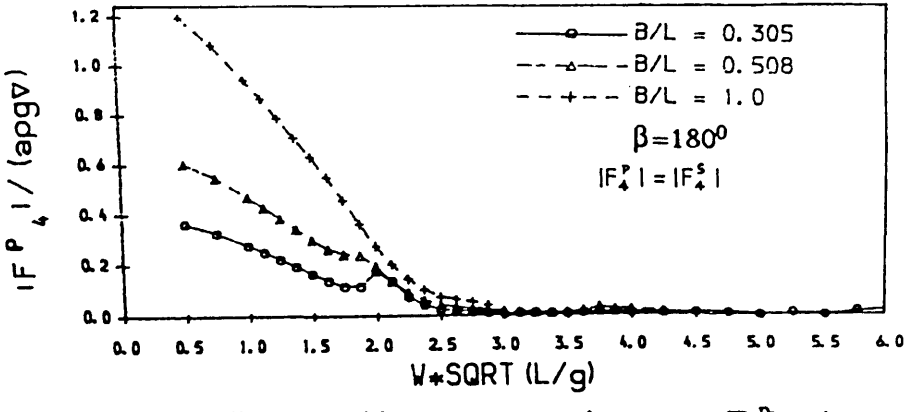

Fig. 4.43 Roll wave exciting moments acting on port (F_4^P) and star (F_4^S) board sides of twin cylinders in head sea

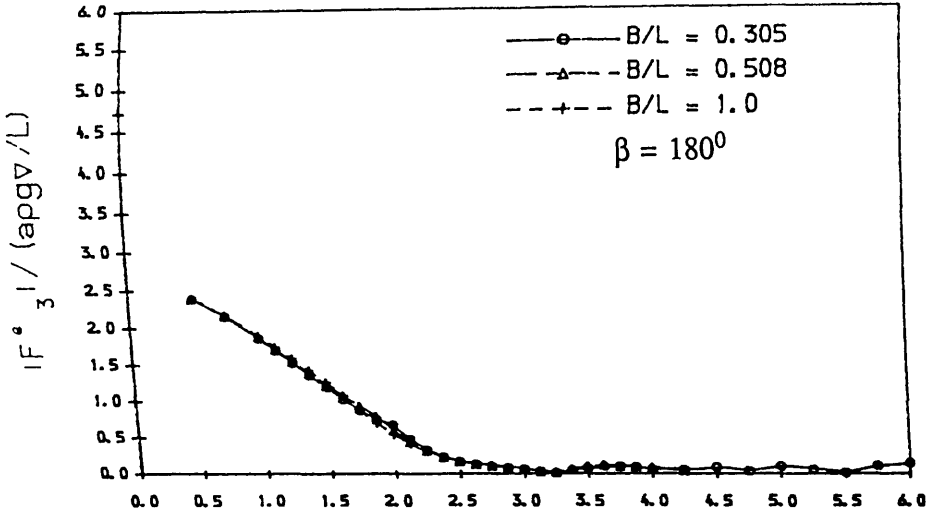

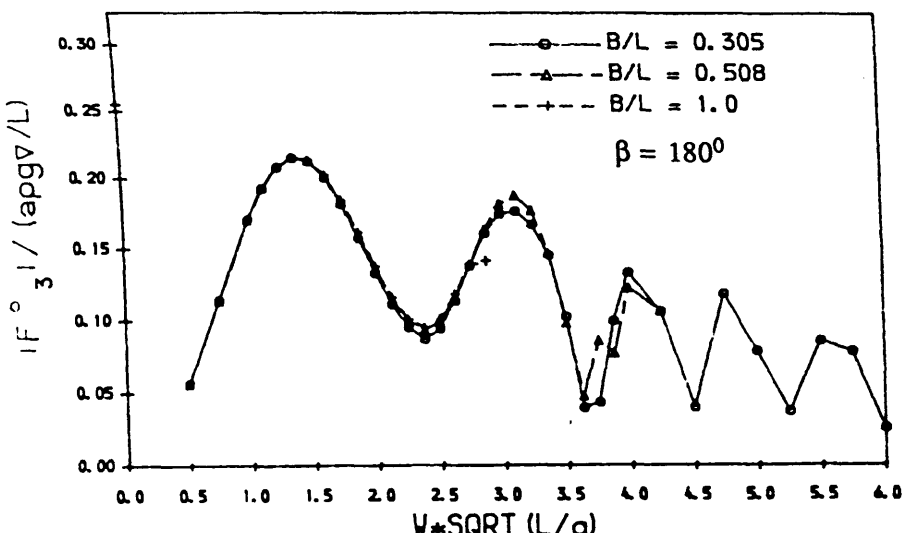

Fig. 4.44 Even and odd parts of heave wave exciting forces on twin cylinders in head sea

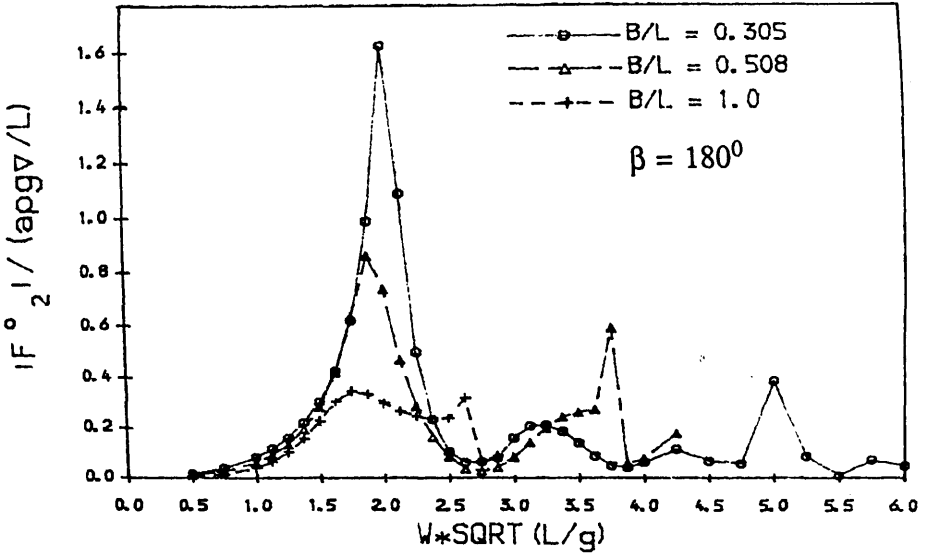

Fig. 4.45 Odd part of sway wave exciting forces on twin cylinders in head sea

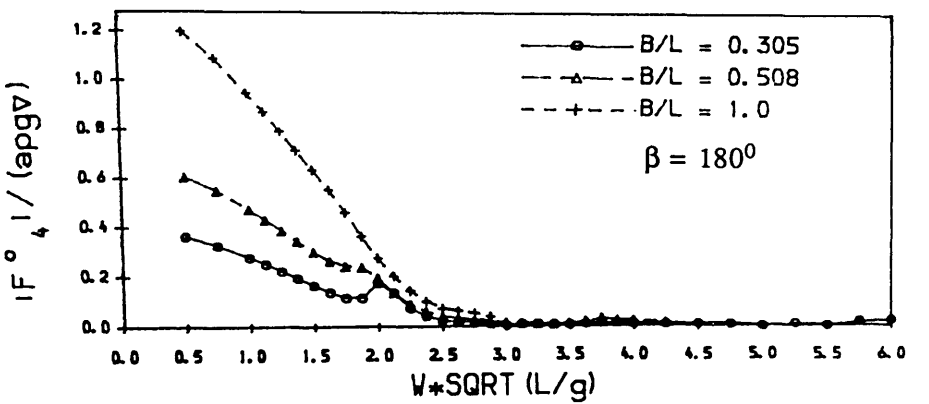

Fig. 4.46 Odd part of roll wave exciting moment on twin cylinders in head sea

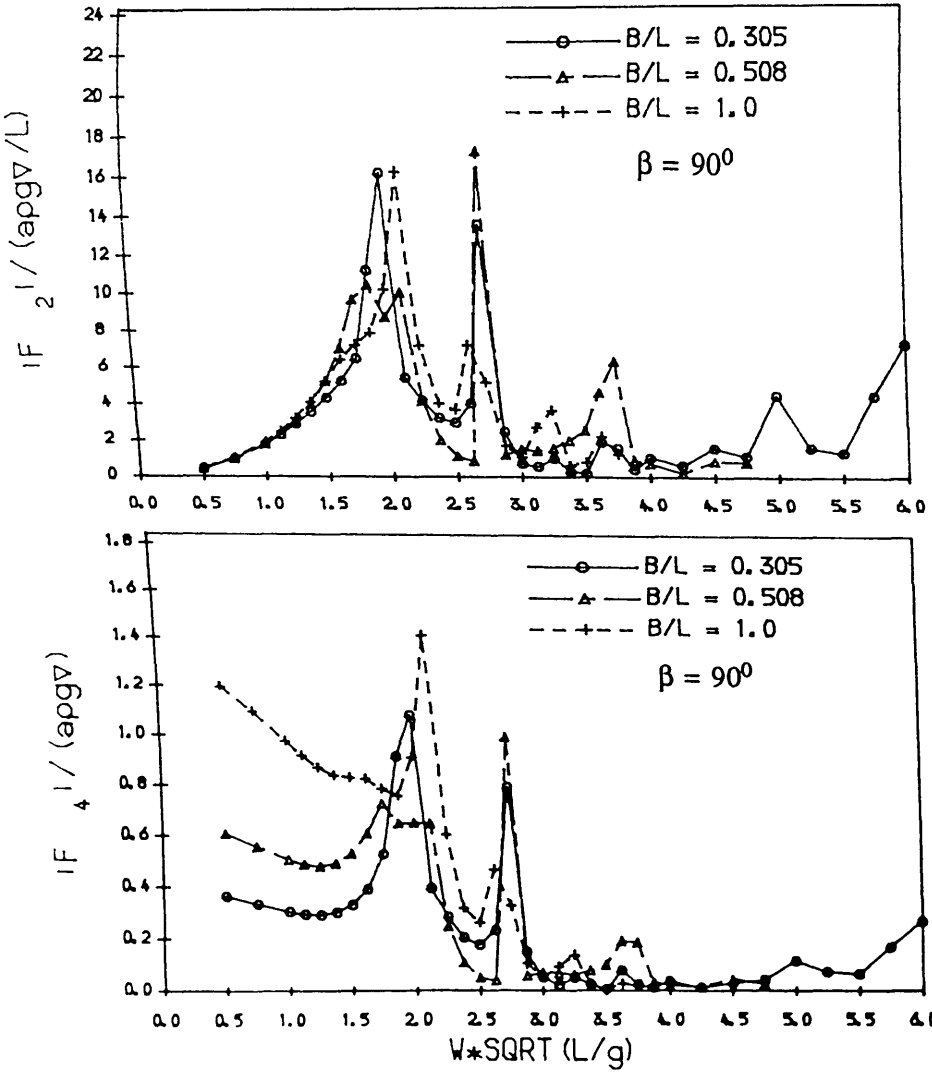

Fig. 4.47 Sway and roll wave exciting forces/moments acting on port board side of twin cylinders in beam sea

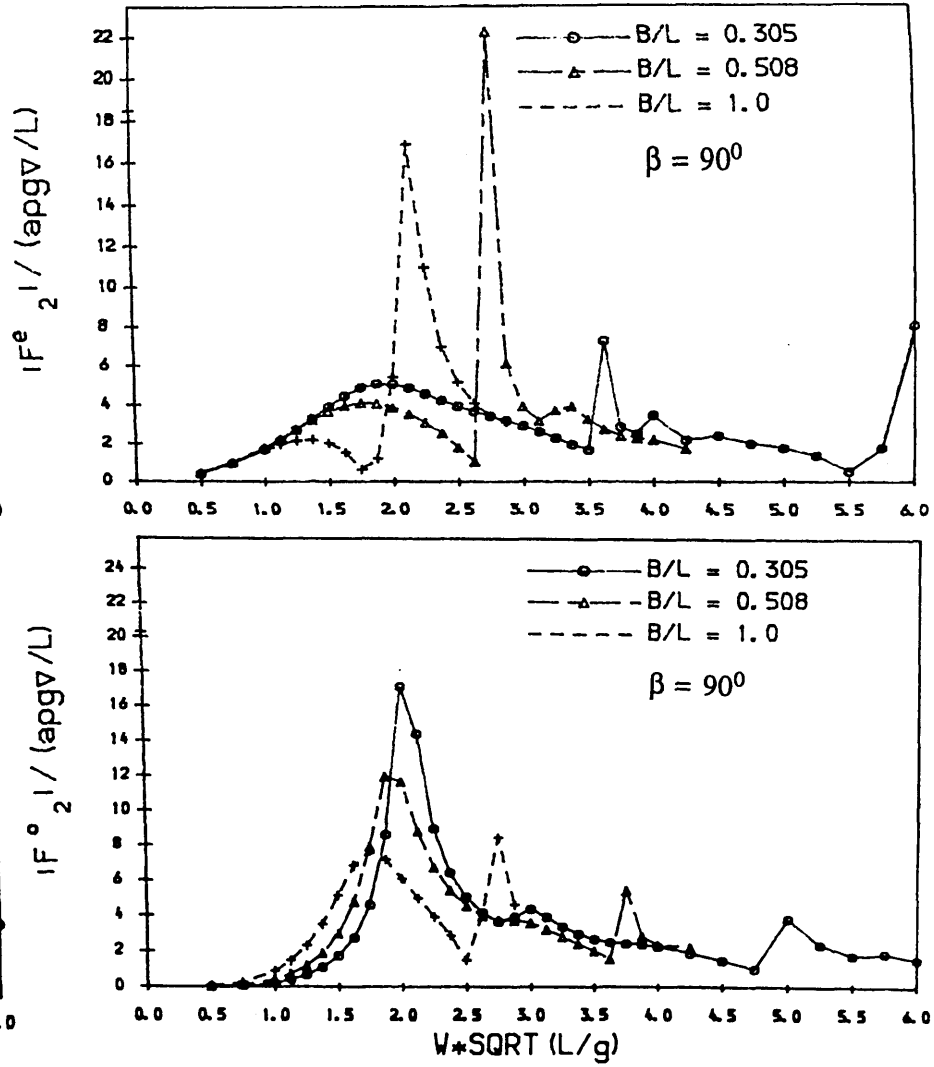

Fig. 4.48 Even and odd parts of sway wave exciting forces on twin cylinders in beam sea

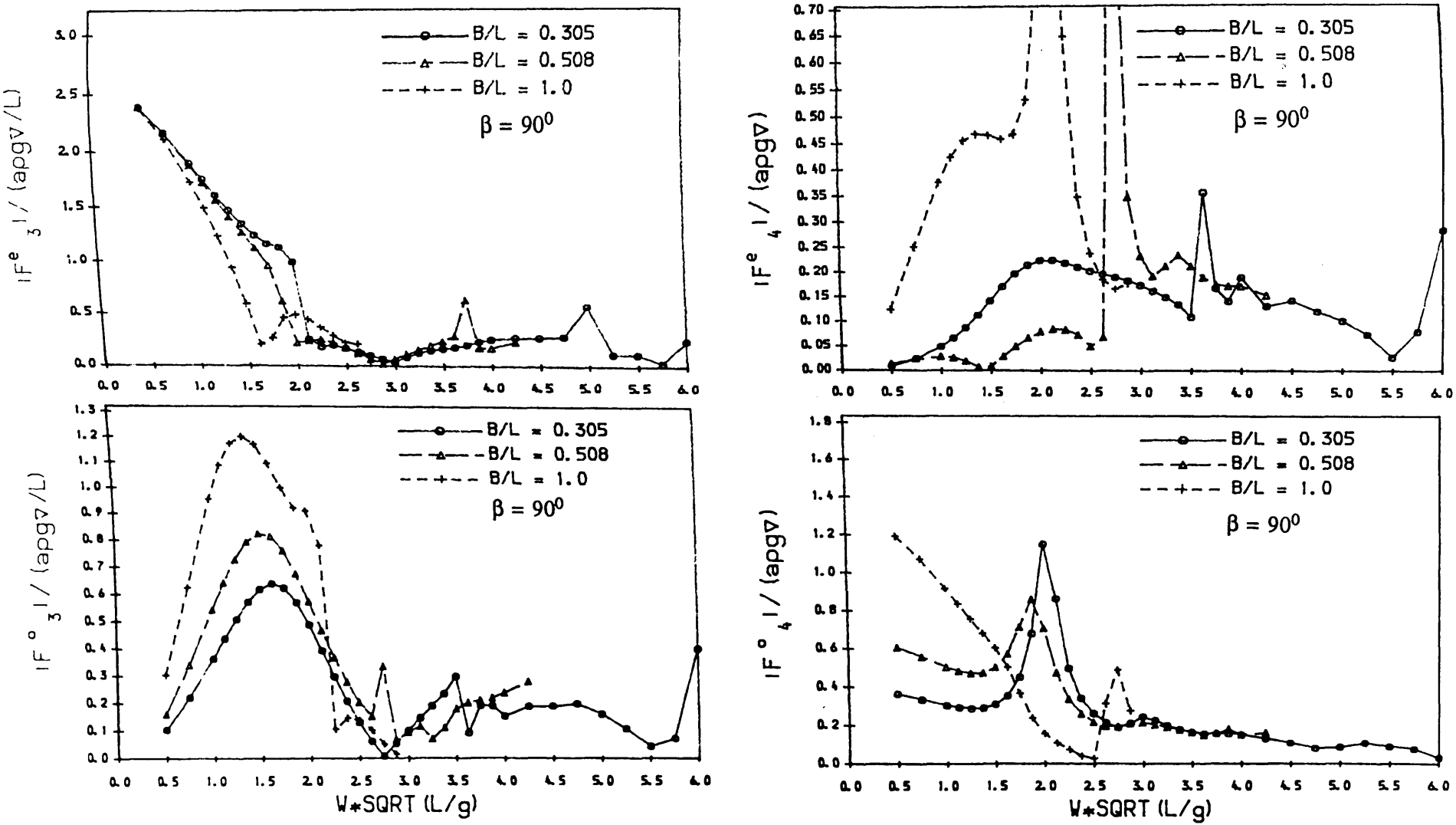

Fig. 4.49 Even and odd parts of heave wave exciting forces and moments on twin cylinders in beam sea

(a) Single strut SWATH

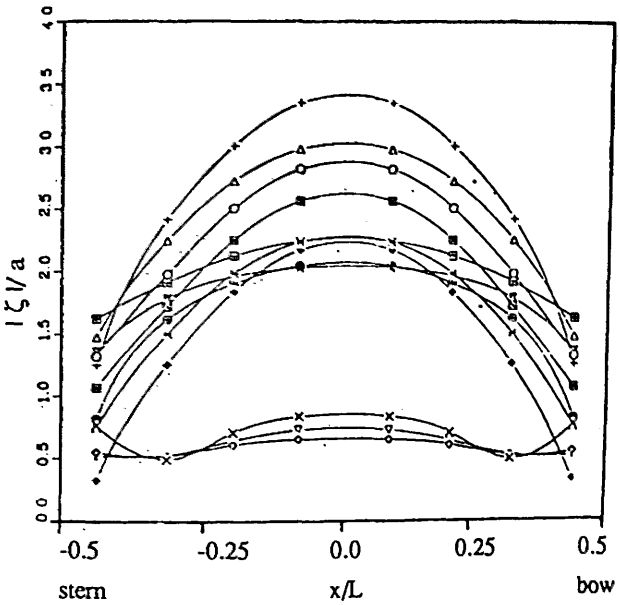

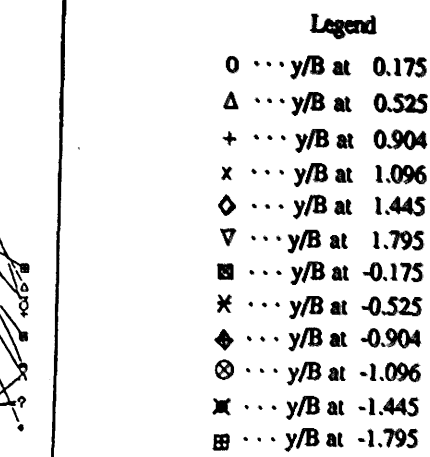

(b) Tandem strut SWATH

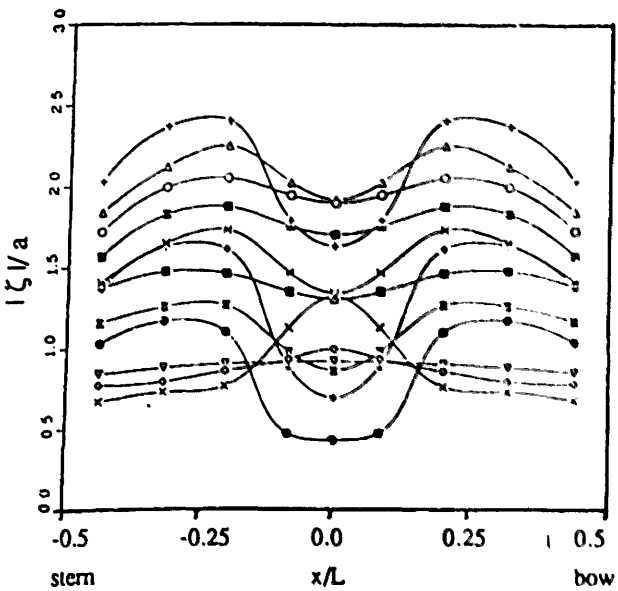

Fig.4.50 Free surface amplitudes plotted along twelve sections parallel to SWATH longitudinal axis (at beam seas)[24]

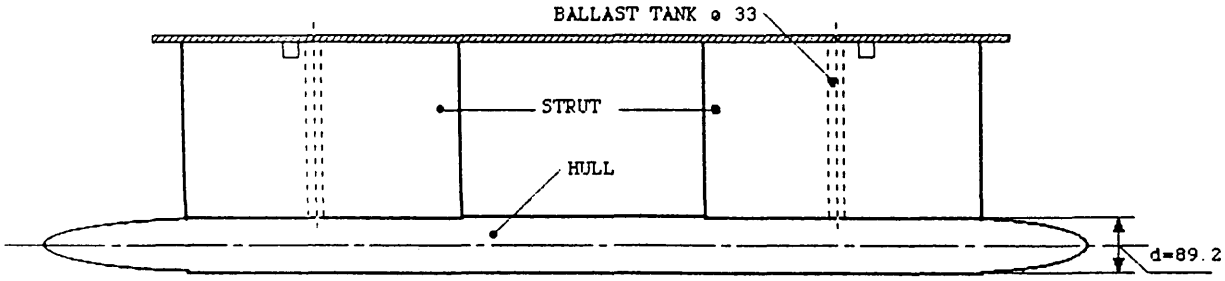

SIDE VIEW

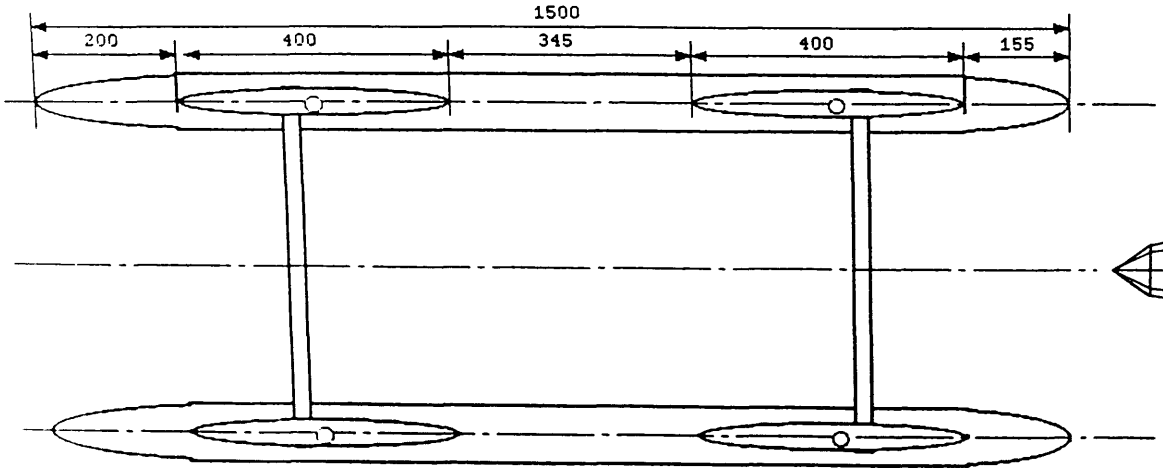

TOP VIEW

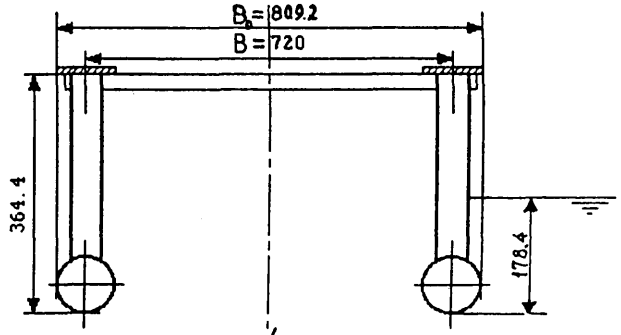

FRONT VIEW

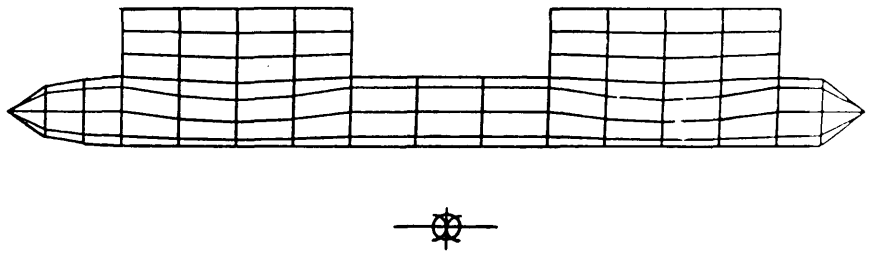

Fig. 4.51 General arrangement of SWATH 1 (the hull form represented by 352 panel elements)

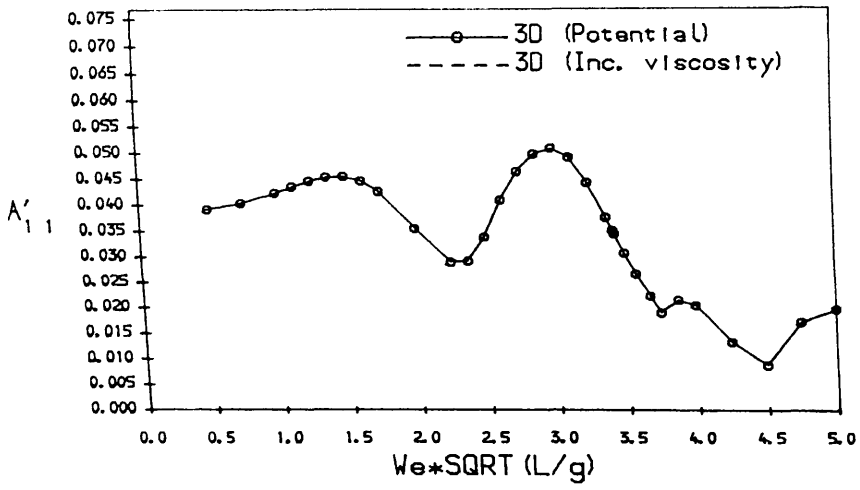

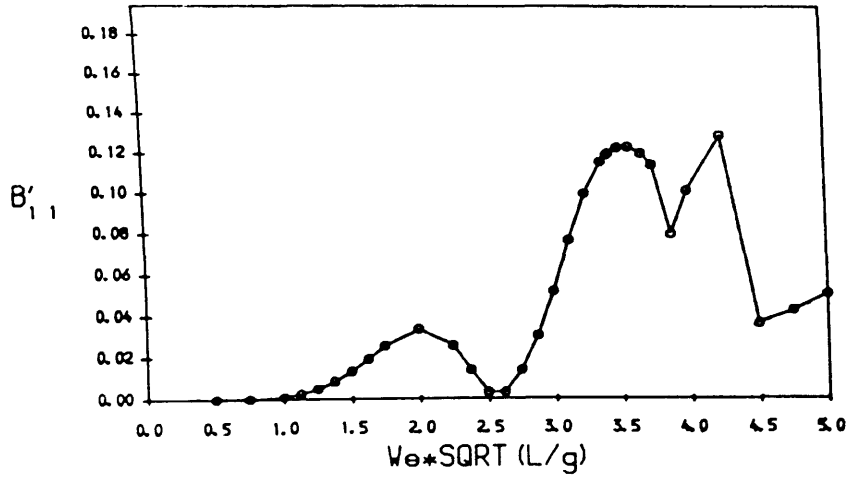

MODE: SURGE, Fn= 0.000

Fig. 4.52 Surge added mass and damping coef. of SWATH 1

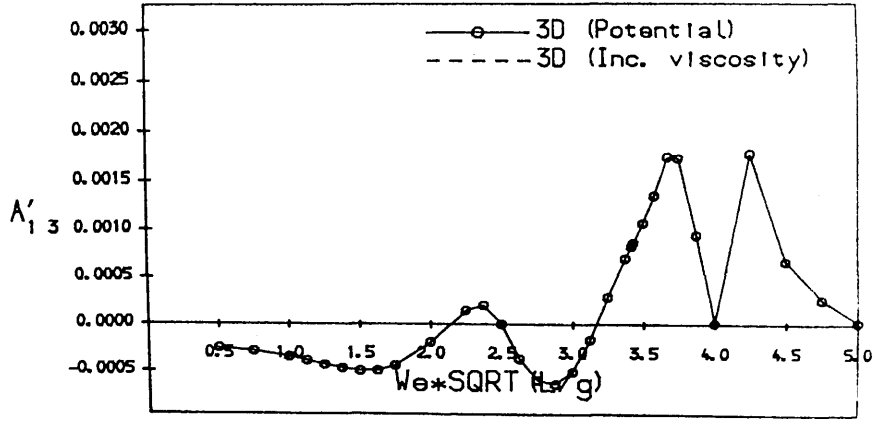

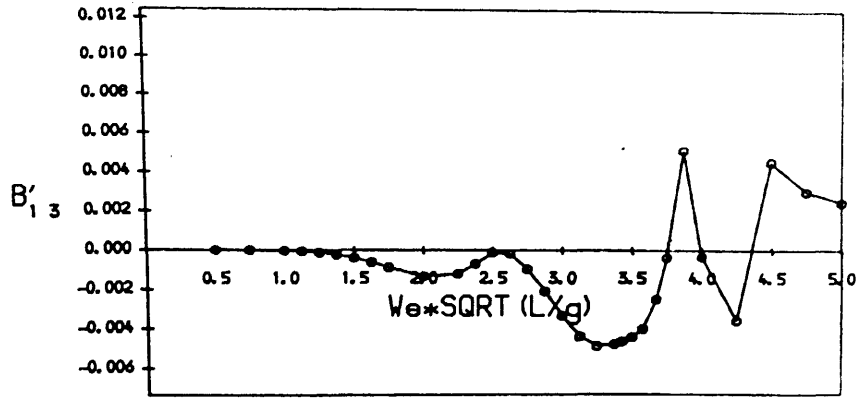

MODE: SURGE-HEAVE, Fn= 0.000

Fig. 4.53 Surge-heave coupling added mass and damping coef. of SWATH 1

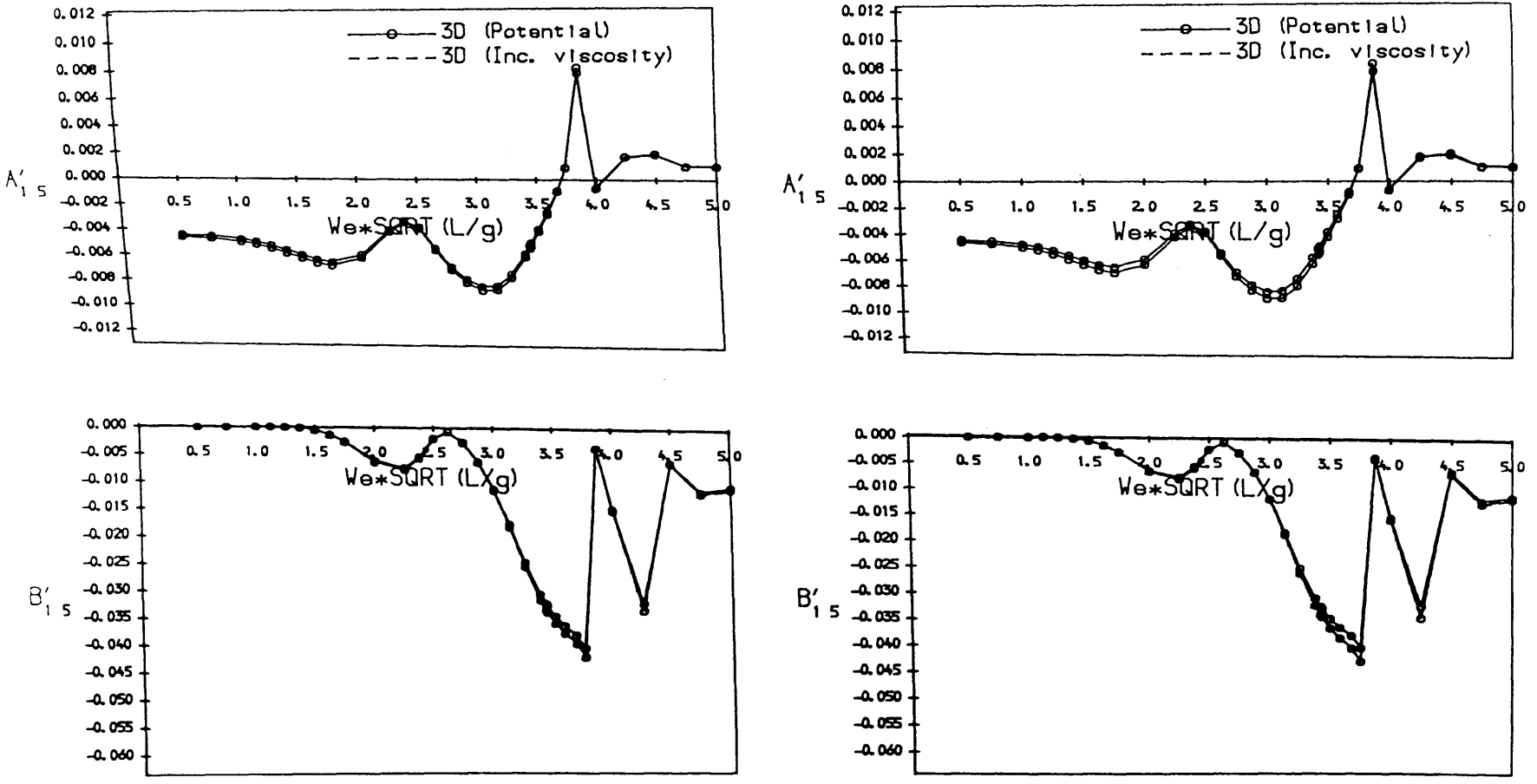

Fig. 4.54 Surge-pitch coupling added mass and damping coefficients of SWATH 1 at F_n=0.0 and F_n=0.261

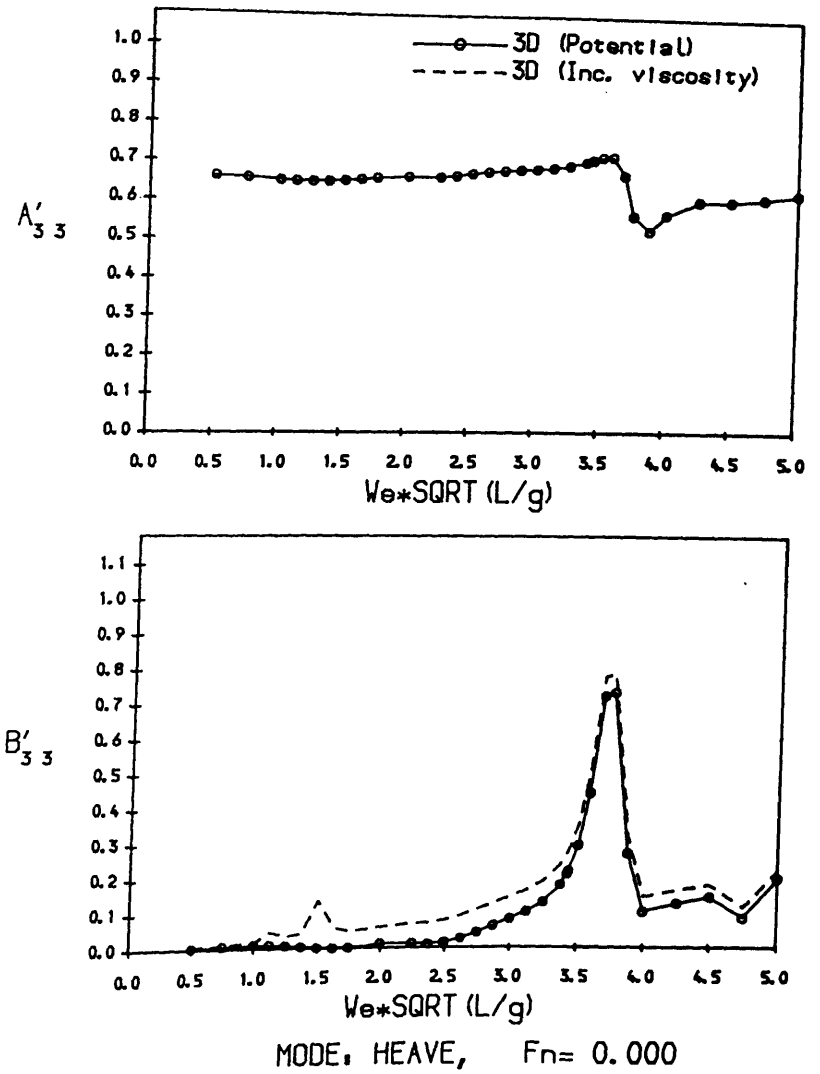

Fig. 4.55 Heave added mass and damping coefficients of SWATH 1

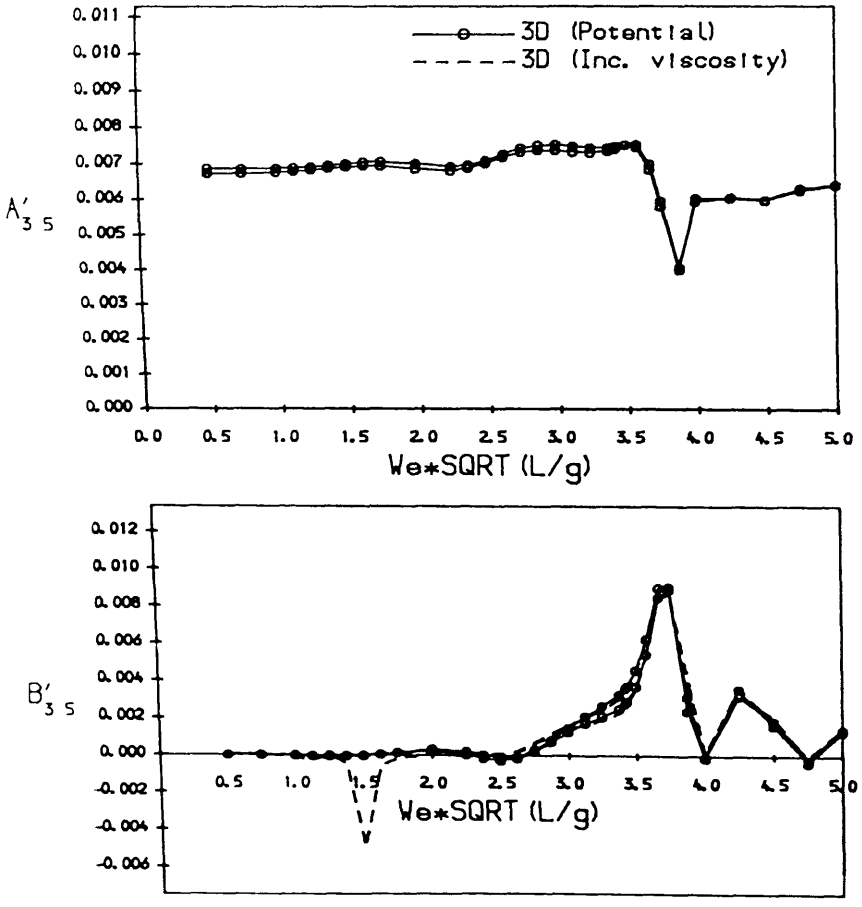

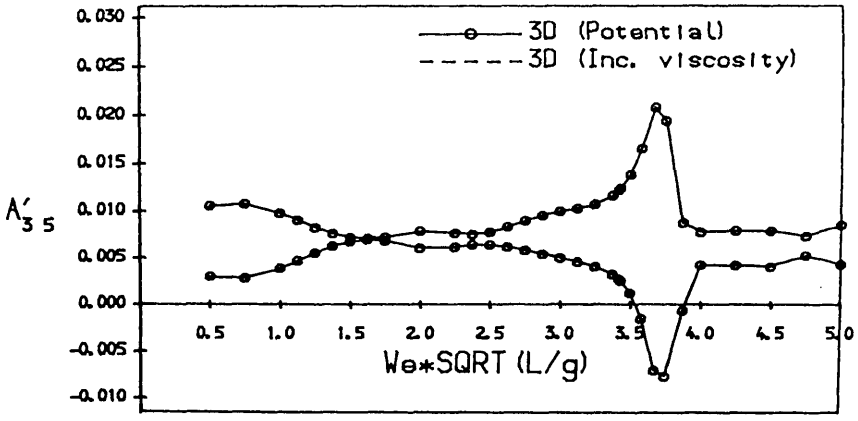

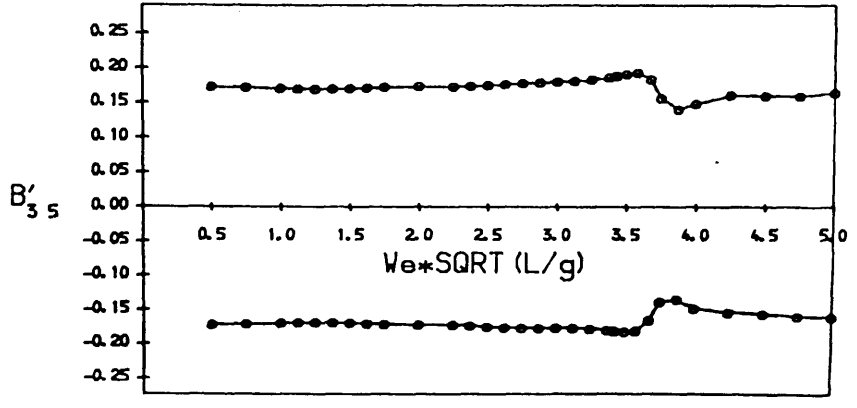

MODE: HEAVE-PITCH, Fn= 0.000

MODE: HEAVE-PITCH, Fn= 0.261

Fig. 4.56 Heave-pitch coupling added mass and damping coefficients of SWATH 1 at F_n=0.0 and F_n=0.261

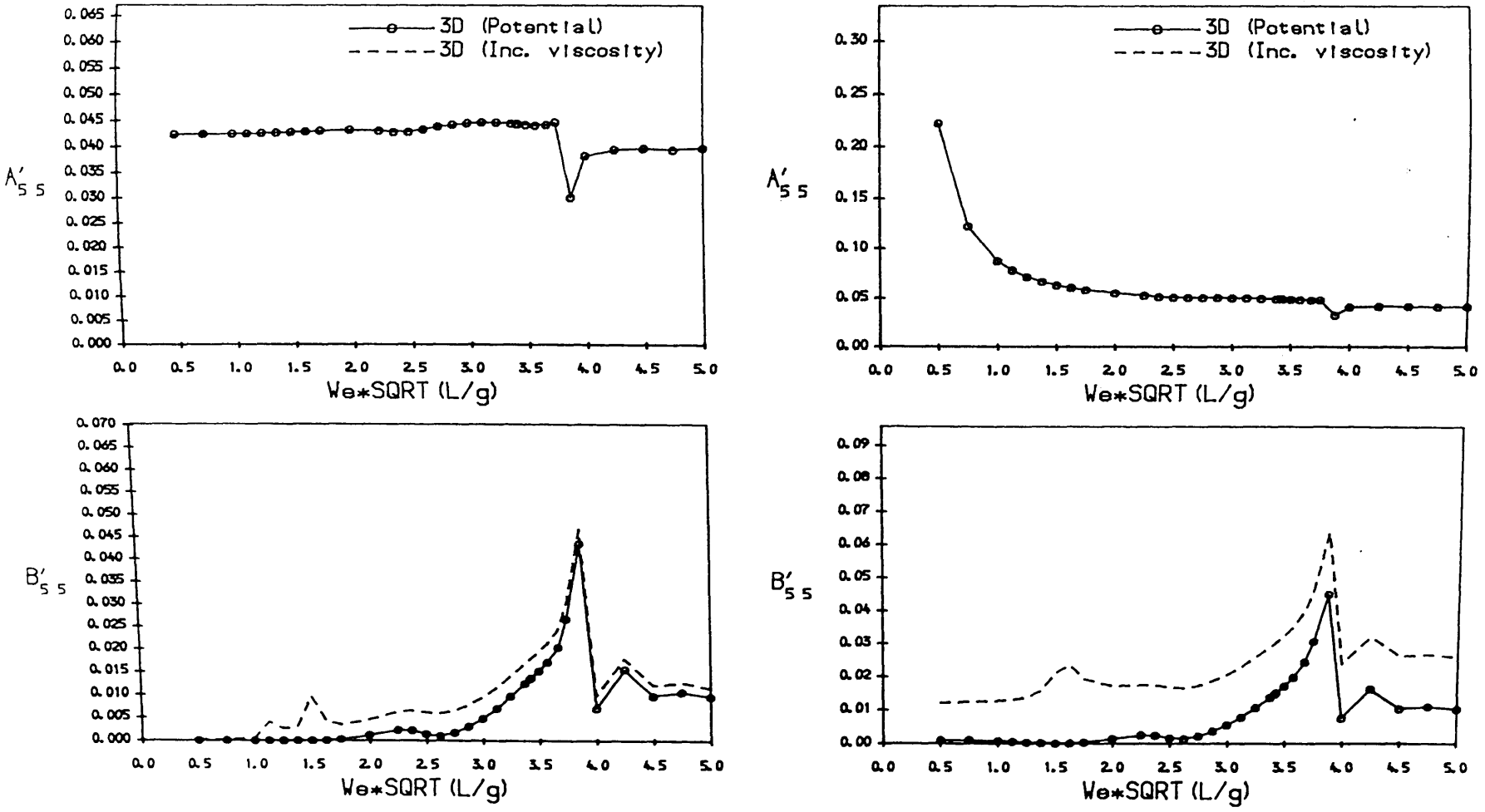

Fig. 4.57 Pitch added inertia and damping coefficients of SWATH 1 at F_n=0.0 and F_n=0.261

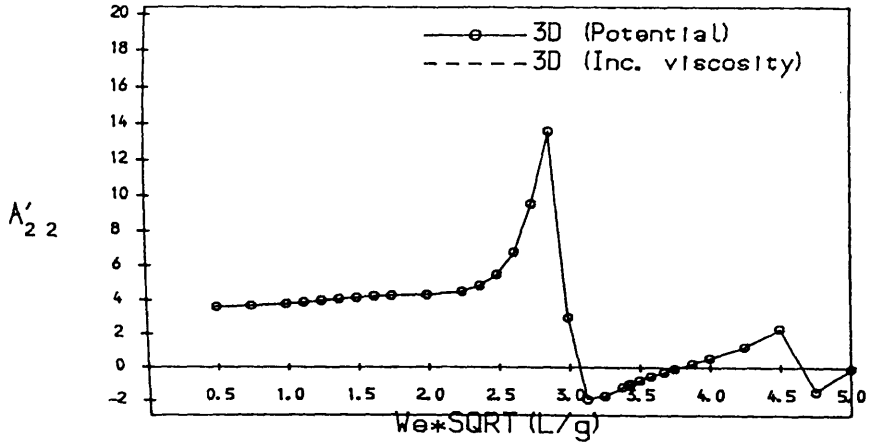

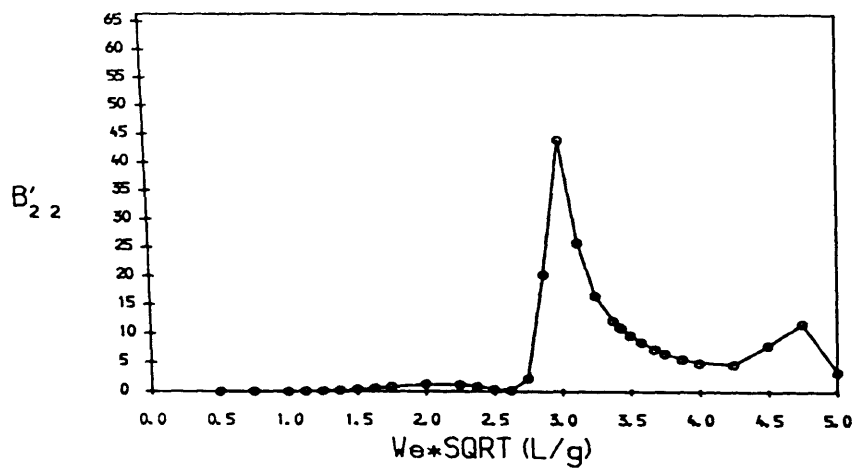

MODE: SWAY, Fn= 0.000

Fig. 4.58 Sway added mass and damping coefficients of SWATH 1

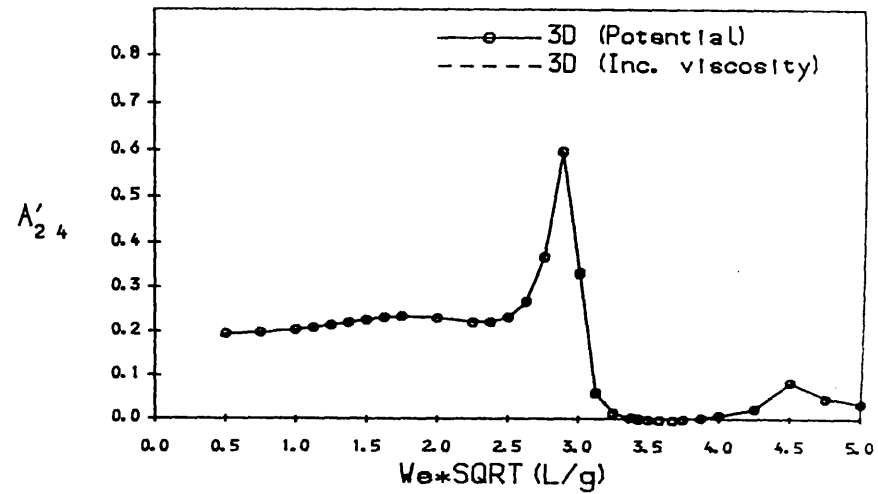

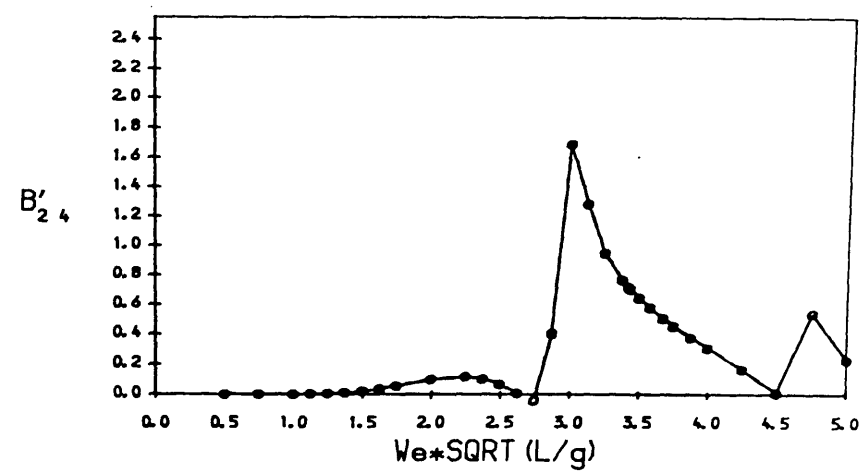

MODE: SWAY-ROLL, Fn= 0.000

Fig. 4.59 Sway-roll coupling added mass and damping coef. of SWATH 1

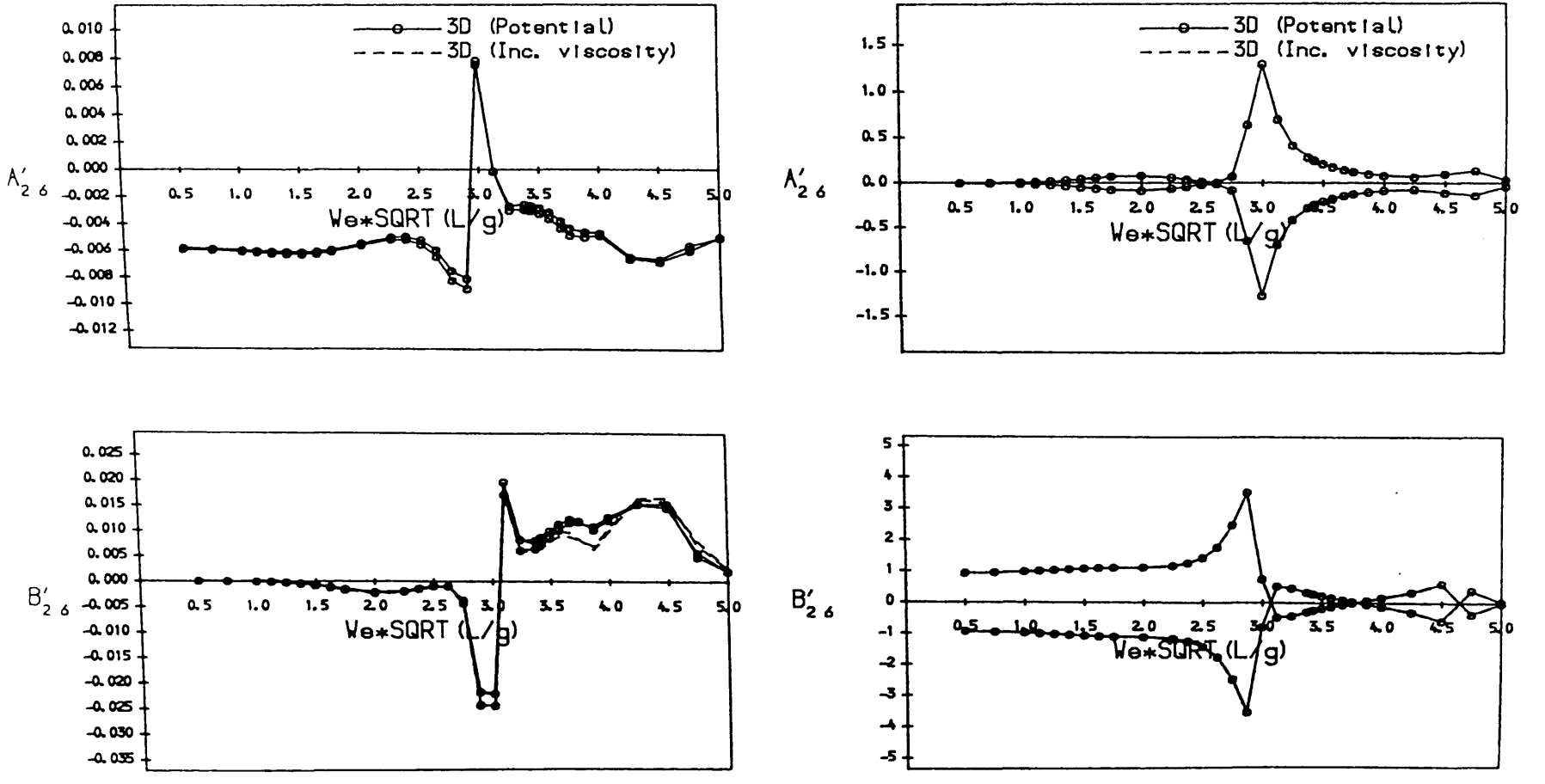

MODE: SWAY-YAW, Fn= 0.000 MODE: SWAY-YAW, Fn= 0.261

Fig. 4.60 Sway-yaw coupling added mass and damping coefficients of SWATH 1 at F_n=0.0 and F_n=0.261

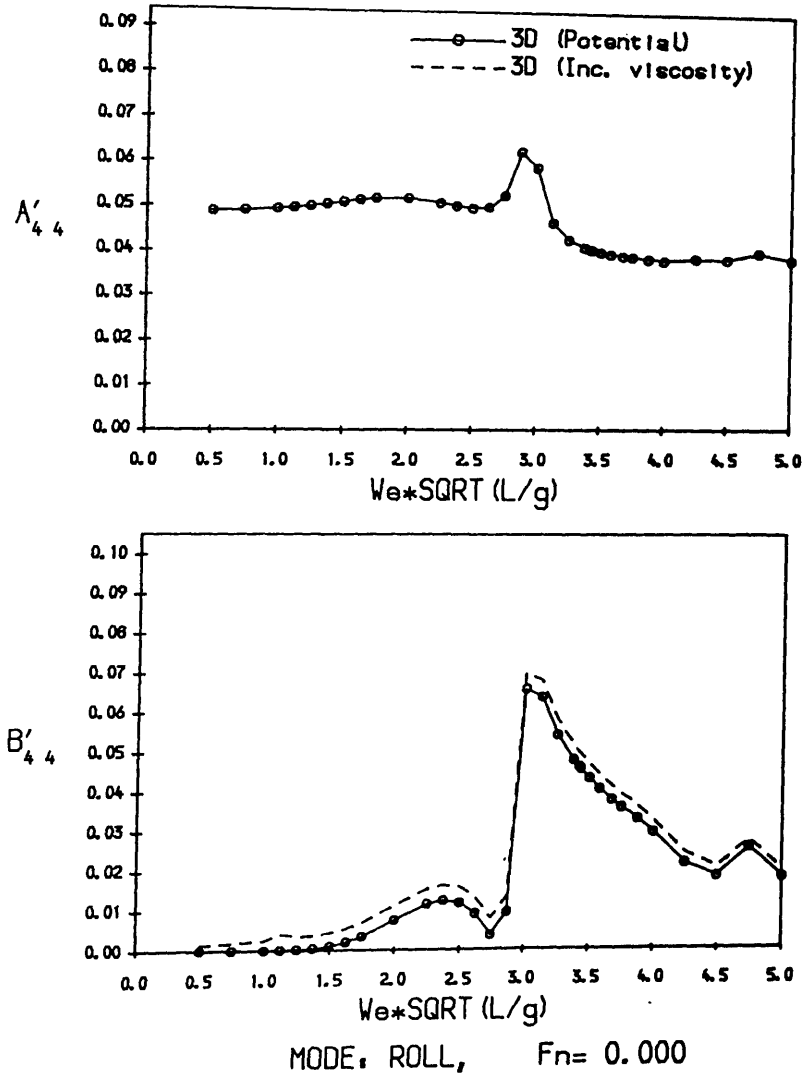

Fig. 4.61 Roll added inertia and damping coefficients of SWATH 1

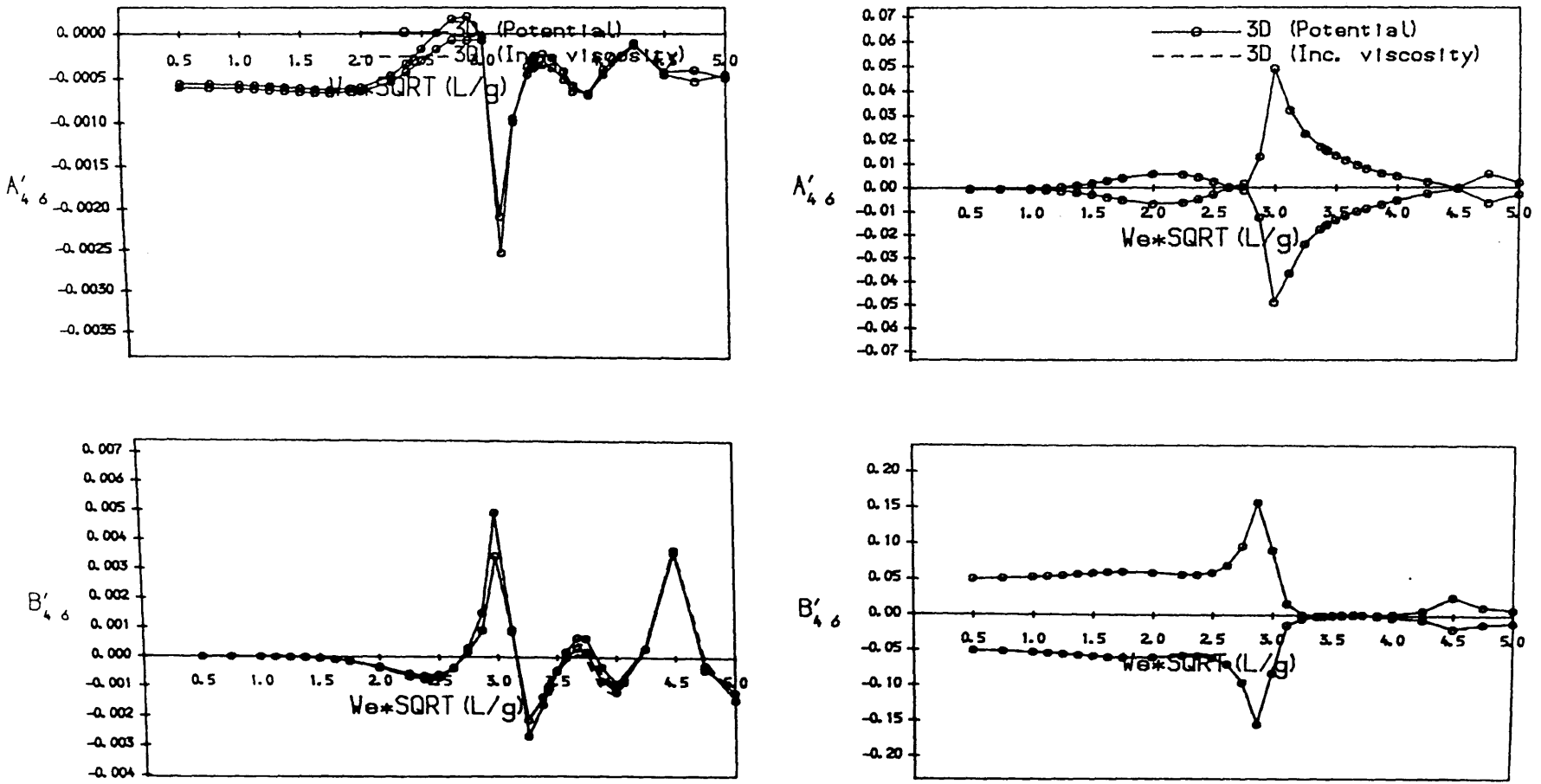

MODE: ROLL-YAW, Fn= 0.000 MODE: ROLL-YAW, Fn= 0.261

Fig. 4.62 Roll-yaw coupling added inertia and damping coefficients of SWATH 1 at F_n=0.0 and F_n=0.261

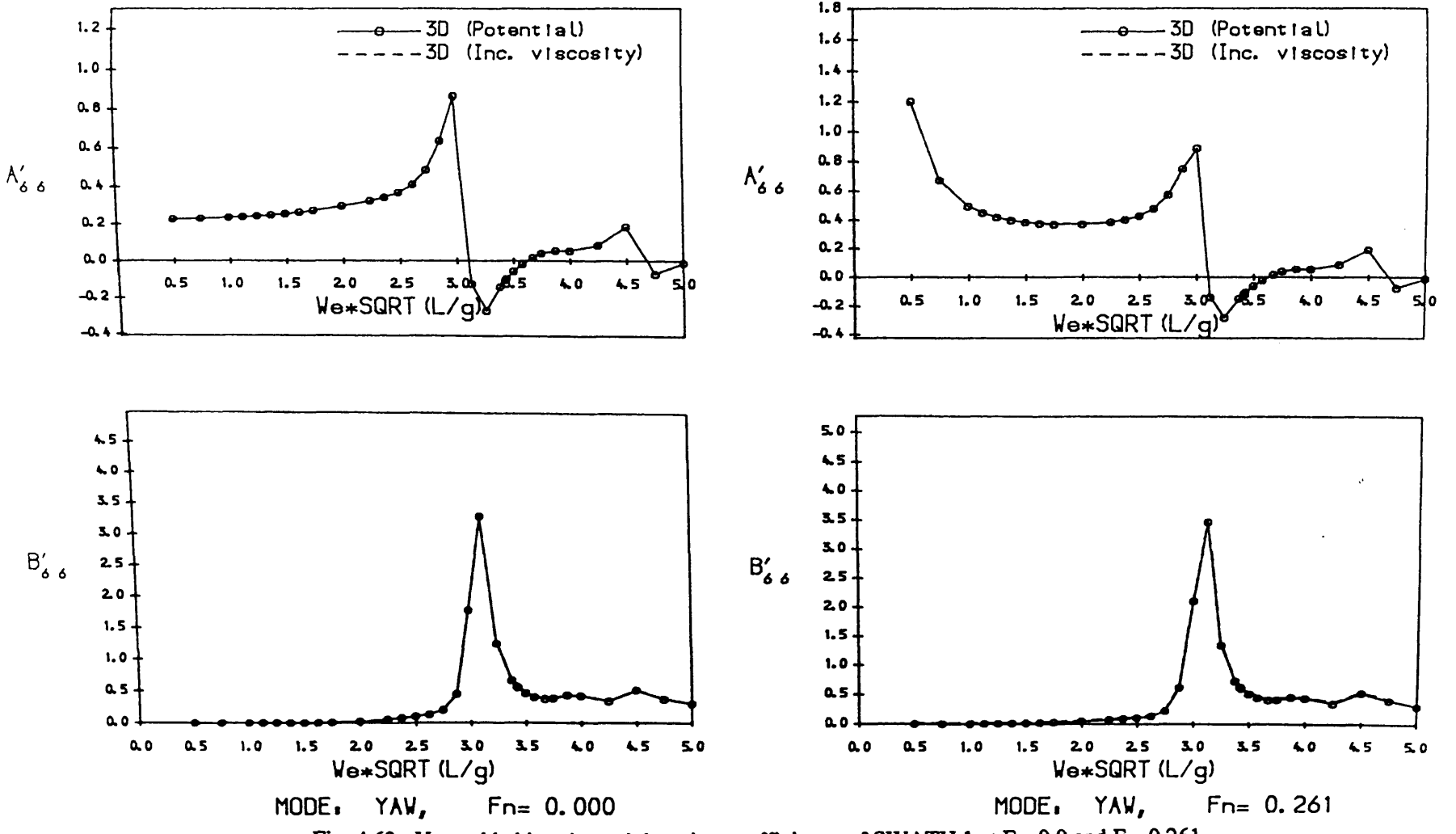

Fig. 4.63 Yaw added inertia and damping coefficients of SWATH 1 at F_n=0.0 and F_n=0.261

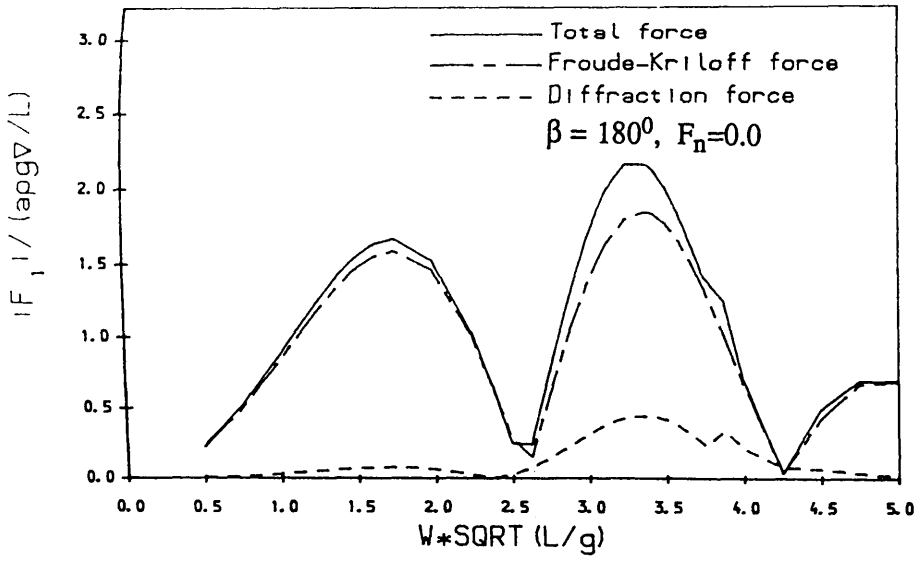

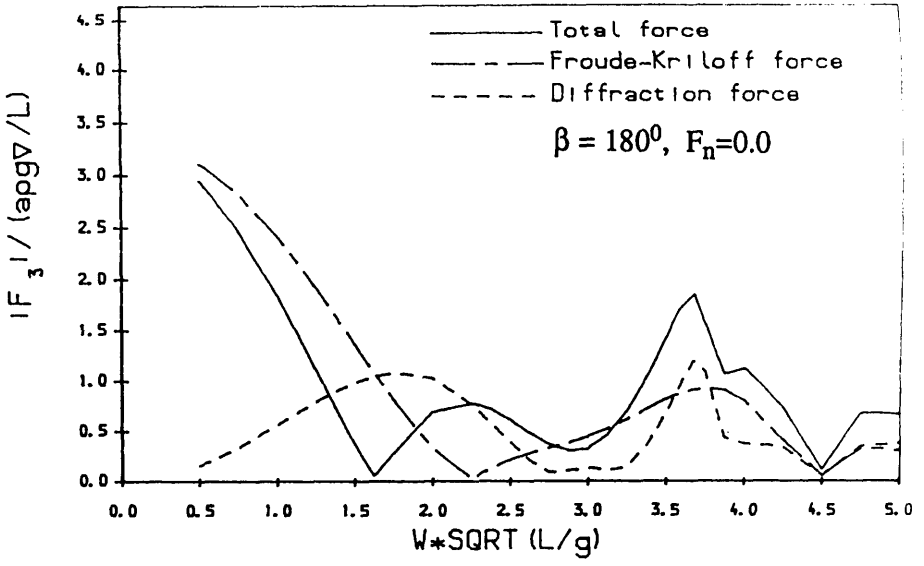

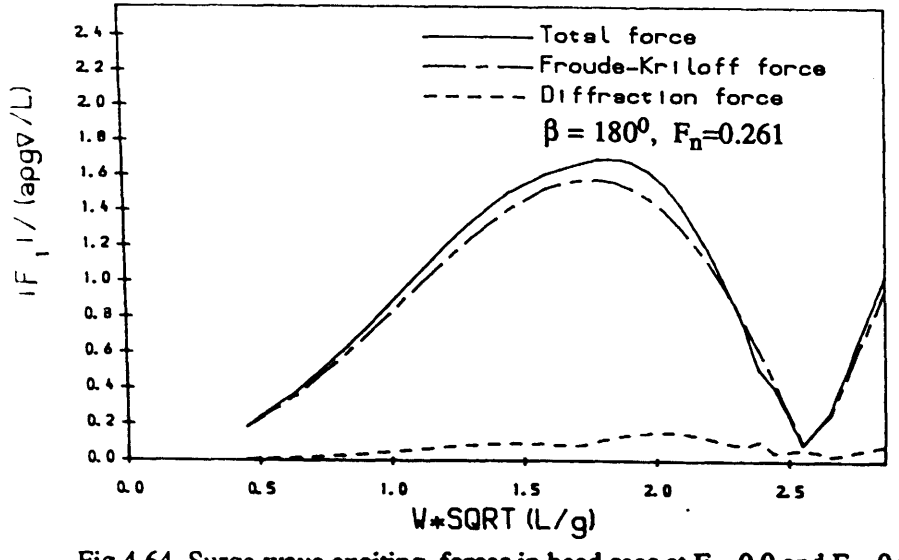

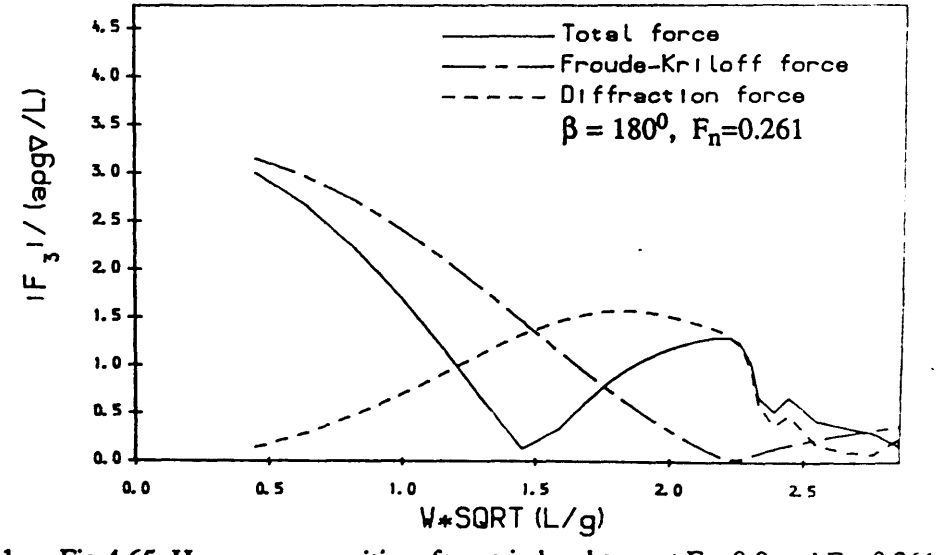

Fig.4.64 Surge wave exciting forces in head seas at F_n=0.0 and F_n=0.261

Fig.4.65 Heave wave exciting forces in head seas at F_n=0.0 and F_n=0.261

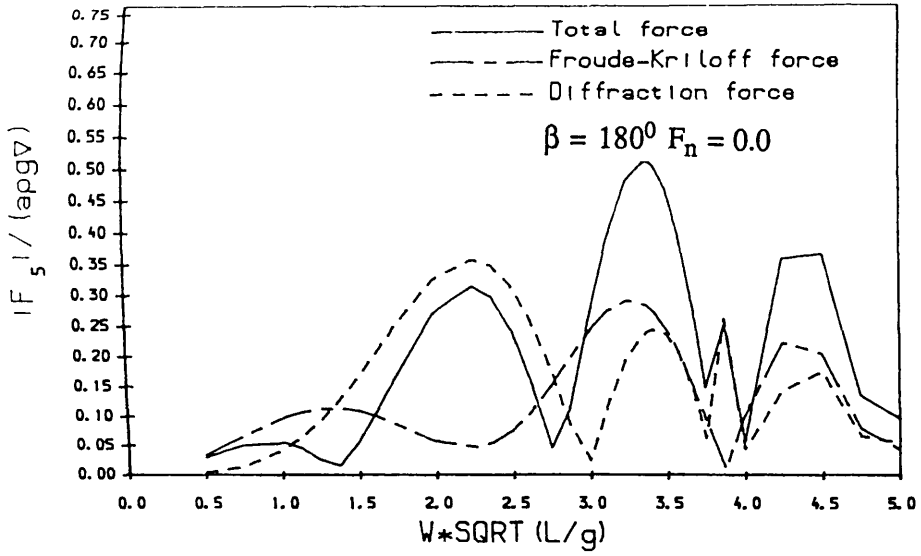

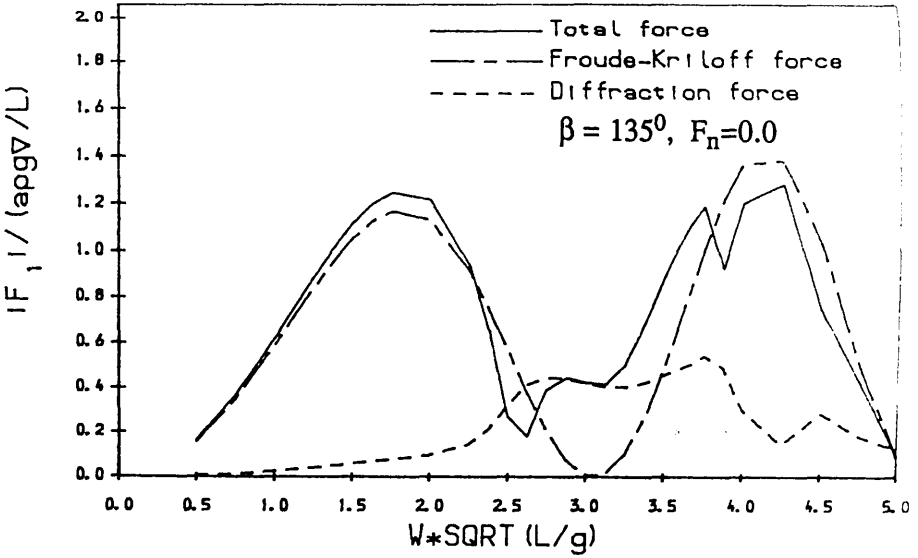

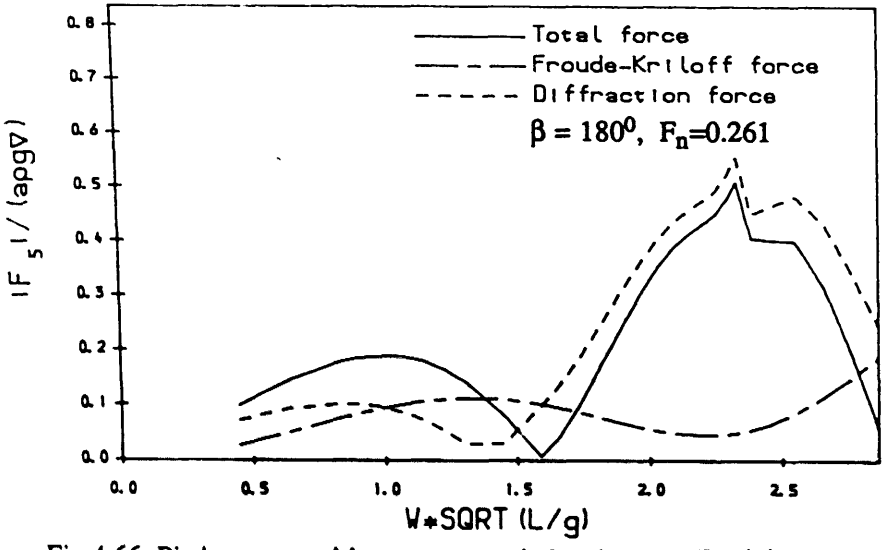

Fig.4.66 Pitch wave exciting moments in head seas at F_n=0.0 and F_n=0.261

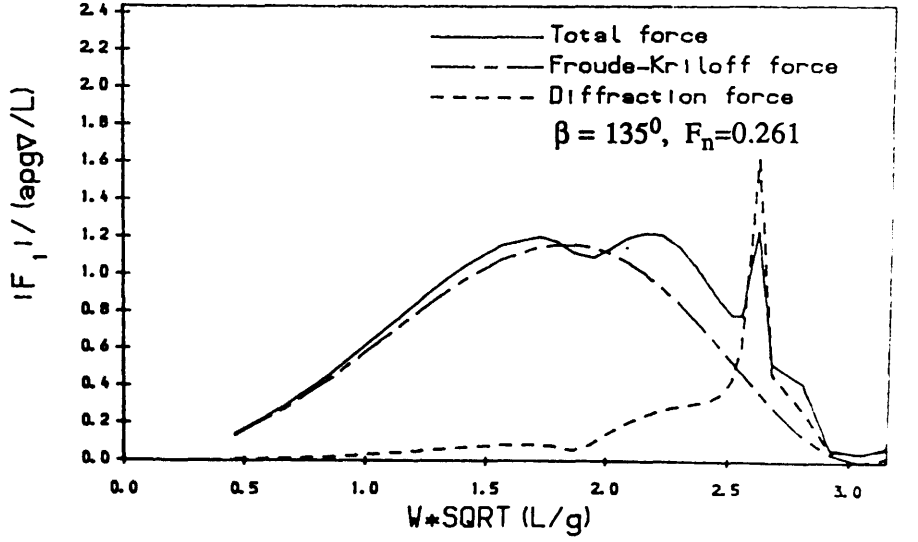

Fig. 4.67 Surge wave exciting forces in bow quartering seas at F_n=0.0 and F_n=0.261

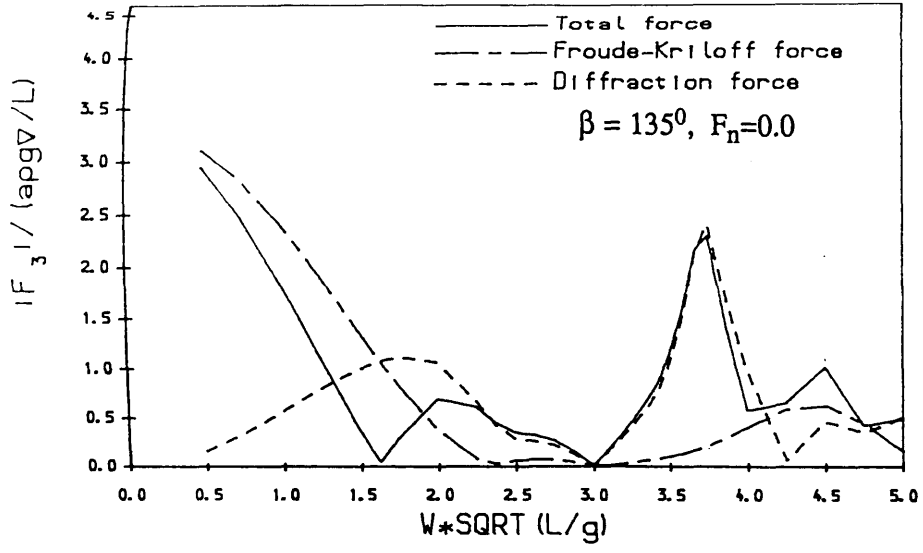

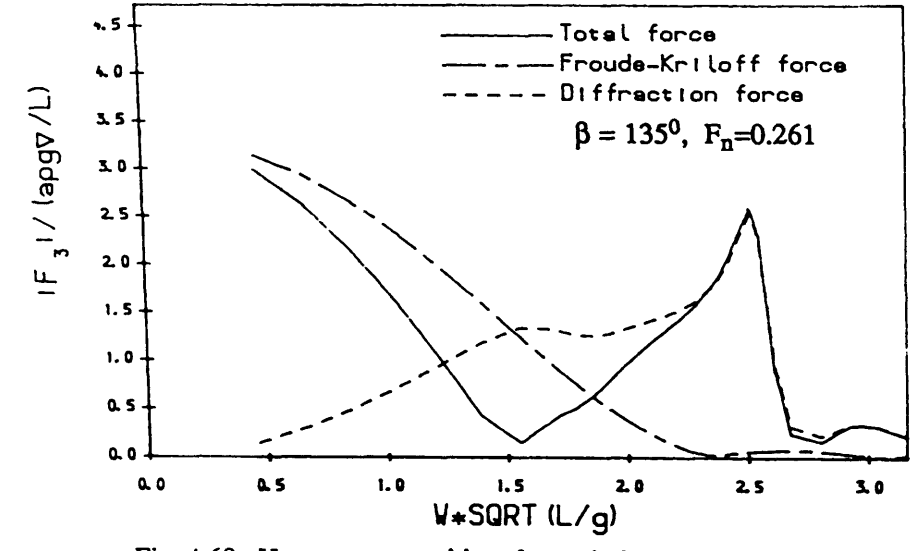

Fig. 4.68 **Heave wave exciting forces in bow quartering seas at F_n=0.0 and F_n=0.261**

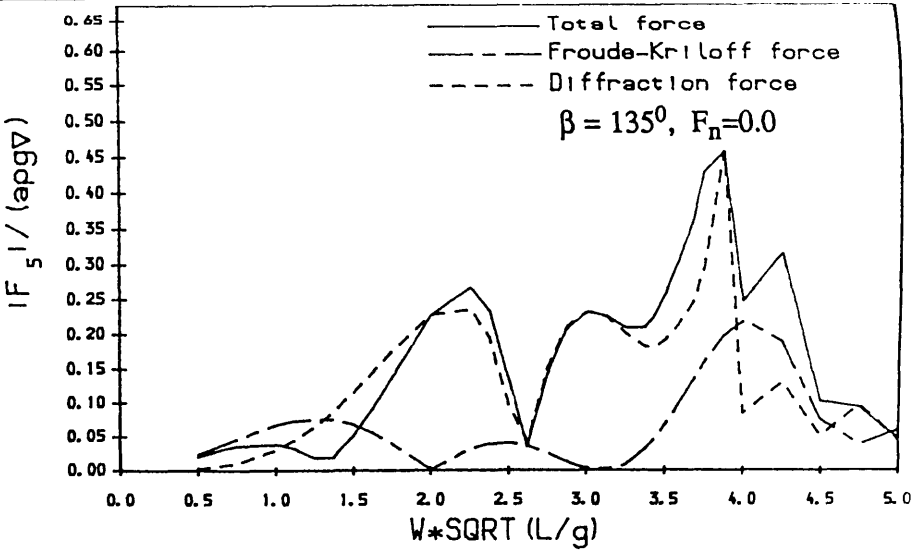

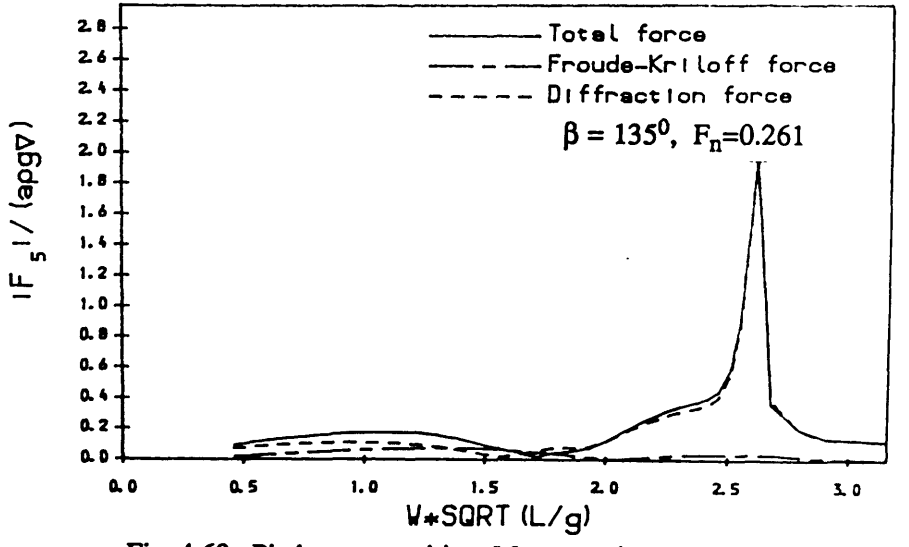

Fig. 4.69 **Pitch wave exciting Moments in bow quartering seas at F_n=0.0 and F_n=0.261**

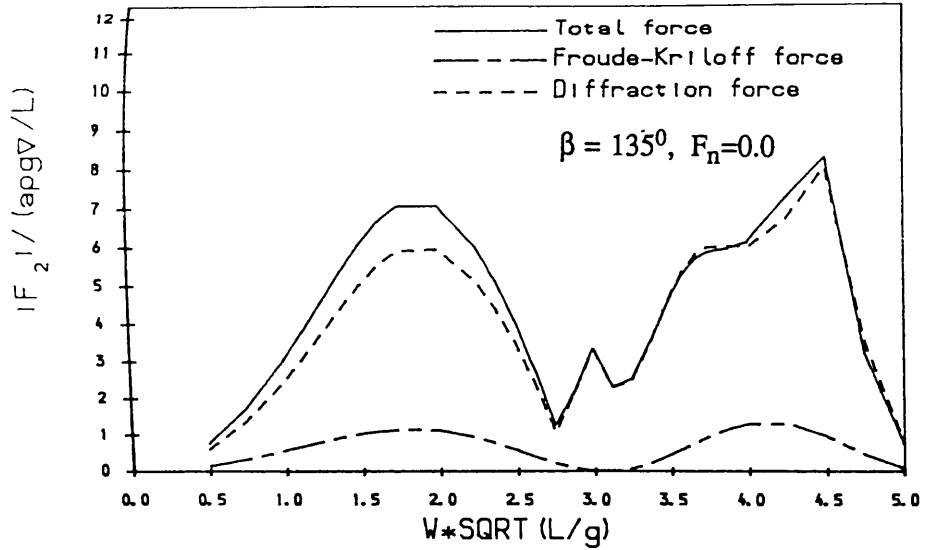

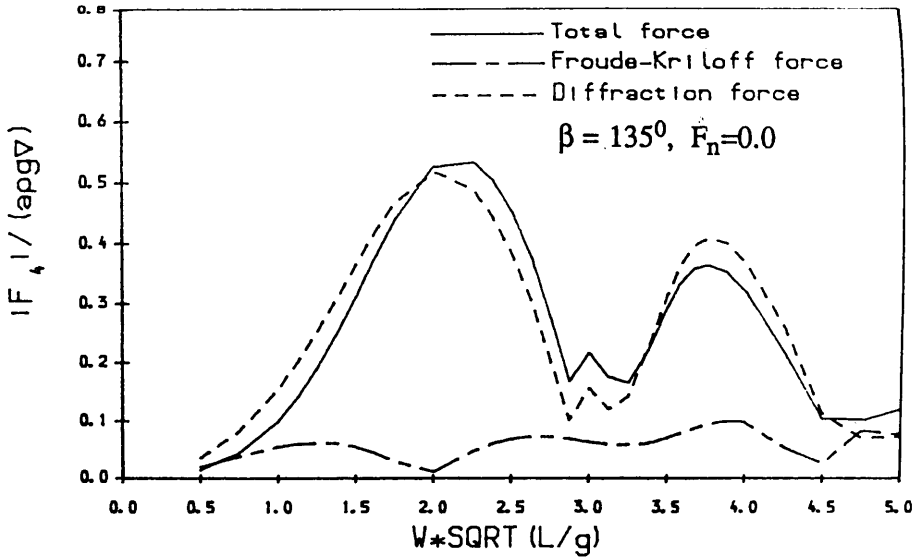

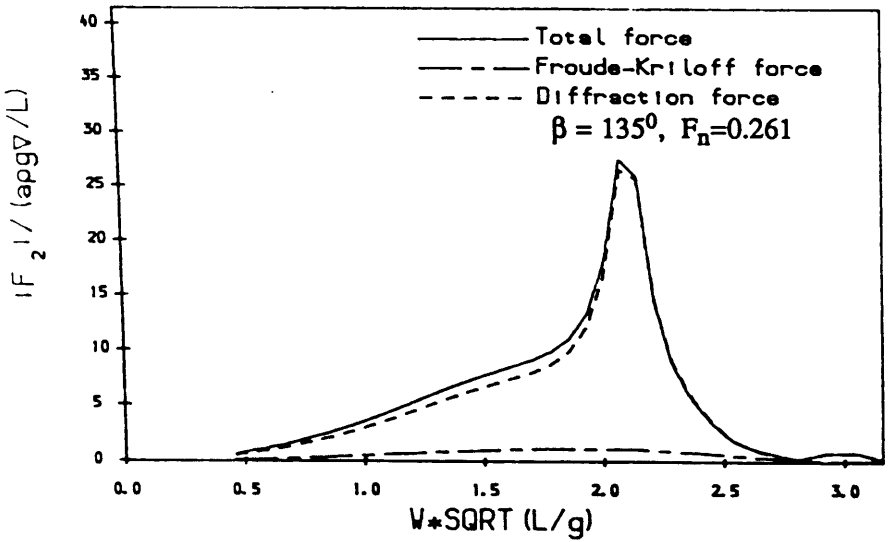

Fig. 4.70 Sway wave exciting forces in bow quartering seas at F_n=0.0 and F_n=0.261

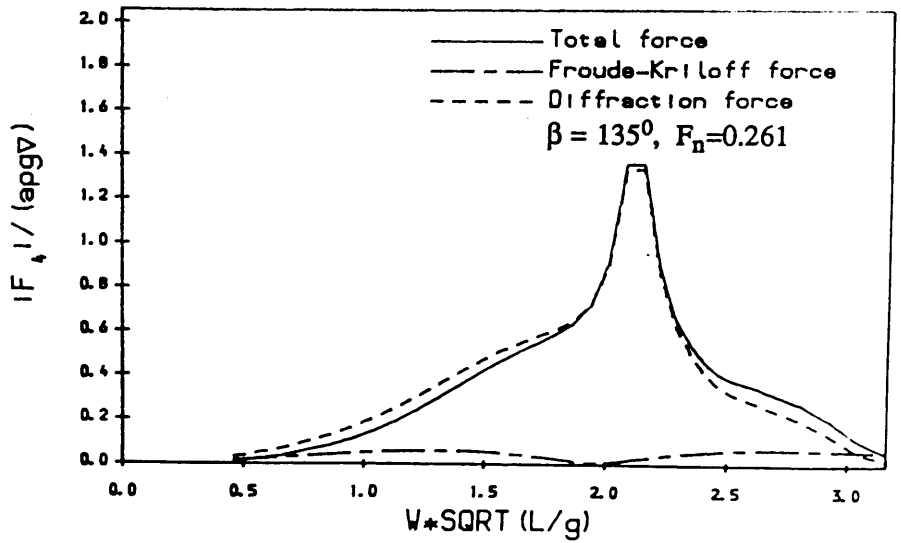

Fig. 4.71 Roll wave exciting moments in bow quartering seas at F_n=0.0 and F_n=0.261

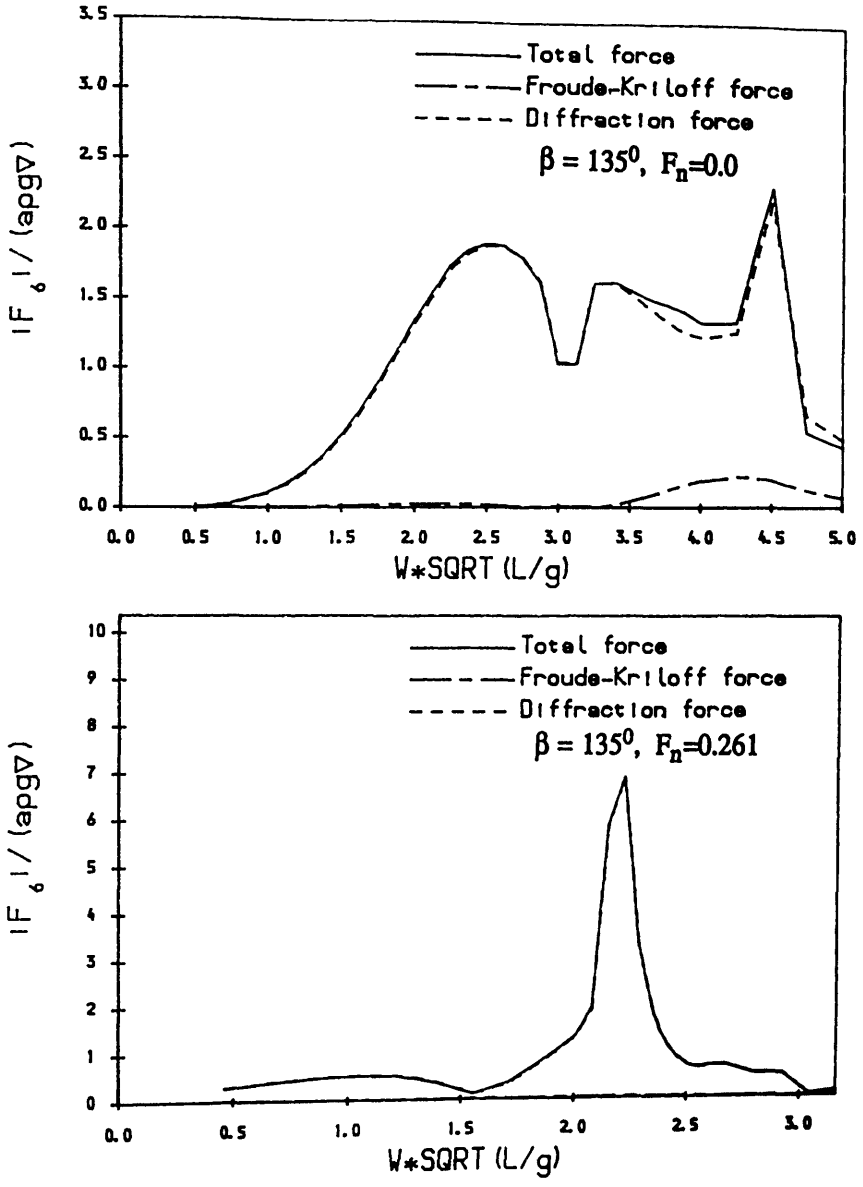

Fig. 4.72 Yaw wave exciting moments in bow quartering seas at F_n=0.0 and F_n=0.261

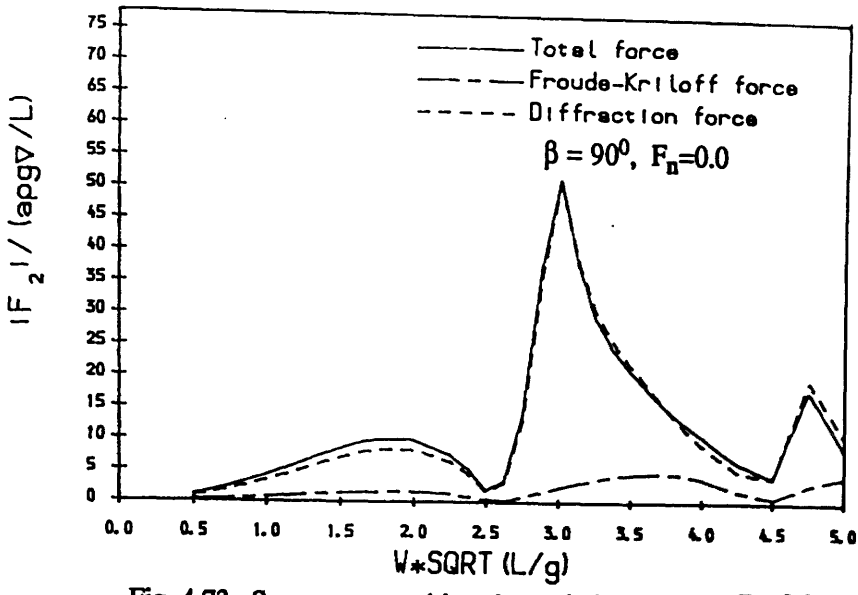

Fig. 4.73 Sway wave exciting forces in beam seas at F_n=0.0

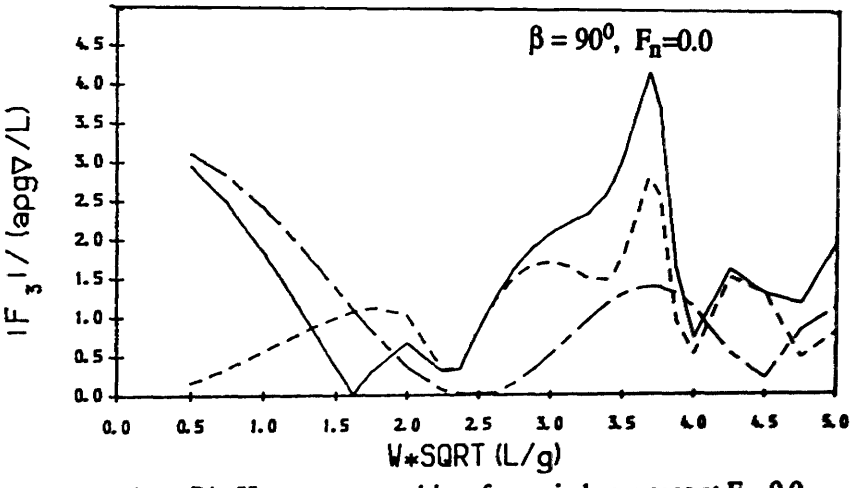

Fig. 4.74 Heave wave exciting forces in beam seas at F_n=0.0

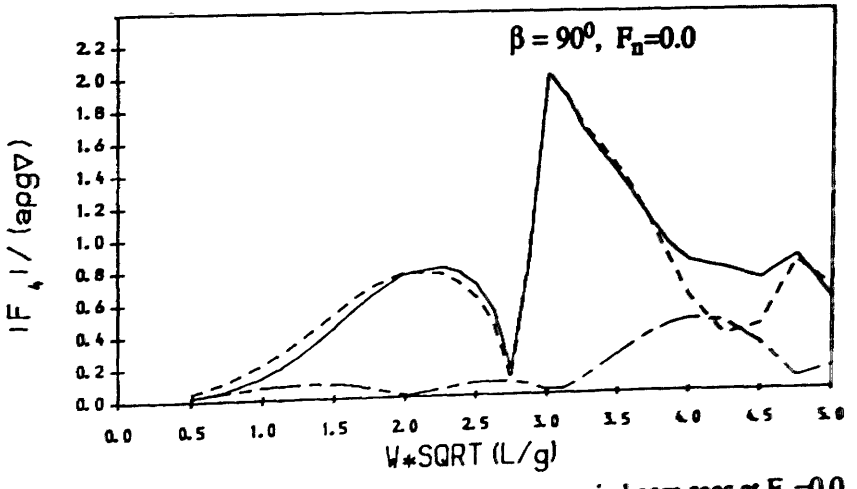

Fig. 4.75 Roll wave exciting moments in beam seas at F_n=0.0

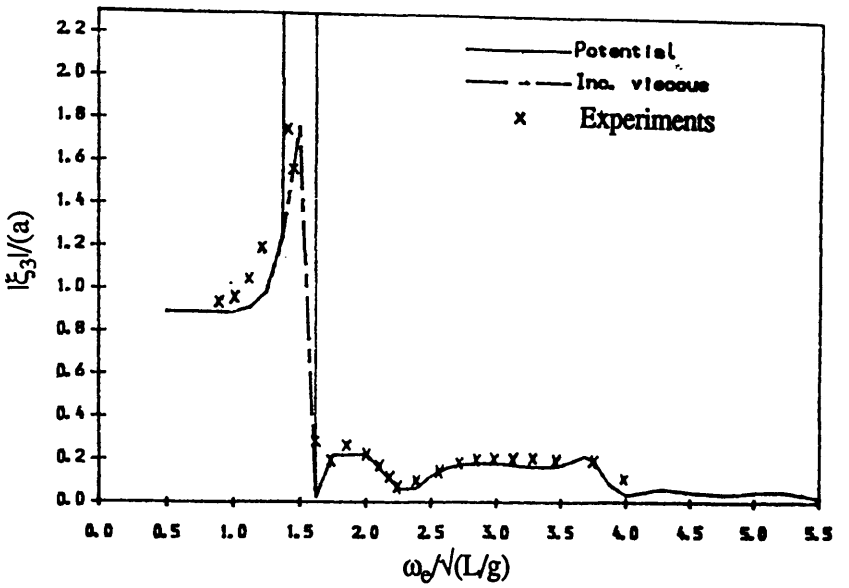

(a) Heave motion responses of SWATH 1 in heave seas

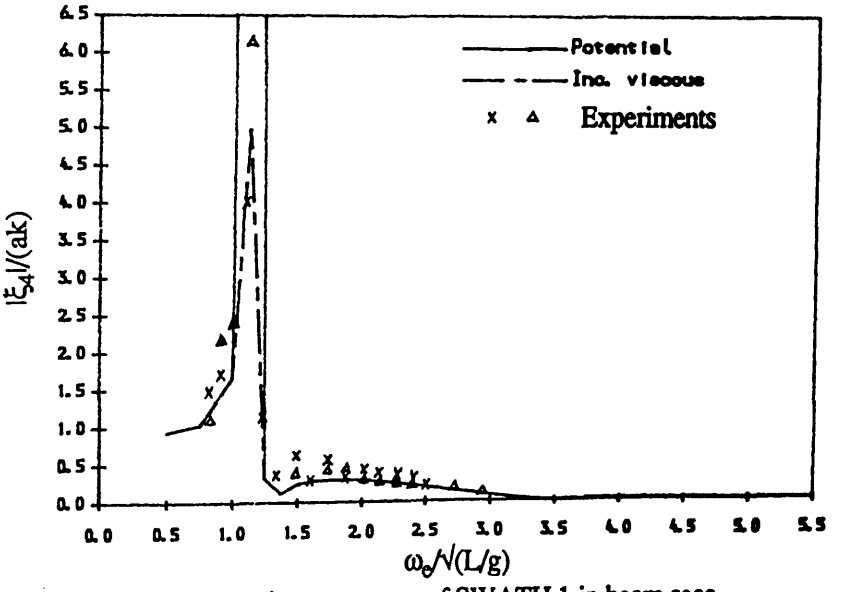

(b) Roll motion responses of SWATH 1 in beam seas

Fig. 4.76 Viscous effect on the motion responses of SWATH 1

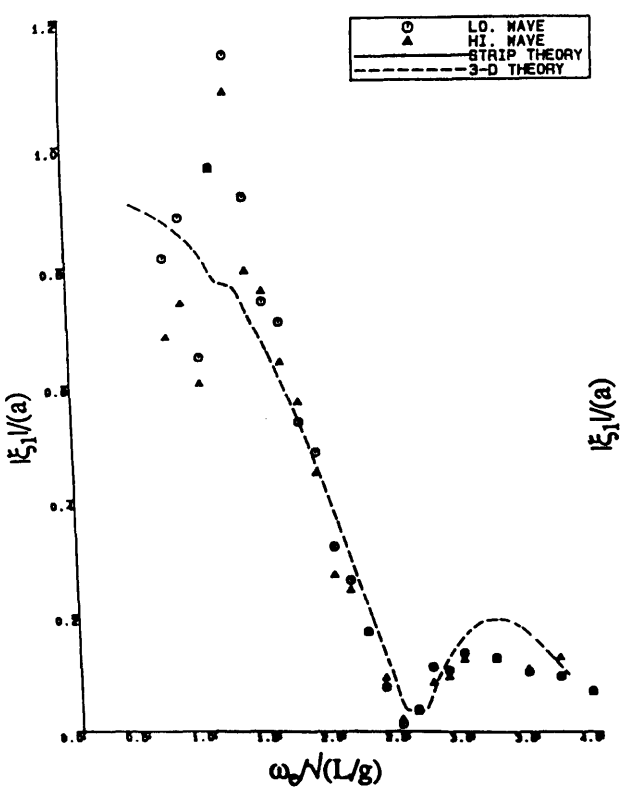

SURGE RESPONSES
SWATH1 MODEL IN REGULAR HEAD SEAS

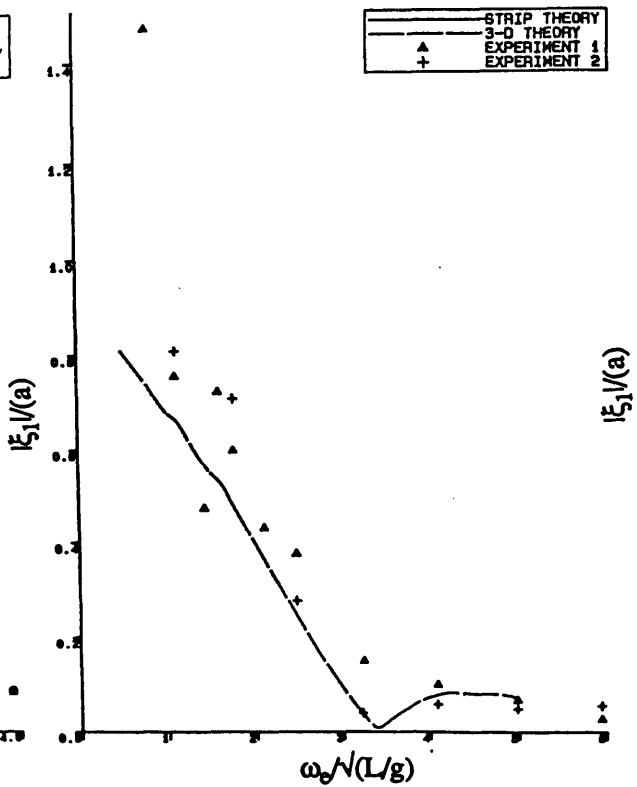

SWATH1 MODEL SURGE RESPONSES
IN REGULAR HEAD SEAS (Fn=0.13)

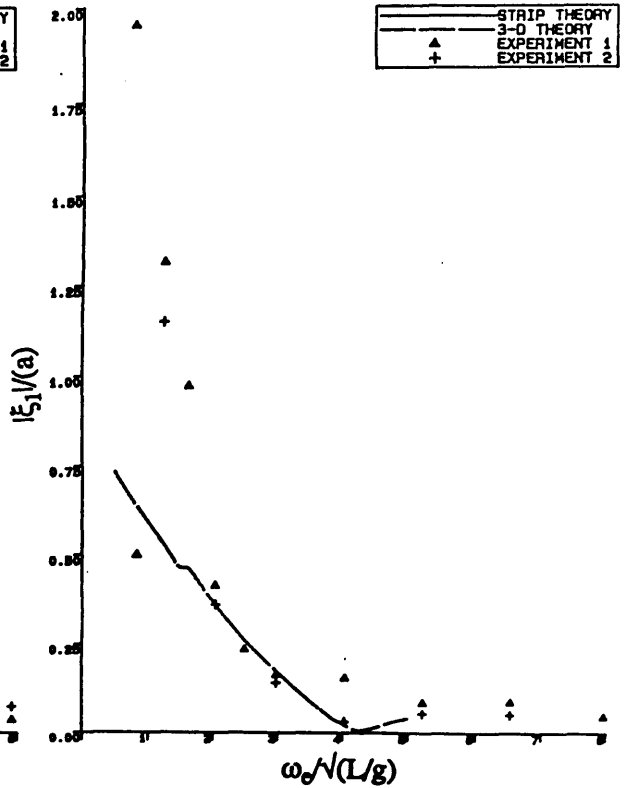

SWATH1 MODEL SURGE RESPONSES
IN REGULAR HEAD SEAS (Fn=0.26)

Fig. 4.77 Surge motion responses of SWATH 1 in head sea at F_n=0.0, F_n=0.13 and F_n=0.261

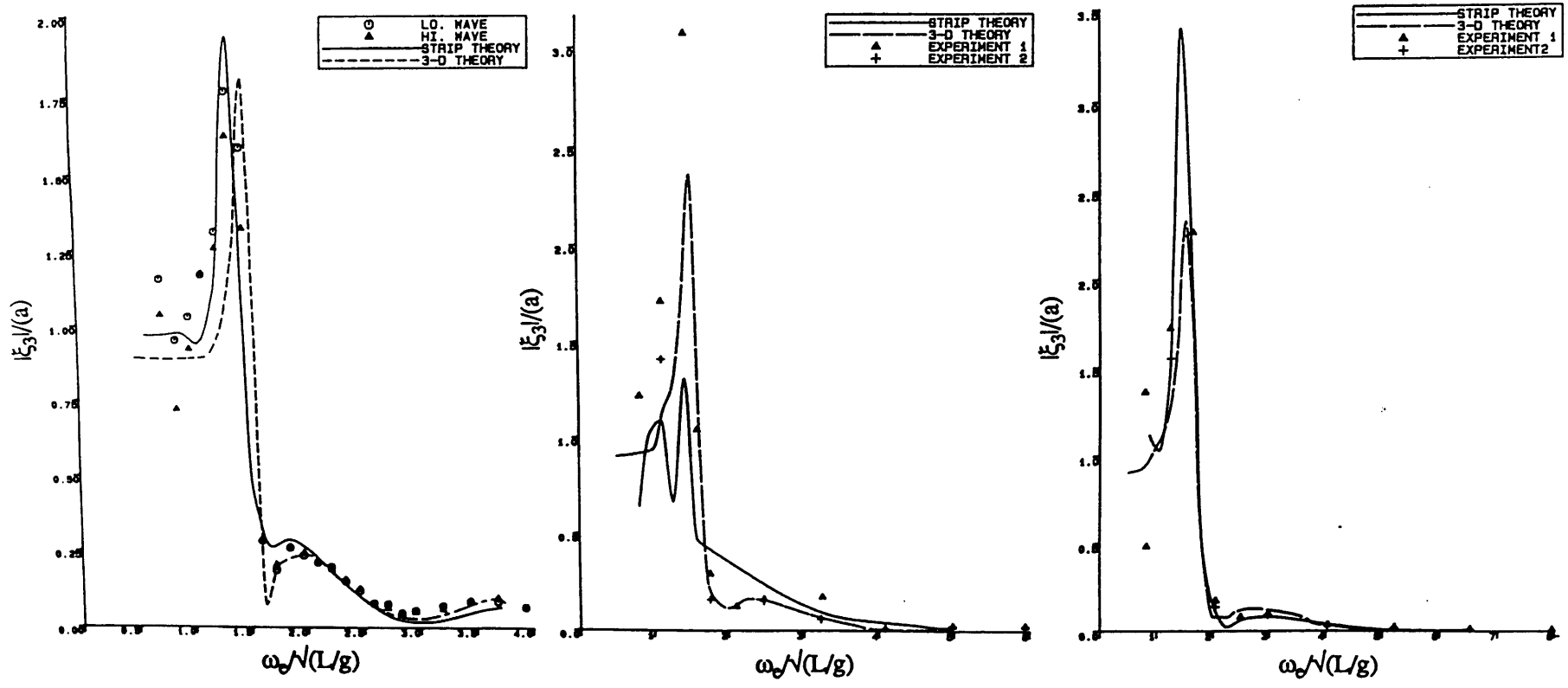

Fig. 4.78 Heave motion responses of SWATH 1 in head sea at F_n=0.0, F_n=0.13 and F_n=0.261

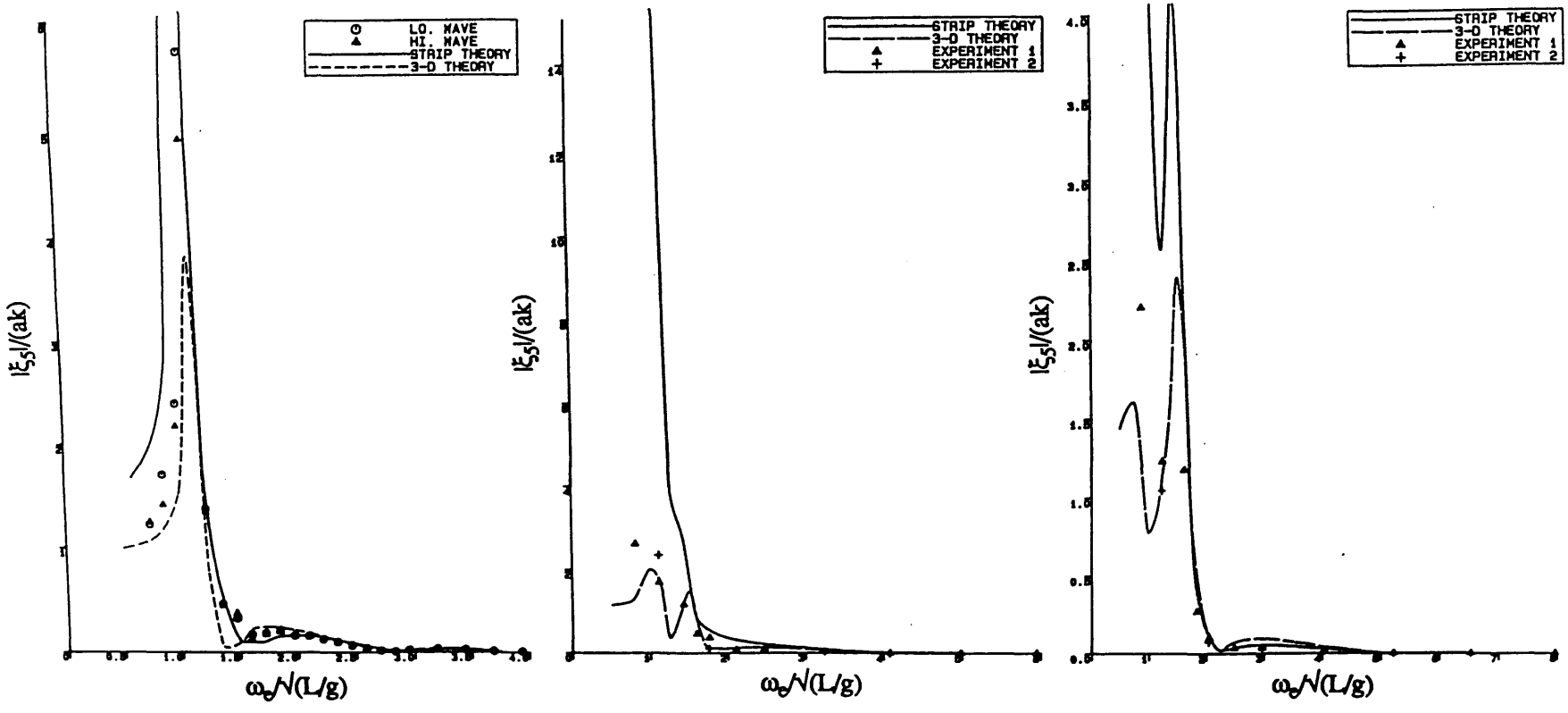

Fig. 4.79 Pitch motion responses of SWATH 1 in head sea at F_n=0.0, F_n=0.13 and F_n=0.261

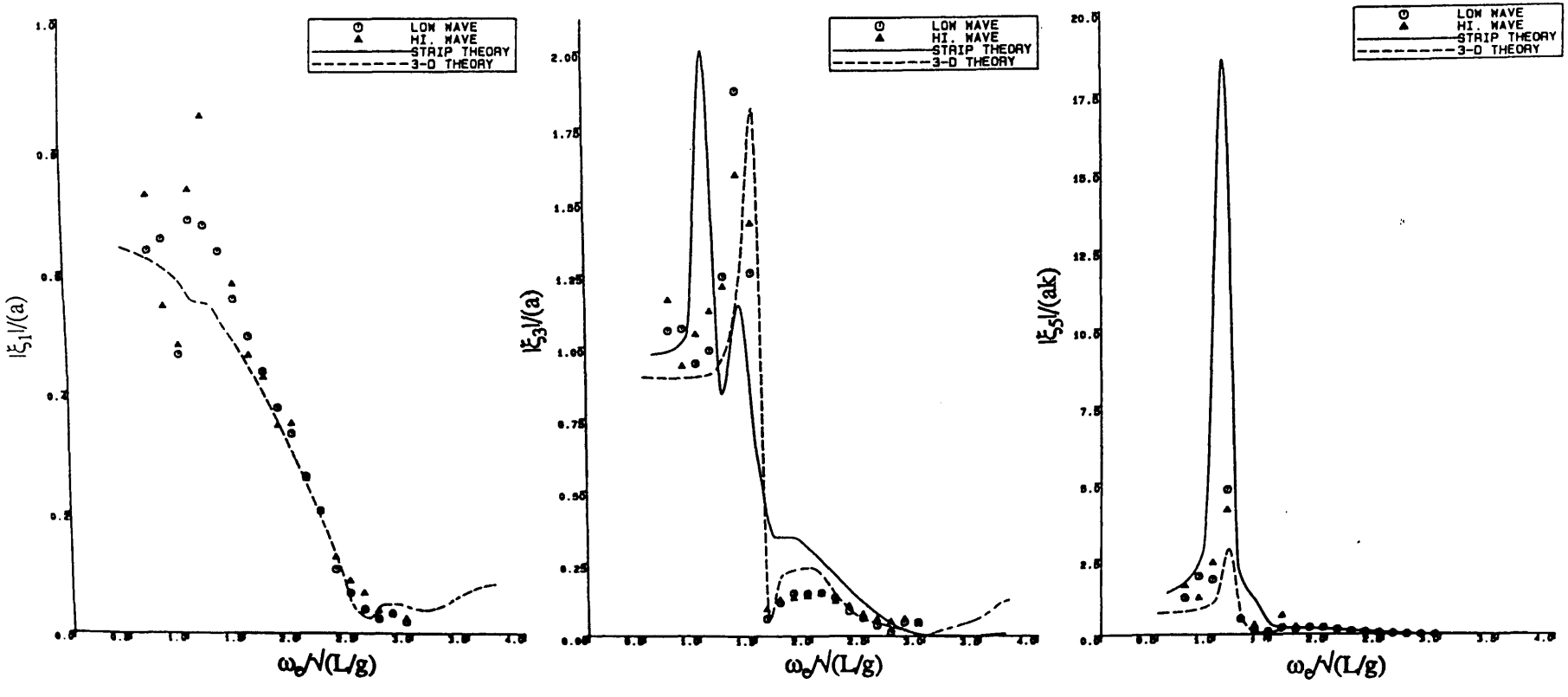

Fig. 4.80 Surge, heave and Pitch motion responses of SWATH 1 in bow quartering sea at F_n=0.0

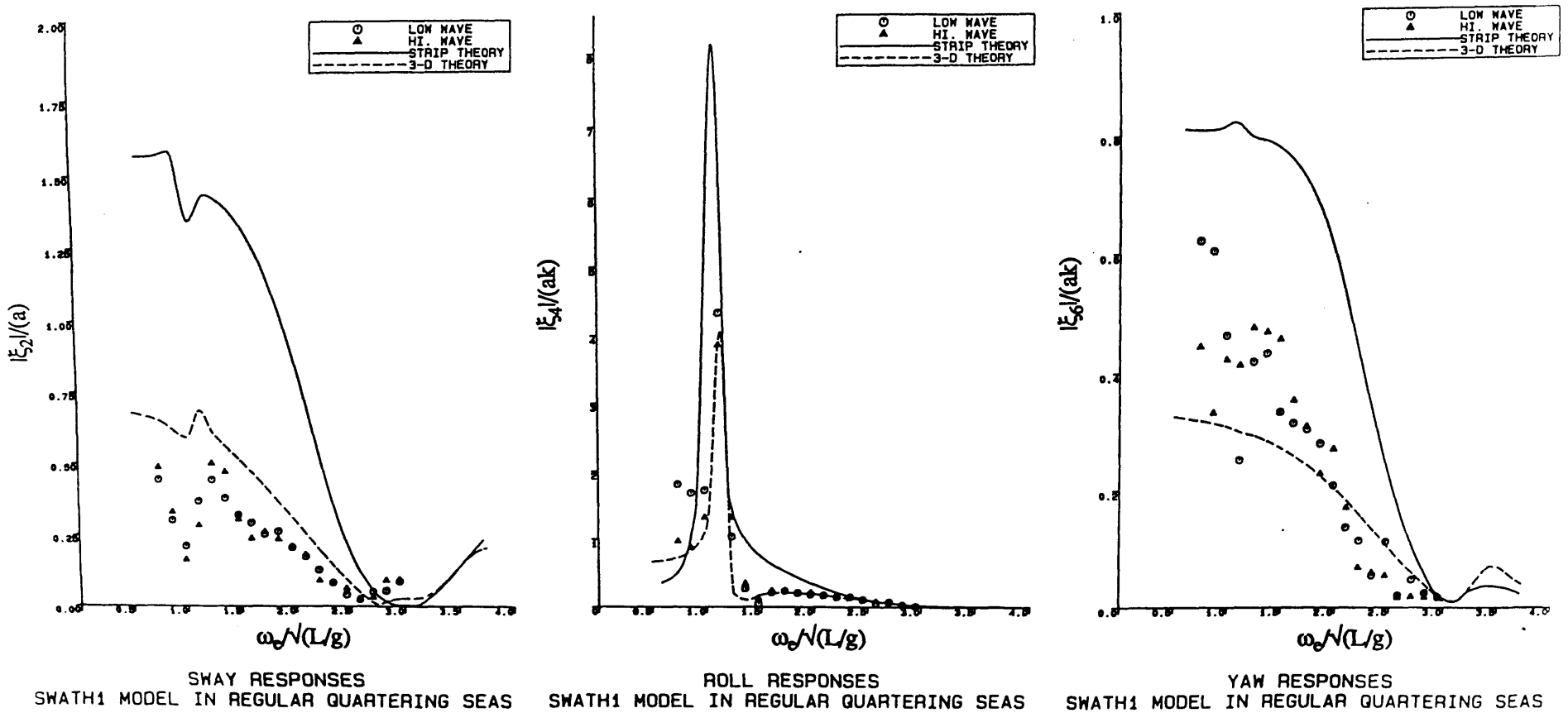

Fig. 4.81 Sway, roll and yaw motion responses of SWATH 1 in bow quartering sea at F_n=0.0

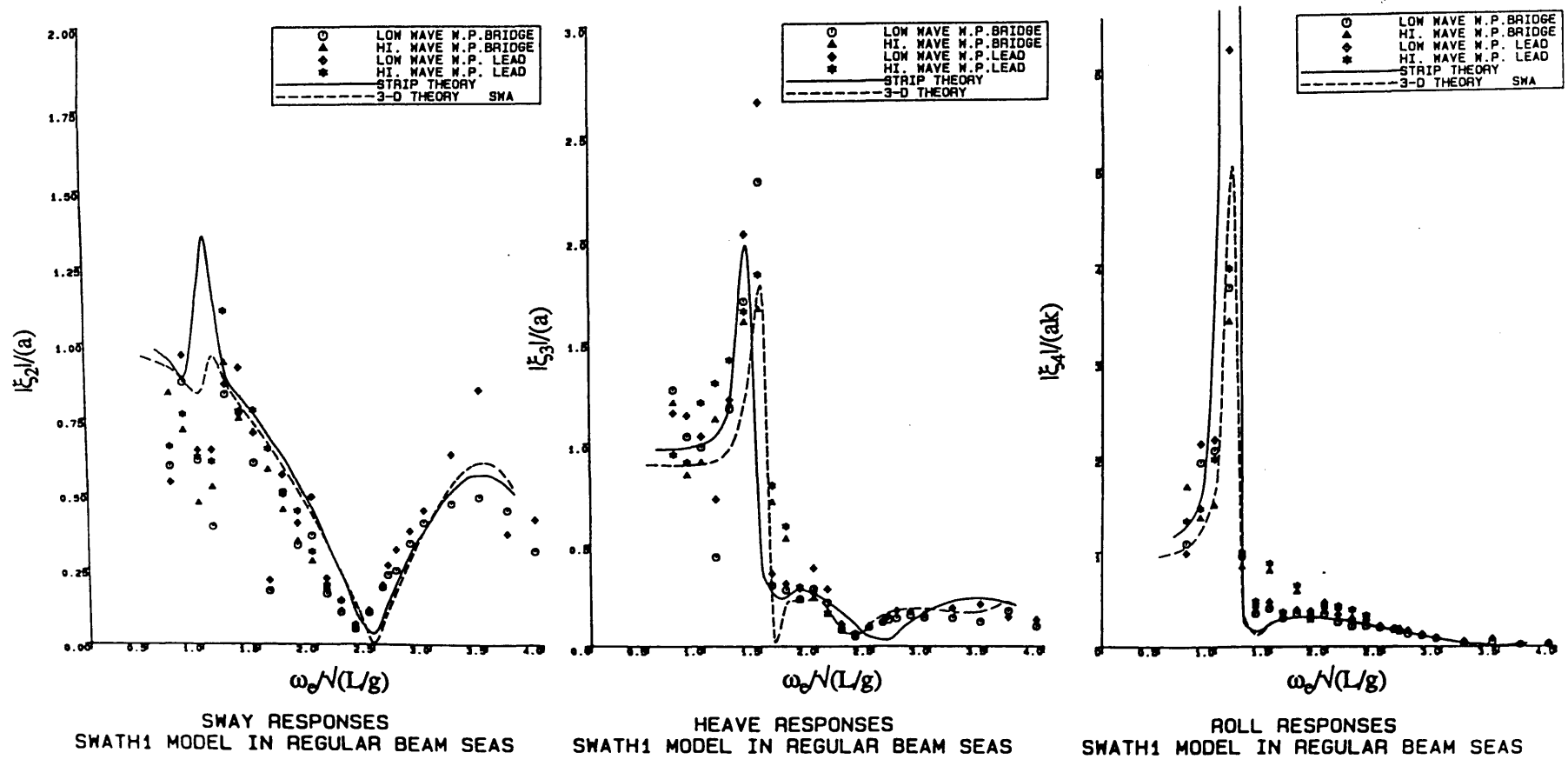

Fig. 4.82 Sway, heave and roll motion responses of SWATH 1 in beam sea at F_n=0.0

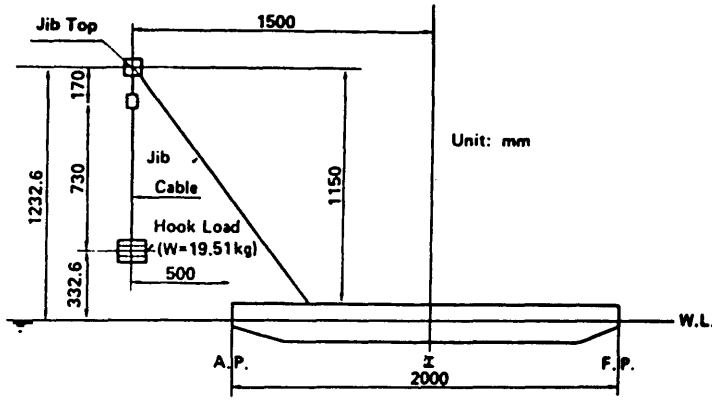

Fig.5.1 Model of ship crane vessel in crane abaft

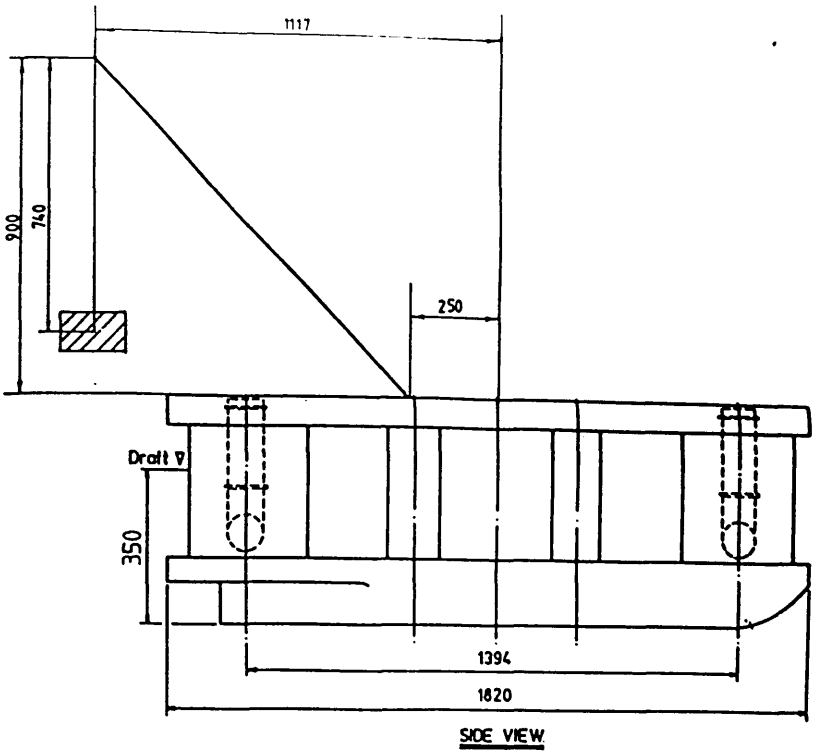

(a) Condition A - crane abaft

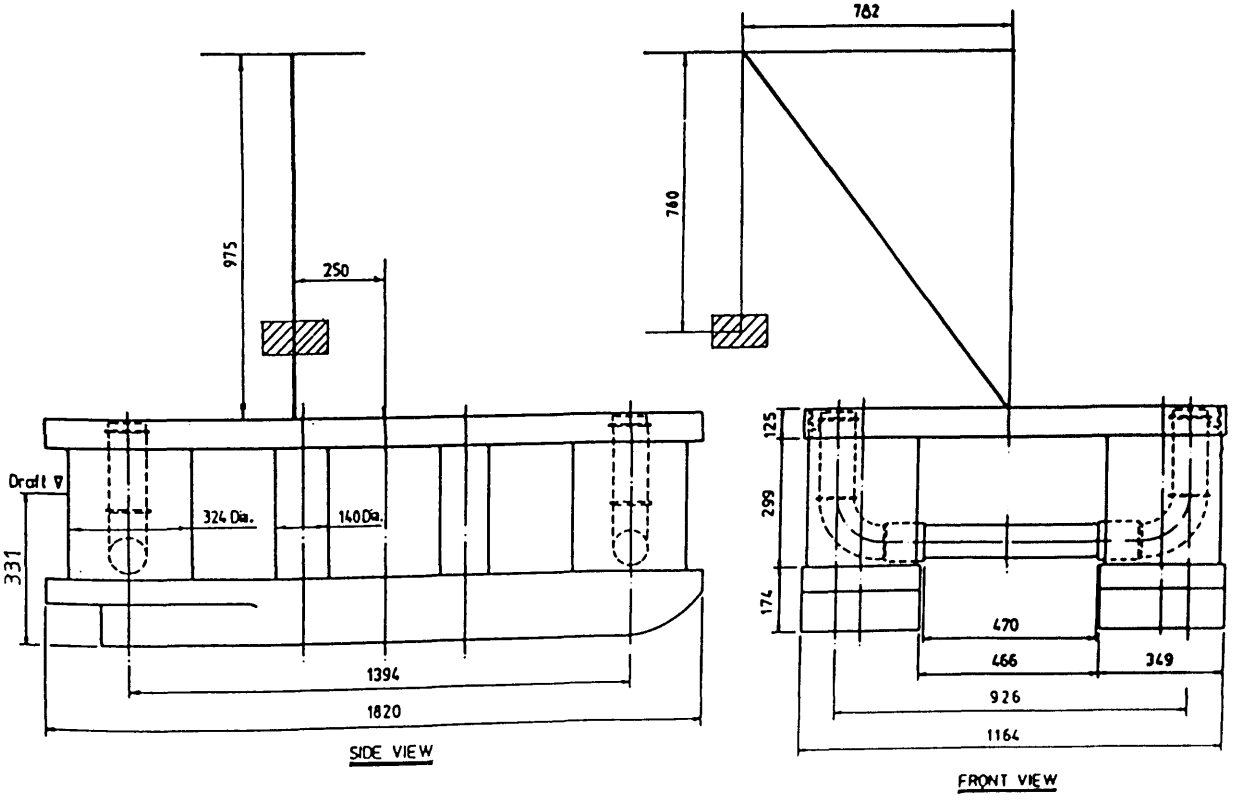

(b) Condition B - crane athwartship

Fig.5.2 Model of semi-submersible crane vessel in two conditions

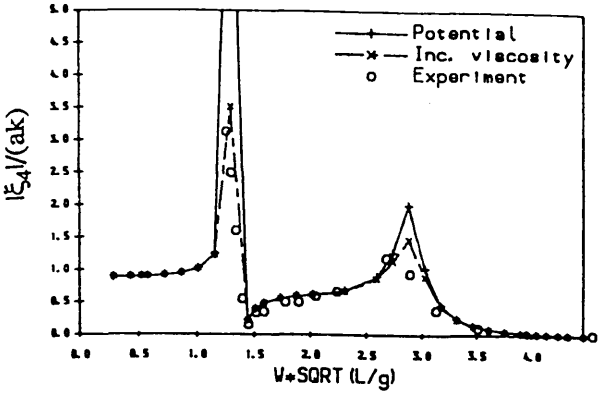

(a) Roll responses in beam seas

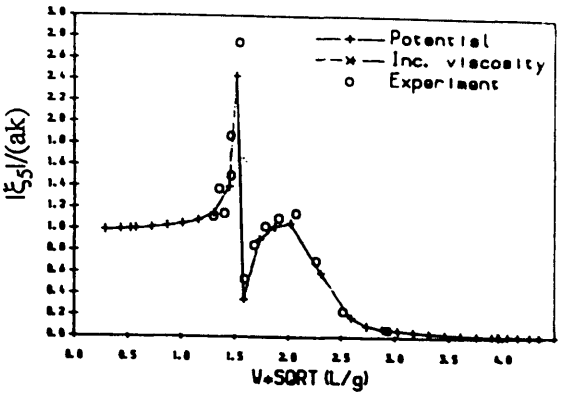

(b) Pitch responses in head seas

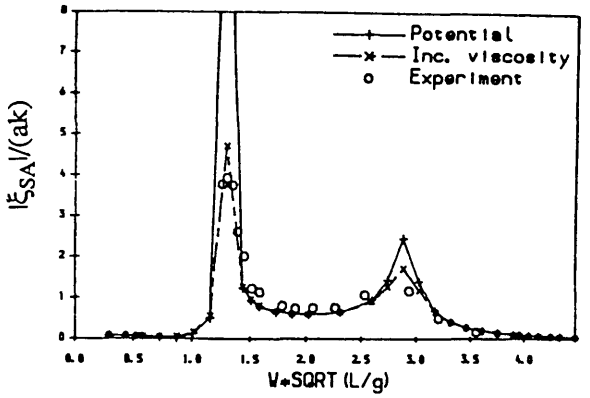

(c) Swing responses of the load in beam seas

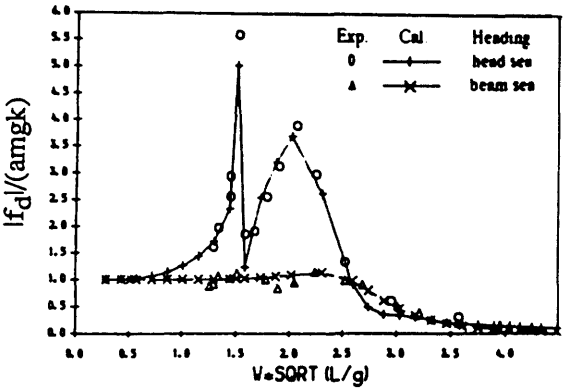

(d) Dynamic tension responses of the cable

Fig.5.3 Motion and dynamic tension responses of ship shaped crane vessel

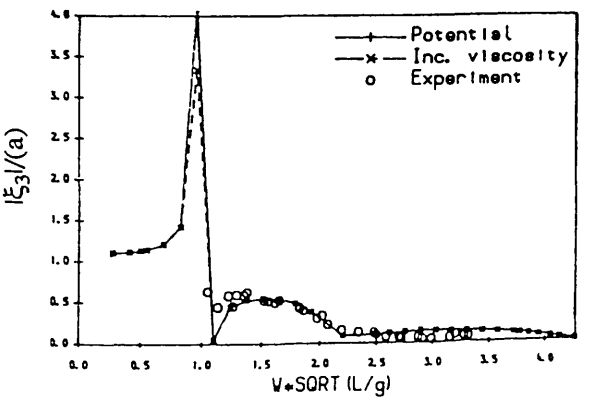

(a) Heave responses in beam seas

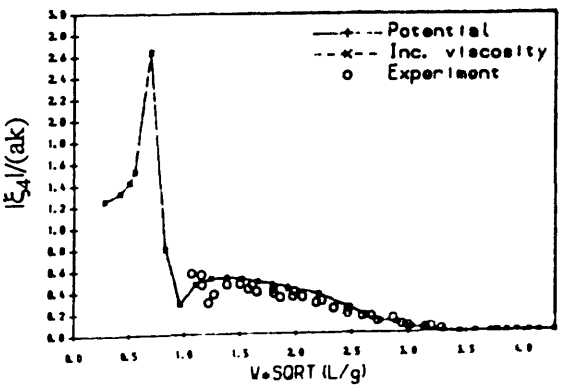

(b) Roll responses in beam seas

Fig.5.4 Motion responses of semi-submersible crane vessel in free floating condition

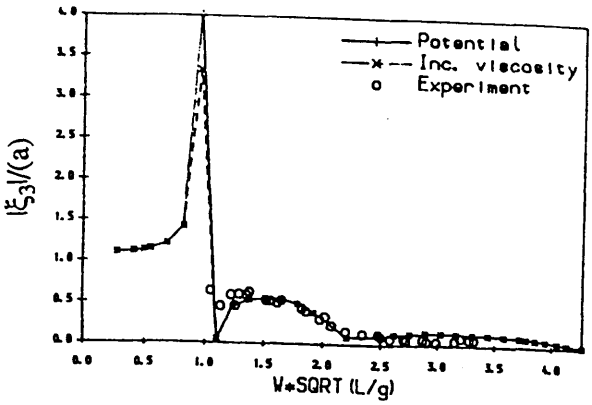

(a) Heave responses in beam seas

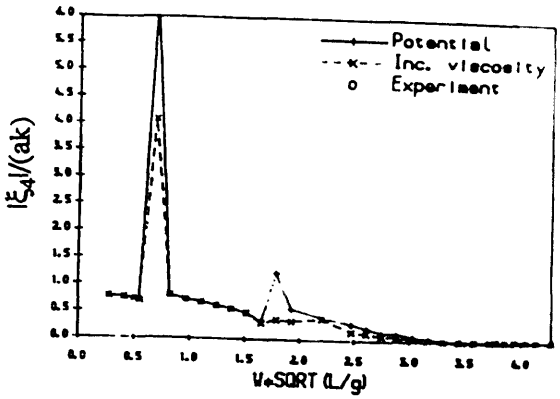

(b) Roll responses in beam seas

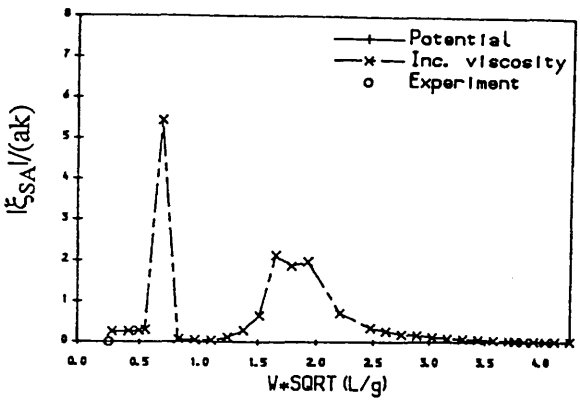

(c) Swing responses of the load in beam seas

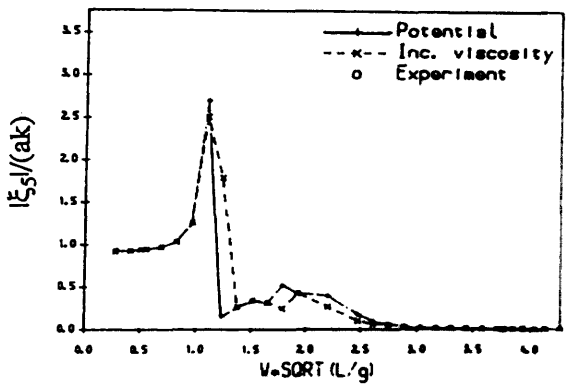

(d) Pitch responses in head seas

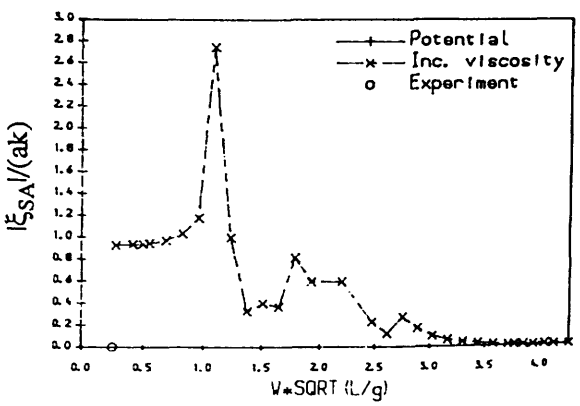

(e) Swing responses of the load in head seas

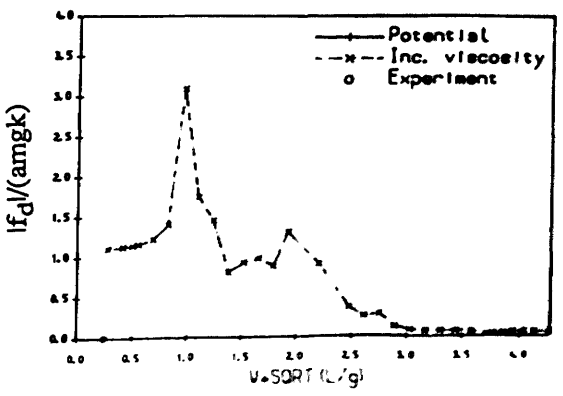

(f) Dynamic tension responses of the cable in head sea

Fig.5.5 Motion and dynamic tension responses of semi-submersible crane vessel (cond. A)

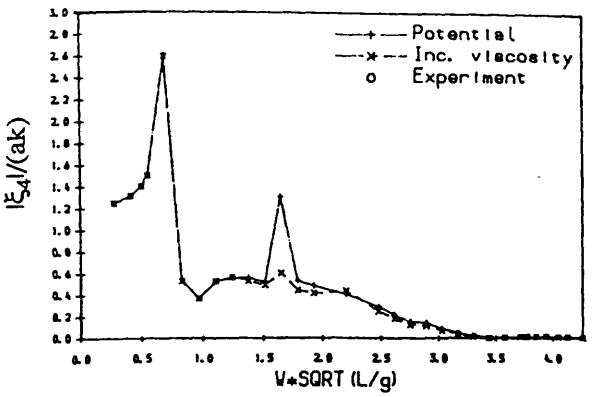

(a) Roll responses in beam seas

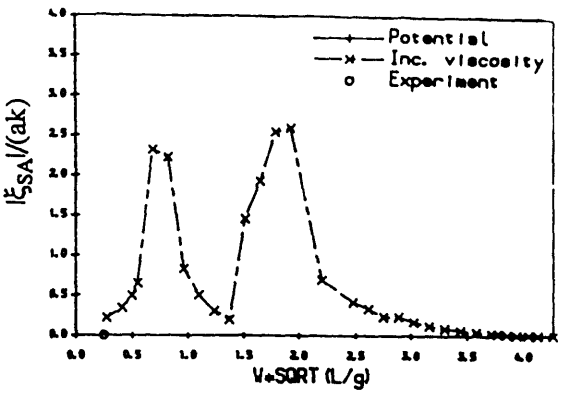

(b) Swing responses of the load in beam seas

Fig.5.6 Motion and dynamic tension responses of semi-submersible crane vessel (cond. B)

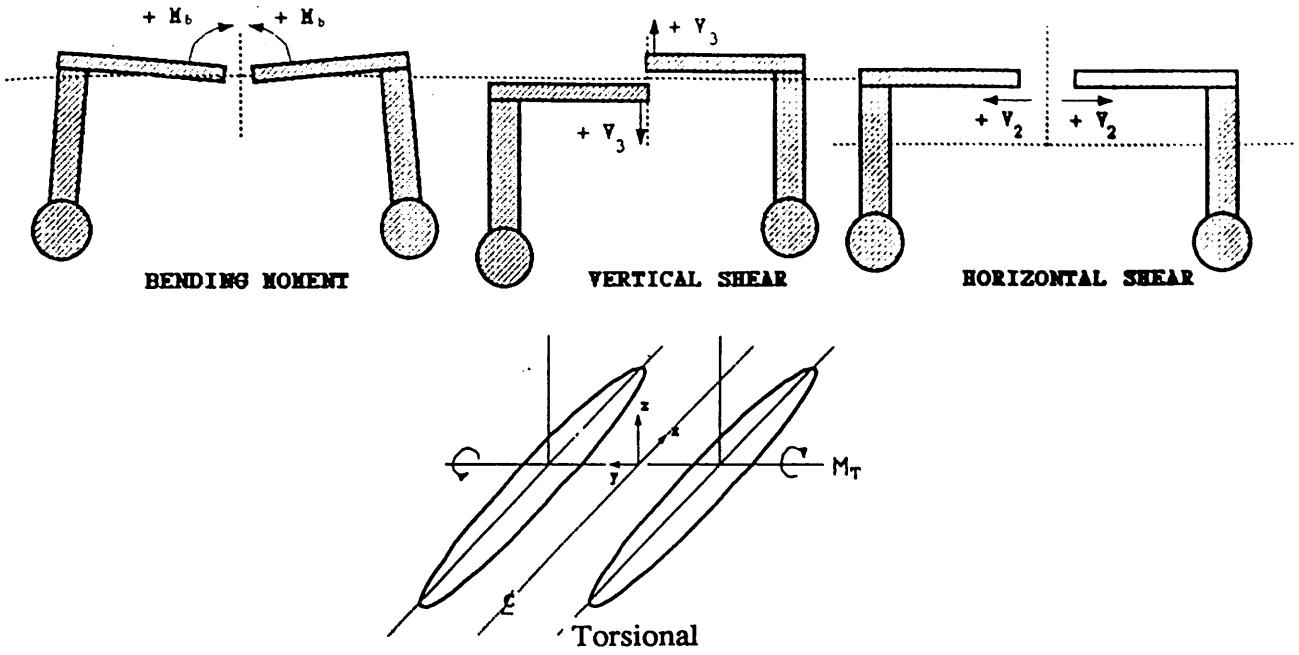

Fig. 6.1 Load conventions on the cross deck of a twin hull ship

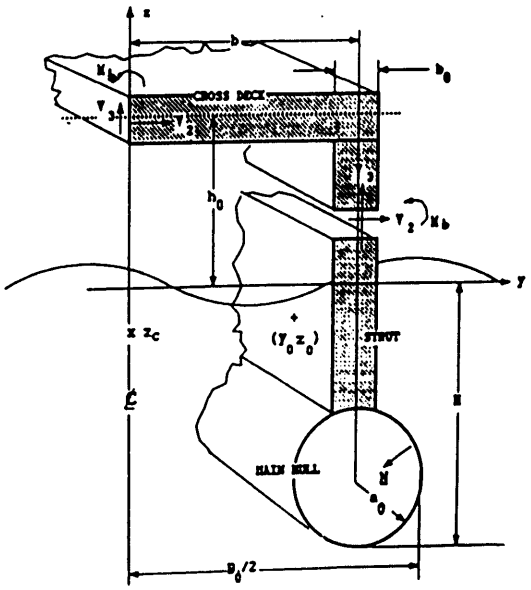

Fig. 6.2 Definition sketch of the cross section of a twin hull ship

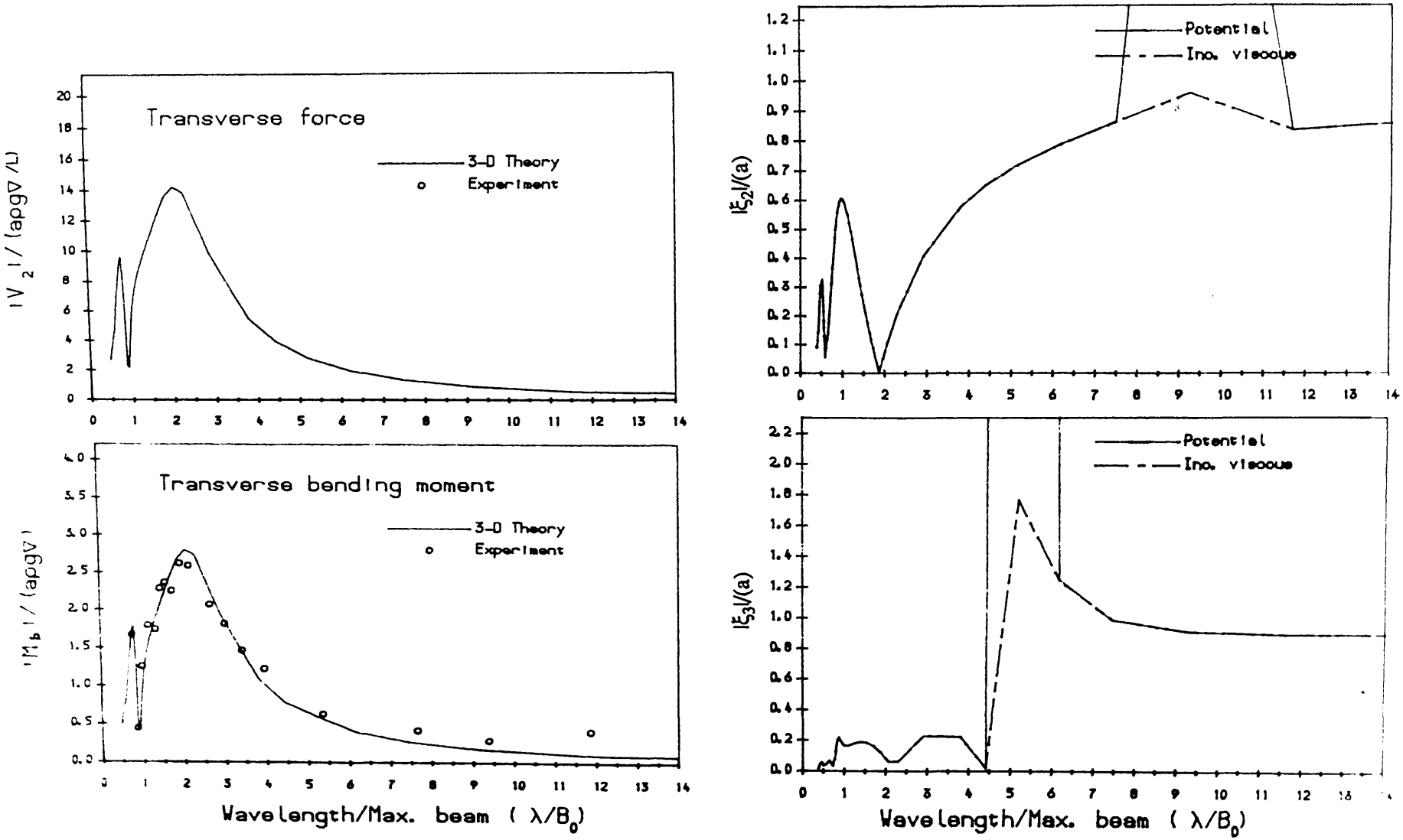

Fig. 6.3 Wave loads at cross deck mid-section and motions of SWATH 1 in regular beam seas

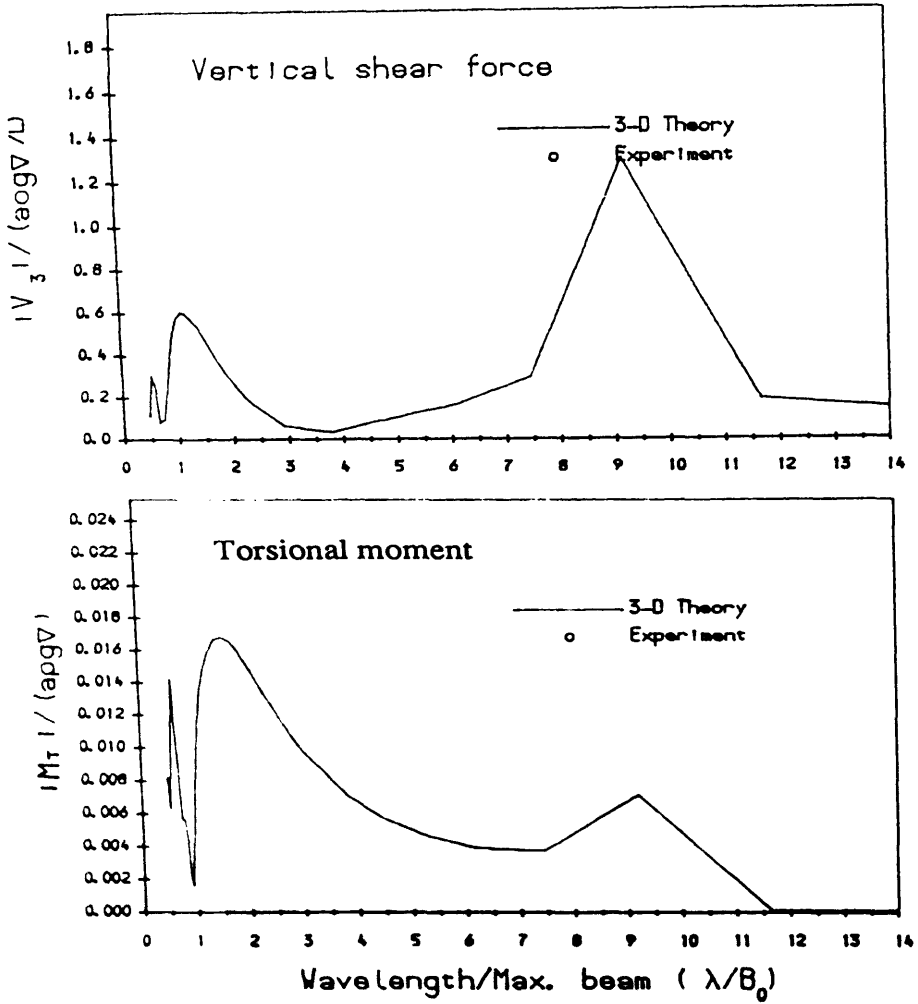

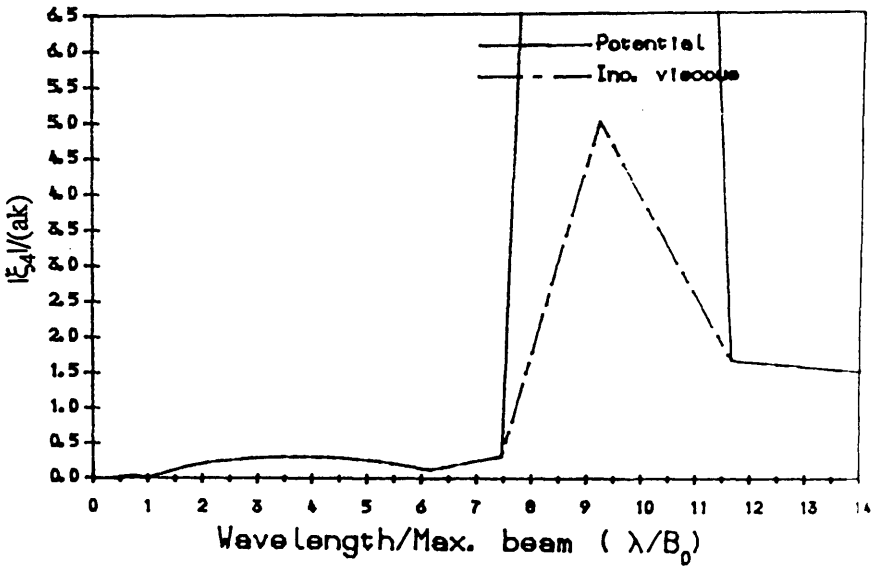

Fig. 6.4 Wave loads at cross deck mid-section and motions of SWATH 1 in regular beam seas

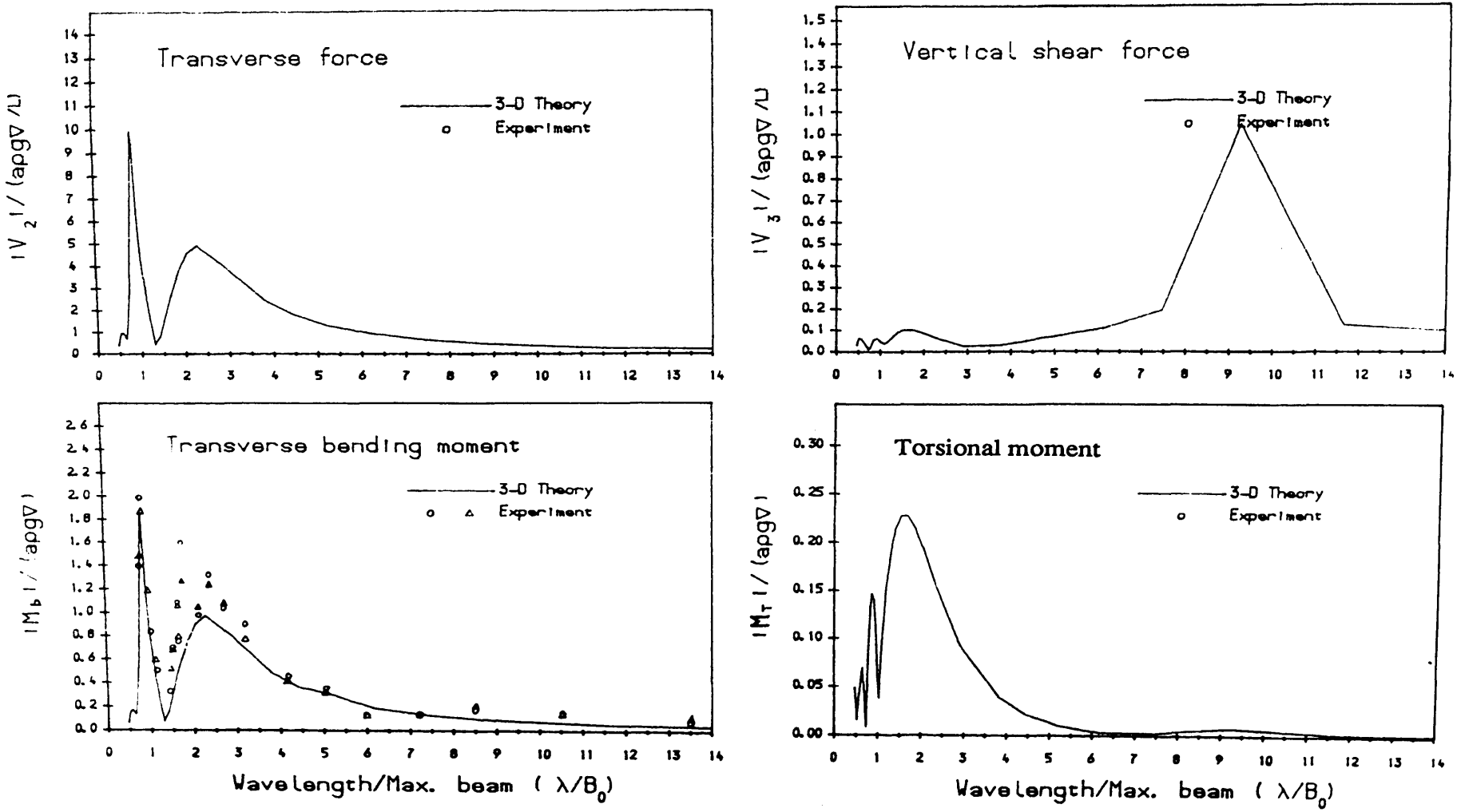

Fig. 6.5 Wave loads at cross deck mid-section of SWATH 1 in regular bow quartering seas

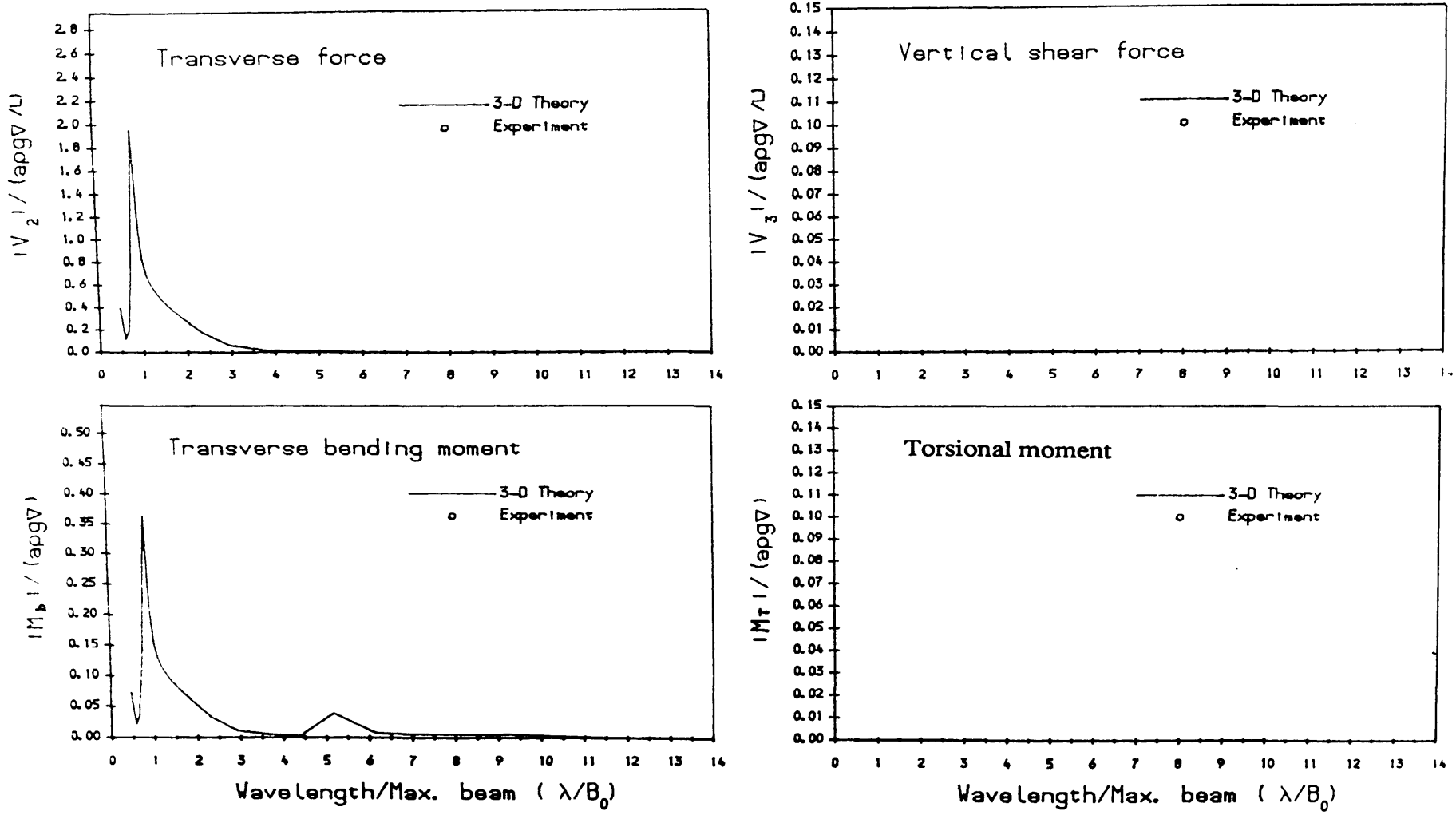

Fig. 6.6 Wave loads at cross deck mid-section of SWATH 1 in regular head seas

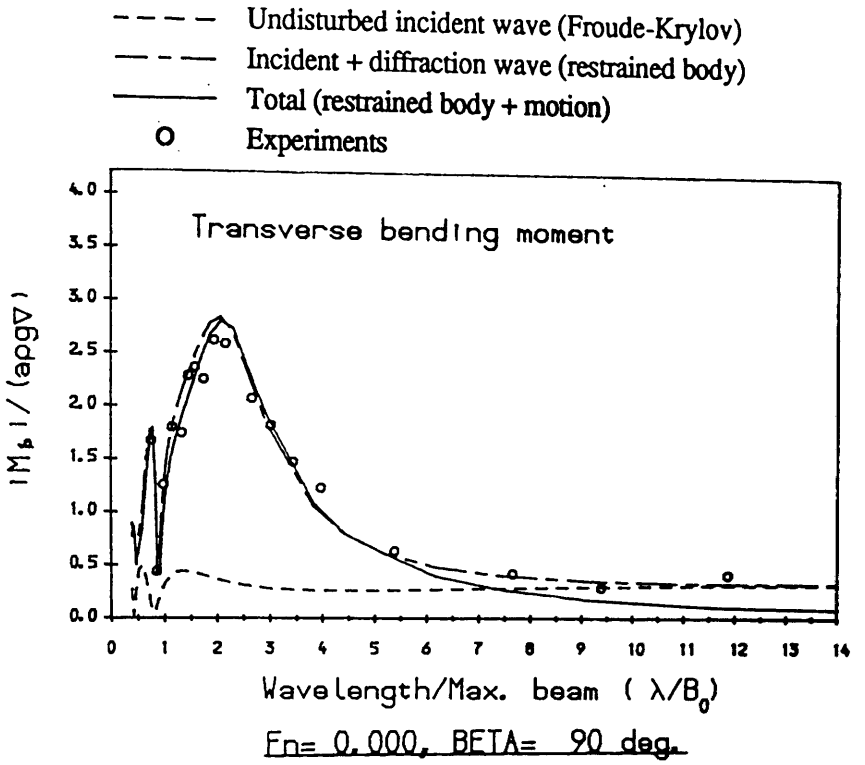

(a) bending moment in regular beam seas

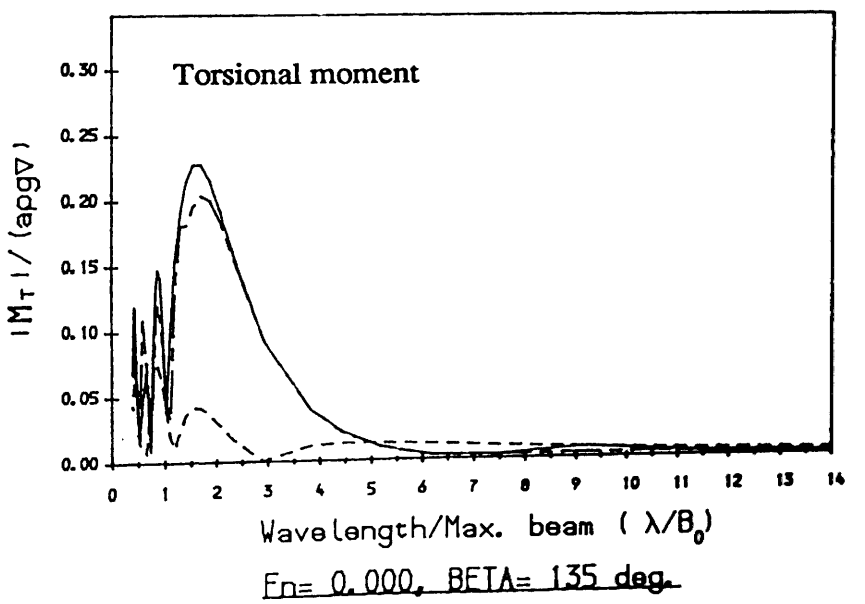

(b) torsional moment in regular bow quartering seas

Fig. 6.7 Decomposition of wave load effects at cross deck mid-section of SWATH 1 in regular beam and bow quartering seas

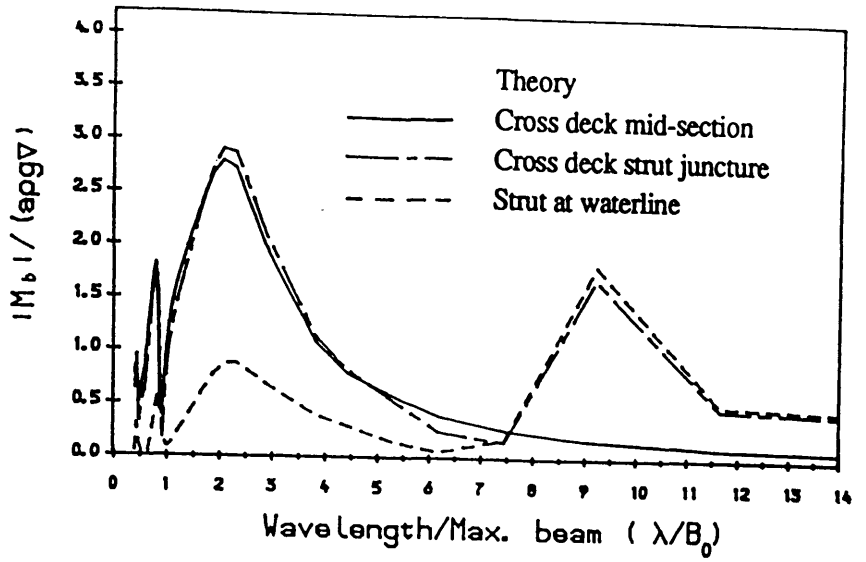

Fig. 6.8 Transverse bending moment of SWATH 1 in regular beam waves at various locations of the hull structure

(a) SWATH 1 (Tandem strut)

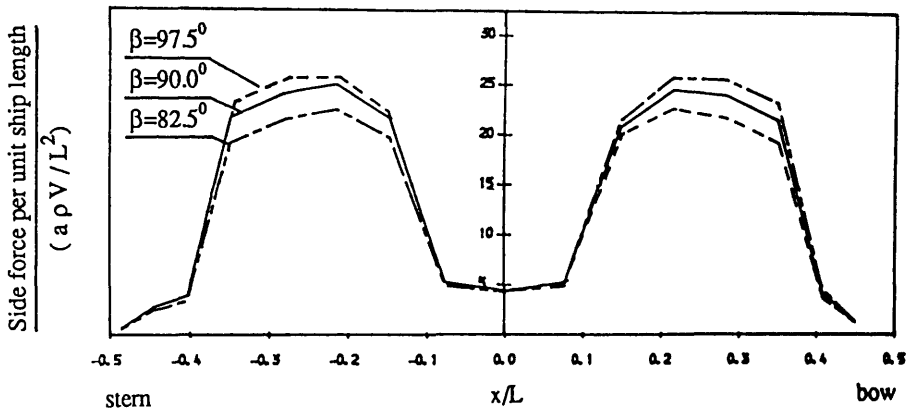

(b) Single strut SWATH

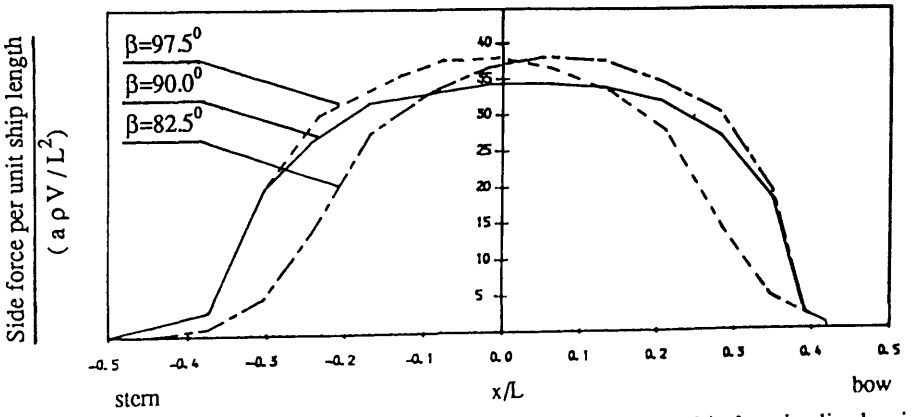

Fig.6.9 Side force distributions along the hull of the SWATH in longitudinal axis at the frequency where the maximum side force and bending moment on the cross deck occur (ω_e= 6.0).

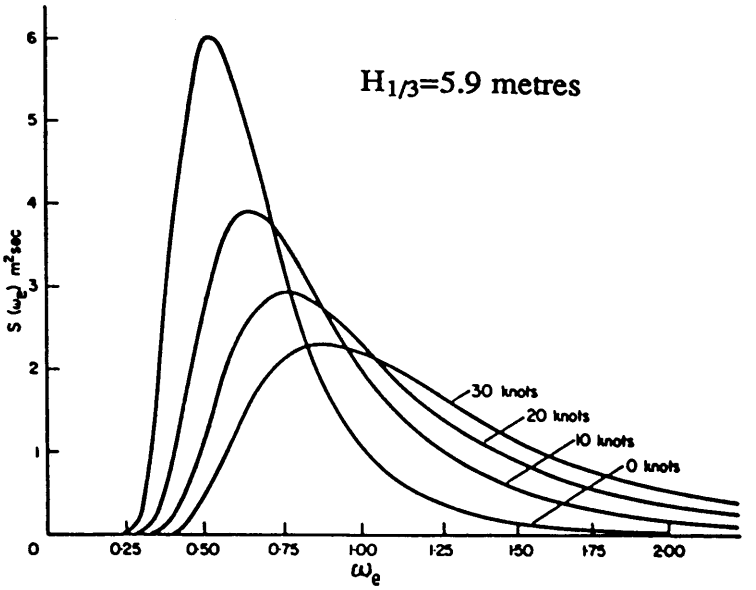

Fig. 7.1(a) Pierson-Moskowitz wave spectrum and the wave encounter spectrum in head sea

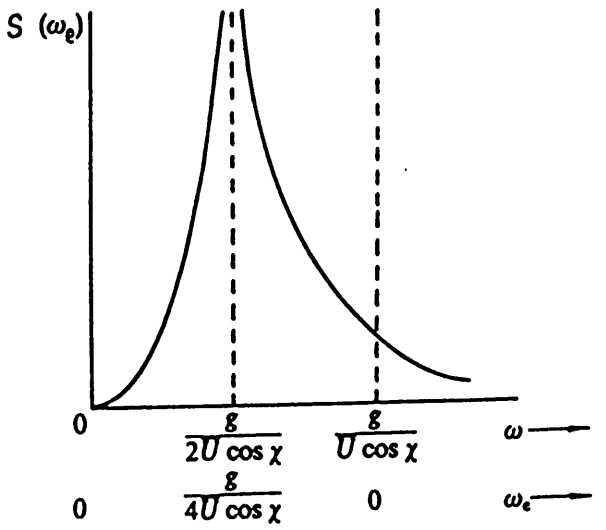

Fig. 7.1(b) A typical wave encounter spectrum in following sea[1]

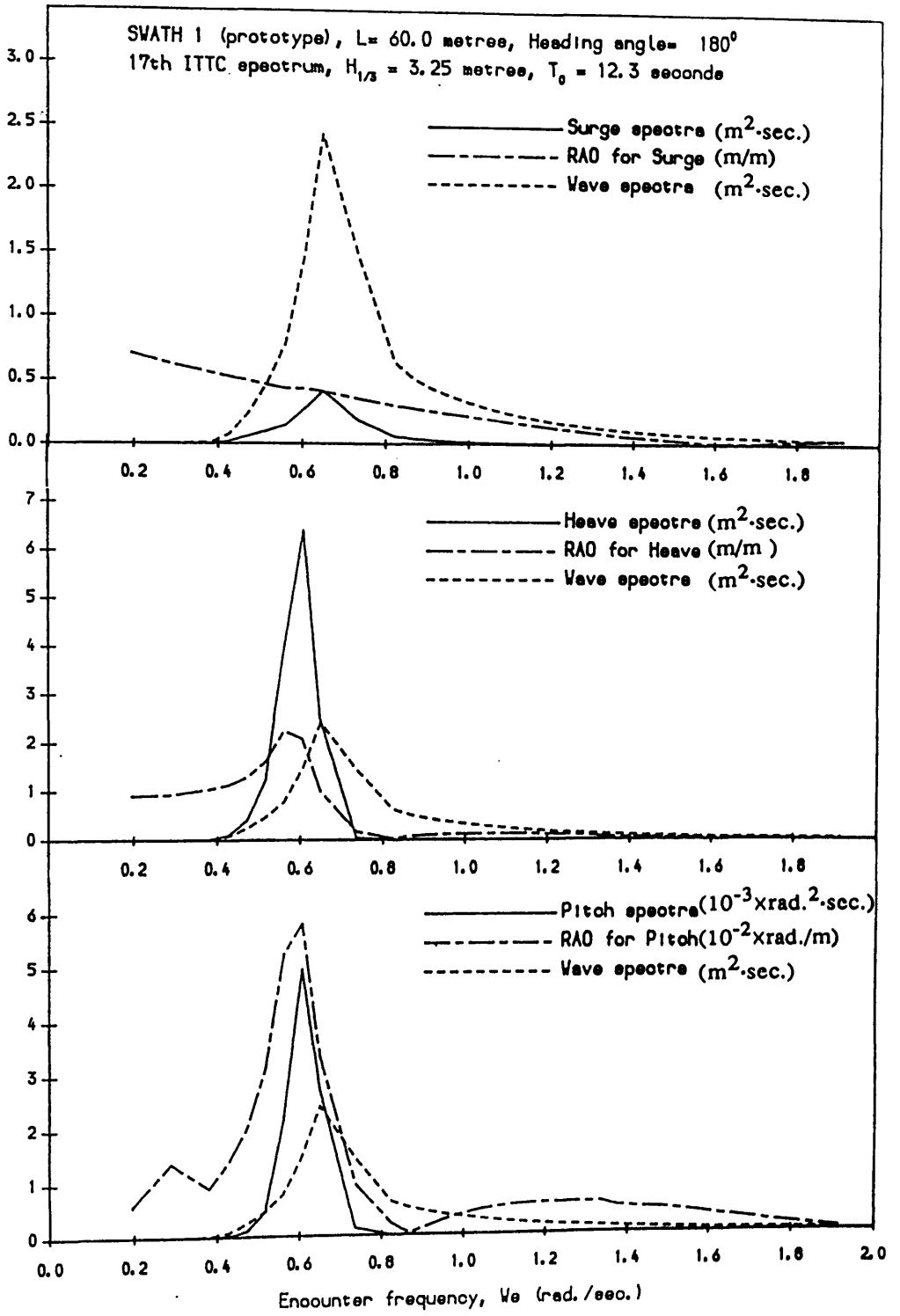

Fig. 7.2 The motion response spectra of prototype SWATH 1 in head sea at 15 knots

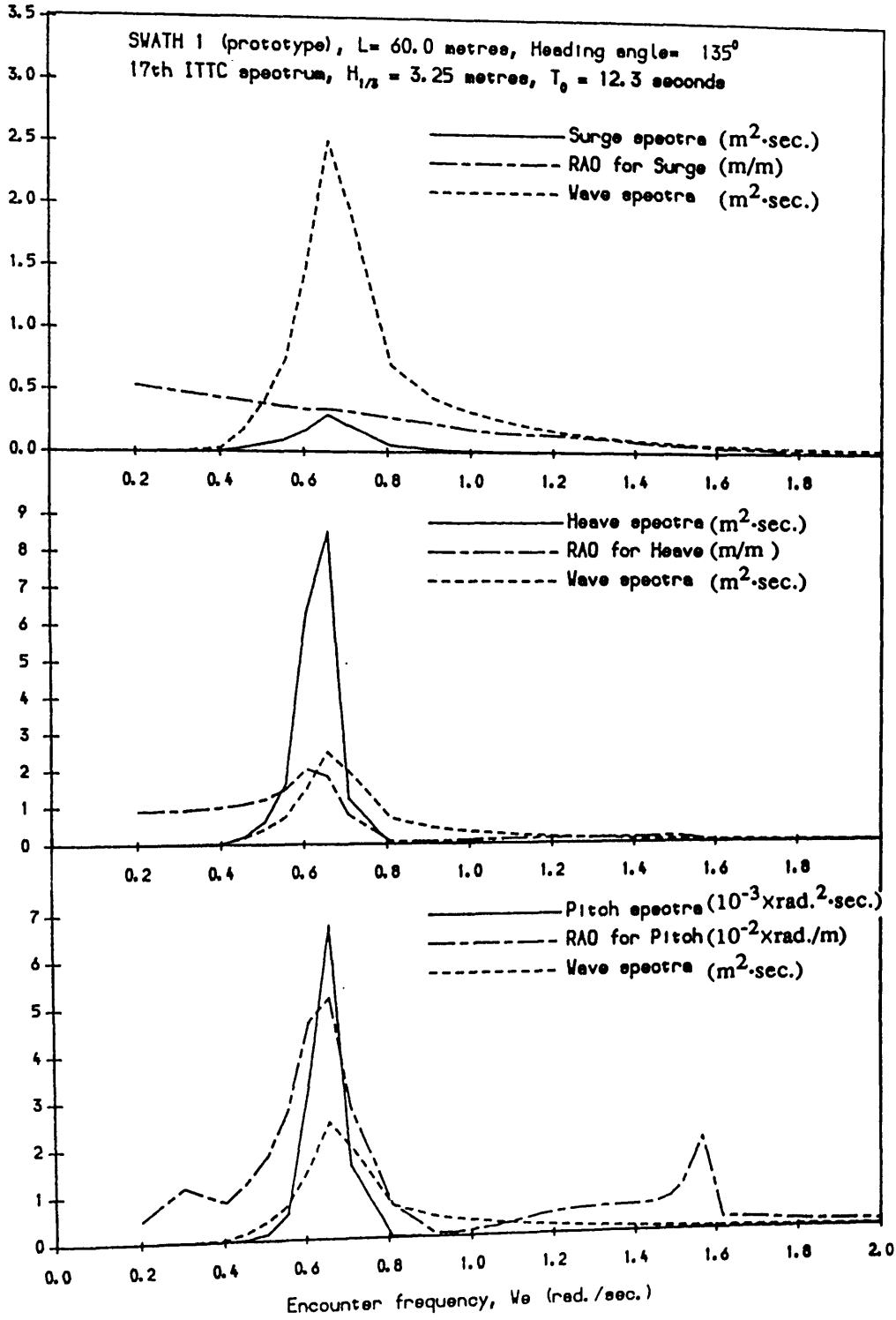

Fig. 7.3 The motion response spectra of prototype SWATH 1 in bow quartering sea at 15 knots (vertical motions)

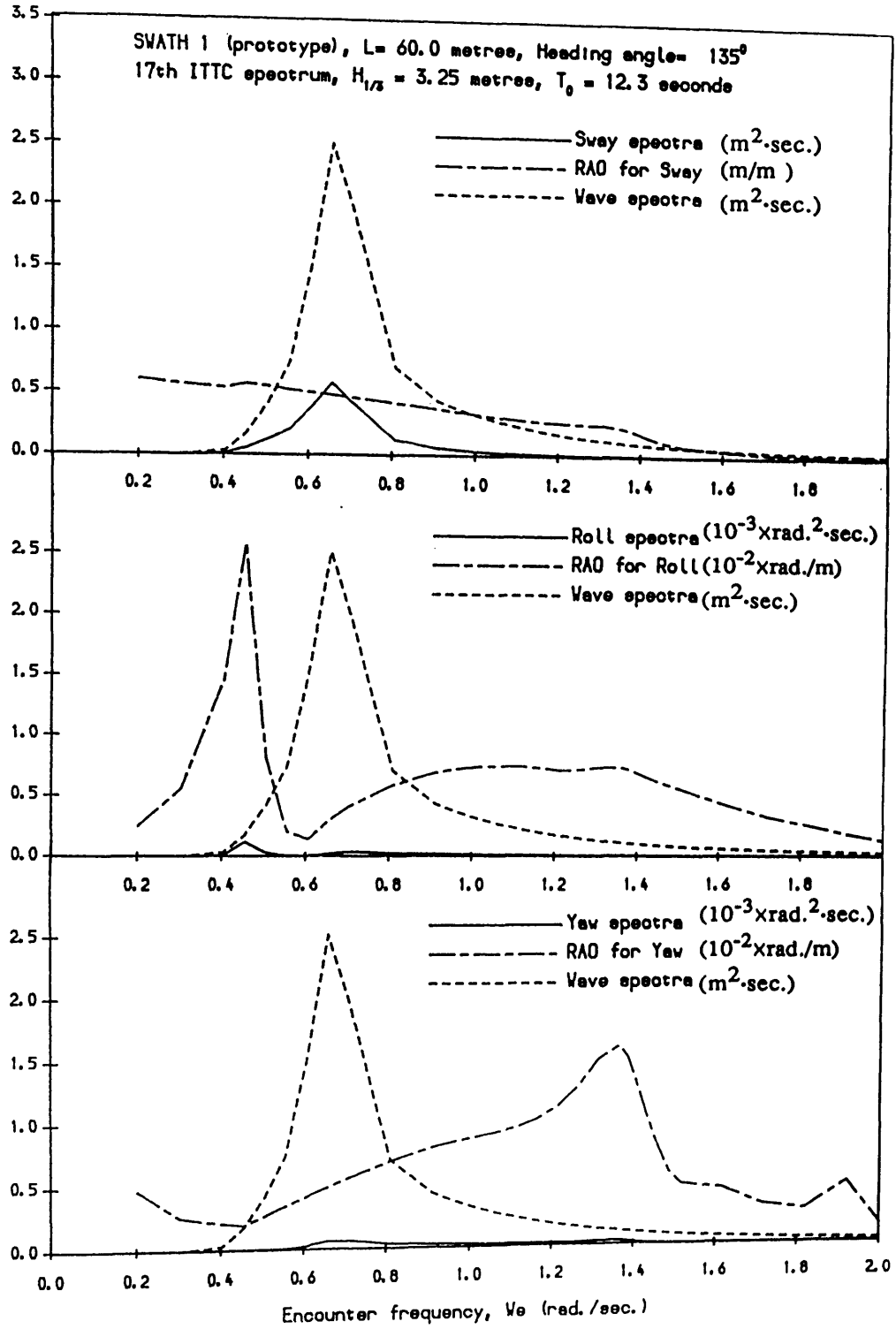

Fig. 7.3 (cont.) The motion response spectra of prototype SWATH 1 in bow quartering sea at 15 knots (transverse motions)

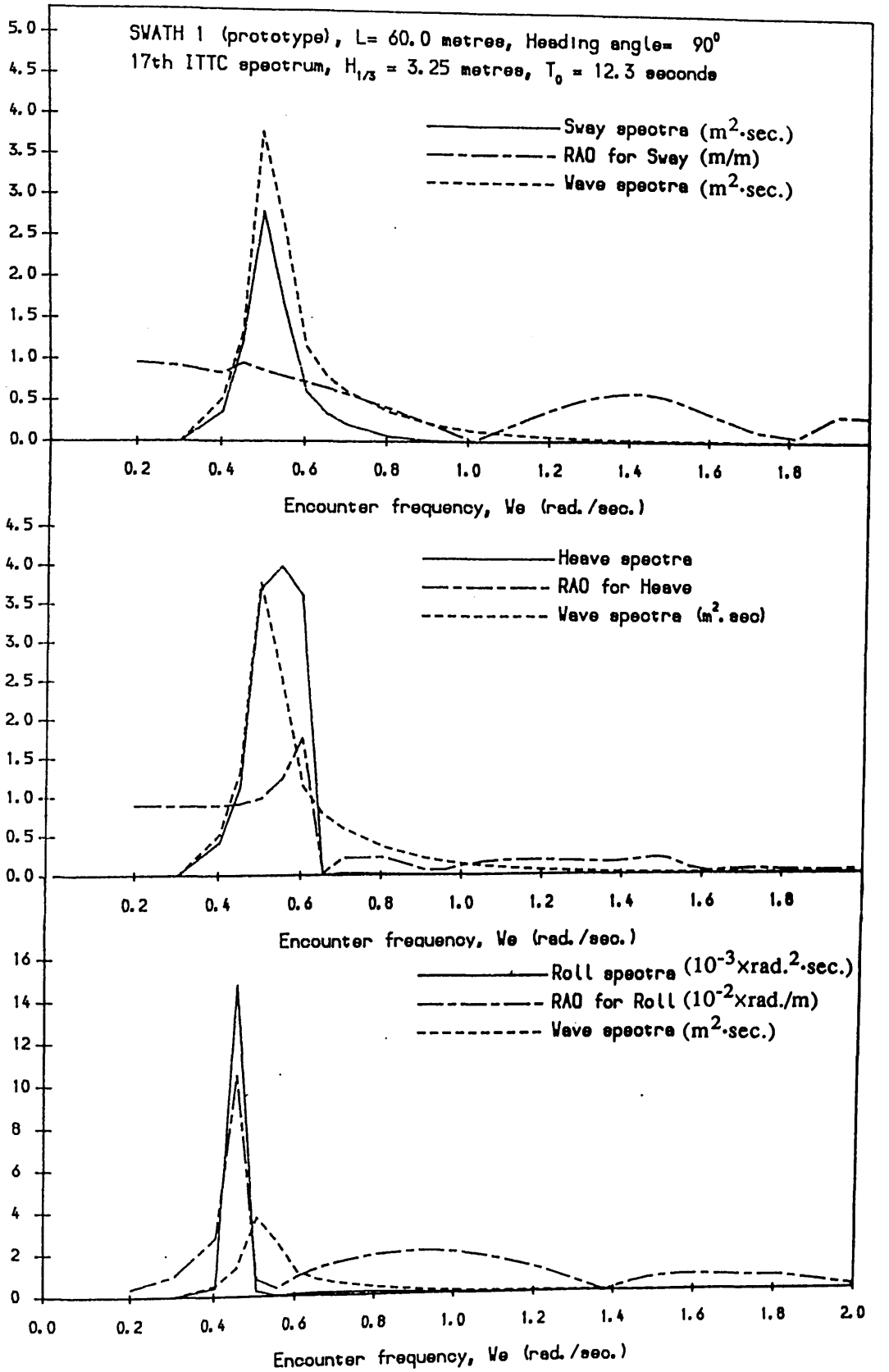

Fig. 7.4 The motion response spectra of prototype SWATH 1 in beam sea at 15 knots

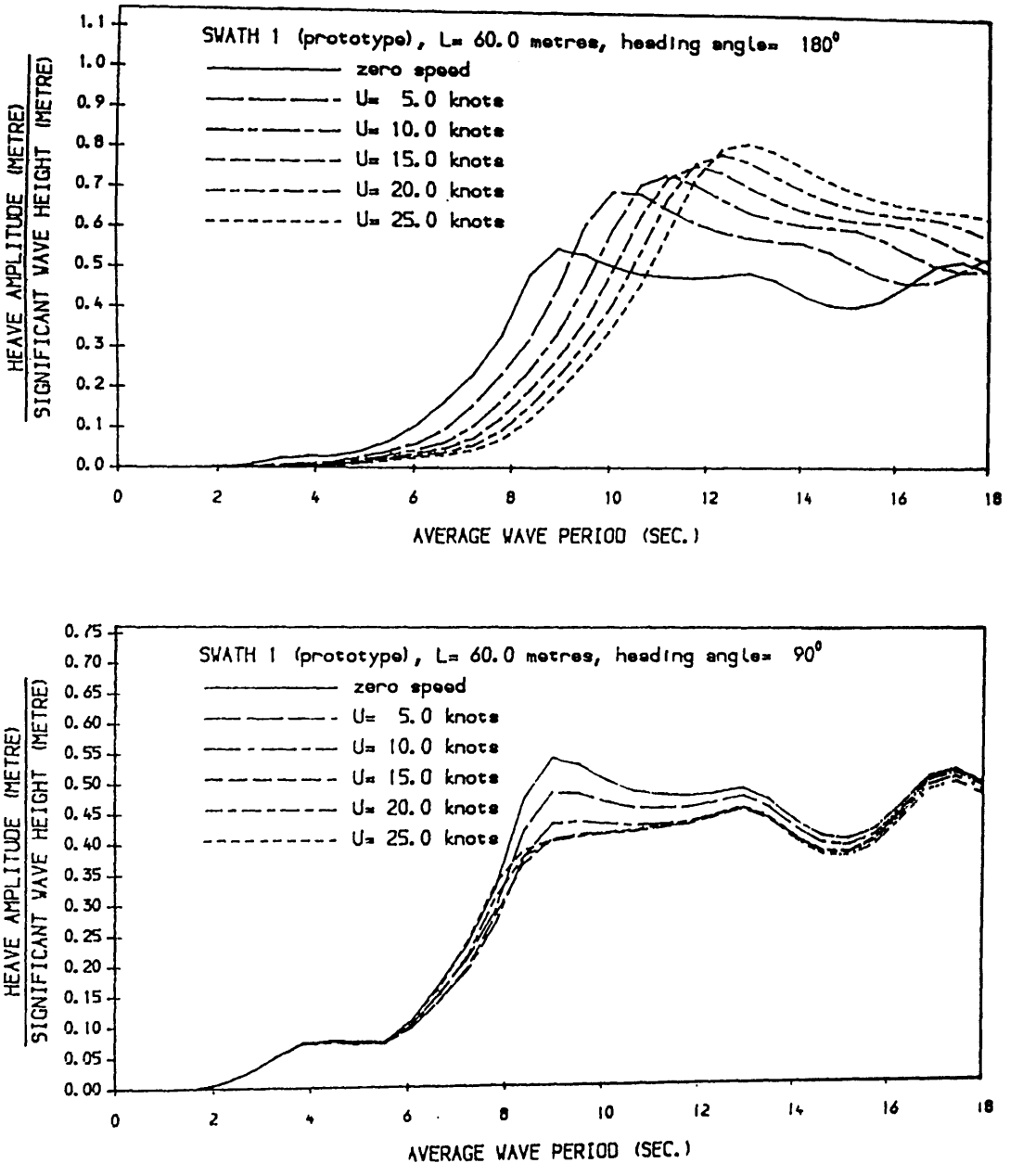

Fig. 7.5 Significant heave responses of prototype SWATH 1 in bow quartering and beam seas at different forward speeds

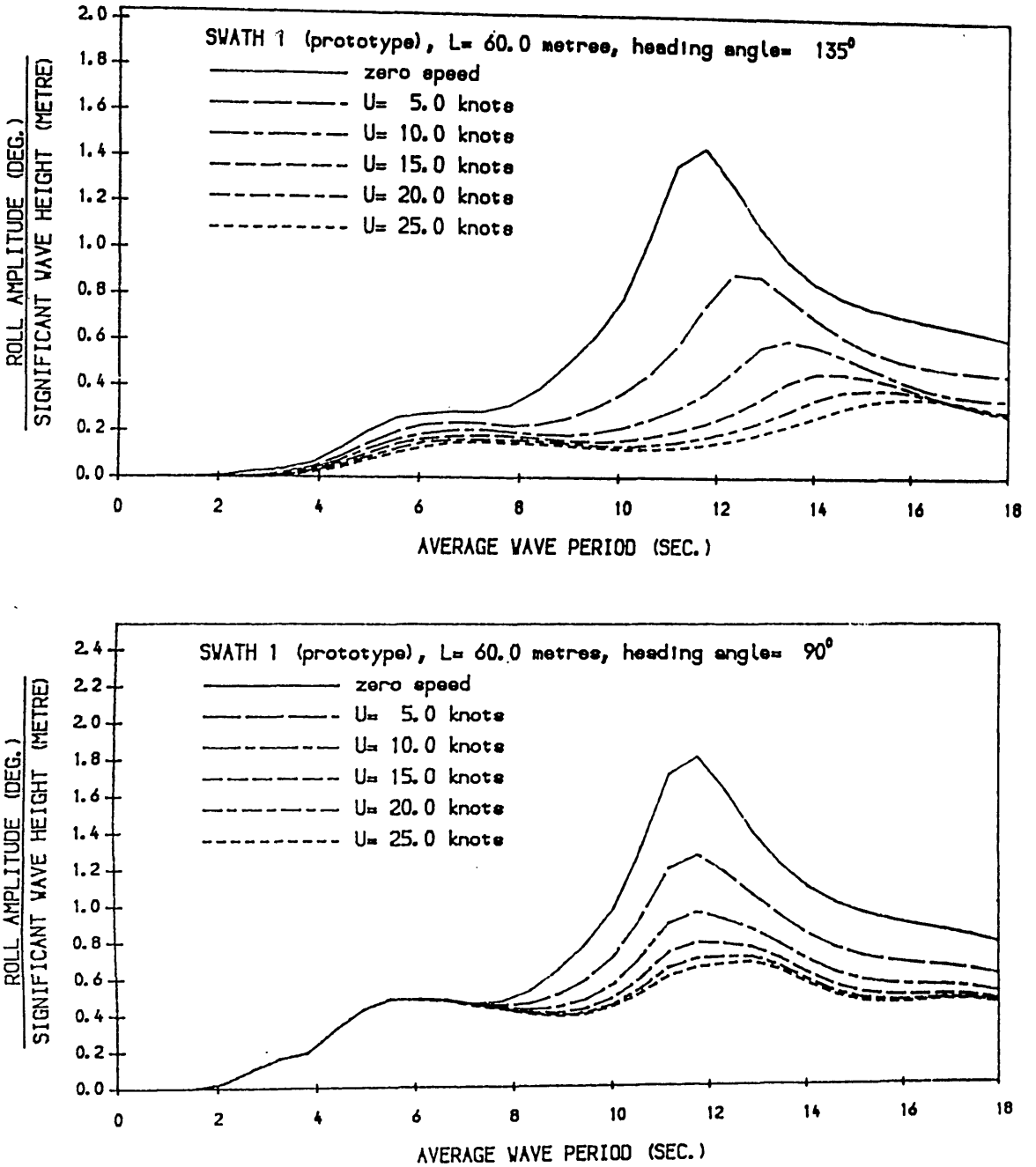

Fig. 7.6 Significant roll responses of prototype SWATH 1 in bow quartering and beam seas at different forward speeds

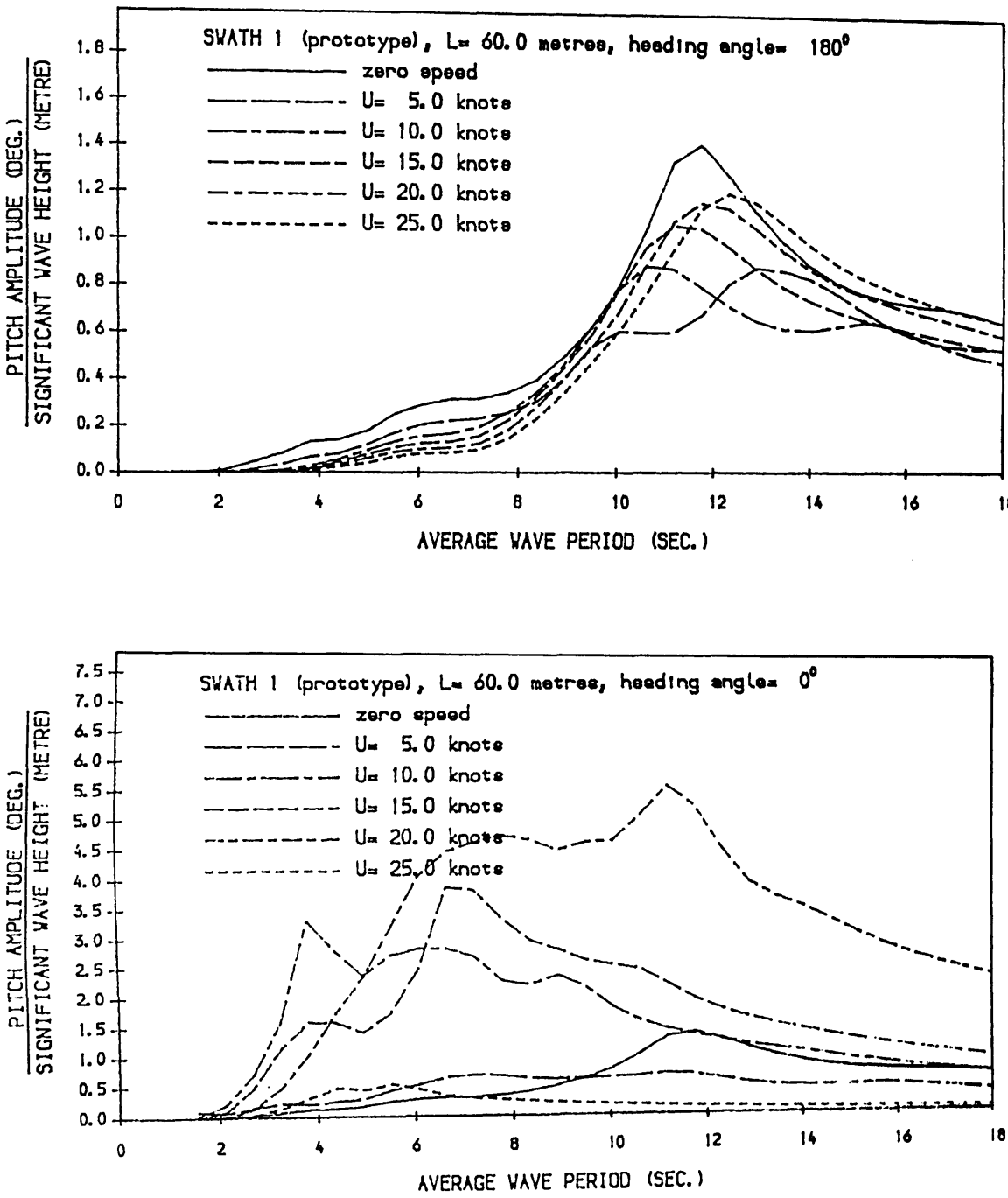

Fig. 7.7 Significant pitch responses of prototype SWATH 1 in head and following seas at different forward speeds

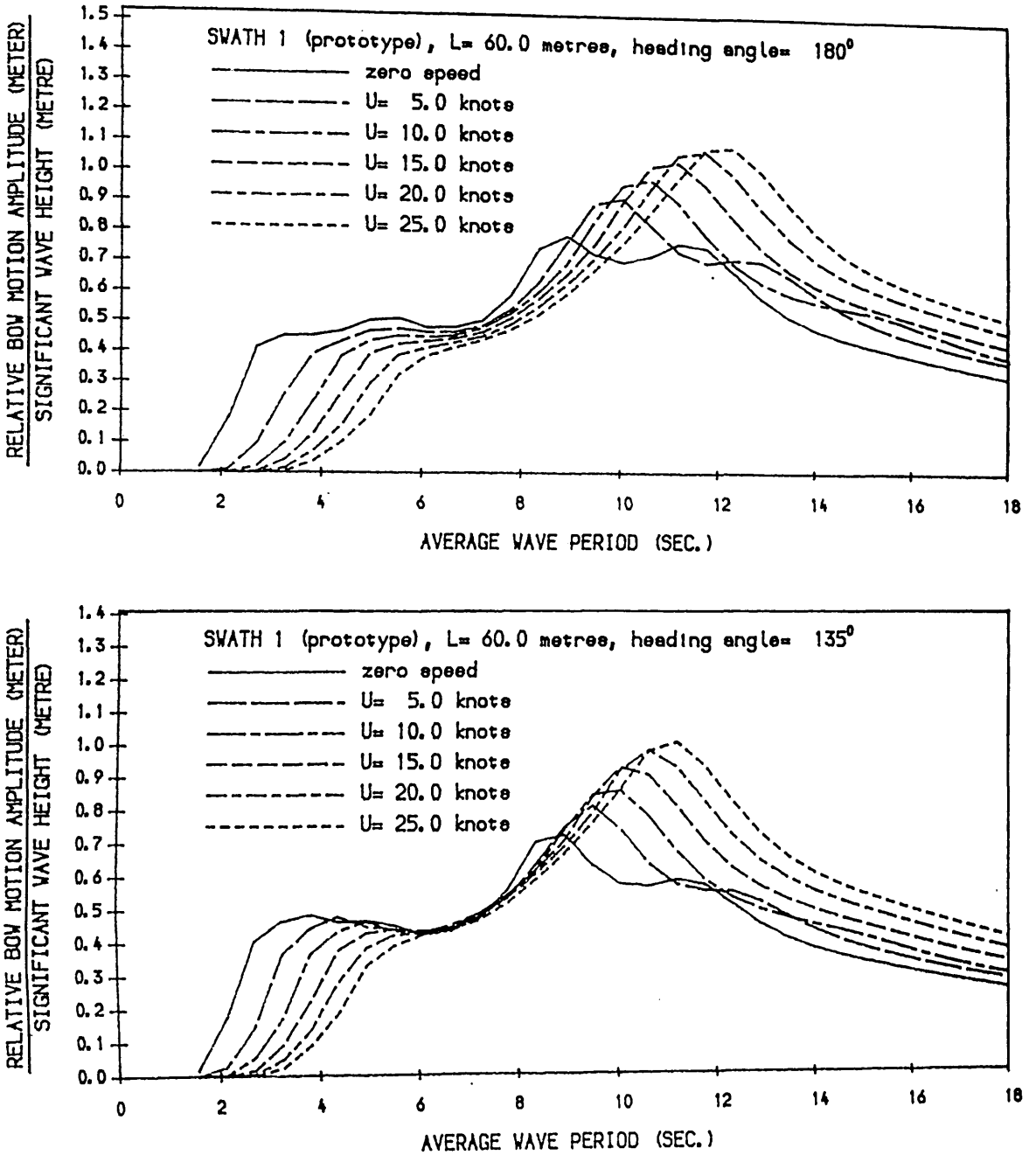

Fig. 7.8 Significant relative bow motion responses of prototype SWATH 1 in head and bow quartering seas at different forward speeds

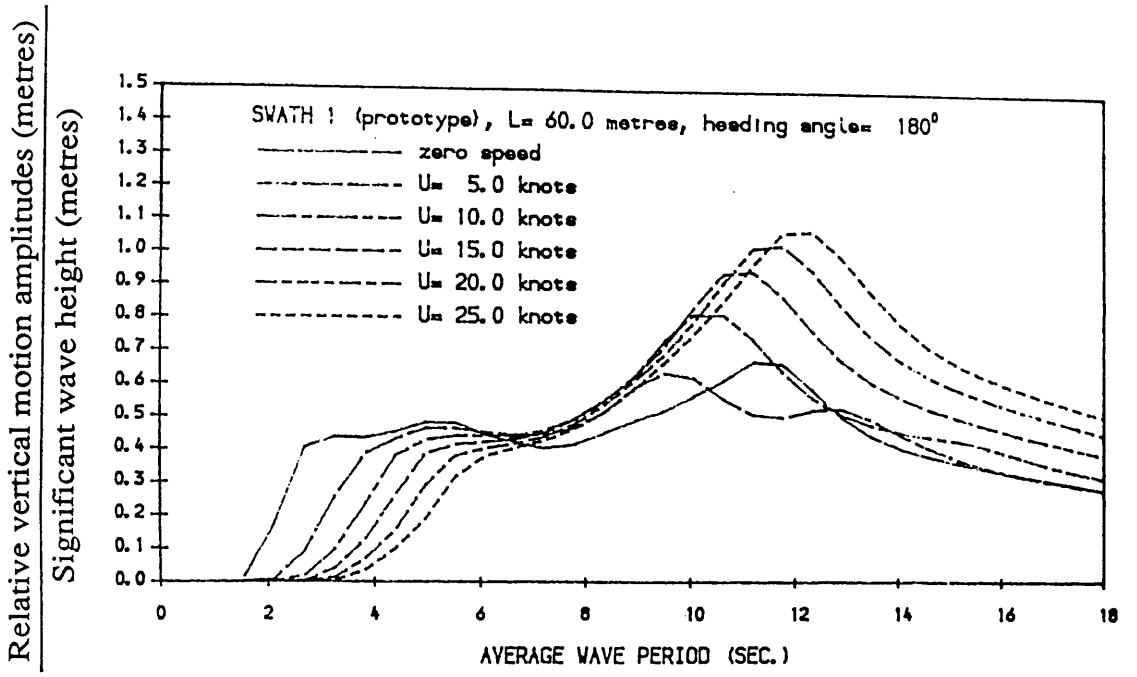

Fig. 7.9 Significant vertical relative motion responses at the propeller of prototype SWATH 1 in head seas at different forward speeds

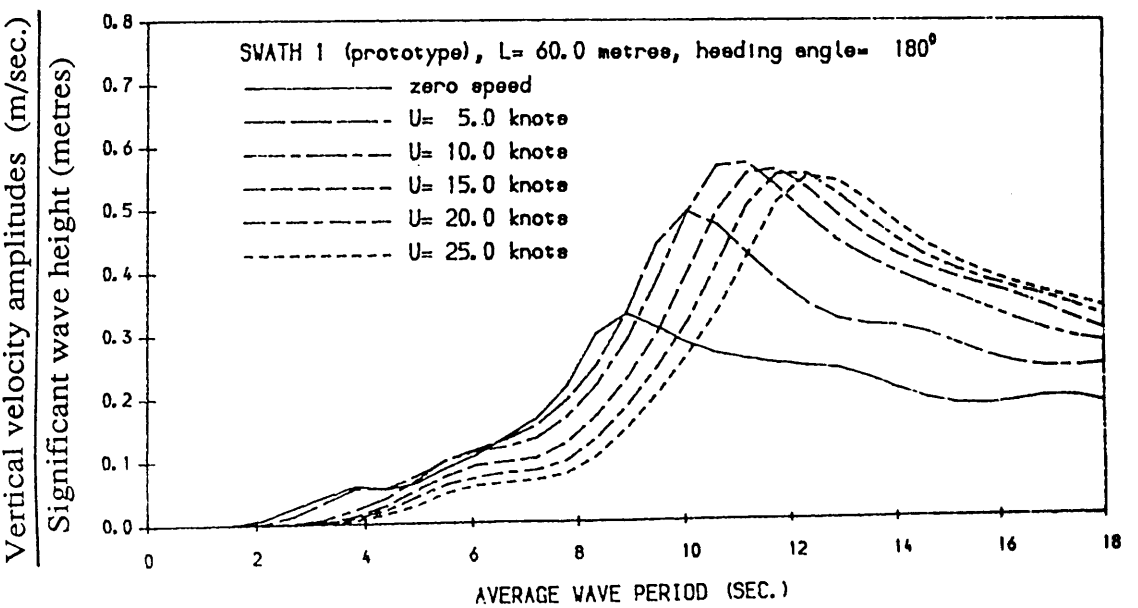

Fig. 7.10 Significant vertical velocity at fight deck of prototype SWATH 1 in head sea at different forward speeds

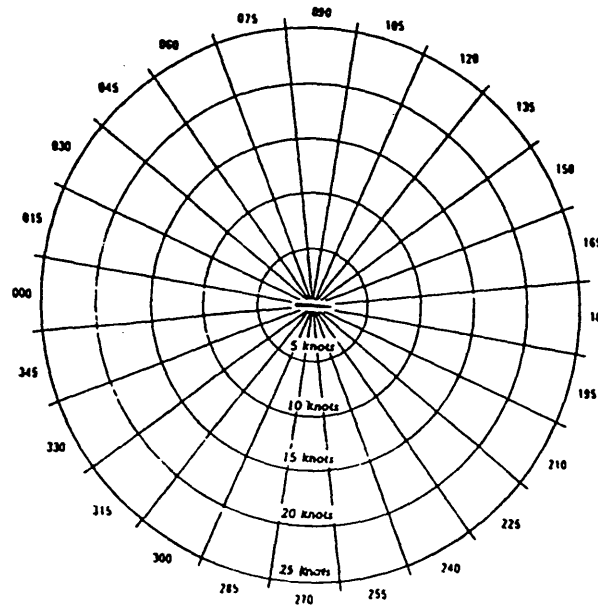

Fig. 7.11 The seakeeping matrix

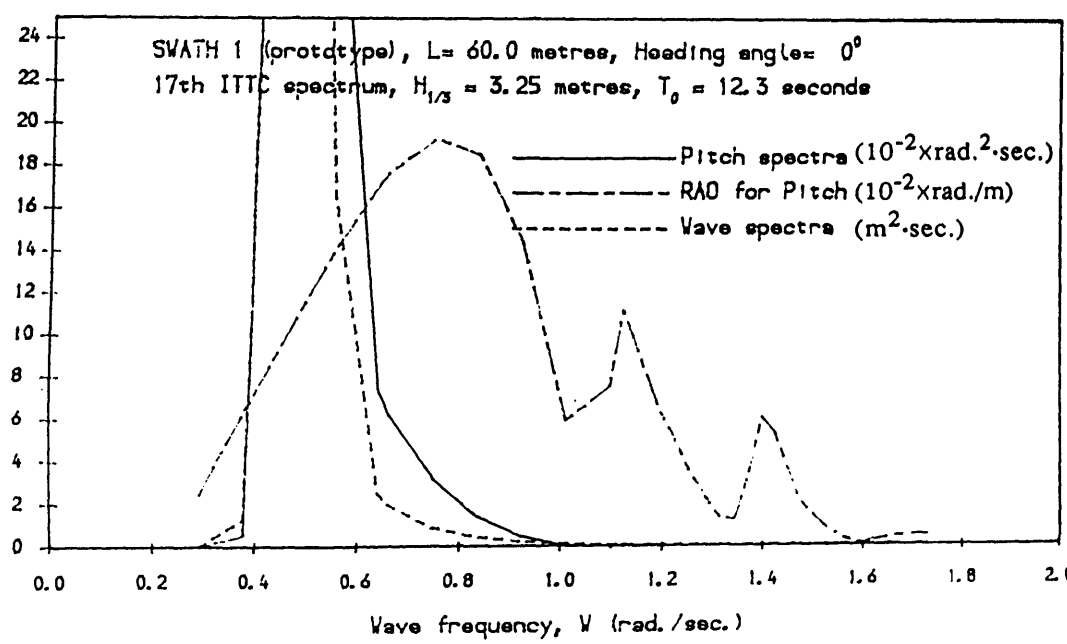

Fig. 7.12 Pitch spectrum of prototype SWATH 1
in following sea at 20 knots

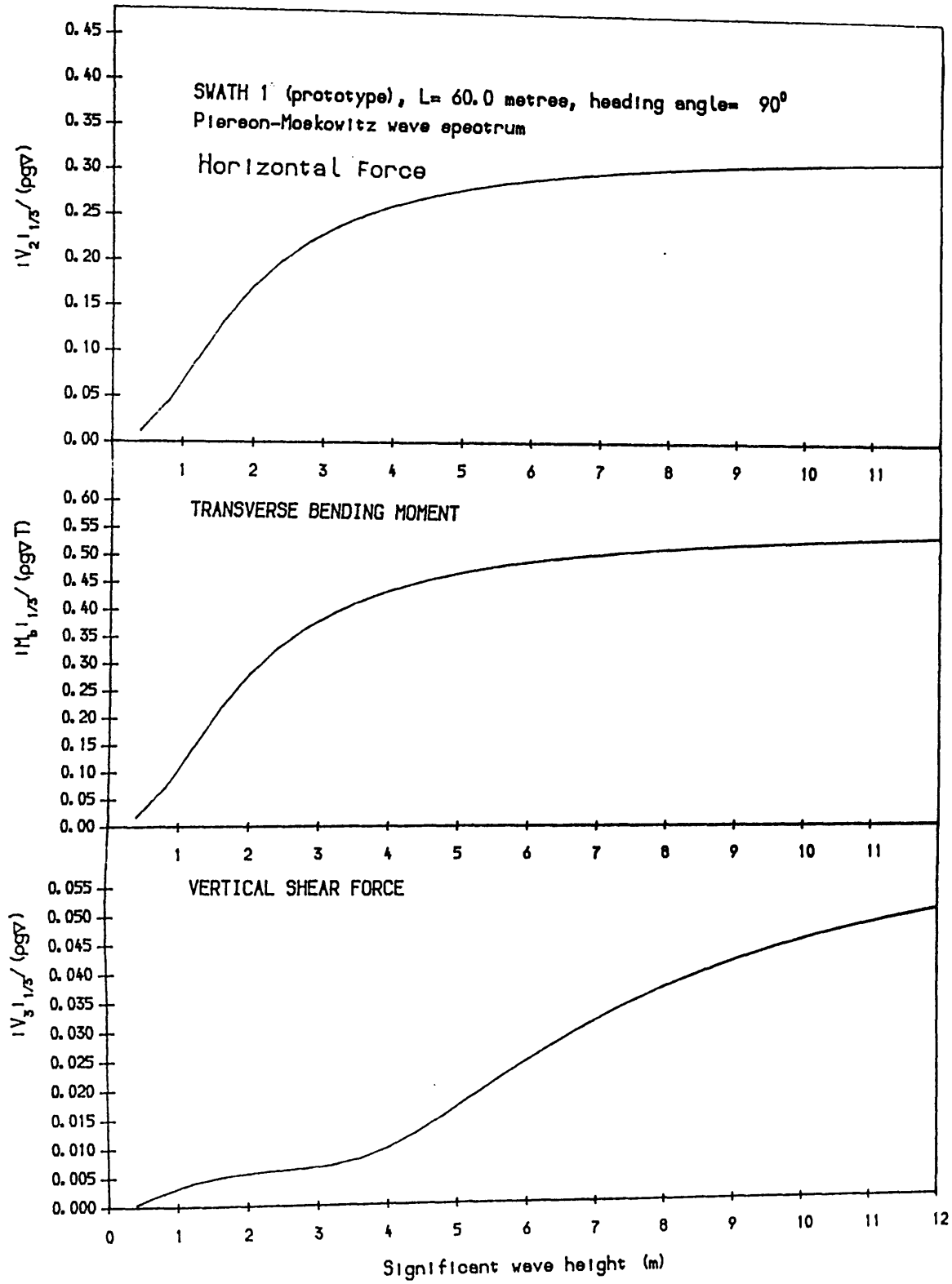

Fig. 7.13 Significant wave loads on the cross-deck structure of prototype SWATH 1 in irregular beam waves

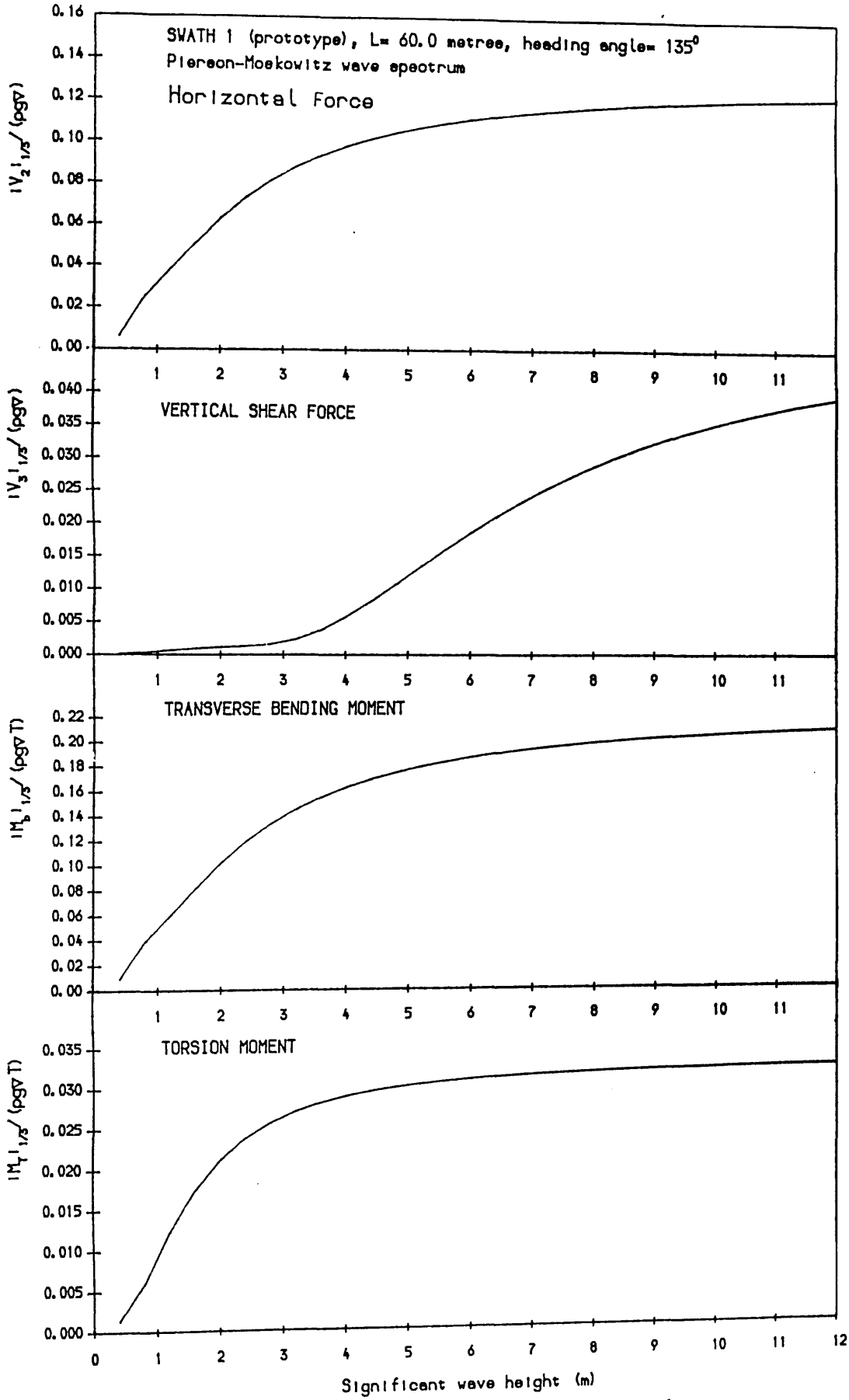

Fig. 7.14 Significant wave loads on the cross-deck structure of prototype SWATH 1 in irregular bow quartering waves